Final Report: HMTAP Task Order 18

Mississippi Coastal Analysis Project

Coastal Documentation and Main Engineering Report

June 17, 2008

FEMA

Federal Emergency Management Agency
Department of Homeland Security
500 C Street, SW
Washington, DC 20472

This project was performed by:

URS Group, Inc.
200 Orchard Ridge Drive, Suite 101
Gaithersburg, MD 20854

and

URS Group, Inc
1625 Summit Lake Drive
Suite 200
Tallahassee, FL 32317

HMTAP Contract No. HSFEHQ-06-D-0162
Task Order Number HSFEHQ-06-J-0018
Assigned on February 6, 2006

Acknowledgements

Emily Hirsch (Technical Monitor - FEMA HQ)
Stephen King (Michael Baker Inc. - Regional Management Center IV)

Table of Contents

Table of Contents

Table of Contents

Tables

Figures

Figures (Cont'd)

Figures (Cont'd)

Figures (Cont'd)

Appendices

This report describes the work performed for the Mississippi Coastal Analysis Project. The project was undertaken in the aftermath of Hurricane Katrina to provide flood hazard risk analysis for the Federal Emergency Management Agency (FEMA) .The analysis will also be used to help Mississippi during the recovery and mitigation efforts.

1.1 PURPOSE AND GOALS

The purpose of the project was to develop revised maps of the coastal flood hazard zones for Hancock, Harrison, and Jackson Counties in Mississippi as defined by the National Flood Insurance Program. This report describes the methodologies developed and the engineering work performed for the Mississippi Coastal Analysis Project.

The overarching goals of this project were to:

- Provide technically sound results using the best-available methods and data
- Meet an aggressive schedule through efficient project management
- Effectively coordinate efforts with other ongoing Federal studies in Mississippi and Louisiana

1.1.1 Best-Available Methods and Data

The Mississippi Coastal Analysis Project had two major components. First, new methods of analysis were developed. Second, these methods were applied to assess the coastal flood hazard in Mississippi.

The first component, that of developing and fully defining new methods of analysis, required the evaluation and integration of many recent advances in the state-of-the-art tools and methods in assessing and measuring hurricane behavior; numerical modeling of hurricanes, storm waves, and storm surge hydrodynamics; and statistical analyses of storm parameters and the coastal flooding hazard. Although these advances represent almost two decades of research and development work, largely in support of the offshore industry, they had not been tailored for application in FEMA coastal flooding projects.

Once the methods had been developed, tested, and verified, they were applied to the analysis of coastal flooding in Mississippi. The application of these new methods represented a considerable revision to the FEMA Coastal Flood Hazard analyses that were in effect prior to this project, which were completed approximately 20 years ago. Since then the number of historic hurricanes has increased and the quality of the data measured during these storms has greatly improved. Predictably, the results presented in this study substantially improve the definition of base flood elevations and the boundaries of mapped flood zones in coastal Mississippi.

1.1.2 Coordination with Ongoing Federal Studies

In Hurricane Katrina's aftermath, several Federal studies of hurricane storm surge behavior focusing on Mississippi and Eastern Louisiana were initiated. These intensive efforts combined the work of several agencies to substantially revise the methods employed to analyze the behavior of coastal hurricane storm surges and to quantify the associated flood risk potential.

The Mississippi Coastal Analysis Project was conducted in coordination with these efforts (refer to Section 2 for additional detail related to coordination efforts).

1.2 PROJECT APPROACH AND TEAM

From the very beginning, FEMA recognized the Mississippi Coastal Analysis Project would occupy a special status among the series of coastal flood analyses they have conducted. The need to satisfy a very aggressive schedule while developing a large number of new analytical methods made it impractical to conform to many of the practices that have characterized previous studies. Furthermore, engaging a number of nationally recognized experts in coastal engineering, geostatistics, meteorology, oceanography, and numerical modeling was necessary.

These experts became members of the overall project team and served both to support technical developments and to provide high-level technical review. This facilitated a fluid approach that allowed the project to adapt to new problems as they were encountered while minimizing delays.

The aggressive schedule also required a relatively large project staff so that work could be divided among many individuals. A uniform application of all methods was emphasized and considerable effort was devoted to documenting quality assurance and quality control activities.

1.2.1 Project Team

The project team comprised the following firms:

- URS Group, Inc. (URS)
- Dewberry Inc.
- Watershed Concepts Inc.
- Ayres Associates
- Oceanweather Inc.
- Risk Engineering Inc.
- Computational Hydraulics and Transport, Inc.
- Dr. Don Slinn

1.2.2 Technical Review Team

The Technical Review Team for the Mississippi Coastal Analysis Project consisted of:

- Dr. Leon Borgman (L.E. Borgman, Inc.)
- Dr. Robert Dean (Consultant)
- Dr. Todd Walton (Consultant)
- Dr. Stephen Baig (National Hurricane Center - National Oceanic and Atmospheric Administration [NOAA])
- Dr. Norman Scheffner (Computational Hydraulics and Transport, Inc.)

- Dr. Don Slinn (Consultant)
- Dr. Gabriel Toro (Risk Engineering, Inc.)
- Dr. Peter Vickery (ARA, Inc.)
- Mr. David Divoky (Watershed Concepts, Inc.)

1.3 REPORT ORGANIZATION

This report is the main source of technical information for the Mississippi Coastal Analysis Project. It provides information on both the derivation of new methods and the modification of existing methods used in this study. It also provides a comprehensive description of how the study methods were applied. This report is supported by a series of more detailed supporting reports (primary author firm noted):

- *Coastal Documentation and Main Engineering Report* (URS Group, Inc.)
- *Historical Flood Perspectives and Basic Coastal Study Area Information* (URS Group, Inc.)
- *Geospatial Technology Task Report* (URS Group, Inc.)
- *Field Investigation of Continuous Seawall* (URS Group, Inc.)
- *Grid Development Report* (URS Group, Inc.)
- *Tide Simulation Report* (URS Group, Inc.)
- *Calibration and Validation of Model Report* (URS Group, Inc.)
- *Wave Setup Methodology for the FEMA Mississippi Flood Study* (Professor Don Slinn)
- *Production Run Report* (URS Group, Inc.)
- *Wave Runup Method* (URS Group, Inc.)
- *Detailed Wave Analysis and Mapping Report* (URS Group, Inc.)
- *Hindcast Wind and Wave Forcing Report in Support of URS FEMA Mississippi Coast Flood Map Update* (Oceanweather Inc.)
- *Wave Setup: A White Paper with Emphasis to Application on the Mississippi Coastline* (Dr. Robert Dean)
- *Summary of Work Performed by Ayres Associates in Support of URS Storm Surge Modeling for FEMA Region 4* (Ayres Associates)
- *Joint Probability Analysis of Hurricane Flood Hazards for Mississippi* (Risk Engineering, Inc.)

One of the stated goals of the Mississippi Coastal Analysis Project was to coordinate, as much as possible, with other ongoing Federal studies in Mississippi and Louisiana. The Mississippi Coastal Analysis Project team coordinated primarily with the Environmental Research and Development Center (ERDC) Coastal Hydraulics Laboratory (CHL) of the U.S. Army Corps of Engineers (USACE) at Vicksburg, MS.

The ERDC-USACE was involved in several major projects, including:

- Interagency Performance Evaluation Taskforce (IPET)
- Mississippi Coastal Improvement Project (MsCIP)
- FEMA Region VI Louisiana Coastal Flood Study
- Louisiana Coastal Protection and Restoration Project (LaCPR)

The first three of these projects were especially important to the Mississippi Coastal Analysis Project. These are summarized in the following sections.

2.1 IPET PROJECT

Much of the IPET project development preceded the Mississippi Coastal Analysis Project work. Subsequent work performed as part of the USACE projects was coordinated with the Mississippi Coastal Analysis Project through exchanges of data and a series of meetings attended by a number of the technical experts from both teams. This cooperation resulted in the development of a set of robust methods that could be compared and checked by the USACE and FEMA project teams.

This report explains the methods that were developed for the Mississippi Coastal Analysis Project. Although these are very similar to the methods developed by USACE for IPET, there are some differences. Readers interested in comparing all of the methods are directed to USACE documents *White Paper on Estimating Hurricane Inundation Probabilities* (Resio et al. 2007), and *Performance Evaluation of the New Orleans and Southeast Louisiana Hurricane Protection System (Interagency Performance Task Force 2008).*

2.2 MISSISSIPPI COASTAL IMPROVEMENT PROJECT (MSCIP)

There was a special relationship between the Mississippi Coastal Analysis Project and the USACE MsCIP and FEMA Region VI Louisiana Coastal Flood Study projects. The MsCIP examined a number of coastal engineering options to reduce the coastal flooding hazard. One important component of this study was to compare past and future storm surge responses under various design options. These options included reconstruction of the offshore barrier islands, additional mainland beach nourishment, as well as construction of hardened structures such as sea walls and a surge protection dike. For each of these options, numerical modeling of storm surge conditions was used to evaluate the coastal flood levels. Some of this work closely paralleled the hydrodynamic modeling that was part of the Mississippi Coastal Analysis Project. Therefore, the two teams coordinated their work to produce a unified set of results for the hurricane surge levels defined by a sequence of recurrence intervals. Detailed information concerning the MsCIP project can be found in the Engineering Appendix to the *Final Report of the Mississippi Coastal Improvement Project* (Wamsley 2007).

2.3 FEMA REGION VI LOUISIANA COASTAL FLOOD STUDY

The USACE FEMA Region VI Louisiana Coastal Flood Study in Eastern Louisiana has also been especially important to the Mississippi Coastal Analysis Project. Very similar data were analyzed with common methods. The results showed good agreement across the border area. Minor differences in the study results were first examined to ensure that they were not symptoms of any underlying problems in either analysis. The results were then presented as a single set of coastal flood levels defined by a sequence of recurrence intervals.

3.1 OVERVIEW OF THE PROCESS OF ANALYSIS

This study of the coastal flood hazards in Mississippi progressed through several distinct steps. First, the characteristics of storms responsible for significant coastal flooding were determined through a statistical study of the regional historical record. These characteristics are site-dependent (storms in Mississippi are different from storms in the Carolinas, for example) and include strength, size, track, and so forth.

Secondly, the storm data was used in conjunction with numerical hydrodynamic models to determine the corresponding storm surge levels throughout Mississippi's coastal counties and to establish the flood elevations corresponding to the 0.2-, 1-, 2- and 10-percent-annual-chance of being equaled or exceeded in any given year.

In a third step, the 1-percent- and the 0.2-percent-annual-chance flood levels were augmented to include the additional hazard associated with wind-generated waves that ride atop the surge, and so raise the flood level. The four flood return periods (10, 50, 100, and 500 years) play central roles in the National Flood Insurance Program (NFIP) administered by FEMA. In particular, FEMA specifies the 1-percent-annual-chance flood level (including the height of the wave crests) as the Base Flood Elevation (BFE) for insurance and floodplain management applications; this level is mapped in FEMA's Digital Flood Insurance Rate Maps (DFIRMs).

3.2 ANALYSIS OF HISTORICAL HURRICANES

The analyses of the coastal flooding hazards use an indirect method based on a probabilistic representation of the occurrence and characteristics of future hurricanes, together with numerical models that calculate the inundation of these hurricanes. First the frequency and intensity of cyclonic storms (hurricanes and tropical storms) must be determined. The behavior of these storms is characterized by a set of meteorological parameters. Typically there are about a half dozen of these parameters that describe the behavior of the event in sufficient detail, so that they can be used as the key parameters for the pressure and wind field in mathematical models.

It is challenging to adequately demonstrate that there is enough information about the historic storms to represent the statistical characteristics of the true range of storm sizes and intensities that may occur in the future. It is recognized that hurricanes, especially intense ones, are rare events. The historic record is only a small sample, from which information is extracted about the full population of events. Thus, clearly defining the limits of this sample so that it contains good quality and truly representative data is important. Even when considerable effort is devoted to this undertaking, good judgment must be combined with statistical methods to ensure the best sample representing the population of all possible events.

Once the characteristics of past events were established, the characteristics of future events were assumed to tend toward the same statistical description. Based on this assumption, the characteristics of a large number of individual future events were defined with different combinations of the meteorological parameters.

This section describes the meteorological parameters used to define tropical storms and hurricanes. The methods used to define a representative sample of the historic storms are explained. Statistical descriptions of these meteorological parameters are presented.

3.2.1 Hurricane Parameters

Hurricane parameters are the variables used in numerical models that represent the main characteristics of the hurricane. Over the past several decades, a sequence of models, such as the wind model used in the NOAA Sea, Lake, and Overland Surges for Hurricanes (SLOSH) Model, the NOAA National Weather Service (NWS)-28 Wind Model, the Vickery and Twisdale (1995) model, the Holland (1980) model, and various implementations of the Planetary Boundary Layer (PBL) model (e.g., Vickery and Twisdale, (1995); Thompson and Cardone, 1996, Vickery et al., 2000) have been used. Most of these models use the following three parameters: 1) the central atmospheric pressure deviation (ΔP), 2) the pressure scale radius (R_p), and 3) the forward speed of the storm center (V_f). Some of these models also use a parameter to alter the spatial gradients in the radial pressure field (the "Holland B" parameter), which in turn alters the peakedness of the wind field. Additional parameters define the geographical location and direction of propagation of the storm. This study utilized the point of landfall (S_i) and the storm track azimuth (θ)[1] for this purpose.

Another commonly used measure of the size of the hurricane is the radius to maximum winds (R_{max}). The radius to maximum winds is the representative distance between the center of storm circulation and the location of the highest sustained wind speed. Under most windfield models, and for typical hurricane sizes, R_p and R_{max} are nearly identical, and some investigators use the two terms interchangeably. This study utilized R_p as its measure of hurricane size, except in the SLOSH runs, where the difference between the two radii was considered explicitly.

The central atmospheric pressure deviation (ΔP) and the central pressure of the storm (CP) are closely related parameters that are interchanged in some usages. Both of these are usually measured in units of millibars (mb). The central pressure is a specific measure of the pressure within the center or eye of the storm. The central pressure deficit or deviation (ΔP) is the difference between the actual central pressure and the atmospheric pressure at a large distance outside of the storm. This study assumes that ambient pressure at a remote distance from the storm has a value of 1013 mb, per common practice, unless otherwise specified.

There are many other factors that influence the time-varying behavior of these large storms. As the quality of observational data from satellites, Doppler radar, ocean data buoys, and other instrument systems has improved, so has the understanding of variations in the internal structure of storms due to eye-wall replacement cycles, oscillations in the radial position of maximum winds, track wobbles, the development of storm bands, and other features. These sources of variability are not included in the list of hurricane parameters because the data are sparse.

3.2.2 Sources of Storm Data

Meteorological data were needed for both the model calibration task and the verification task, and to provide the historical basis for the storm climatology. Data were collected from a variety of sources, as described below.

NOAA has collected measurements of historic cyclonic storms in waters surrounding the United States for many years. These have been compiled into the Atlantic basin hurricane database (HURricane DATabase, commonly referred to as HURDAT – see Jarvinen et al. 1984) which is

[1] Compass direction of the storm track at landfall, measured clockwise from North.

available to the public. HURDAT is the official record of tropical storms and hurricanes for the Atlantic Ocean, Gulf of Mexico, and Caribbean Sea, including those that have made landfall in the United States. It has recently been revised to include data going back to 1851. The data consist of the latitude and longitude of the storm center (i.e., eye), central pressure, and maximum wind speed at 6-hour intervals.

Additional data sources include: NOAA Technical Report NWS 38 (Ho et al. 1987), NOAA Technical Memo NWS TPC-4 (Blake et al. 2005), NOAA Technical Memo NWS TPC-1 (Hebert et al. 1996), and the National Hurricane Center (NHC) Tropical Cyclone reports for the individual storms. In addition to these public agency sources, a detailed list of storm characteristics from recent storms has been developed by Oceanweather Inc. (OWI); this list includes updates provided by David Levinson at the NOAA National Climate Data Center (Levinson, pers. comm. 2007).

3.2.2.1 Hurricane Katrina

Detailed data were developed for Hurricane Katrina to support its use in calibrating the numerical model framework. The pertinent data sets consist of:

- Aircraft reconnaissance obtained from NOAA and U.S. Air Force hurricane hunter aircraft, including vortex messages and continuous flight-level wind speed, direction, and D-Value
- Gridded and image fields of marine surface wind composites from the National Hurricane Research Division (NHRD) HWind analysis
- Synoptic observations from NOAA buoy and Coastal Marine Automated Network (C-MAN) stations
- Synoptic observations from transient ships and coastal and land stations
- Composite NWS radar imagery and Doppler radar PBL flow velocity estimates
- Loops of NOAA Geostationary Operational Environmental Satellite (GOES) visual, infrared, and water vapor imagery
- National Centers for Environmental Prediction (NCEP) model wind fields
- Quick Scatterometer (QUIKSCAT) winds
- TOPography EXperiment (TOPEX) for Ocean Circulation altimeter winds and waves
- European Remote Sensing (ERS-2) satellite altimeter winds and waves
- Data from offshore platforms equipped with meteorological packages

3.2.2.2 Hurricanes Camille and Betsy

Data from public sources were used for Hurricanes Camille and Betsy. These included the USACE Mobile District Hurricane Camille Report (1970); the reports by Hamilton and Steere (1969) and the *Hindcast Wind and Wave Forcing in Support of URS FEMA Mississippi Coastal Flood Map Update* supporting report; and the papers by Goudeau and Conner (1968), Frank (1970), and Simpson et al. (1979).

3.2.2.3 Historical Hurricane Data

The major source of data for historical storms was the TROPical (TROP) files provided by OWI. These files were derived from detailed reviews of a wide range of meteorological data on hurricanes in the Gulf of Mexico. The characteristics obtained from the TROP files are the offshore central pressure, track coordinates, storm radius, forward velocity of the storm center, and azimuth of the track (the latter two were derived from the coordinates and associated timestamps). For values of parameters at landfall, a separate list was compiled by Dr. Peter Vickery of ARA. Some of the data sources had conflicting information, and Dr. Vickery supplied a list of the preferred landfall central pressures for all 188 storms in the historic record since 1900. It was also necessary to augment these data with information from NWS 38 and HURDAT for some of the weaker historic storms.

3.2.3 Historic Storms

3.2.3.1 Period of Record

The selection of the period of record is important because of the need to use as much data as possible, while maintaining a meaningful standard for the data itself. The HURDAT[2] data were recently expanded to include data from 1885 to 1900 and most recently from 1851 to 1885. The quality of the data varies considerably over the period from 1851 to present. Methods used to collect coastal and inland weather measurements were improving by the beginning of the 20th century, but measurements offshore were sparse and erratic until nearly mid-century. This situation changed dramatically during World War II (WWII) in the 1940s with the initiation of aircraft missions to measure storm parameters. Since that time, the quality of both offshore and onshore data has risen continuously. Aircraft instrumentation and navigation has also improved continuously since WWII. Satellite observations were added during the 1960s, and these too have become increasingly more sophisticated and useful. More instrument systems have been introduced in recent decades. Ocean data buoys with meteorological and oceanographic sensors have been deployed since the 1970s. A variety of Doppler radar installations came online during the 1990s. Within the last few years, mobile meteorological stations have been added to increase the spatial density of storm measurements.

After review of the many forms of data, both the USACE team and the URS team decided to designate the beginning of the period of record for the studies as the initiation of the offshore aircraft measurements during WWII. This decision was reviewed by personnel from the National Hurricane Center (NHC) who agreed that this initial date was a reasonable choice, especially because the numerical hydrodynamical calculations require information about the characteristics of the storm while it is offshore. The period of record used for this study was 1940 to 2006.

3.2.3.2 Large-Scale Temporal Variability

There is often a concern about multi-year temporal variability in studies involving hurricanes and tropical storms. Some multi-year periods have more frequent storms than others. The period of

[2] http://www.aoml.noaa.gov/hrd/hurdat/index.html

record for the Mississippi Coastal Analysis Project is sufficiently long to span a variety of these multi-year patterns.

There is a growing concern that climate change and global warming may lead to a change in the frequency or intensity of hurricanes. Although this has been suggested by various researchers, there does not appear to be a substantial body of evidence to quantify these effects at this time. Long-term climate trends such as this may also bring about changes in the rate of ongoing sea level rise. Fortunately, changes in the behavior of hurricanes and in global sea level occur in time scales that are certainly no shorter than decades. FEMA provides for periodic reevaluation of coastal flood maps. Accordingly, no special provisions for long-term changes in hurricane behavior or sea-level rise are included in this project.

3.2.3.3 Storm Sample Zone

Although hurricanes are devastating storms, the length of coastline that each event affects is only a fraction of the length of the northern Gulf Coast. In the past it was argued that, given a large enough sample of storms, the characteristics of hurricanes would be the same over most of the Gulf (Bea et al. 1983). This would mean that the observed local variations in the number or intensities of landfalling storms come purely from the sparse nature of the data.

More recently, evidence has accumulated that the characteristics of hurricanes are not uniform over the Gulf of Mexico (Cooper 1992). Time-averaged patterns in the circulation of the atmosphere and Gulf waters are thought to give rise to statistically significant regional differences in storm characteristics. That is, the frequency and intensity of storms is now thought to vary across the Gulf and along its shoreline.

Figure 3-1 shows the storm rate for the whole Gulf of Mexico. The storm rate varies across the Gulf over distances of hundreds of kilometers. The north-central Gulf has the highest storm rate and this is believed to be a consequence of both the shape of the Gulf and the pattern of the prevailing winds, which steer the hurricane. The typical location of the warm Loop Current may also affect rates in a less direct manner. More importantly, the Loop Current and the warm eddies that it generates have been linked to the geographical variation in hurricane intensity (Chouinard et al. 1997b, Cooper 1992, Hong et al., 2000).

These regional patterns in the characteristics of cyclonic storms pose a number of difficulties to the analysis of the coastal flood hazard in Mississippi. The straight line distance from border to border is only on the order of 70 miles (mi). Since WWII, five hurricanes have made landfall on this coast (Ethel, 1960; Camille, 1969; Elena, 1985; Georges, 1998; and Katrina, 2005). This would be a small number of hurricanes on which to base a statistical description of the storm parameters. The limitations in extending the record further back in time have already been discussed. However, it is also apparent that storms making landfall 50–100 kilometers (km) to either side of the Mississippi coast could equally well have struck within the State if the steering-wind patterns had been slightly different. The characteristics of landfalling storms vary little over distances of the order of the length of the Mississippi coast. Thus, the sample of historic storms can be taken over a length of coast that extends beyond Mississippi.

In order to identify the sample of historic storms that can be used as the basis for the storm climatology, it is necessary to define where and how they are measured. In this study, the

characteristics of the storms as they made landfall were used because the amount and quality of measurements is greater nearshore and onshore than offshore.

Simplified Shoreline

Designating a simplified shoreline to avoid crenulations that could confuse the designation of the landfall points is also useful. The schematic shoreline for the north central Gulf of Mexico presented in NOAA Technical Report NWS #38 (Ho et al. 1987) was adopted. However, to avoid the possibility of multiple landfall points for a single storm track, the NWS #38 schematic shoreline was further simplified to eliminate the outline of the "birdfoot" delta of the Mississippi River. This delta feature is mostly a narrow wetland with a size that is small relative to the dimensions of hurricanes. Consequently, it will not influence hurricane behavior in the same way as a mainland coast The resulting project shoreline is shown on Figure 3-2.

Sample Zone

With the project shoreline defined, the length of shoreline to use for collecting hurricane statistics had to be established. An optimal length is established through a tradeoff between reducing statistical uncertainty by considering a longer length of coast, thereby increasing the number of events in the sample, and increasing spatial resolution by considering a narrower length of coast.

In the era of FEMA coastal flood hazard analyses that were previously used on the Mississippi coast, a fixed length was used to define a capture zone. This zone usually extended some distance to either side of the coast of interest, but there were no established methods that uniquely defined how far this distance should reach. There was a sharp cut-off at the ends of this zone, which raised another potential problem. Because the number of landfalls per unit length is small, the designated length may just miss the landfall location of one or more significant hurricanes. If the zone is arbitrarily lengthened to include these data, they may have a disproportionately large effect on the statistical description of the storm characteristics.

Over the past decade the offshore industry has advanced the methods used to define the size of the zone for the population sample. Chouinard et al. (1997b) has introduced the use of the Gaussian Kernel Approach. In this method, each storm in the region near the site of interest is given a weight that decreases smoothly as distance to the site increases. The use of a smooth kernel may be viewed as an extension of the traditional discrete capture zone approach (i.e., a smooth Gaussian shape with a certain width replaces a box-car function with a width equal to the width of the capture region). Furthermore, Chouinard's method provides an objective procedure to define the width of the Gaussian function used to calculate these weights in a manner that provides the optimal balance between statistical precision and spatial resolution.

The process starts by taking historical storm data from a shoreline length that extends well beyond the study area. This provides the raw data used in the Gaussian Kernel Approach. For this study, the initial data were taken from all of the post-1940 storms making landfall in the Initial Capture Zone (ICZ) between 85^{o} W and 95^{o} W.

Because the Mississippi coast is short relative to the patterns of parameter variation shown on Figure 3-1, only a single site was analyzed to calculate the storm climatology. A coastal

reference point ([CRP] with coordinates 30.20 N, 89.30 W) was located approximately 30 km (i.e., approximately one radius of maximum winds) west of the coastline midpoint (Figure 3-2).

The tracks of all hurricanes making landfall in the ICZ were identified. These tracks were extrapolated back offshore as straight lines with the azimuth unchanged from the shore crossing. The Gaussian Kernel Approach was used with all of the initial data to evaluate an appropriate length scale. A length scale of 200 km to either side of the CRP was selected. The reasons for selecting this length are given in the following sections.

Storm Populations

To accommodate the aggressive project schedule, the storm population was partitioned between the "greater" and the "lesser" storms (defined below). An analysis conducted by Risk Engineering indicated that the flood levels for annual recurrence rates of 1 percent or less are largely controlled by hurricanes with central pressure below 965 mb, hereafter referred to as "greater storms." Most of the later phases of the project (Wave Height Analyses for Flood Insurance Studies [WHAFIS] analysis and much of the mapping) depended on knowing the flood levels corresponding to the 1-percent-annual-exceedance rate. Accordingly, the analysis was first carried out for these greater storms. Subsequently, an additional analysis was conducted for the lesser storms. Based on previous experience, storms with central pressures between 982 mb and 965 mb control surge elevations that are characteristic of 10-percent-annual-exceedance rates. The same procedures were followed in both phases of these analyses.

The initial data sample consisted of 33 hurricanes, 15 of which were greater storms and 18 of which were lesser storms. The two storm populations were analyzed and modeled separately. The resulting surges were then combined.

3.2.4 Defining the Characteristics of Historical Hurricanes

In order to develop a statistical characterization of past storms, the storm rate and each of the five meteorological parameters were analyzed separately. The Chouinard method was used in characterizing the storm rate (λ), the landfall track azimuth (θ), and the central pressure deficit (ΔP). The pressure scale radius (R_p), which was taken as dependent on ΔP, and the forward speed of the storm (V_f) were analyzed using conventional regression and distribution-fitting statistical methods, respectively.

For each storm in the sample, the minimum track-to-CRP distance (track-CRP) for use in the Chouinard method was calculated using a straight-line track constructed using the landfall location and the storm azimuth at landfall. Therefore, the variant of the Chouinard method used in this study works with the distance at the point of closest approach (computed using this idealized track), in conjunction with the storm parameters at landfall. This is in contrast with Chouinard's original procedure, which works with the parameters at the point of closest approach.

The size of the storm sample was effectively determined by the kernel size (see Equation 1 below). The *Cross-Validation* method developed by Chouinard (Chouinard and Liu 1997a; Chouinard et al. 1997b) was used to determine the optimal kernel size using a technique known as *Cross Validation*. For a given choice of kernel size, the cross-validation calculates a quantity called the cross-validation square error (CVSE), which measures the combined effect of

statistical uncertainty and lack of fit (i.e., poor spatial resolution). The kernel size that resulted in the smallest mean-square error when averaged over all of the trial realizations was selected. Details on this method are fully explained in the supporting project report, *Joint Probability Analysis of Hurricane Flood Hazards for Mississippi*.

Three different kernels were determined with this cross-validation method. Two of these were used to evaluate the storm rate and one was used to determine the central pressure deviations.

3.2.4.1 Storm Rate

The optimal size of the Gaussian kernel used in determining the omni-directional storm rate for the Mississippi coast was developed with the Chouinard method. Figure 3-3 shows a plot of the CVSE against the unsigned distance from the CRP. Based on the results shown on this figure, the optimal kernel size is in the range of 150 to 200 km.

The Gaussian weighting or kernel function is of the form:

$$w_i = \frac{1}{\sqrt{2\pi}h_d}\exp\left[-\frac{1}{2}\left(\frac{d_i}{h_d}\right)^2\right] \quad (1)$$

where d_i is the individual minimum distance measurement for a given storm and h_d is the kernel size for distance. With this, the storm rate (λ) is computed from:

$$\lambda = \frac{1}{T}\sum_{i=1}^{N} w_i \quad (2)$$

where T represents the length of the period of record in years and N is the total number of storms within the time period, location, and pressure range under consideration. The omni-directional storm rate for the Mississippi coast was determined to be 2.88E-4 storms per year per kilometer for the greater storms (central pressure < 965 mb) and 2.57E-4 storms per year per kilometer for the lesser storms (965 mb $\leq$ central pressure < 982 mb). Observations show that the track position parameter is uniformly distributed.

3.2.4.2 Landfall Track Azimuth

The landfalling data and methods used to determine the omni-directional storm rate were also used to determine the directional storm rate and to characterize the storm track azimuth at landfall. Figure 3-4 shows a plot of the CVSE for the calculation of directional rates, which depends on both the distance kernel size and the angular kernel size. For this area the optimal kernel size for the directional storm rate (200 km) is not sharply defined, especially for the larger directional spreads. It is in the range of 170 km to 220 km which is similar to the size obtained earlier for the omni-directional rates. For the sake of consistency, the distance kernel size of 200 km was used for all analyses.

Figure 3-5 shows the directional rates for the greater storms obtained using the smoothing parameters obtained in Figure 3-4. Dividing these rates by the omni-directional rate determined earlier, results in the probability distribution of storm azimuth, which is well approximated by a Beta distribution with probability density function proportional to $x^{r-1}(1-x)^{t-1}$, where

$x = (\theta + 180)/360$, r = 10.2, and t = 11.7 (the associated mean and standard deviation are −12.4 degrees and 37.5 degrees, respectively). Figure 3-6 shows similar results for storms with central pressures between 965 and 982 mb. The resulting distribution of azimuths is well approximated by a normal distribution with mean and standard deviation of −9.9 degrees and 58.7 degrees, respectively.

3.2.4.3 Central Pressure

Central pressure as a measure of storm intensity is characterized by the pressure deficit ΔP. For the storms used to calibrate and verify the models the actual atmospheric pressures at the storm center and well outside of the storm were used. For the storms created for the forward modeling this parameter was calculated as $\Delta P = 1013 \text{ mb} - \text{Central Pressure}$ (i.e., it is assumed that the far-field pressure is always 1013 mb). Based on experience from previous studies, the shape of the distribution of ΔP for storms with central pressures below 965 mb (i.e., $\Delta P > 48\text{mb}$) is taken as a 3-parameter Weibull, i.e.,

$$P[\Delta P > x] = \exp[(\Delta P_0 / U)^k - (x/U)^k]; \quad x > \Delta P_0 \tag{3}$$

where the Weibull scale parameter U and shape parameter k are obtained by fitting the data, as described below, and ΔP_0 is the minimum value under consideration (i.e., 48 mb for the largest storms; note that it is important to use a value of ΔP_0 that is consistent with the calculation of rates).

The Weibull parameters U and k were obtained using the approach of Chouinard et al. (1997b), where each storm was assigned a weight that depends on the distance to the site of interest, using an optimal kernel function similar to the one used in the calculation of rates. Then parameters U and k are solved for using the method of a weighted maximum likelihood. In solving the maximum-likelihood problem, an additional constraint was added, which forced the Weibull density function to be monotonically non-increasing in the range of $\Delta P > 48\text{mb}$.

Figure 3-7 shows the cross-validation results for a Chouinard analysis of the central pressure distribution for the greater storms (central pressures below 965 mb). These results suggest an optimal kernel size in the range of approximately 100 km to 140 km. This range is roughly comparable to the kernel size range of 150 km to 200 km determined in the storm rate analysis and 170 km to 220 km from the track azimuth analysis. In all cases, these optimum values are not sharply defined so that a general representative length scale is all that is needed. For the sake of consistency with the directional-rate calculations, a kernel size of 200 km was used for all analyses.

The statistical uncertainty in the storm parameter values was determined using a "bootstrapping" procedure (Efron 1982). For the bootstrapping procedure, a synthetic storm catalog with the same duration as the actual catalog was created using a re-sampling randomization scheme. For each new realization from the re-sampling, the optimum kernel size was used to calculate a new set of parameter values (i.e., rate and Weibull parameters). This was repeated 1,000 times, and the mean values, variances, and co-variances of these parameters were determined. These values were then used to establish the mean values for the rate and the cumulative distribution function of the pressure deficit. The rationale for using the mean distribution for ΔP, rather than the

best-estimate distribution that one obtains by applying the Chouinard procedure (1997) to the historical hurricane catalog, is based on decision theory (McGuire et al. 2005).

The resulting mean distribution of ΔP is a weighted average of Weibull distributions and does not necessarily follow a Weibull distribution. Conveniently enough, a Weibull distribution with U=48.6 mb and k=1.8 provides a good approximation of the mean distribution of ΔP for the range of ΔP of interest to this study.

A slightly different approach was followed for the lesser storms, as described below. The first step was to fit a Weibull distribution to the $\Delta P > 31$ mb data (the combined data from the lesser and greater storms) using the same weighted maximum likelihood procedure, with a kernel width of 200 km, but without imposing the monotonicity constraint on the probability density. The next step was to perform bootstrapping in the same manner discussed above, obtaining a Weibull approximation to the mean distribution of ΔP. The final step was to remove the greater storms from this distribution by introducing an upper bound at $\Delta P = 48\text{mb}$ and re-normalizing the distribution. The resulting cumulative distribution has the form:

$$P[\Delta P > x] = \frac{\exp\left[-\left(\frac{x}{U}\right)^k\right] - \exp\left[-\left(\frac{48\text{ mb}}{U}\right)^k\right]}{\exp\left[-\left(\frac{31\text{mb}}{U}\right)^k\right] - \exp\left[-\left(\frac{48\text{ mb}}{U}\right)^k\right]} \qquad 31\text{mb} \le \Delta P \le 48\text{mb} \tag{4}$$

with U=46.6 mb and k=1.95. The rate for lesser storms given earlier is consistent with this distribution.

3.2.4.4 Pressure Scale Radius (R_p)

Considerable attention was given in this study to establishing whether the storm radius (R_p) was statistically independent of the central pressure of a storm. Figure 3-8 shows a plot of these two parameters measured at landfall for all hurricanes in the TROP files that made landfall between 85 and 95 degrees west.

As shown in Figure 3-8, the data for landfalling storms are sparse, and the correlation of the parameters is not strong. However, the decision on whether to consider these two parameters to be correlated has important consequences. If there is no negative correlation, then future storms with large radii and low central pressures are more likely than they are under the commonly made assumption of negative correlation.

A recent paper by Shen (2006) provides some insight into the relationship between R_p and ΔP. This paper examines the kinetic energy balance within a hurricane and concludes that, given the same large-scale environmental conditions, hurricanes with smaller radii have a higher potential intensity. This result is not sensitive to changes in model parameters.

To overcome the scarcity of data in Figure 3-8, more information was taken from the larger amount of data available for storms offshore in the whole Gulf of Mexico. Figure 3-9 shows a plot of all Gulf of Mexico R_p- ΔP data for storms with $\Delta P > 48\text{mb}$ in the TROP files. Each point along the track (typically taken at 6-hour intervals) yields one R_p- ΔP pair, as long as the point is on Gulf of Mexico waters. Therefore, this figure and the analysis that follows include multiple R_p- ΔP pairs for each storm.

Figure 3-9 illustrates that R_p has a large scatter for any given value of ΔP. It also suggests a moderate negative correlation between R_p and ΔP, and it does not show an obvious dependence on latitude (within the range of latitudes of the Gulf). These data were used to perform a regression analysis of $\ln(\Delta P)$ on $\ln(R_p)$. In addition, a log-normal shape was adopted for the conditional distribution of $R_p \mid \Delta P$, based on earlier studies (e.g., Wen and Banon 1991; Toro et al. 2004). In summary, the conditional distribution of $R_p \mid \Delta P$ for the greater storms is treated as lognormal, with a mean value of $406.2\Delta P^{-0.711}$ nautical miles (nmi) and a standard deviation of $187.7\Delta P^{-0.711}$ nmi.

Although there is still some uncertainty about the correlation of $R_p/\Delta P$, the trend for the offshore storms and the modeling results by Shen (2006) suggest that these should not be treated as independent parameters. This approach is consistent with the approach described by Resio et al. (2007) for USACE and in other studies (e.g., Wen and Banon 1991; Toro et al. 2004).

In the Mississippi Coastal Analysis Project, the functional relationship between R_p and ΔP derived from data taken from the whole Gulf of Mexico was used with the central pressures measured at landfall. The assumption is that the relationship between R_p and ΔP that was evident in the larger offshore data set also holds as the storms approach land.

The lognormal model for $Rp \mid \Delta P$ developed for the greater storms was found to over-predict the values of R_p for the lesser storms when applied to lower values of ΔP. Thus, it was necessary to perform a new analysis including these storms. The data for this analysis were selected by determining the value of R_p at the time when the storm reached its maximum ΔP within the Gulf [R_p (offshore), or $R_{p(o)}$ for brevity], and then pairing this value with the value of ΔP at landfall. This data selection approach is more consistent with the R_p- ΔP relationship in the Joint Probability Method (JPM) calculations used in this study (see Section 3.3) than the approach used above for the greater storms. Furthermore, the data were restricted to the 1950-2006 interval in order to use more reliable values of $R_{p(o)}$, and the data point for Hurricane Juan (1985) was excluded because its value of $R_{p(o)}$ in the TROP files (100 nmi) was considered an outlier.

Figure 3-10 shows these data, as well as the percentiles of the lognormal model for the distribution of $R_p \mid \Delta P$ derived from them (Figure 3-9). Figure 3-10 demonstrates that the two models are similar in the ΔP range of interest for the 1-percent-annual-chance exceedance rate flood (i.e., ΔP 60-90 mb), but they differ significantly for the lesser storms. Therefore, the lognormal model for $R_p \mid \Delta P$ based on Figure 3-10 was used for the lesser storms. This model corresponds to a lognormal distribution with a mean value of $79.58\Delta P^{-0.33}$ nmi and a standard deviation of $36.78\Delta P^{-0.33}$ nmi.

3.2.4.5 Storm Forward Speed and Landfall Position

The hurricane parameter that has the least effect on the magnitude of a storm surge is the forward speed of the storm center. Data for this parameter were taken at landfall for the 1940-2006 time period. For the greater storms, data from the TROP files were used. The probability density for the forward speed of the greater storms is shown on Figure 3-11 and for the lesser storms on Figure 3-12. The data for the forward speed of the storm (V_f) fit a lognormal distribution.

The landfall positions (S) were treated as a uniform distribution because the occurrence rate is approximately constant within the region of interest.

3.2.4.6 Other Storm Parameters

Although most of the older diagnostic models of hurricane winds and pressures used the five parameters (ΔP , R_p, V_f, θ, and S) as inputs, others were considered. The PBL model used in this study, and other similar models, includes the Holland B (*B*) parameter, which alters the shape of the radial distribution of winds.

Figure 3-13 presents example pressure and gradient wind speed profiles for a stationary hurricane having a central pressure of 943 mb, and a far field pressure of 1013 mb, showing the effect of changes in the Holland B parameter on the pressure and wind speed profiles. The maximum wind speed decreases with decreasing values. As this parameter decreases, the model hurricane becomes broader. For example, with a Holland B of 0.75, the wind speed is reduced by nearly 50 percent of the maximum value. Hurricanes modeled with large values of Holland B are typically considered "tight" storms, and are most often associated with small storm pressure radii. Hurricanes modeled with small values of Holland B are broader.

The Holland B parameter was accorded a special treatment in all of the FEMA and USACE projects for Mississippi and Louisiana. Based on studies described in Resio et al. (2007), storm-to-storm variation of this parameter was taken to be negligible, and the variation as the storm approached the coast was taken to be systematic, as described below.

As storms with pressure radii greater than 10 nmi approach within 90 nmi of the shore, the value of the Holland B parameter is taken to decrease linearly from 1.27 to 1.0 at the shoreline. This change continues after landfall, such that it reaches a value of 0.9 after 3 hours. Storms with pressure radii smaller than 10 nmi are taken to maintain the value of 1.27 as they approach the coast.

In the future, the understanding of the behavior of hurricane wind and pressure fields will likely expand, and more sophisticated mathematic models, perhaps with additional parameters, will be developed. At this time, it is clear that the representations of wind and pressure fields in the current generation of models are idealized. In the absence of more detailed representations, the effects of the real departures are recognized and treated as statistical variabilities, as described later in Section 5.2.

3.3 DEVELOPMENT OF THE JPM-OS METHOD FOR MISSISSIPPI

The storm surge analysis method used in this project required defining a set of hypothetical synthetic storms with characteristics that match those of the population of past storms (developed using the historical storm sample as described in Section 3.2). The synthetic storms needed to represent the full range of conditions contained in the historic storm population, and their occurrences needed to be weighted in the right proportions. Synthetic storms defined by combinations of meteorological parameters that have not occurred in the past, but were deemed plausible by the probabilistic descriptions developed in the previous section, were included.

The JPM developed by Myers (Myers 1975, Ho and Myers 1975) was selected for statistical analysis by FEMA for this project after some initial work with other approaches. In order to apply the JPM in combination with the computationally demanding Advanced Circulation (ADCIRC) hydrodynamic model, a particularly efficient procedure for the JPM analysis needed to be developed. A new approach was developed to reduce the total number of storms needed for

the JPM procedure without deteriorating the accuracy of the results. The modified JPM is called JPM-Optimum Sampling (JPM-OS), and is described more fully in Section 3.3.2.

3.3.1 Description of the JPM Method

As mentioned earlier in this report, the process of determining the annual probability of coastal flood elevations for the indexed occurrence probabilities would be simpler if there were a large number of actual measurements of coastal floods at all geographical locations of interest over an adequate period of time. If that were the case, historical data could be used. However, if the historical data are insufficient, this approach leads to a high degree of uncertainty and is not recommended.

If sufficient historical surge height data are unavailable, a more elaborate method is necessary. This method relies on probabilistic models of the storm occurrence, in time and of the storm characteristics, together with numerical models that calculate the coastal flood elevation given these storm characteristics. These models include the model for storm track and for the evolution of the storm characteristics (conditional on the characteristics at landfall), the windfield model, the surge model, etc. (see Section 4.1) and are represented symbolically as $\eta\ (\Delta P, Rp, V_f$ landfall location$, \theta, ...) = \eta(\underline{X})$[3], where vector $\underline{X}$ represents all storm characteristics. The annual probability of a coastal flooding elevation at a site in excess of a value η is defined in terms of the following three quantities:

- The annual rate of storms of interest
- The joint probabilities of the storm characteristics
- The storm-generated flood elevations at that site, given the storm characteristics

The combined result is expressed by the multiple integral

$$P[\eta_{\max(1\ yr)} > \eta] = \lambda \int \ldots \int_{\underline{x}} f_{\underline{X}}(\underline{x}) P[\eta(\underline{x}) > \eta] d\,\underline{x} \qquad (5)$$

where λ is the mean annual rate of storms of interest for that site, $f_{\underline{X}}(\underline{x})$ is the joint probability density function of the storm characteristics of these storms, and $P[\eta(\underline{x}) > \eta]$ is the conditional probability that a storm of certain characteristics $\underline{x}$ will generate a flood elevation in excess of η. This probability would be a Heaviside step function $H[\eta - \eta(\underline{X})]$ if vector $\underline{X}$ contained a complete characterization of the storm and if one could calculate the flooding elevation $\eta\ (\underline{X})$ exactly for any given $\underline{X}$, but these conditions cannot be satisfied in practice. This integral (Equation 5) considers all possible storm characteristics for the population of storms of interest and calculates the fraction of these storms that produce flooding elevations in excess of the value of interest η, using the total probability theorem (Benjamin and Cornell 1970).

The right hand side in Equation 5 represents the mean annual rate of storms that produce surges exceeding η at the site. If this rate is low, and the physical process of hurricane occurrences is

[3]All landfalls are referenced to a point located at the center of the study area. The parameter defining landfall location is thus the signed distance from the reference point for which the probability distributions were derived.

independent enough so that the probability of two or more exceedances of η in one year is much lower than the probability of one exceedance, this rate represents a good approximation of the annual exceedance probability. These conditions are satisfied for the exceedance probabilities of interest in this study, specifically, the 10-, 2-, 1- and 0.2-percent-annual-chance of exceedance probabilities.

Equation 5 is the basis of the JPM. The probability density in Equation 5 is now taken as the joint probability of a combination of hurricane parameters. The associated flood elevation at any given point is determined as the maximum level produced by the numerical model. Equation 5 defines a smooth function of η that can be used to determine the flood levels associated with any probability of being exceeded.

3.3.1.1 Practical Formulation of the JPM

As previously mentioned, enhanced measurements with satellites, ocean data buoys, Doppler radar, and other systems have recently demonstrated the complexity in the internal structure and variability of hurricane behavior. Therefore, as noted by Resio et al. (2007), the total number of storm parameters that would allow the function defined in Equation 6 to be fully evaluated would be very large. It is important to acknowledge that modeling of the storm behaviors that control the coastal flood hazard is incomplete if it is driven only by the five traditional "major" parameters. In addition, the numerical hydrodynamic models for the hurricane effects are not perfect, despite their recent progress.

Therefore, the actual elevation $\eta(\underline{X})$ is expressed in terms of the model-calculated elevation $\eta_m(\underline{X})$ as $\eta(\underline{X}) = \eta_m(\underline{X}) + \varepsilon_m$, where ε_m is a term that accounts for variations in the actual values of $\eta(\underline{X})$ that are not accounted for by the windfield and hydrodynamic models. This difference is treated as a random quantity independent of $\underline{X}$. If the model is unbiased, ε_m has a mean value of zero. Using the above representation, the actual conditional probability $P[\eta(\underline{x}) > \eta]$ is written as:

$$P[\eta(\underline{X}) > \eta] = P[\eta_m(\underline{X}) + \varepsilon_m > \eta] = P[\varepsilon_m > \eta - \eta_m(\underline{X})] \quad (6)$$

The ε_m term, referred to as the "epsilon term," is designed to include all of the causes for deviations of actual storm surges from the estimates obtained using numerical models of hurricanes, such as the PBL model used in this project. The ε_m term accounts for variations in the surge heights caused by storm wind and pressure field asymmetries, variations in maximum wind intensity and the radius of maximum wind around the storm, eyewall replacement cycles, propagation of spiral bands, and other similar phenomena. The term is also used to account for various other numerical model deficiencies, many not specifically identified, which contribute to differences between the modeled and measured maximum surge heights. The overall analysis is made more complete by including a term representing the effects of these deficiencies.

In addition, it is convenient to partition the vector of storm characteristics $\underline{X}$ into two parts, as follows: (1) a vector of principal quantities $\underline{X}_1 = (\Delta P, Rp, V_{f,}\text{landfall location}, \theta)$, whose probability distributions are represented explicitly and whose effects are also represented explicitly in the model calculations, and (2) a vector of secondary quantities $\underline{X}_2 = (B, \text{tide...})$,

whose distributions (relative to their base-case values) and effects are jointly represented in an approximate manner by random terms $(\varepsilon_B, \varepsilon_{\text{tide}}, ...)$ (which have units of elevation). These secondary quantities are set to their base-case values in the model runs. Although these epsilons are conceptually different from the modeling error ε_m introduced in the previous paragraph, they are combined operationally into one random quantity as $\varepsilon = \varepsilon_m + \varepsilon_B + \varepsilon_{tide} + ...$ The characterization of these epsilons is discussed below.

Incorporating these considerations, Equation 5 becomes:

$$P[\eta_{\max(1\,yr)} > \eta] = \lambda \int ... \int_{\underline{X}_1} f_{\underline{X}_1}(\underline{x}_1) P[\eta_m(\underline{x}_1) + \varepsilon > \eta]\, d\underline{x} \qquad (7)$$

where $\underline{X}_1 = (\Delta P, Rp, V_f, \text{landfall location}, \theta)$ (the subscript 1 [as in X_1] will be dropped in the remainder of this report for the sake of simplicity). Both the coastal flood hazard studies described in Resio et al. (2007) and this Mississippi Coastal Analysis Project adopted the JPM formulation that includes the epsilon term.

The components of the epsilon term used in the Mississippi Coastal Analysis Project were as follows:

ε_1 = This is the contribution from the astronomical tide. The range of astronomical tide is relatively small in the Mississippi coastal area and there is a strong fortnightly modulation. A storm can make landfall at any phase of the tide. This epsilon term is used to represent the effect of random phasing of the maximum storm surge and the astronomical tide.

ε_2 = This epsilon term represents the changes in surge heights due to unaccounted variability in the value of Holland B. This parameter is used in the PBL numerical model of hurricane winds and pressures to account for the radial gradients. The use of ε_2 completes the representation of effects described by the Holland B parameter because it combines with the systematic along-track variations discussed in Section 3.2.4.6.

ε_3 = This epsilon term represents the departures between modeled and measured surge levels and is used to express variations in the surge heights due to lack of accuracy in the modeling results.

ε_4 = This epsilon term represents the internal variability of the structure of hurricanes and accounts for the variation in the resulting surge levels due to unrepresented variations in the characteristics of individual storms and their tracks.

Assuming that the various epsilon terms are probabilistically independent and that their effects combine additively, the standard deviation of epsilon is computed as the square root of the sum of the squares of the standard deviations of the individual epsilons. In addition, the combined epsilon is assumed to have a normal distribution shape (the assumptions of independence and additive combination suggest that the normal assumption is a good approximation). The evaluation of this term is explained in Section 5.2.

3.3.2 JPM-OS Development Strategy

A full JPM analysis could require modeling of a synthetic storm population of over 1,000 storms. Therefore the goal of the optimum sampling approach was to derive the same statistical results from JPM using the fewest number of storms and therefore reduce storm surge modeling computer run time. An analysis was performed to reduce the number of synthetic storms to be modeled while maintaining the essential accuracy of the JPM. This analysis included sensitivity tests that explored the variations of computed surge heights in response to changes in the values of the storm parameters. An objective method was applied to develop several JPM-OS candidates for synthetic storm populations. Each of these candidate synthetic storm populations was tested against a screening level implementation of the full JPM analysis of Mississippi coastal flooding to establish which minimum combination of storms best matched the results of the full JPM analysis. The NOAA SLOSH model setup for the Mississippi coast was used as a diagnostic tool for both the sensitivity and the screening analyses.

3.3.3 Overview of the SLOSH Model

The NOAA SLOSH model was chosen to conduct the sensitivity tests and comparative tests of the JPM-OS cases because it had previously been configured for the Mississippi coastline and it offered a rapid processing speed (typically less than 2 minutes on a standard desktop PC for a single storm simulation). The model, set up for the Mississippi Gulf Coast Basin, was provided by NOAA.

The SLOSH model is used by the NHC to estimate storm surge heights and winds resulting from historical, hypothetical, or predicted hurricanes by accounting for pressure, radius, forward speed, track, and winds (Jelesnianski et al. 1992). It is a two-dimensional, depth-integrated finite difference code. SLOSH utilizes a curvilinear grid system to allow high resolution in the area of forecast interest, computes surges over bays and estuaries, retains some non-linear terms in the equations of motion, and allows for the representation of sub-grid scale features such as channels, barriers, and flow of surge up rivers. The telescoping grid provides a large geographical area with detailed land topography. The smallest grid represents an area of about 0.1 square mile (sq mi). This grid size permits inclusion of topographic details such as highway and railroad embankments, causeways, and levees. The largest grid cell is approximately 11.6 sq mi. The model accounts for astronomical tides by specifying an initial tide level, but does not include rainfall amounts, riverflow, or wind-driven waves.

3.3.4 Sensitivity Analysis

The sensitivity analysis focused on five meteorological storm parameters: the central pressure deficit (ΔP), the radius to maximum winds (R_{max}), the forward speed of the storm (V_f), the azimuth angle of the storm landfall crossing (θ), and the landfall position (S_i). Note that the SLOSH model uses R_{max} instead of R_p in its windfield model. To accommodate this, all R_p values used elsewhere were converted to corresponding values of R_{max} using the equation:

$$R_{\max} = 0.5387 + 0.9524R_p - 0.00575R_p^{\ 2} + 1.17 \times 10^{-5} R_p^{\ 3} \qquad (8)$$

where both radii are in nautical miles. This equation was fit to values provided by Cardone (personal communication to G. Toro, 1999). For small values of R_p (e.g., $R_p < 10$ nautical

miles), the two radii are nearly identical. The difference between R_p and R_{max} becomes greater as the size of the storm increases, with R_p being greater than R_{max}. For example, a typical storm with an R_p of 20 nmi has an equivalent R_{max} of 17.4 nmi.

The sensitivity analysis was designed using a baseline storm, with a systematic variation of each storm parameter. The baseline storm was included in each parameter variation. Figures 3-14a – 3-14d show the Mississippi region, with the baseline storm track and the coastal and inland points for which the simulated surge heights were recorded. The points were selected to provide coverage of the coastline, inland bays and rivers, and upland areas. The baseline storm track started approximately 362 mi due south of the Central Mississippi coast, with a due north track line. The parameters for the baseline storm are shown in Table 3-1.

Table 3-1. Baseline Storm Parameters

Parameter	Value	Units
ΔP	70	mb
R_{max}	30	mi
V_f	12	mph
θ	0	degrees
S_i	See Figure 3-15	latitude and longitude

For each parameter, the values were varied over a range that spanned the typical variations found in historical storms. The values used in the sensitivity analysis are listed in Table 3-2 for each parameter.

Table 3-2. Values for Each Parameter

Parameter	# of cases	Values
ΔP	9	30, 40, 50, 60, 70, 80, 90, 100, 110
R_{max}	10	6, 12, 18, 24, 30, 36, 42, 48, 54, 60
V_f	7	6, 8, 10, 12, 14, 16, 18
θ	7	-45, -30, -15, 0, 15, 30, 45 (see Figure 3-16)
S_i	7	see Figure 3-15

The complete set of parameter values comprises 40 simulations, of which 5 are identical to the baseline storm. Each storm was simulated with the SLOSH model and the maximum surge height recorded at each of the 147 output points distributed across the whole Mississippi coastal area. The output data files were then re-formatted and consolidated into a single database for analysis. When no surge was recorded at a station for a particular location, the value was recorded as null in the database.

The sensitivity analysis was designed to determine the sensitivity of the surge response to the meteorological storm parameters, for various geographical settings, and whether topographic

effects would amplify or distort the patterns of surge level responses. For this purpose, the output points were divided into three groups: coastal, riverine, and inland. Coastal output points were located along the open shoreline. Riverine output points were located in lowlands adjacent to streams and within stream valleys. Inland output points were located in upland places between valleys and away from the coast. For each group of points, the dependence of the surge height was plotted versus the parameter values. When the simulation did not produce a surge at a particular location (i.e., null value), the curve for that location had missing values. These conditions appear as an incomplete curve in most instances.

Plot lines have been color-coded in a rainbow-chromatic color scale, with colors ranging from the red palette in the west to the blue palette in the east (refer to Figures 3-17 through 3-22). The color ramp scale uses the following progression: violet-red-orange-yellow-white/gray-green-blue-indigo-gray/blue-black with intermediate colors used as necessary for the inland stations. Line types were also varied as needed, including solid, dashed, dotted, and dash-dotted lines.

By normalizing both the range of the parameter and its associated surge response by their respective maximum values, the relative importance of each parameter was represented. The dominant factors are the storm strength and proximity represented by the central pressure deficit and landfall proximity. Variations in storm radii have only about half the effect of variations in the pressure deficit. Variation in both forward speed and track azimuth at landfall have even smaller effects. These related responses, as well as the shape of the response curves, were later used to decide the best ways to make discrete representations of the statistical storm parameter functions.

The response of the surge heights to systematic changes in the parameter values is relatively smooth at the open coast but progressively less so inland. This response shows the importance of local topography, and thus, the importance of modeling overland flooding rather than extrapolating values inland.

3.3.5 Central Pressure Deficit

Figures 3-17, 3-18, and 3-19 show the results for the variation of central pressure for the coastal, riverine, and inland points. In each plot, each individual curve represents the dependence of the surge height at a single point. The results for the coastal stations reveal expected behavior of a relatively linear increase in surge height with an increase in central pressure deficit. There are deviations from a strictly linear dependence at a few locations which reflect the way the storm surge propagates around hills. A similar pattern is evident for the riverine stations, though there are more curves with deviations from a linear dependence than for the coastal stations. The results for the inland stations show the most variability in terms of deviation from a strictly linear dependence; distinct groupings of results appear to be related to geographic and topographic influences. Comparison of these results with the others given in this section indicates that the central pressure deficit parameter dominates the surge height response.

3.3.6 Forward Speed

Figures 3-20, 3-21, and 3-22 show the dependence of the surge height on forward speed for the coastal, riverine, and inland points. The curves can be divided into three general categories: increasing surge height with an increase in forward speed, decreasing surge height with an increase in forward speed, and initial increase followed by a decrease in surge height with an

increase in forward speed. As seen previously in central pressure deficit plots, the dependence of the surge height on increasing forward speed results in more erratic behavior for the inland stations than for the coastal and riverine stations.

In order to investigate the geographic influences on the results for the forward speed analysis, the curves were divided into three categories described above and plotted spatially. The locations with their designations are shown in Figure 3-23. The plotted results suggest that stations to the far west of the storm track have a decreasing surge height with an increase in storm forward speed, and conversely, stations to the far east of the storm track have an increasing surge height with an increase in storm forward speed. Stations with increasing followed by decreasing surge heights with increasing forward speed tend to be located to the west of the storm track but closer to the storm track than those stations that experience only a decrease in surge with increasing forward speed.

Comparison of these results with others given in this section shows that of the five parameters analyzed, the forward speed parameter has the least influence on the surge heights.

3.3.7 Storm Track Azimuth

The results for the dependence of the surge height on storm track azimuth angle are shown in Figures 3-24, 3-25, and 3-26. The results reveal different behavior between many of the points. However, except for a few of the locations, the results show one of two general patterns: the surge height either monotonically increases or monotonically decreases as the storm approach angle rotates from NW to NE. A spatial plot of the locations is shown in Figure 3-27, which indicates which points incurred an increasing or decreasing surge height with the storm track approach angle. The plotted results suggest that points far to the east of the landfall point experience a decrease in surge height as the storm angle rotates clockwise. For points moderately to the east and to the west of landfall, there appears to be an increase in surge height as the storm track is rotated clockwise (from −45 to 45 degrees). The variations in surge height caused by differences in the track azimuth have less control on the surge heights than any of the other parameters except forward speed.

3.3.8 Radius to Maximum Winds (R_{max})

Figures 3-28, 3-29, and 3-30 show the results of varying the R_{max}. Note that for stations west of the baseline track, the increase in R_{max} increases the distance between the station and the location where the maximum winds make landfall (MWL). For points east of the baseline track, the increasing R_{max} first decreases the distance between the station and the MWL, but then it increases the distance. For points even farther east, the distance between the station and the MWL always decreases as the R_{max} increases. To account for the locations of stations relative to the MWL, the plots are reconstructed with the stations' distance from the MWL as the independent (x-axis) variable. Figure 3-31 shows the convention for defining the distance for MWL, and the resulting curves are shown in Figures 3-32, 3-33, and 3-34 for coastal, riverine, and inland stations. The distance definition convention causes the curves in the Figures 3-32 through 3-34 to be plotted with the x-axis in reverse from previous plots.

These tests showed that R_{max} is second only to the ΔP parameter in controlling surge heights.

3.3.9 Landfall Location

The results for the seven storm tracks considered are shown in Figures 3-35, 3-36, and 3-37. In these plots the landfall location is referenced to the Track ID location, which increases eastward (see Figure 3-15). The storm track data were plotted in terms of the distance between the station and the MWL. Because each storm included in this set varied landfall location while keeping the same R_{max}, the data were plotted in terms of the distance from the MWL. In this study, this is essentially 30 mi east of the actual landfall location. The results for these curves, using the distance from the MWL to R_{max} location as the independent variable, are shown in Figures 3-38, 3-39, and 3-40.

3.3.10 Spatial Distribution of Landfall Locations

In addition to the analysis of the meteorological parameters, an analysis was conducted to determine the sensitivity of the surge results to the spatial distribution of landfall locations. Of particular interest were: (1) the extent westward from the Mississippi/Louisiana border and the extent eastward of the Mississippi/Alabama border that storms needed to be distributed, and (2) the maximum spacing between storm tracks that could be used. The details of the analyses used to address these two distribution parameters are available in Scheffner (2006). The study consisted of developing a database of storm surges generated using the SLOSH model. The storm locations were chosen to span a large distance to the west and east of the two Mississippi borders with relatively dense spacing. Each storm had the same meteorological parameters and only differed by their landfall location. The storm parameters were: ΔP = 80 mb, θ = due north, V_f = 9.98 mph, and R_{max} = 25 mi. The storms were spaced at one-half the radius to maximum winds and extended 250 mi to the west of the Mississippi/Louisiana border, and 150 mi east of the Mississippi/Alabama border for a total of 33 storm tracks. Each simulation's surge heights were recorded at 40 output stations, which included 20 stations just offshore and 20 stations just inland of the coastline with an average of 4.5 mi between the points.

The simulated surge heights were then used in an Empirical Statistical Technique (EST) approach (Borgman et al. 1992, Scheffner and Borgman 1996, Scheffner et al. 1996) to estimate the 10-, 50-, 100-, and 500-year surge heights at the output stations. A sequence of subsets was then created by methodically reducing the total number of storms by decreasing the lateral extent of the storm distribution and by increasing the spacing between storm tracks. Each subset was then used in an EST analysis to produce 10-, 50-, 100-, and 500-year flood surge heights. The surge heights for each subset were compared to those obtained using the entire database to ascertain the minimum lateral extent and maximum spacing that could be used without compromising the validity of the estimated surge heights. The results of this analysis indicated that a spacing of one radius to maximum winds, a lateral extent of 3 to 4 radii to maximum winds to the west of the Mississippi/Louisiana border, and 1 radius to maximum wind to the east of the Mississippi/Alabama border were sufficient to provide adequate storm track representations. A project memo by Dr. N. Scheffner more fully describes this work (Scheffner 2007).

3.4 THE JPM-OS (MISSISSIPPI) METHOD

The above-described sensitivity analysis established the relative importance of the meteorological parameters with respect to the surge heights to be ΔP, S_i, R_p (or R_{max}), V_f, and θ.

This information was used in specifying the correlation distances and selecting the discretization schemes for the development of the JPM and JPM-OS schemes.

Several JPM-OS schemes were developed and then their results were compared to the results from a full JPM base case ("Gold Standard") analysis, which was run with nearly 3,000 storm simulations. The results from these comparisons were used to select the final JPM-OS scheme from the various test cases. Details on the methodology used to develop these schemes and results from the comparisons are provided below.

The variant of the JPM-OS used in this study approach approximates the integral in Equation 7 as a weighted summation as follows:

$$P[\eta_{\max(1\,yr)} > \eta] = \lambda \int \ldots \int_{\underline{x}} f_{\underline{X}}(\underline{x}) P[\eta_m(\underline{x}) + \varepsilon > \eta]\, d\underline{x} \approx \sum_{i=1}^{n} \lambda_i P[\eta_m(\underline{x}_i) + \varepsilon > \eta] \qquad (9)$$

where each $\underline{x}_i = (\Delta P_i, Rp_i, V_{f,i}, \mathrm{S_i}, \theta_i)$ may be interpreted as a synthetic storm, $\lambda_i = \lambda p_i$ may be interpreted as the annual occurrence rate for that storm, and $\eta_m(\underline{x}_i)$ may be interpreted as the estimate from the hydrodynamic model of the surge elevation generated by that storm. For this approach to be practical, the storm characteristics $\underline{x}_i$ and their rates λ_i must be specified so that the integral can be approximated with sufficient accuracy (for all η values of interest), using a reasonably low value of *n* (i.e., a reasonably low number of synthetic storms and corresponding numerical model runs).

The approach used to define the synthetic storm characteristics and their rates may be summarized by the following three steps:[4]

1. Discretize the distribution of ΔP into three broad slices, roughly corresponding to hurricane Categories 3, 4, and 5.
2. Within each ΔP slice, discretize the joint probability distribution of ΔP(*within slice*) , R_p, V_f, and θ using the optimal sampling procedure known as Bayesian Quadrature (Diaconis 1988; O'Hagan 1999; Minka 2000). This procedure represents the response portion of the integrand (i.e., the term $P[\eta_m(\underline{x}) + \varepsilon > \eta]$) as a random function of $\underline{x}$ with certain correlation properties, and calculates the values of $\Delta P_i, R_{p_i}, V_{f,i}, \theta_i$, and the associated probability, so that the variance of the integration error is minimized. This minimization consists of two nested operations as follows: inner optimization: find the optimal values of the probabilities for given values of the x_i's (performed analytically); and outer optimization: determine the optimal values of the x_i's (performed numerically). The correlation properties of the random function (which take the form of correlation distances) depend on how sensitive the response is to each variable (shorter correlation distances for the more important variables). These correlation distances were set based on judgment and on the results of the sensitivity tests described in Section 3.3.
3. Discretize the distribution of landfall location by offsetting each of the synthetic storms defined in the previous two steps. The track spacing is equal to R_p and is measured

[4] This description applies to the greater storms. A slightly modified approach was followed for the lesser storms.

perpendicular to the storm track. The probability p_i assigned to each artificial storm is easily computed as the product of the probabilities resulting from the three steps. This probability is then multiplied by the rate λ to obtain the artificial storm's rate λ_i.

Further details on the JPM-OS methodology are provided in the supporting project report titled *Joint Probability Analysis of Hurricane Flood Hazards for Mississippi* (Risk Engineering).

Before going further, it is useful to make some comments regarding the JPM-OS approach summarized above.

- Although the synthetic storms and their rates are generated as a numerical device to approximate the integral in Equation 7, it is useful to view them as a set of representative storms, which serve as a proxy for all possible future storms, with their associated occurrence rates. Similarly, these synthetic storms and their rates may be viewed as a compact discrete representation of the multi-dimensional probability distribution of possible future storms and their characteristics.
- The discretization of the distribution of ΔP prior to the Bayesian Quadrature may seem superfluous, but experience gained by Risk Engineering during this and earlier studies indicates that this step improves the efficiency of the overall scheme. This observation is likely related to some of the probability distribution transformations used in the JPM-OS methodology.

3.4.1 Development of Candidate JPM-OS Schemes

Several JPM-OS candidate schemes were developed. Each of these was used to complete an analysis of the 1-percent- and 0.2-percent-annual-exceedence rate recurrence levels at a series of 147 representative locations across coastal Mississippi. For each candidate scheme, the number of points within each ΔP slice and the correlation distances were specified. Prior to the SLOSH comparisons, internal checks were made to verify that low-order marginal distribution moments (i.e., the means, standard deviations, skewness, and kurtosis, for the distributions of the five storm parameters) were preserved by the JPM-OS scheme.

3.5 JPM-OS EVALUATION

To test the validity of the JPM-OS storm selection, the 1-percent-annual-exceedence rate surge heights obtained using the smaller storm set associated with the JPM-OS schemes were compared with the 100-year surge heights obtained using a greater storm set, representative of a traditional JPM approach, as described in this section. The analysis provided a quantitative basis for testing alternative JPM-OS storm selection strategies and minimizing the total number of storms, while simultaneously demonstrating the reliability of the JPM-OS approach.

The analysis was used to determine both the total number of storms that are required in the JPM-OS selection and the choices for the correlation distances to use in the Bayesian Quadrature. These choices, in turn, determine each storm's parameter values (i.e., central pressure, radius to maximum winds, track, etc.) and rate λ_i.

3.5.1 JPM-Reference ("Gold Standard")

A large set of synthetic storms was generated and implemented in a mock surge analysis in order to create a standard for comparing alternate JPM-OS schemes. This large set was intended to represent the traditional JPM approach.

The set consisted of 2,967 storms with three values for forward speed, four values for the track angle relative to the coastline, six different central pressure values, and five different values for R_{max}, totaling 360 unique storm parameter sets and their associated annual rates, drawn from the probability distributions and rates developed earlier. The selection of the five R_{max} values was different for each ΔP value in order to represent the correlation between these parameters (see Section 3.2.4.4).

The sensitivity tests described in Section 3.2 provided guidance for the arrangement of tracks for the storms. The counter-clockwise rotation of the hurricane winds made the distribution of tracks different beyond each of the Mississippi borders. Only one track was needed east of Mississippi, but three were needed beyond the western border. The storm tracks for the 360 parameter combinations were obtained by first using a randomly selected starting point west of the Mississippi/Louisiana border. Additional tracks were spaced at intervals equal to one radius to maximum winds to the east until at least one storm track was assigned east of the Mississippi/Alabama border. The starting location west of the Mississippi/Louisiana border was chosen randomly to equal some distance approximately three and four radii to maximum winds west of the border. Thus, there were always a minimum of three storm tracks located west of the Mississippi/Louisiana border. The actual number of tracks associated with each of the 360 storm parameter sets depended on the actual distance of the radius to maximum winds of each data set. The total number of tracks used for each unique parameter set ranged from 5 to 21. When summed over all 360 storm sets, the total number of storms equaled 2,967.

The parameter values and annual rates for the 360 storms were defined as follows. The values and probabilities for each parameter were determined using the one-dimensional quadrature approach described by Miller and Rice (1983). For R_p, values were drawn from the conditional distribution of radius given as ΔP. For input to SLOSH these were converted to corresponding values of R_{max}. However, for consistency with other parts of this report, these are tabulated as R_p values. For each resulting storm (i.e., for each combination of parameters), the storm event rate was obtained by multiplying the probability associated with each of the storm parameter values (i.e., $p(\Delta P_i) \times p(R_{p,i} \mid \Delta P_i) \times p(V_{f,i}) \times ...$) and then multiplying that result by the storm spacing (which is equal to the storm's radius to maximum wind) times the annual rate of a Category 3 or higher storm occurring in the Gulf Coast area (3.02x1-4 storms/km/yr).

The parameters used in the large set of synthetic storms—designated JPM-Reference—and the normalized probabilities are described in Tables 3-3a, b, c and d.

Table 3-3a. Storm Set Parameters and Probabilities for JPM-Reference: Discrete Distribution of Central Pressure Deficit

Central Pressure Deficit (mb)	Probability
45.6	0.04958
48.6	0.16607
56.1	0.28435
69.1	0.28435
87.6	0.16607
111.8	0.04957

Table 3-3b. Storm Set Parameters and Probabilities for JPM-Reference: Discrete Conditional Distribution of R_p Given Central Pressure Deficit

Central Pressure Deficit (mb)	Values of Rp (nmi)				
45.6	6.94	13.43	24.38	44.28	85.71
48.6	6.63	12.84	23.32	42.34	81.96
56.1	5.99	11.59	21.05	38.23	74.00
69.1	5.16	10.00	18.15	32.96	63.80
87.6	4.36	8.44	15.33	27.84	53.88
111.8	3.67	7.10	12.89	23.41	45.31
	Probability				
	0.011	0.222	0.534	0.222	0.011

Table 3-3c. Storm Set Parameters and Probabilities for JPM-Reference: Discrete Distribution of Forward Speed

Forward Speed (meter/second)	2.99	6.04	12.23
Probability	0.16667	0.66667	0.16667

Table 3-3d. Storm Set Parameters and Probabilities for JPM-Reference: Discrete Distribution of Azimuths

Azimuths (Theta) *	-73.0	-32.7	7.3	49.4
Probability	0.13299	0.36701	0.36701	0.13299

*(direction to; degrees clockwise from North)

Each storm was simulated with the SLOSH model and the maximum surge was recorded at the same 147 points used in the sensitivity analysis. For each output point the 100-year surge height was calculated from the 2,967 surge values. This was accomplished by sorting the storm surge heights at each point in descending order. The event probabilities were then summed, starting with the largest storm surge height. This procedure produced a curve approximating the cumulative probability of surge height. The 100-year surge height was obtained by interpolating the surge height on the curve corresponding to the 0.01 value for the cumulative probability. This process was applied to all 147 points to develop the 100-year surge heights associated with each JPM storm set.

3.5.2 JPM-OS Schemes and Comparisons

Five JPM-OS alternative schemes and the corresponding storm sets were developed and tested. The storm parameters and normalized event probabilities for two example storm sets are listed in Tables 3-4 and 3-5. The actual event probability was obtained by multiplying the probabilities by the storm spacing (which is equal to the storm's radius to maximum winds) and the rate of Hurricane Category 3 and higher storms in the Gulf Coast area. The total unique sets of storm parameters (except landfall position) for JPM-OS-3, JPM-OS-4, JPM-OS-5, JPM-OS-6, and JPM-OS-7 were 37, 37, 23, 19, and 17 respectively. When these storms were assigned to tracks along the Mississippi, Louisiana, and Alabama coastlines using the same procedure used in developing the storm sets for the JPM-Reference storm set, the total number of storms was 303, 303, 193, 158, and 147, respectively.

The surge from each storm within each JPM-OS candidate scheme set was calculated with the SLOSH model and the maximum surge was recorded at the same 147 points used in the sensitivity analysis (Section 3.2). For each output point, the 100-year surge height was calculated using the same approach used in developing the JPM-Reference surge elevations (Section 3.5.1). Figures 3-41 and 3-42 show the comparison of the JPM-OS-6 and JPM-OS-7 to the JPM-Reference results for each point. There are some points where the difference is large, due to the use of the surge elevation rather than the water depth. These points typically occur at the inland edge of the storm surges, where the results from one storm set just manages to flood the point, while the other does not, so there is no valid elevation for comparison. In other cases, anomalous comparisons resulted for special and rare combinations of large grid elements and subgrid drainage representations. These distorted results were eliminated from the comparisons. The outlier points were removed from the data sets before the summary analysis was conducted.

The differences between each example JPM-OS set of results and the JPM-Reference are summarized by the average error, the average absolute value of the error, and the root mean square (RMS) error in Tables 3-6 and 3-7 for the 1-percent and 0.2-percent-annual-exceedence rate- surge heights (100- and 500-year floods). The latter surge height was obtained using the same procedure as for the 1-percent-annual-exceedence rate -surge height, but interpolating the height corresponding to the 0.002 value of the cumulative probability.

Table 3-4. Storm Parameters Set for JPM-OS-6 (SLOSH)

Central Pressure Deficit (mb)	Heading (deg)	Radius To Maximum Winds (miles)	Forward Speed (mph)	Number of Tracks	Normalized Probability
66.16	-38.91	18.9	13.6	7	0.142556
55.29	-13.49	35.2	13.6	6	0.128424
46.96	-38.92	23.2	13.6	7	0.142549
55.29	-13.49	12.0	13.6	10	0.128424
55.29	56.66	21.1	13.6	7	0.115047
92.93	-12.81	15.3	13.4	9	0.030331
78.52	-12.82	28.5	13.5	6	0.047395
78.53	47.33	17.0	9.8	8	0.037305
78.53	-12.82	9.9	13.5	11	0.047395
78.53	-12.86	17.0	32.7	8	0.030949
70.02	-12.82	18.3	13.4	8	0.030331
78.53	-71.04	17.0	9.8	8	0.037297
128.5	-12.81	12.5	13.4	10	0.009529
103.5	-12.82	24.4	13.5	7	0.014890
103.5	47.33	14.4	9.8	9	0.011720
103.5	-12.82	8.3	13.5	12	0.014890
103.5	-12.86	14.4	32.7	9	0.009724
94.46	-12.82	15.2	13.4	8	0.009529
103.5	-71.04	14.4	9.8	8	0.011718

Table 3-5. Storm Parameters Set for JPM-OS-7 (SLOSH)

Central Pressure Deficit (mb)	Heading (deg)	Radius To Maximum Winds (miles)	Forward Speed (mph)	Number of Tracks	Normalized Probability
70.1	-67.61	22.8	13.6	7	0.094940
66.64	10.93	34.6	13.6	6	0.073940
60.25	17.53	20.0	7.3	7	0.112354
54.95	10.93	10.9	13.6	10	0.073942
60.25	17.53	20.0	25.2	7	0.112354
46.15	10.93	20.1	13.6	7	0.073942
52.77	-67.61	17.3	13.6	8	0.094940
88.29	10.93	18.6	13.6	8	0.073941
78.78	-22.83	11.3	13.6	10	0.103835
48.81	-22.83	32.8	13.6	6	0.103835
128.5	-12.81	12.5	13.4	10	0.009529
103.5	-12.82	24.4	13.5	7	0.014890
103.5	47.33	14.4	9.8	9	0.011720
103.5	-12.82	8.3	13.5	13	0.014890
103.5	-12.86	14.4	32.7	9	0.009724
94.46	-12.82	15.2	13.4	8	0.009529
103.5	-71.04	14.4	9.8	9	0.011718

Table 3-6. Error Between JPM-OS and JPM-Reference for a 100-Year Storm

100-year surge	OS-6	OS-7
RMS Error (ft)	0.47	0.54
Average Error (ft)	-0.02	-0.02
Average (/Error/) (ft)	0.34	0.45
Minimum Error (ft)	-1.40	-1.07
Maximum Error (ft)	1.20	1.44
No. of Pts. > 1.0 ft	6	3

Table 3-7. Error Between JPM-OS and JPM-Reference for a 500-Year Storm

500-year surge	OS-6	OS-7
RMS Error (ft)	0.59	1.04
Average Error (ft)	0.14	-0.43
Average (/Error/) (ft)	0.47	0.80
Minimum Error (ft)	-1.20	-3.62
Maximum Error (ft)	1.62	1.76
No. of Pts. > 1.0 ft	11	37

Based on the comparisons given in Tables 3-6 and 3-7, the JPM-OS-6 storm set was selected. This provided the definition of the JPM-OS analysis of the greater storms.

The comparisons between the JPM-Reference storm sets and the five JPM-OS candidate schemes provided criteria for the selection of a scheme with sufficient accuracy and demonstrated the validity of the resulting JPM-OS storm representations. This validation is important because this JPM-OS scheme is relatively new and because the selection of the correlation distances involved some judgment (see Section 3.4).

The SLOSH model comparisons were not done for the lesser storms, but the statistical-moment comparisons and comparisons using a simple parametric surge model were done. The range of pressure deficits for the lesser storms is much smaller than for the greater storms. Because of this, only one slice was used.

3.6 APPLICATION OF THE QUADRATURE JPM-OS APPROACH

This section describes the application of the Quadrature JPM-OS approach to hurricanes affecting the Mississippi coast. Results for the greater storms (ΔP > 48mb) and lesser storms (ΔP =31 to 48 mb) are provided in separate sections.

3.6.1 JPM-OS Scheme for Greater Storms

The JPM-OS-6 case, described in Section 3.5.2, was used for the full analysis using the numerical modeling approach discussed later in this report. However, a small adjustment was made in ΔP between the SLOSH mock runs (described in Section 3.5) and the full model

framework production runs. Also, the layout of the storm tracks in the ADCIRC modeling differed from the SLOSH modeling. The ADCIRC model required slightly fewer tracks (six less). The SLOSH runs are noted as JPM-OS-6 (SLOSH) and the full production run values are noted as JPM-OS-6 (ADCIRC).

Figure 3-43 illustrates the resulting synthetic storms (for one landfall location). Each chart on the main diagonal shows the probability distribution of the corresponding quantity (in the form of a histogram), as represented in the JPM-OS-6 discretization. Each off-diagonal scatter diagram shows how each pair of quantities (i.e., ΔP and R_p) are jointly distributed in the JPM-OS-6 (ADCIRC) scheme, with the areas of the circles being proportional to the associated annual rate. Table 3-10 lists the corresponding parameter values, probabilities, and rates.

Table 3-8 shows the three slices of the ΔP distribution, their probabilities, and the number of modes in the Bayesian-Quadrature discretization for each slice in the JPM-OS-6 (ADCIRC) case used in the production runs. Table 3-9 shows the corresponding correlation distances, and Table 3-10 shows the storm parameter distribution for this case.

Table 3-8. Discretization of ΔP into Slices in the JPM-OS-6 (ADCIRC) Scheme for Greater Storms

Slice	Category 3	Category 4	Category 5
ΔP range (mb)	48-73	73-98	98-135
Probability	0.657	0.261	0.082
# of nodes in Bayesian Quadrature	5	7	7

Table 3-9. Correlation Distances in the JPM-OS-6 (ADCIRC) Scheme for Greater Storms

Correlation Distance (std normal units)			
ΔP (within slice)	R_P	V_f	Θ
4	2.5	6	5

Table 3-10. Parameters of the JPM-OS-6 (ADCIRC) Scheme for Greater Storms

StormID (OWI notation)	ΔP (mb; coast)	R_p (nmi; offshore)	V_f (m/s)	θ (deg)	Probability	Annual Rate (for each track)
JOS6001	66.69	18.61	6.047	-38.91	1.33E-01	1.32E-03
JOS6002	57.17	39.82	6.047	-13.49	1.20E-01	2.55E-03
JOS6003	49.72	22.93	6.047	-38.92	1.33E-01	1.63E-03
JOS6004	57.17	10.83	6.047	-13.49	1.20E-01	6.94E-04
JOS6005	57.17	20.77	6.047	56.66	1.08E-01	1.19E-03
JOS6006	92.95	14.7	5.943	-12.81	3.42E-02	2.68E-04
JOS6007	78.59	30.8	6.014	-12.82	5.34E-02	8.77E-04
JOS6008	78.59	16.56	4.349	47.33	4.20E-02	3.71E-04
JOS6009	78.59	8.904	6.014	-12.82	5.34E-02	2.54E-04

StormID (OWI notation)	ΔP (mb; coast)	R_p (nmi; offshore)	V_f (m/s)	θ (deg)	Probability	Annual Rate (for each track)
JOS6010	78.59	16.56	14.54	-12.86	3.49E-02	3.08E-04
JOS6011	70.02	17.98	5.943	-12.82	3.42E-02	3.28E-04
JOS6012	78.59	16.56	4.346	-71.04	4.20E-02	3.71E-04
JOS6013	128.7	11.66	5.943	-12.81	1.06E-02	6.58E-05
JOS6014	103.7	25.3	6.014	-12.82	1.65E-02	2.23E-04
JOS6015	103.7	13.6	4.349	47.33	1.30E-02	9.44E-05
JOS6016	103.7	7.313	6.014	-12.82	1.65E-02	6.44E-05
JOS6017	103.7	13.6	14.54	-12.86	1.08E-02	7.83E-05
JOS6018	94.47	14.53	5.943	-12.82	1.06E-02	8.20E-05
JOS6019	103.7	13.6	4.346	-71.04	1.30E-02	9.43E-05

1. The annual rate for each storm is calculated as the storm probability displayed here, times the annual rate of greater storms (2.88E4 storms/km/yr), times the storm spacing (Rp) in km.
2. The annual rates in Column 7 are the lambda terms in the report text.

3.6.2 JPM-OS Scheme for Lesser Storms

A simpler approach was used for the lesser storms (ΔP =31 to 48 mb). In particular, the distribution of ΔP was not divided into slices because these storms span a narrower range of ΔP and because the associated probability distribution is less skewed. Thirteen nodes were employed. Table 3-11 lists the correlation distances used.

Table 3-11. Correlation Distances in the JPM-OS-6 Scheme for Lesser Storms

Correlation Distance (std normal units)			
ΔP	R_P	V_f	Θ
2.5	3	5	5

The JPM-OS scheme was initially developed using the $R_p \mid \Delta P$ distribution shown in Figure 3-7. The resulting parameter values were then used to generate the synthetic storms and perform the wind, wave, and surge calculations. Later in the project, the $R_p \mid \Delta P$ distribution for the lesser storms was changed to that shown in Figure 3-8. The weights were adjusted to reflect the new distribution without a significant loss of accuracy in the JPM-OS scheme. Table 3-12 lists the corresponding parameter values, probabilities, and rates.

The JPM-OS scheme (with the adjusted weights) was validated using an approach simpler than that used for the greater storms. The validation was completed using a parametric surge model somewhat simpler than the model of Irish et al. (2008) instead of using the SLOSH model. The validation also only considered one location and one storm track, and it used a 36-node JPM-OS scheme as the standard for comparison. Checks on statistical moments were also performed.

Table 3-12. Parameters of the JPM-OS Scheme for Lesser Storms

StormID (OWI notation)	ΔP (mb; coast)	R_p (nmi; offshore)	Vf (m/s)	θ (degrees)	Probability	Annual Rate (for each track)
CAT2001	46.38	41.59	5.42	8.758	4.74E-02	9.37E-04
CAT2002	37.75	53.63	3.00	23.55	2.93E-02	7.47E-04
CAT2003	44.28	21.64	3.40	63.87	7.61E-02	7.83E-04
CAT2004	40.71	12.72	4.93	-9.324	1.76E-01	1.06E-03
CAT2005	31.78	44.24	4.88	-11.27	3.92E-02	8.25E-04
CAT2006	32.11	17.19	6.10	31.22	9.30E-02	7.60E-04
CAT2007	34.67	24.32	6.94	-71.07	8.75E-02	1.01E-03
CAT2008	47.53	16.94	4.38	-31.63	6.26E-02	5.04E-04
CAT2009	42.09	27.82	3.71	-59.19	9.49E-02	1.25E-03
CAT2010	34.67	24.31	2.46	-5.25	8.75E-02	1.01E-03
CAT2011	44.28	21.64	10.50	-13.83	7.62E-02	7.83E-04
CAT2012	37.75	53.63	7.89	-45.75	2.93E-02	7.46E-04
CAT2013	37.04	29.79	6.64	46.64	1.01E-01	1.44E-03

Notes

1. The annual rate for each storm is calculated as the storm probability, times the annual rate of storms (2.567E-4 storms/km/yr), times the storm spacing (R_p) in km.
2. The annual rates in the last column are the lambda terms in the report text.

3.7 GENERATION OF SYNTHETIC STORMS

The numerical wind and wave calculations require as inputs the entire history of the synthetic storm, from the time it enters the Gulf. This history consists of hourly values of the coordinates of the storm center, pressure deficit, the pressure radius, and forward velocity. The sequence of values from the storm parameters associated with each Quadrature JPM-OS node is generated as described below. All the storms considered here make landfall at the Coastal Reference Point. Each set of synthetic storm parameters define a group of synthetic storms. All storms in the group have the same parameter values and annual occurrence rates, but they follow different tracks. These tracks are parallel to each other and are spaced one R_p apart.

The approach used to generate the storm tracks—given $(\Delta P, V_f, \theta)_{coast}$ and $R_{p(offshore)}$ —is a purely deterministic approach and is largely based on the approach developed by USACE in their probabilistic surge studies for Mississippi and Louisiana (Resio et al. 2007).

USACE projects preceding and paralleling the Mississippi Coastal Analysis Project introduced the concept that the major Gulf hurricanes tend to originate outside its boundaries (Resio, 2007, personal communication). The tracks tend to enter the Gulf through the Florida or Yucatan Straits and to follow a relatively consistent set of tracks. The geometry of the tracks is somewhat similar to those of Hurricanes Betsy, Rita, Ivan, Camille, Katrina, and Andrew (designated by USACE as the BRICKA tracks). The synthetic storm tracks used in the Mississippi Coastal Analysis Project followed this concept, although a different algorithm was used to generate the track geometry.

Storms moving along these tracks were subject to systematic changes as they approached the coast. Storms with $R_{p(offshore)} > 10$ nmi vary in their pressure deficit, radius, and Holland B linearly over the last 90 nmi prior to landfall, according to the following rules:

R_p (landfall) = 1.3xR_p (offshore)

Holland B (offshore) = 1.27

Holland B (landfall) = 1.0

Holland B (3 hours after landfall) = 0.9

Decrease in ΔP (mb) = R_p (offshore, nmi) – 6 (maximum increase is 18 mb, minimum is 5 mb)

Storms with $R_{p(offshore)} < 10$ nmi, on the other hand do not undergo any weakening or changes in R_p and Holland B prior to landfall. A discussion of these systematic changes as the storms approach landfall is given in Resio (2007).

After landfall, linear variation continued for 2 hours, with the same slopes applied prior to landfall. Weakening of ΔP continued after this point, following the exponential-decay model of Vickery and Twisdale (1995).

This formulation for the evolution of central pressure and other hurricane parameters prior to landfall is the first published formulation that permits the incorporation of these effects within the context of a JPM analysis. This formulation is based on Resio's (2007) analysis of recent well-documented storms. In its present form, this formulation is purely deterministic, in the sense that all synthetic storms with the same R_p undergo the same changes in ΔP, R_p, and Holland B. The reader is referred to Resio (2007) for further details on this formulation.

Figures 3-44 and 3-45 show the tracks for the greater and lesser synthetic storms, respectively. Tracks that made landfall with a north-northwest azimuth are similar in appearance to the BRICKA tracks. All these storms make landfall at the CRP (as defined in Section 3.2.3). These storms are referred to as the *master of reference tracks*. Each of the master synthetic storms was then offset by R_p, creating multiple offset synthetic tracks that cover the entire Mississippi coast. The latter synthetic storms are the ones actually used in the probability calculations. Figure 3-46 shows the track and the variation in time of the key storm parameters for one master synthetic storm. The top panel of Figure 3-46 shows the track of the synthetic storm (in color; the *master track*), as well as the offset tracks. The offset tracks have a spacing of R_p and a uniformly distributed random offset from the master track.

The three bottom panels of Figure 3-46 show the variation in time of the key storm parameters for the master track. The time of landfall is represented by a short vertical stroke.

The purpose of using a random landfall point for each set of synthetic storm tracks and spacing these by R_p was to distribute the tracks with reasonable uniformity. Figures 3-47 and 3-48 show the distributions for the greater and lesser synthetic storms respectively.

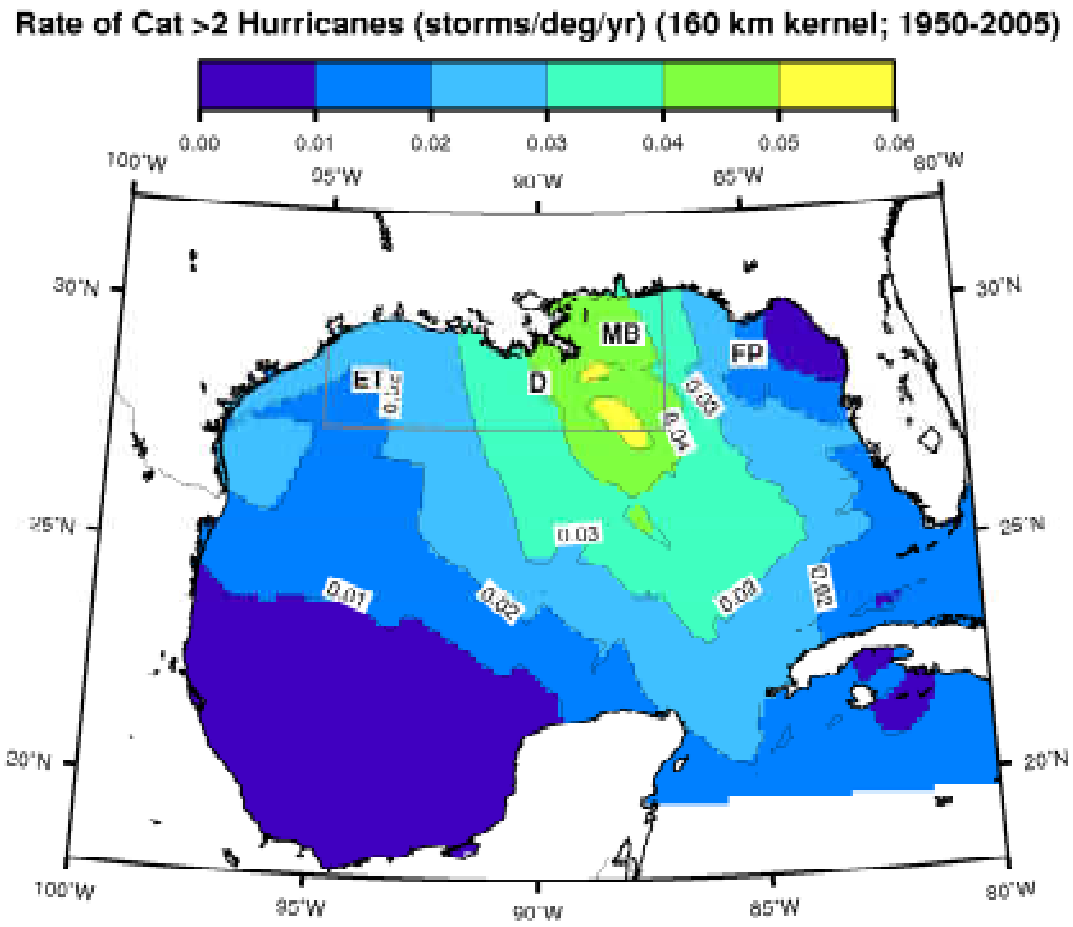

Figure 3-1. Analysis of Hurricane Frequency from an Analysis Using an Optimized Spatial Kernel [Source: *Joint Probability Analysis of Hurricane Flood Hazards for Mississippi*].

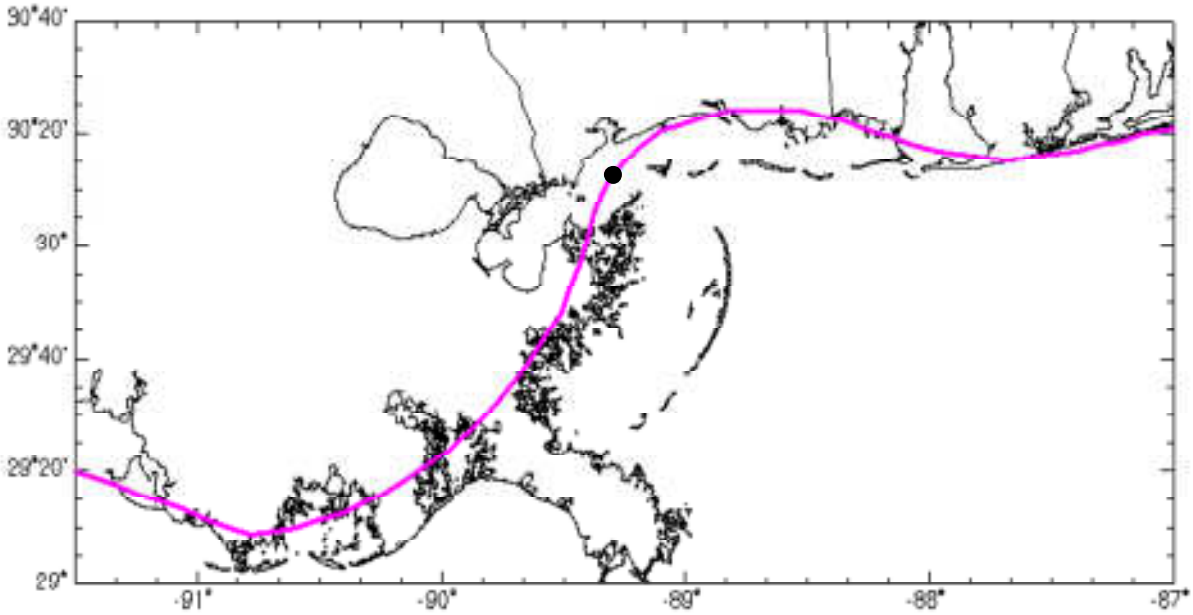

Figure 3-2. Simplified Project Shoreline with Coastal Reference Point Shown by ●.

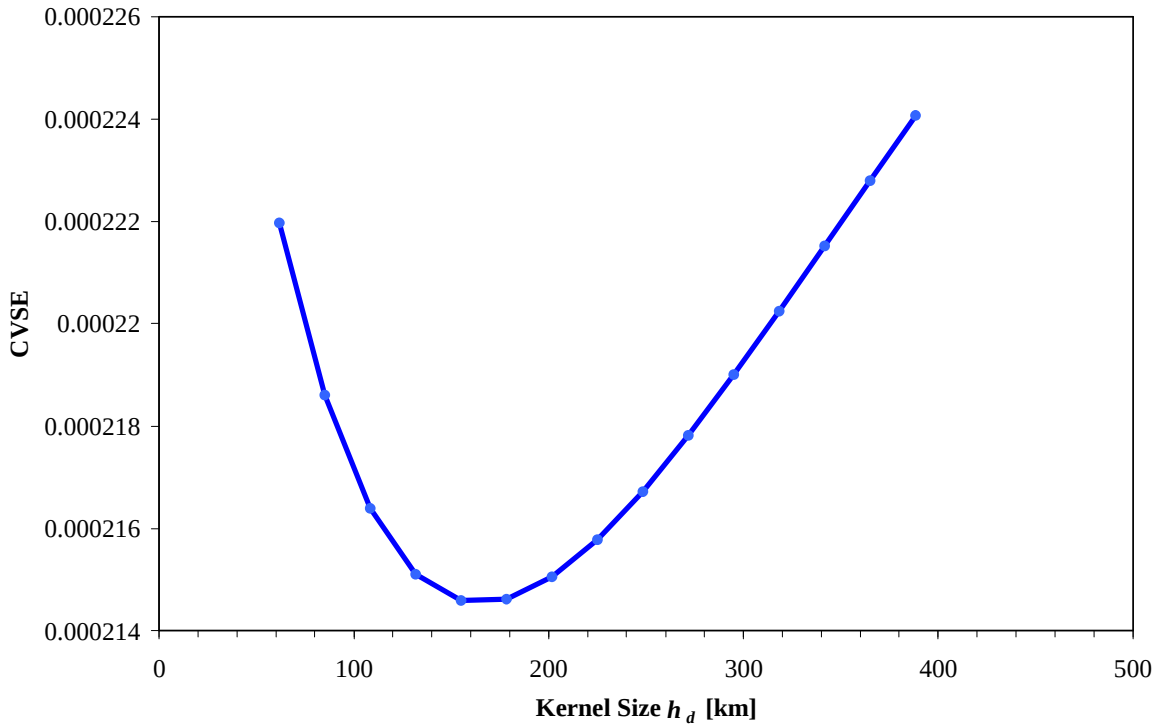

Figure 3-3. CVSE for the Omni-Directional Storm Rate Relative to Hurricanes with Central Pressure Deviations Greater than 45 mb.

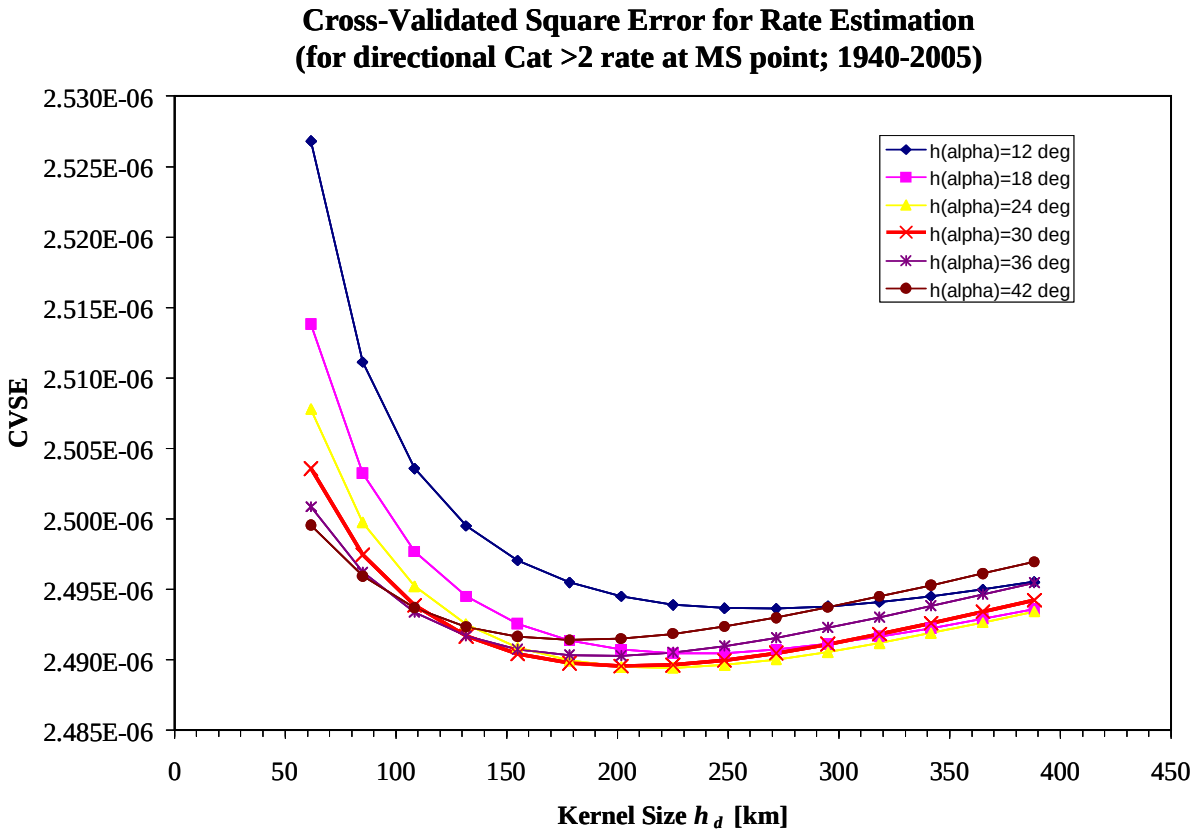

Figure 3-4. CVSE Results for the Directional Storm Rate and Angle Width.

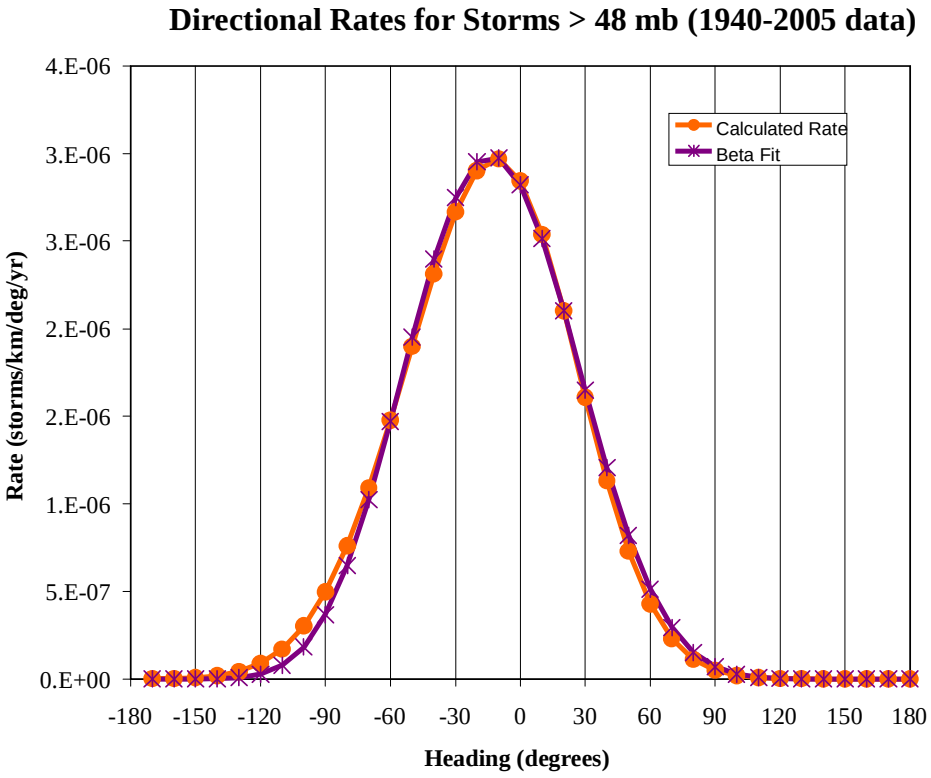

Figure 3-5. Directional Rates and Beta Distribution of Storm Azimuth for Storms with Central Pressures Below 965 mb.

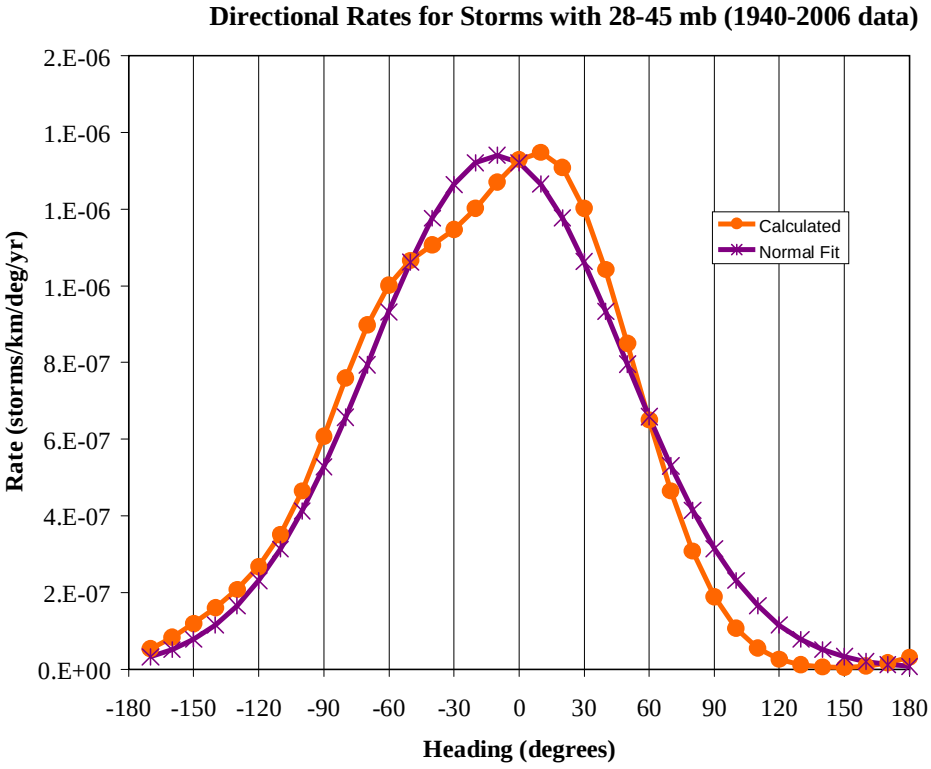

Figure 3-6. Directional Rates and Normal Distribution of Storm Azimuth for Storms with Central Pressures Between 965 and 982 mb.

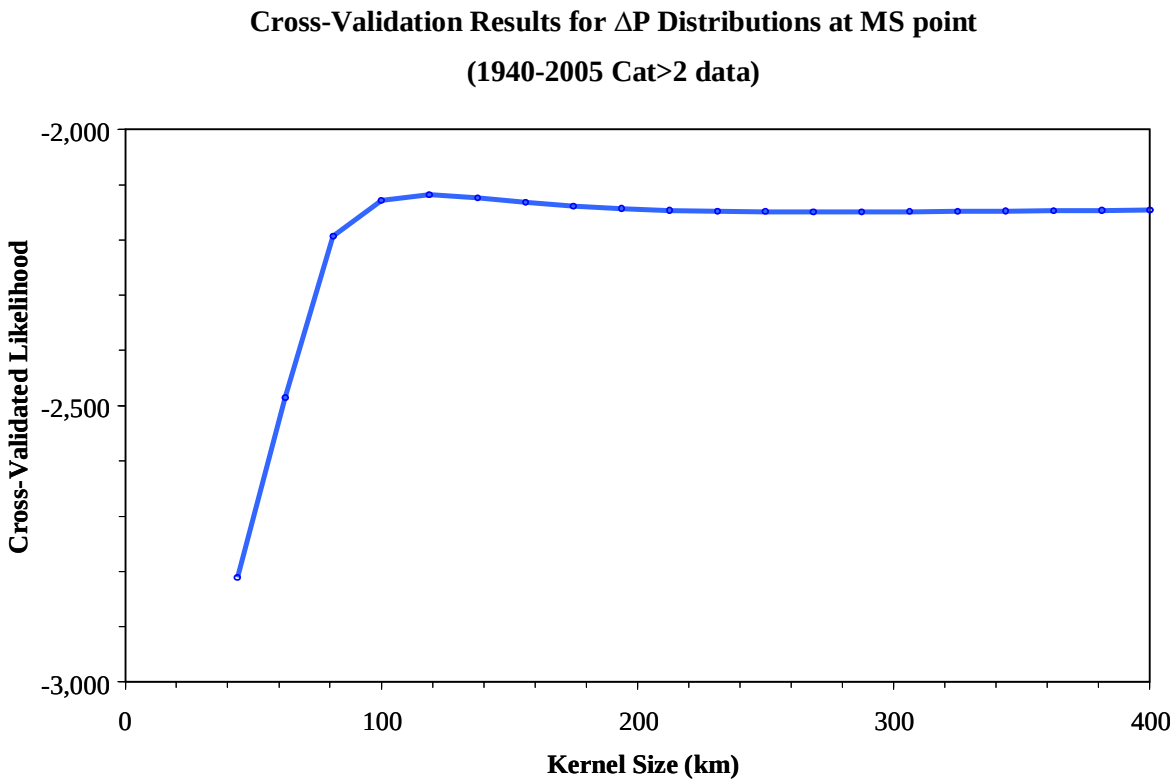

Figure 3-7. Cross-Validation Results for Central Pressures of the Greater Storms.

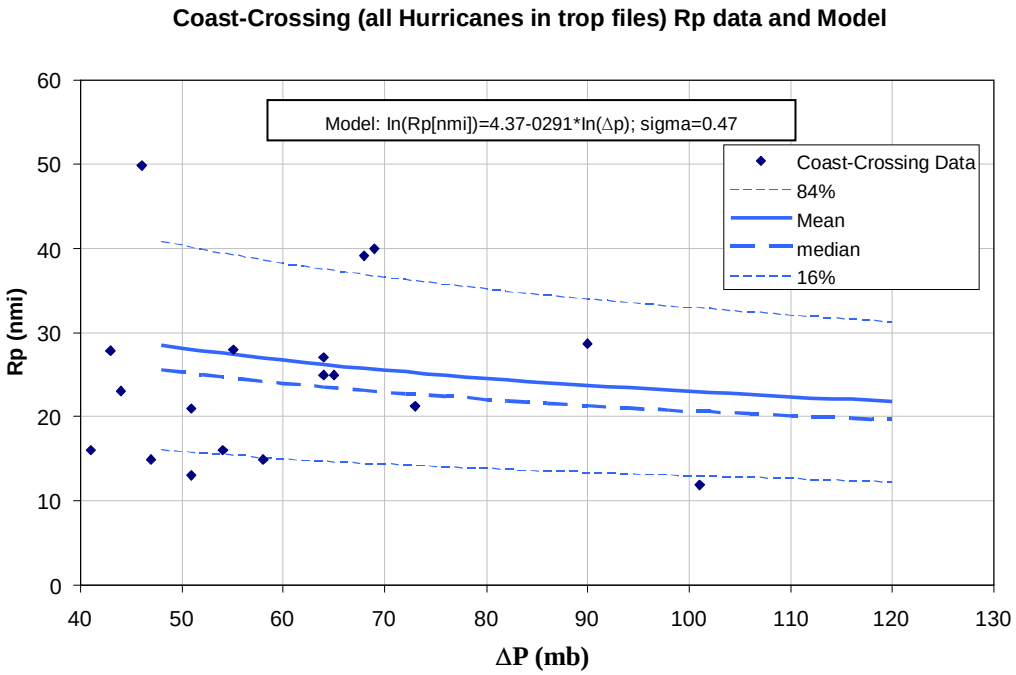

Figure 3-8. The Pressure Radius versus Central Pressure Deviation for Storms at Landfall in the Gulf of Mexico.

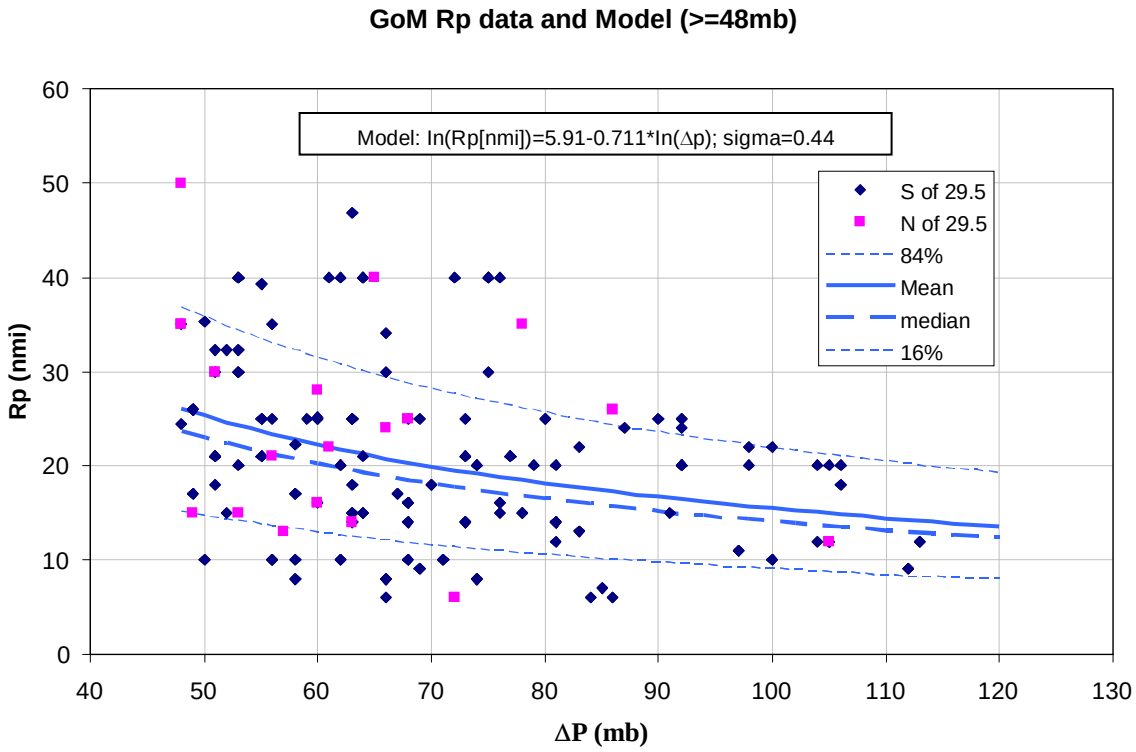

Figure 3-9. The Pressure Radius versus Central Pressure Deviation for Storms in the Open Gulf of Mexico.

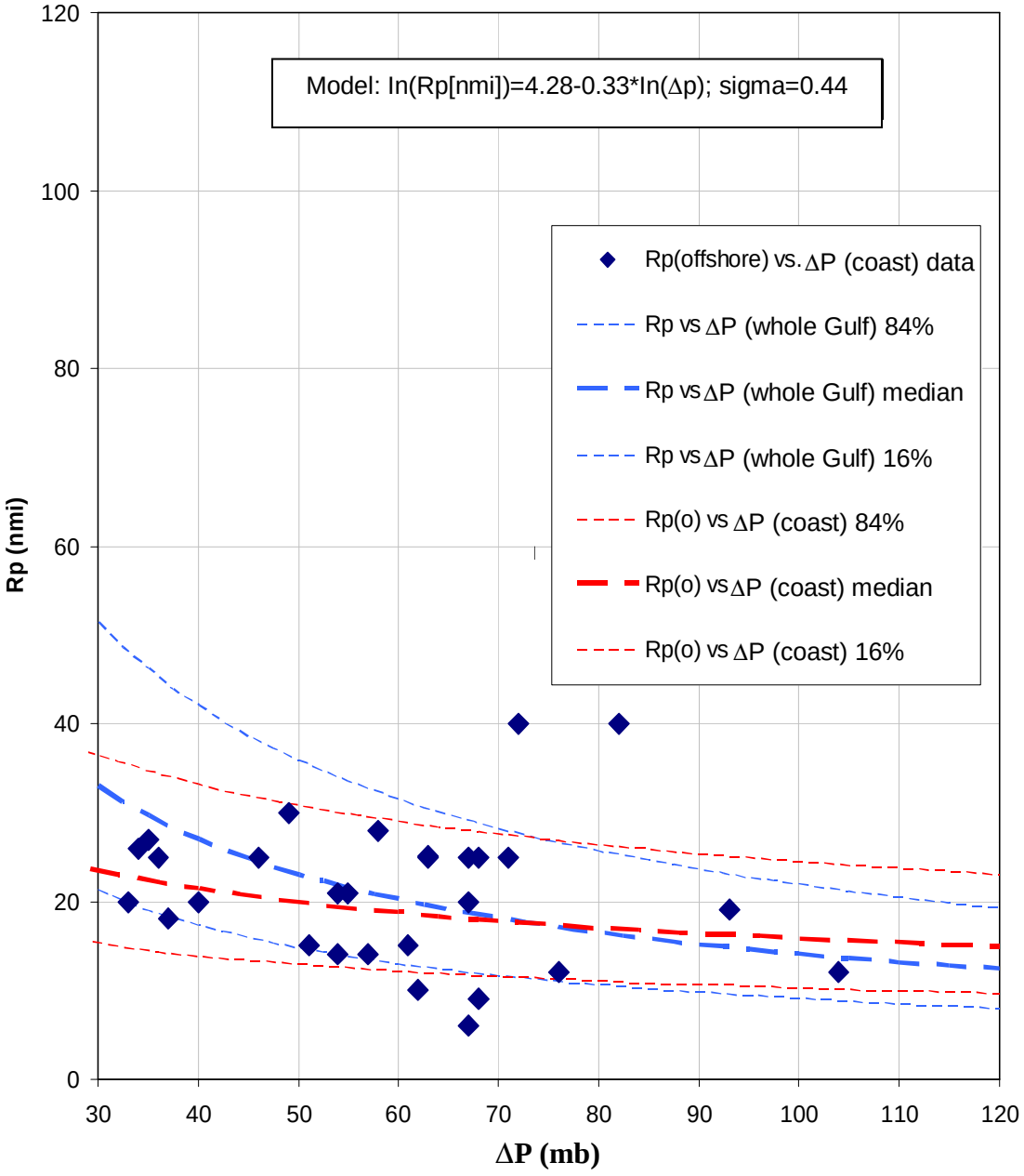

Figure 3-10. The Offshore Pressure Radius versus Landfall Central Pressure Relation for Post-1950 Storms with Central Pressures Below 982 mb in the Gulf of Mexico [Source: *Joint Probability Analysis of Hurricane Flood Hazards for Mississippi*.]

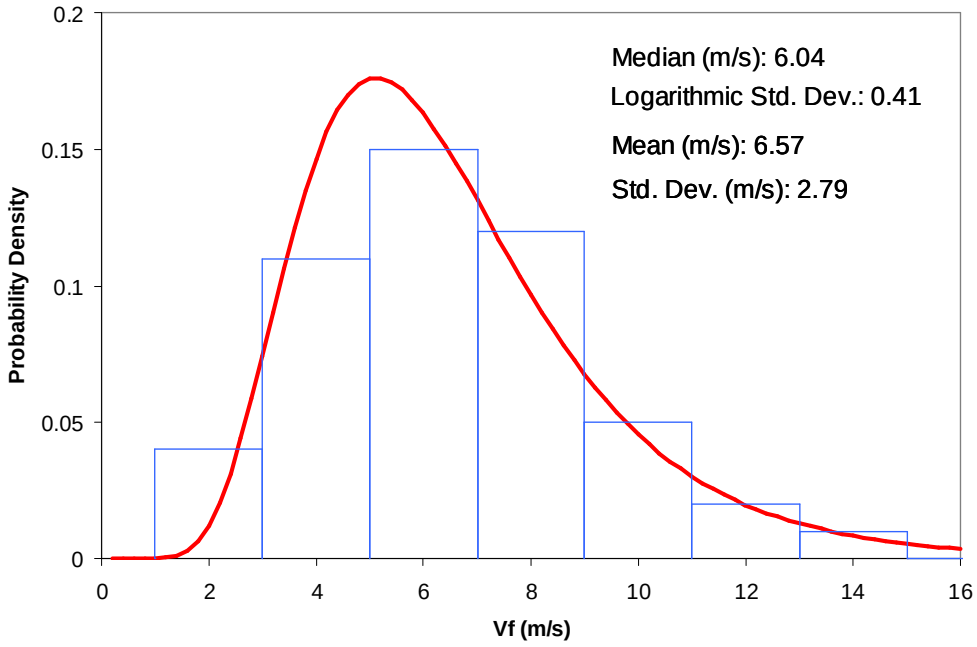

Figure 3-11. Probability Density for Storm Forward Speed for Greater Storms.

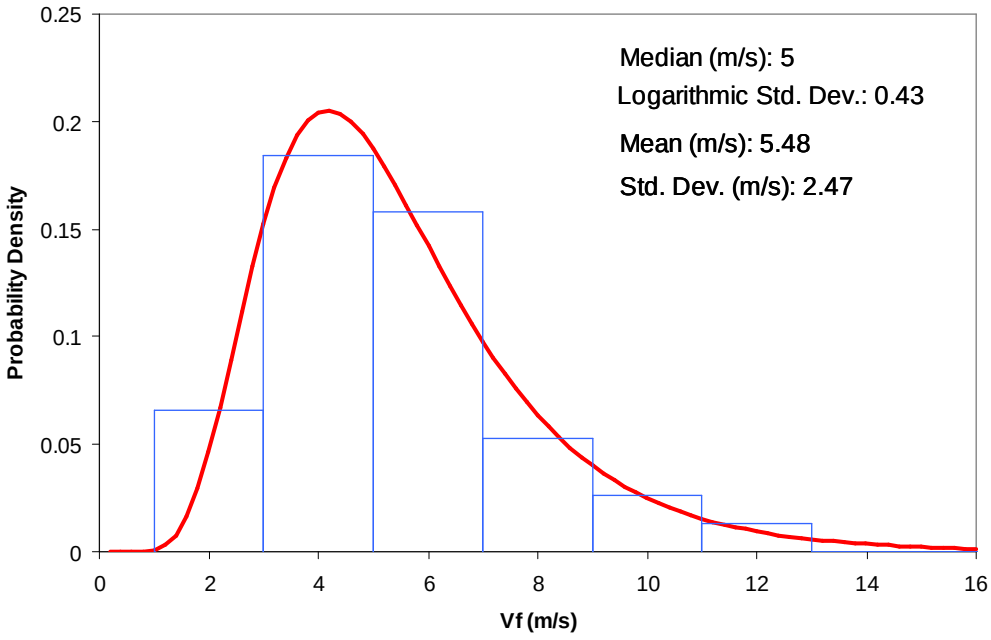

Figure 3-12. Probability Density for Storm Forward Speed for Lesser Storms.

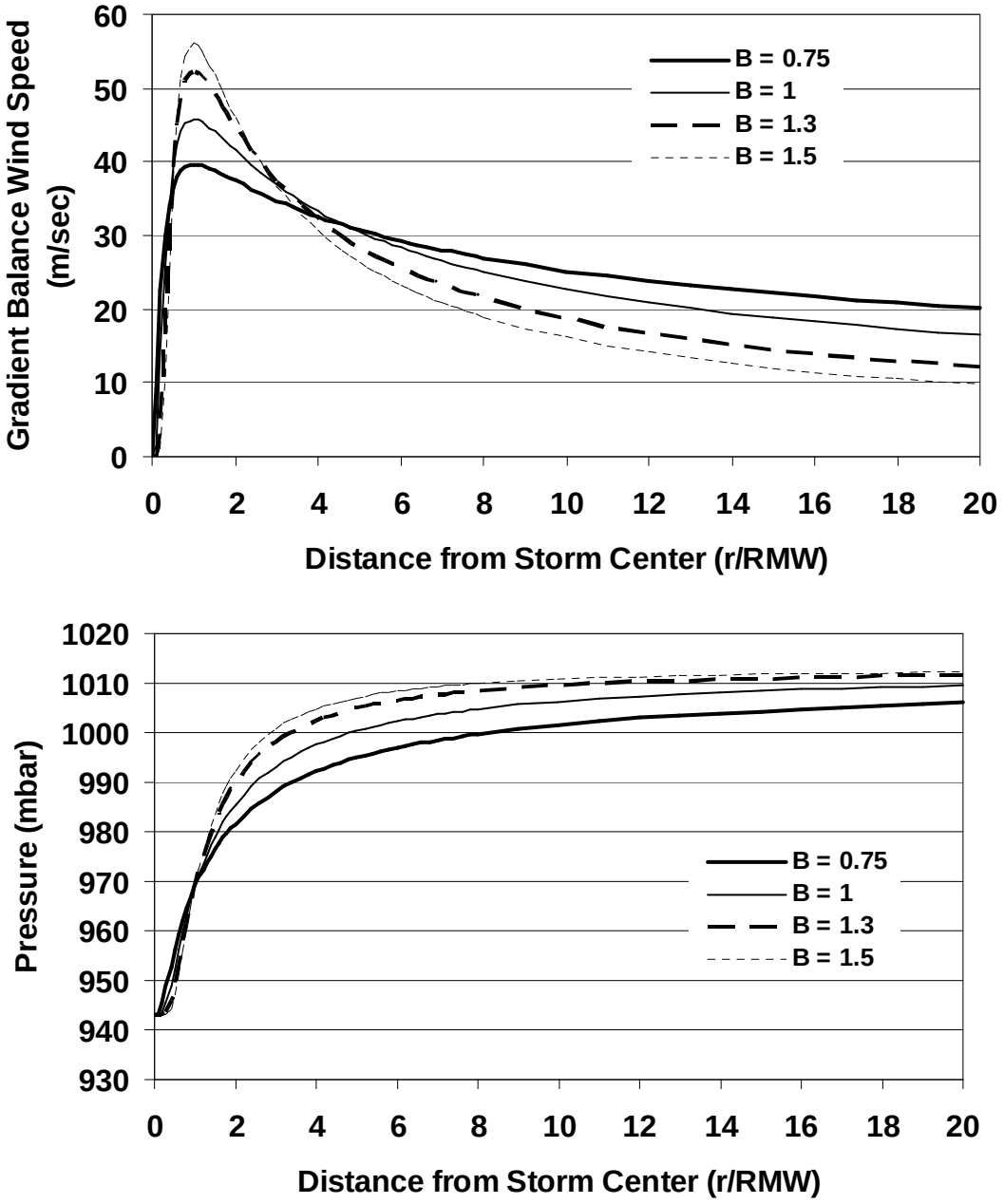

Figure 3-13. Effect of Holland B Parameter on Wind Speeds and Pressures.

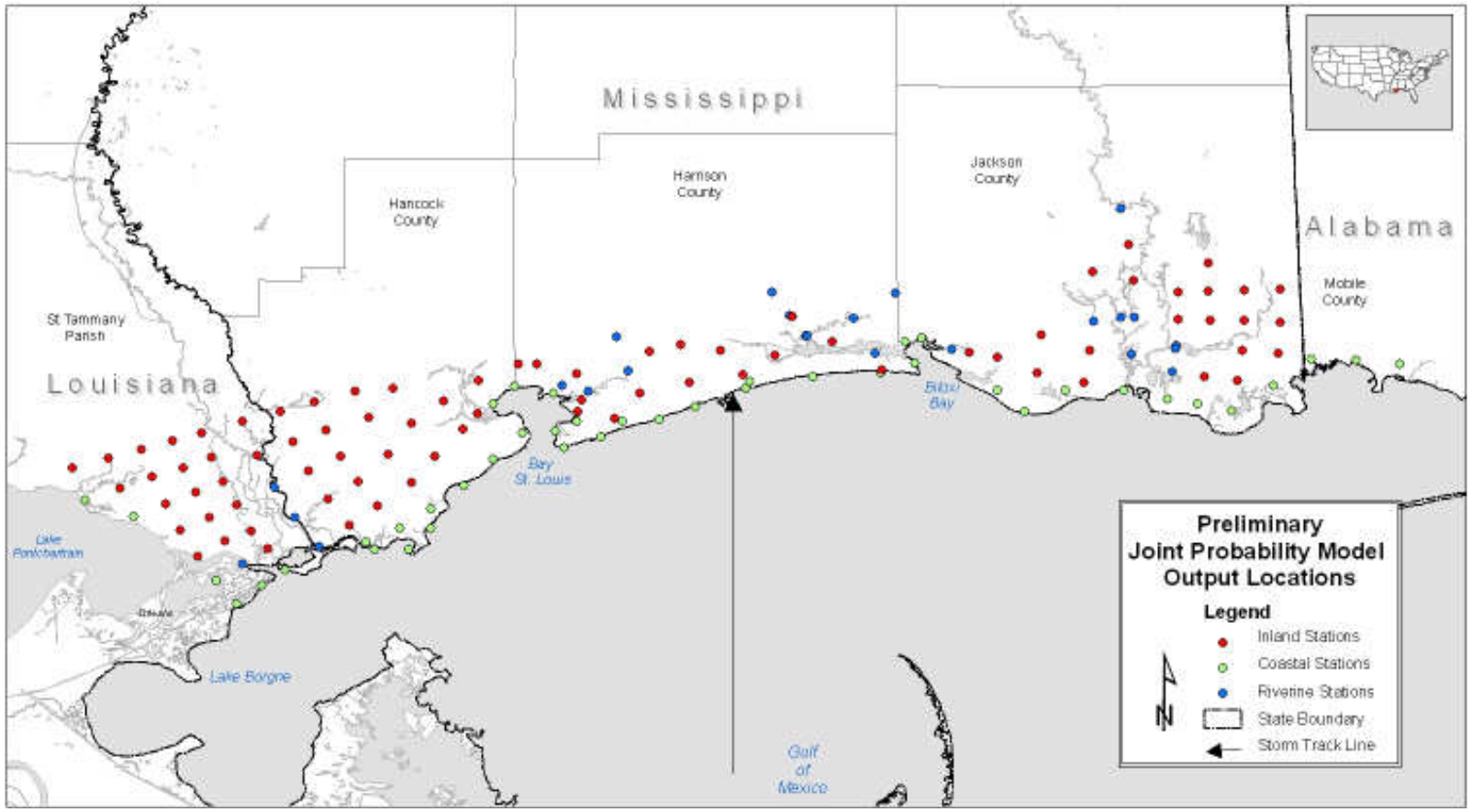

Figure 3-14a. Preliminary Joint Probability Model Output Locations.

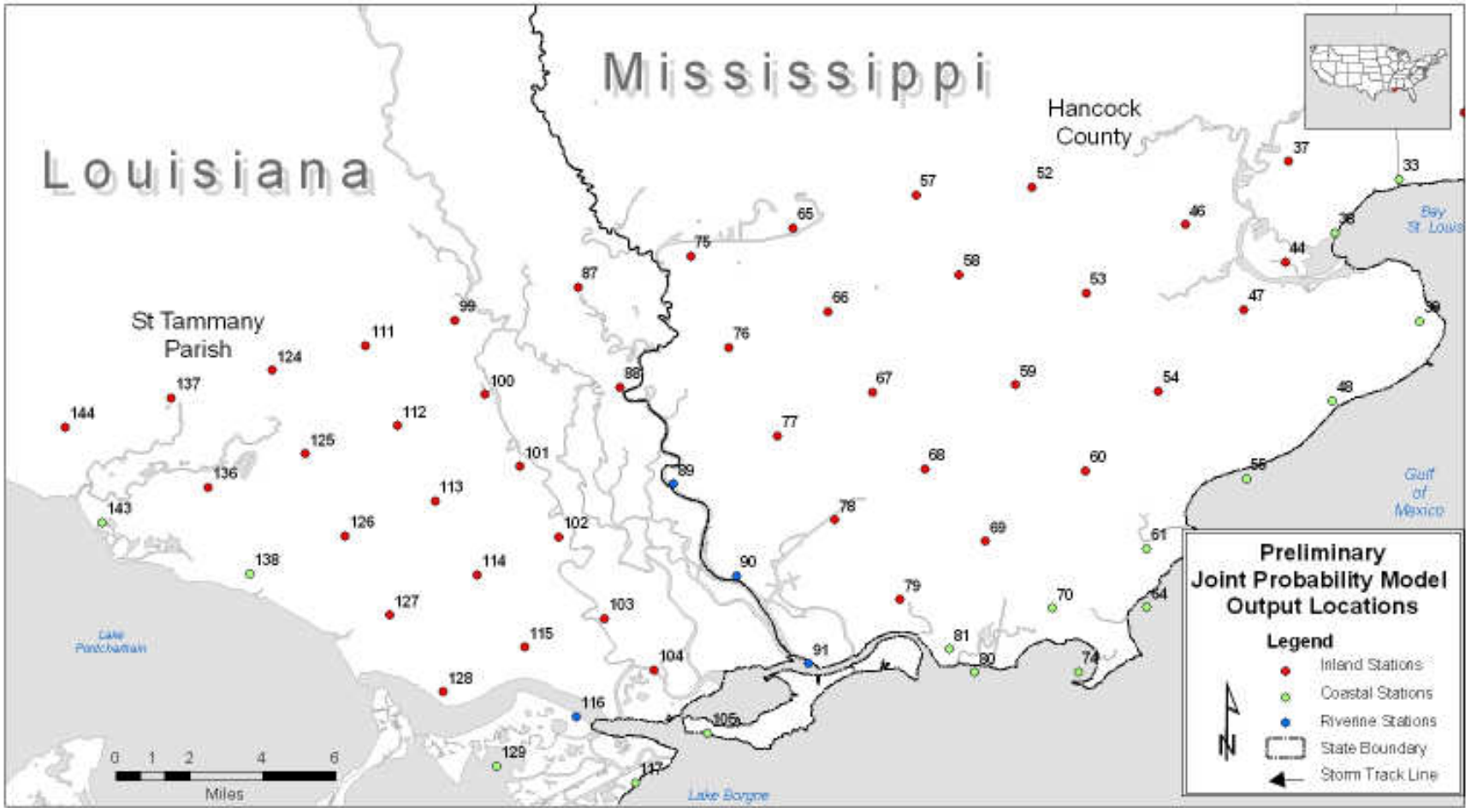

Figure 3-14b. Preliminary Joint Probability Model Output Locations Western Portion of the Grid.

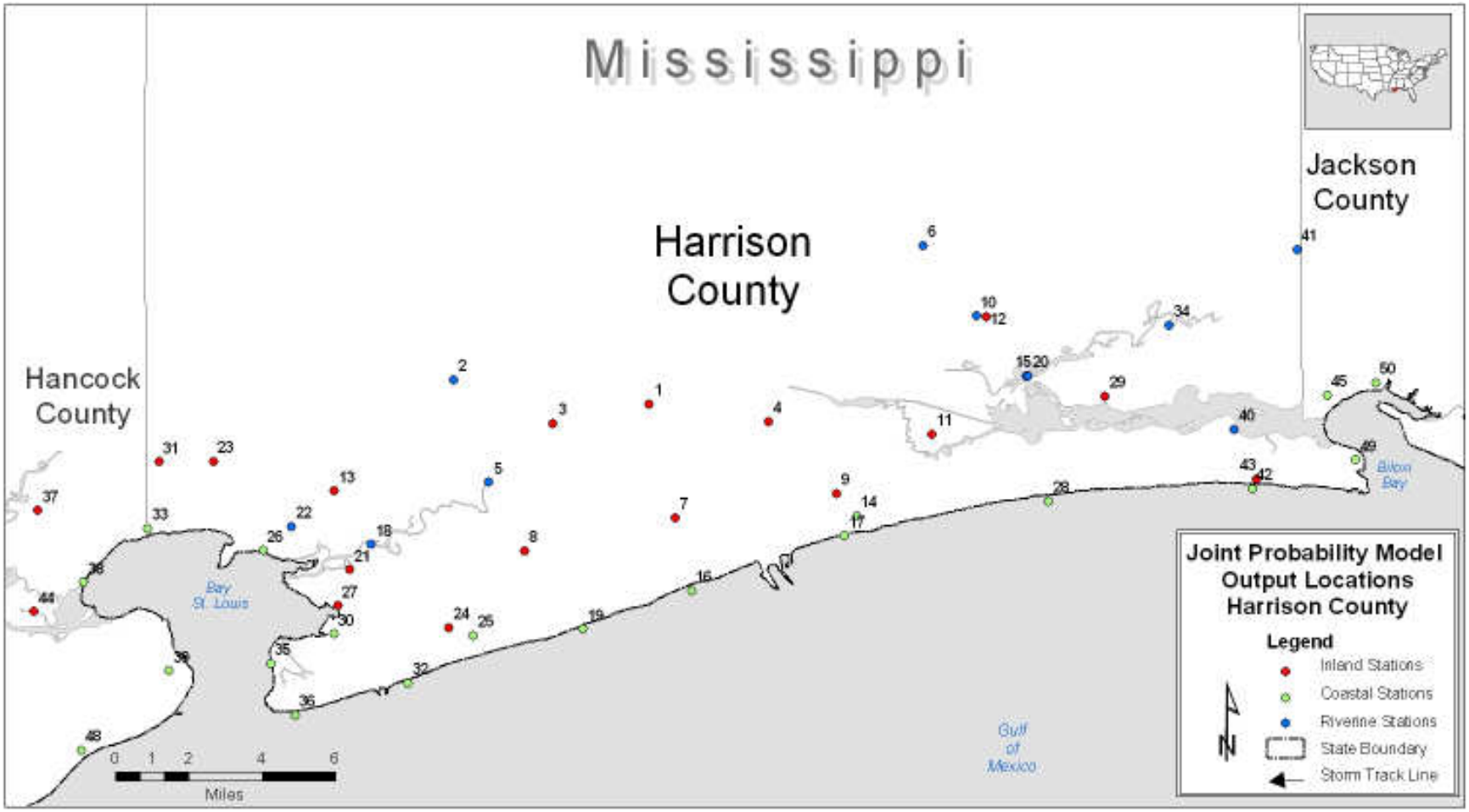

Figure 3-14c. Preliminary Joint Probability Model Output Locations Central Portion of Grid.

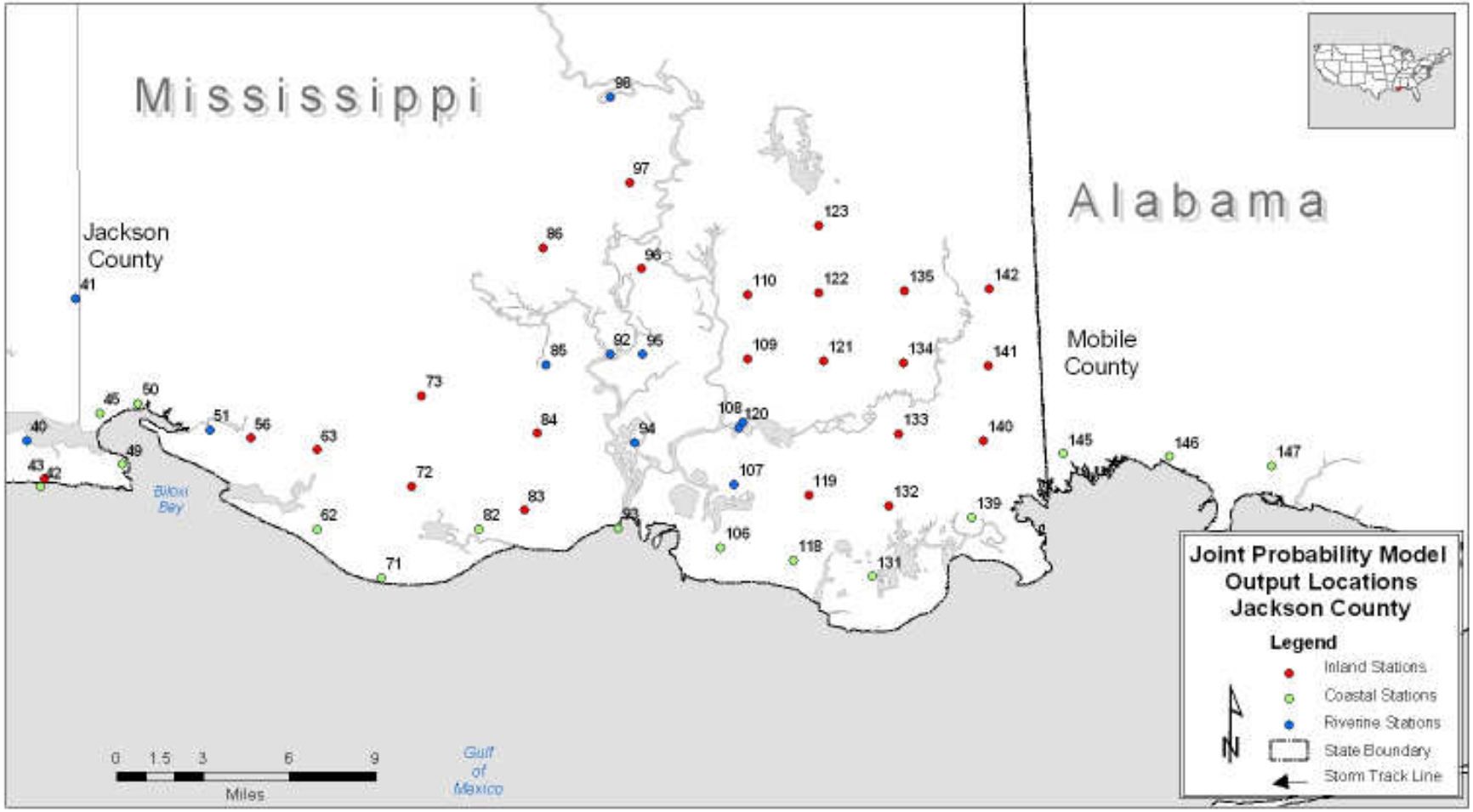

Figure 3-14d. Preliminary Joint Probability Model Output Locations Eastern Portion of the Grid.

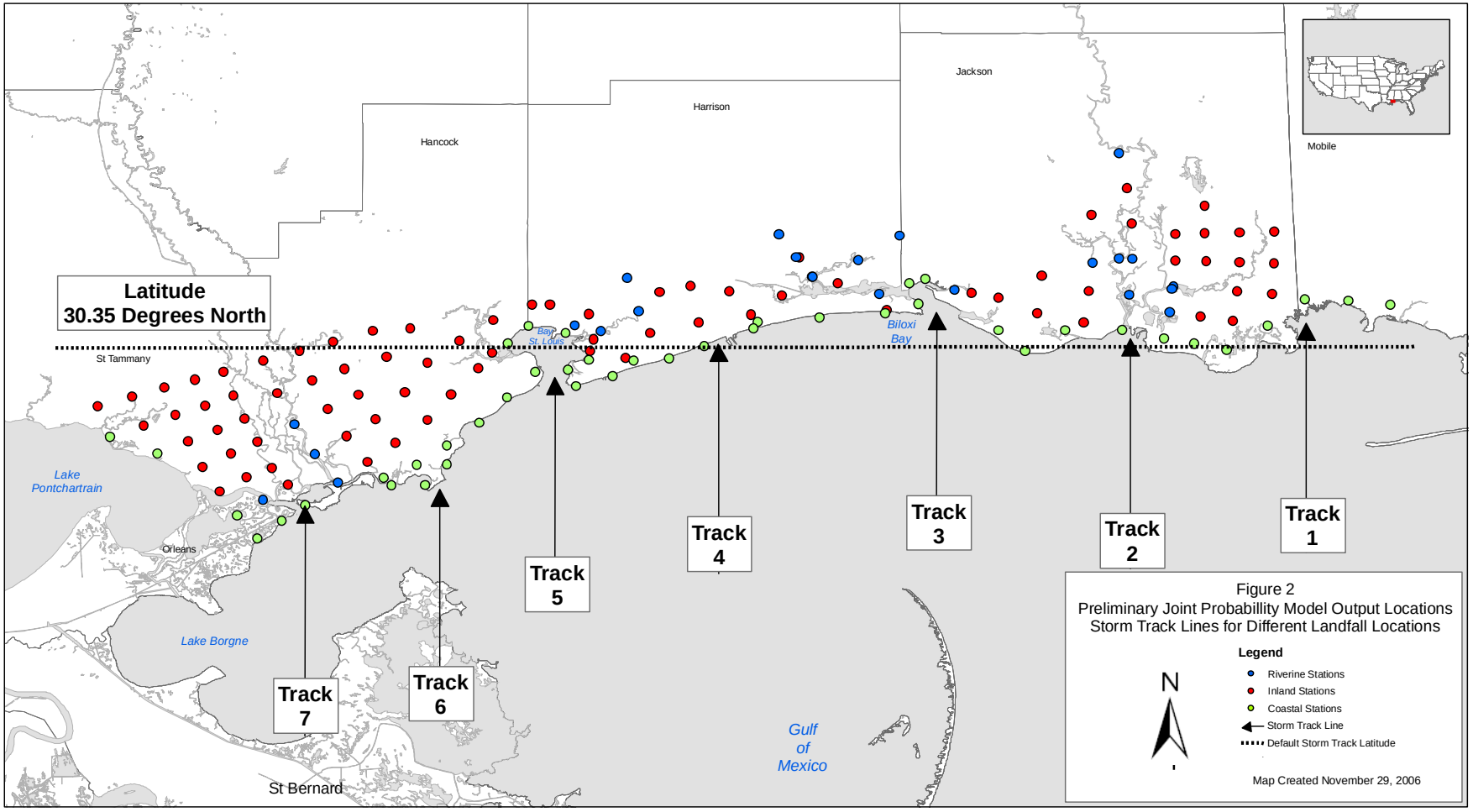

Figure 3-15. Preliminary Joint Probability Model Output Locations Storm Track Lines for Different Landfall Locations.

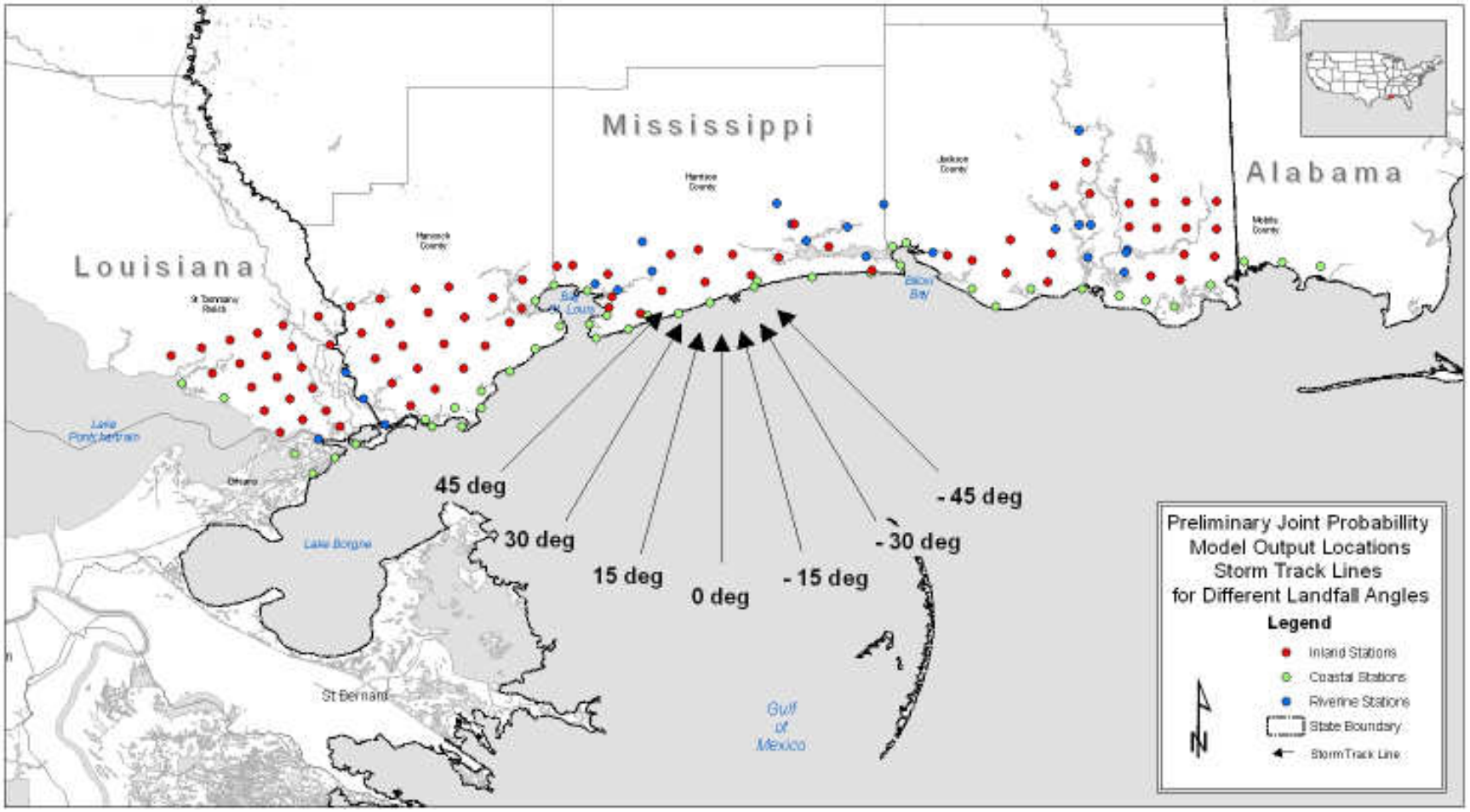

Figure 3-16. Preliminary Joint Probability Model Output Locations Storm Track Lines for Different Landfall Angles.

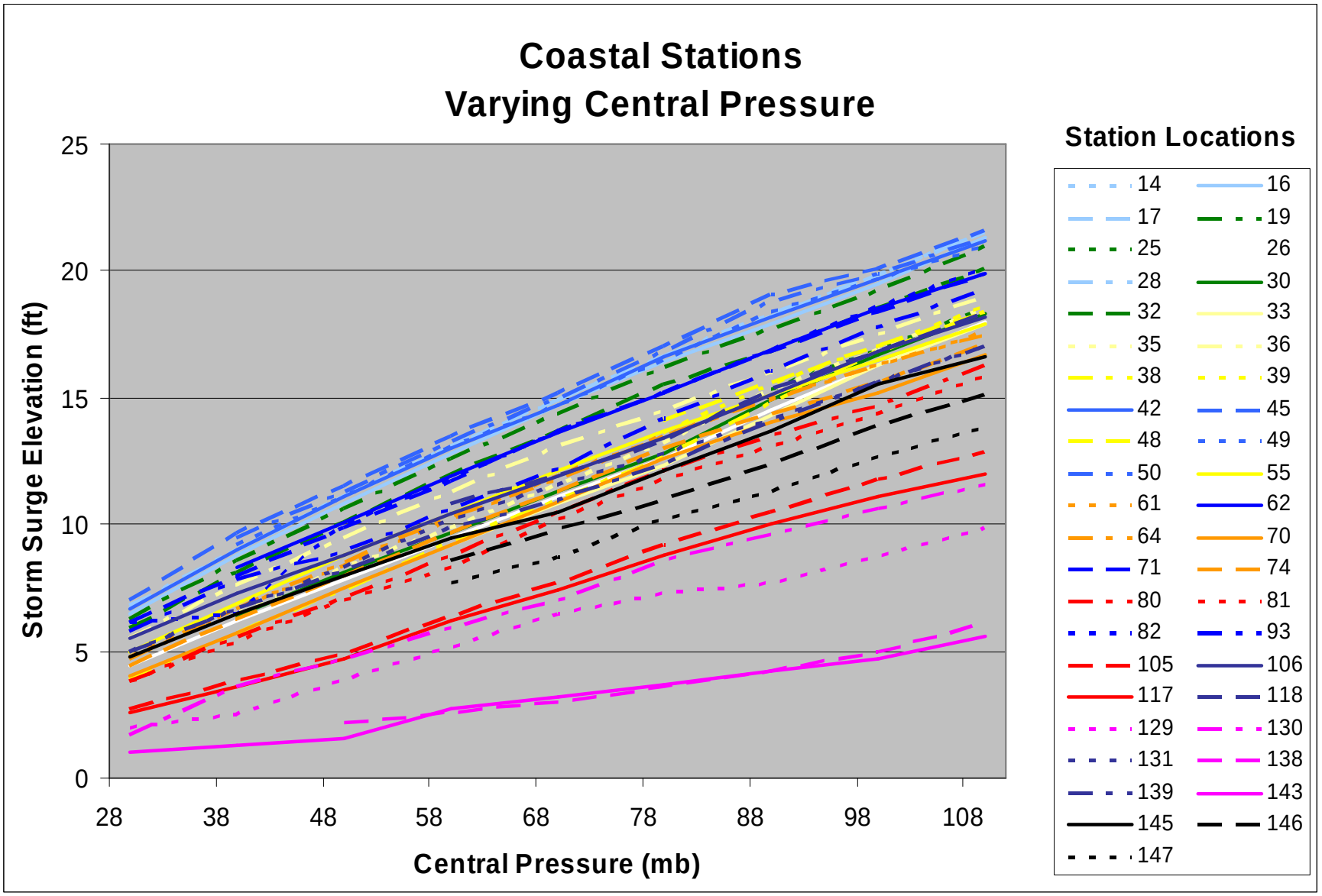

Figure 3-17. Coastal Stations Varying Central Pressure.

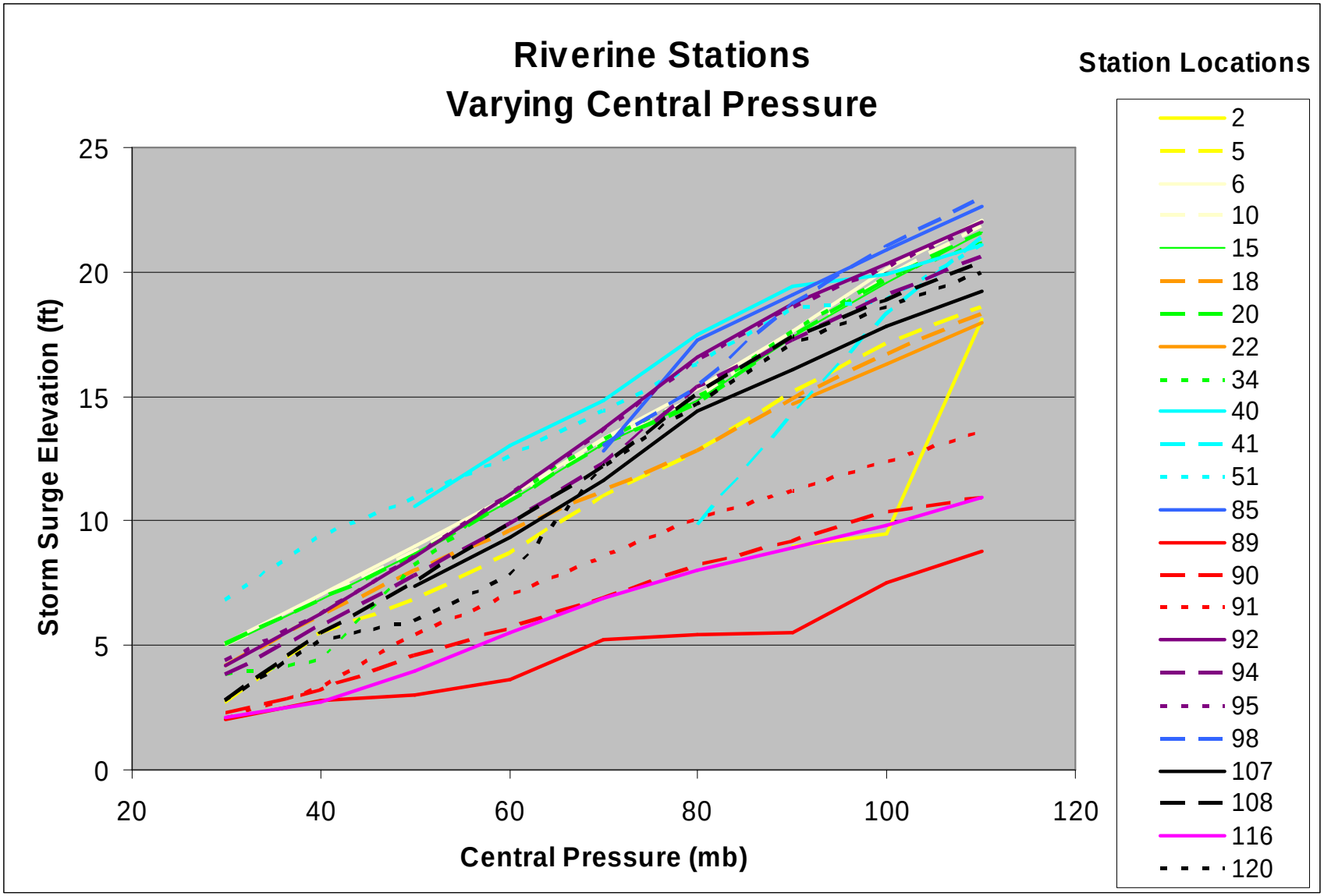

Figure 3-18. Riverine Stations Varying Central Pressure.

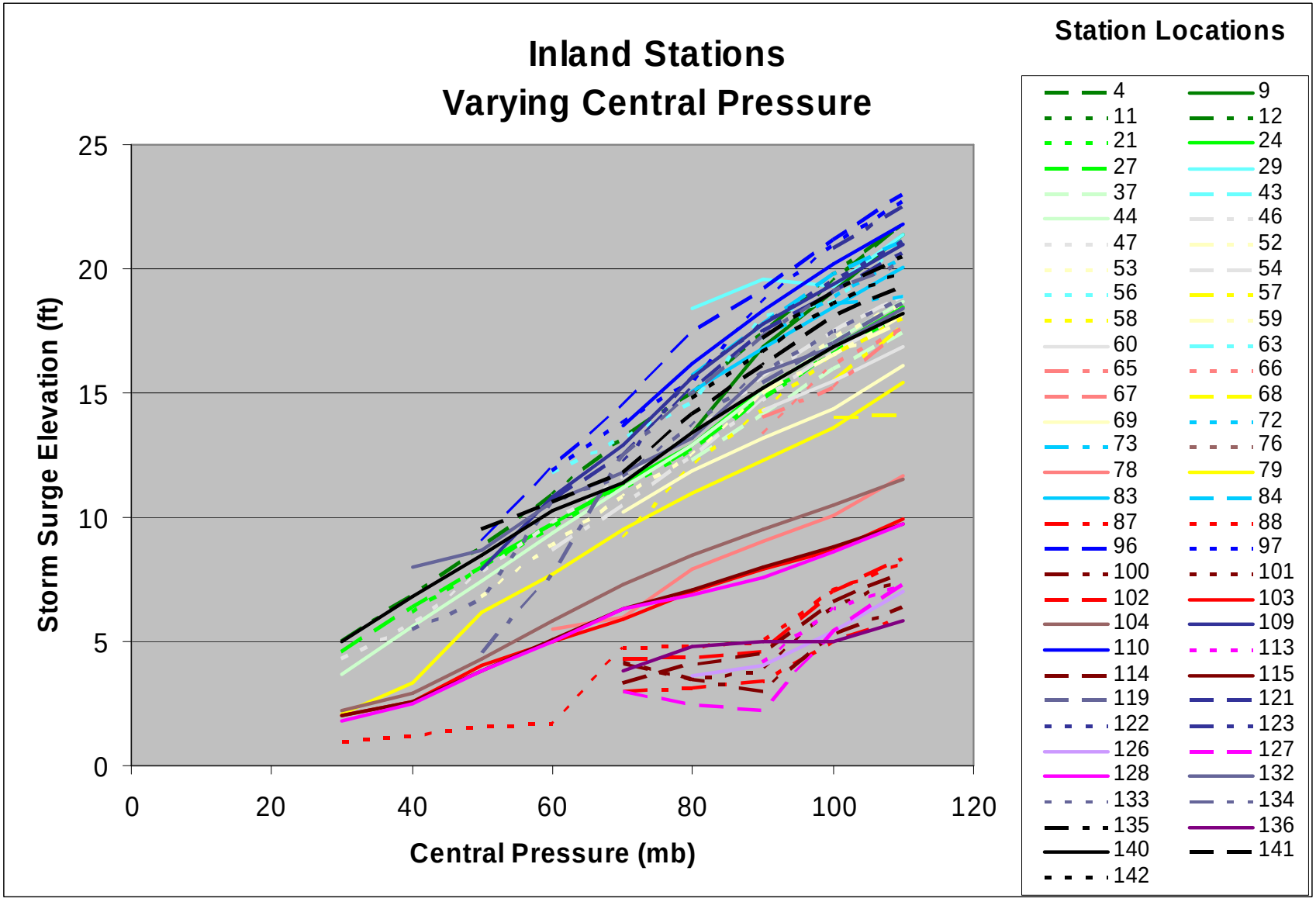

Figure 3-19. Inland Stations Varying Central Pressure.

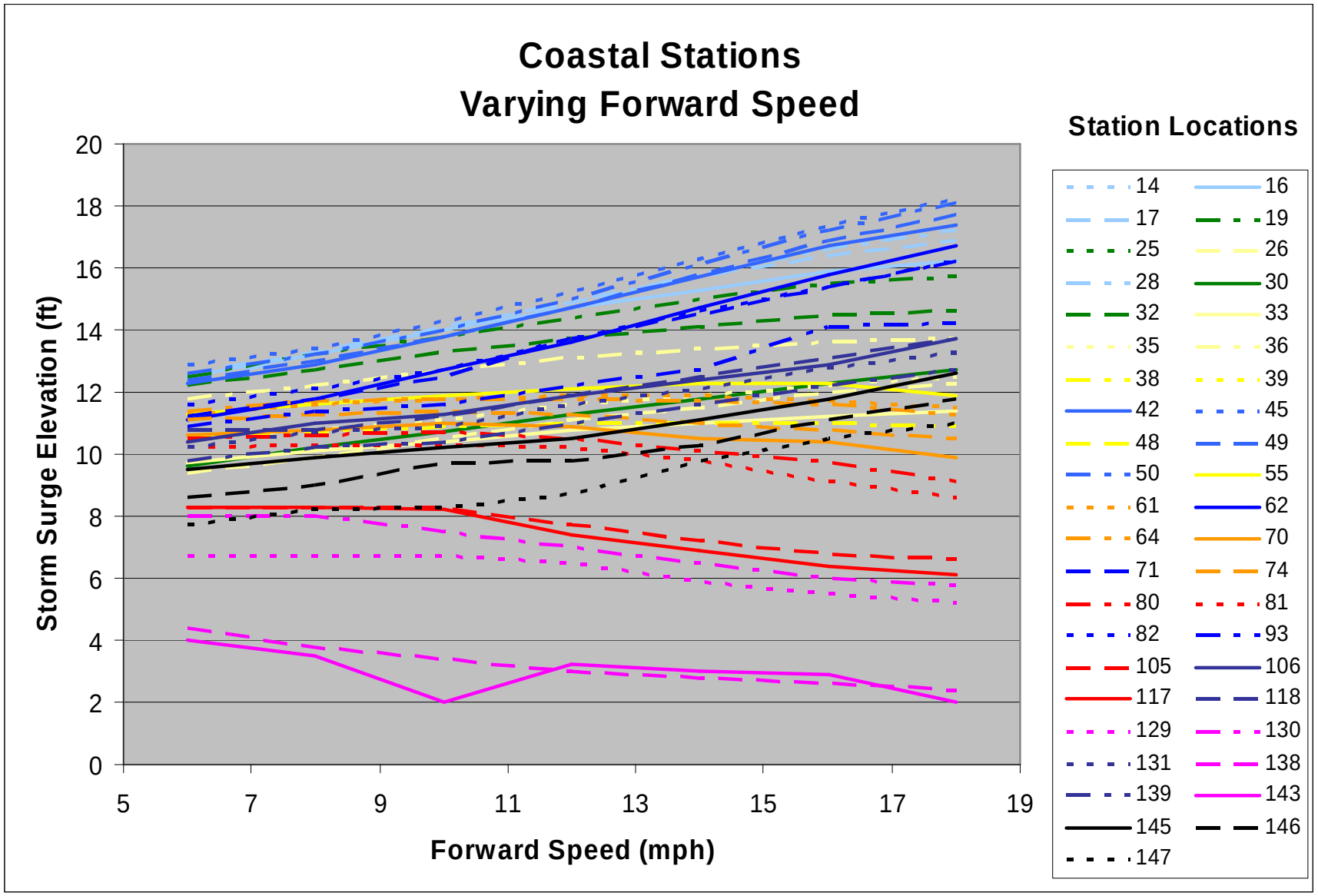

Figure 3-20. Coastal Stations Varying Forward Speed.

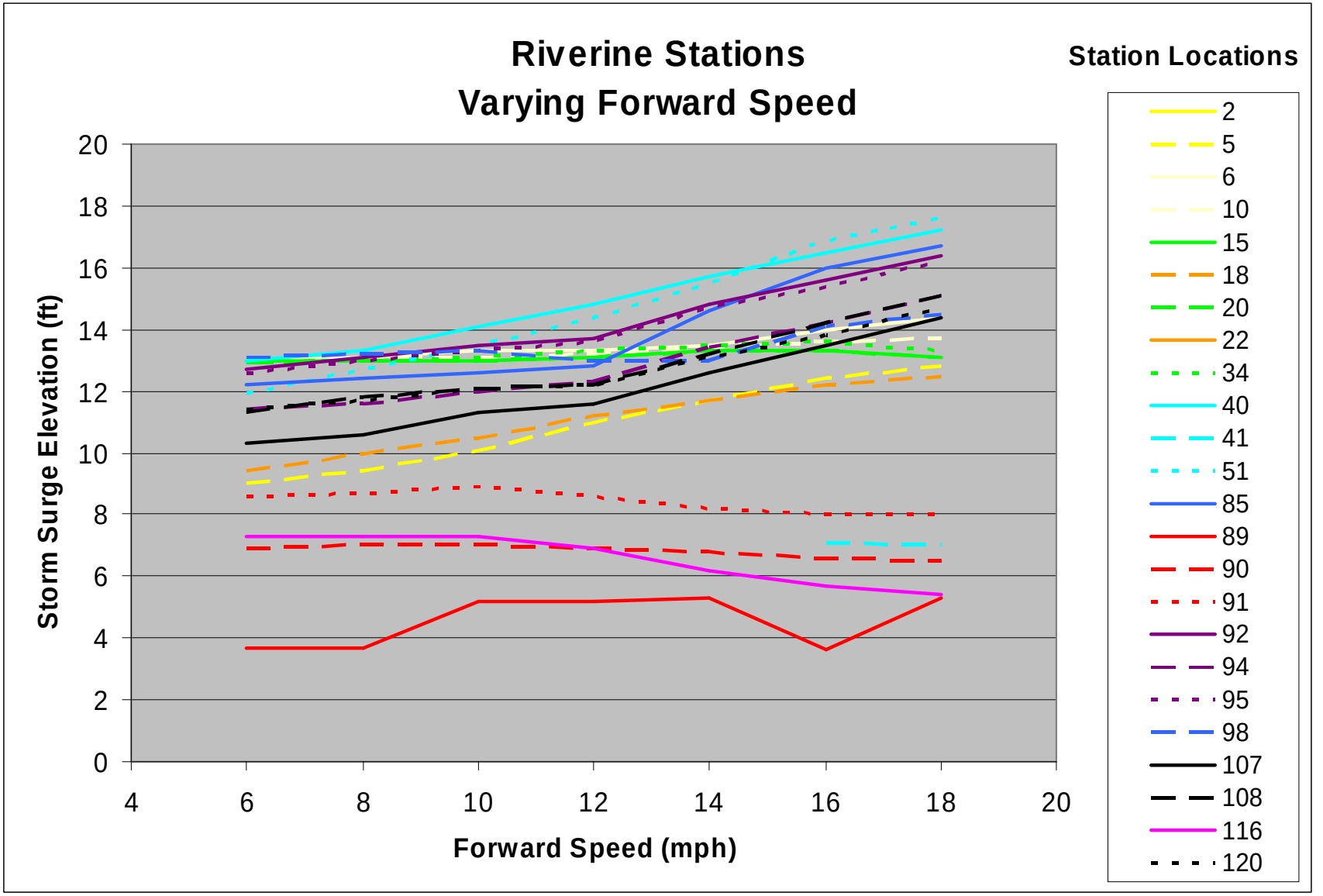

Figure 3-21. Riverine Stations Varying Forward Speed.

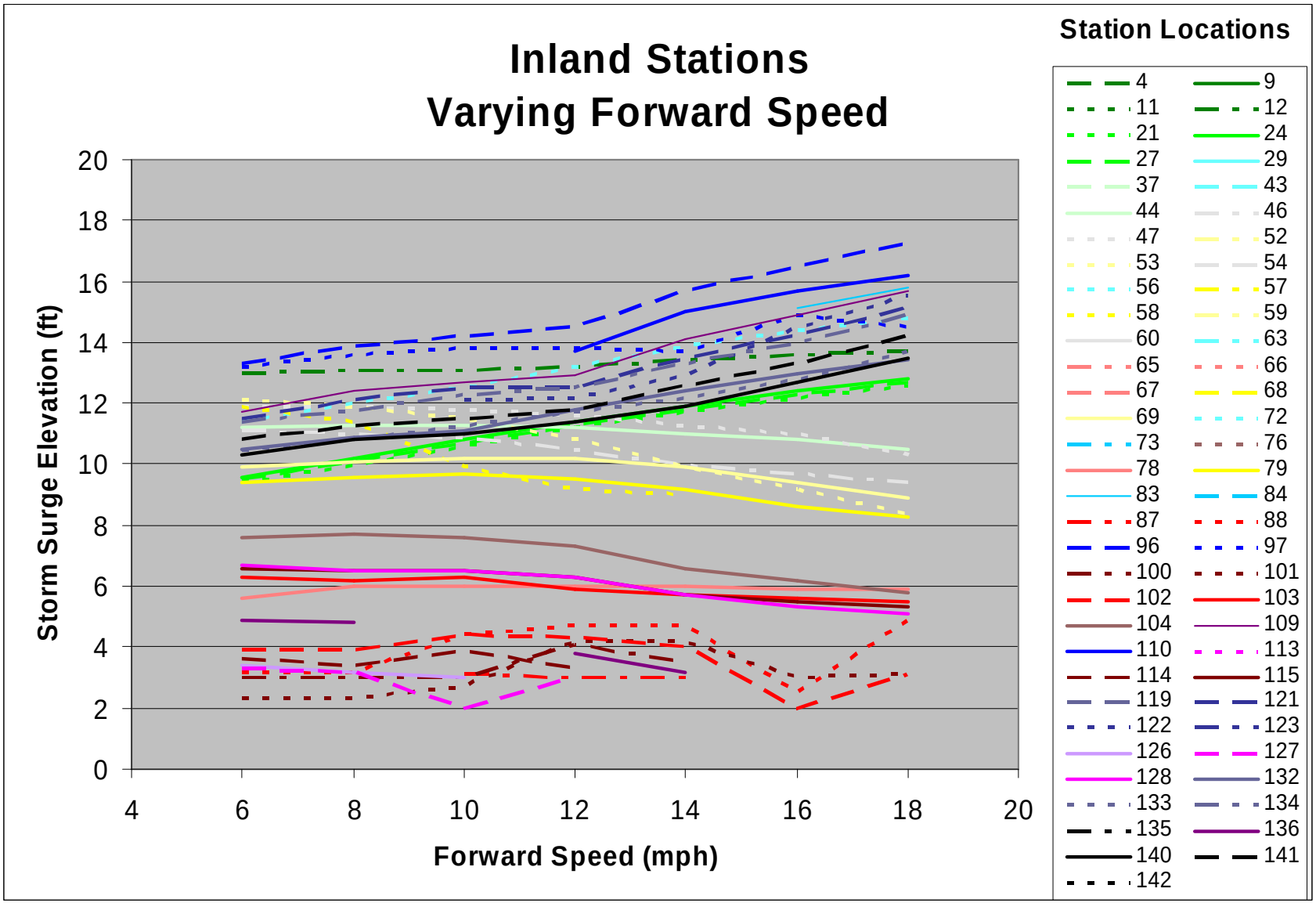

Figure 3-22. Inland Stations Varying Forward Speed.

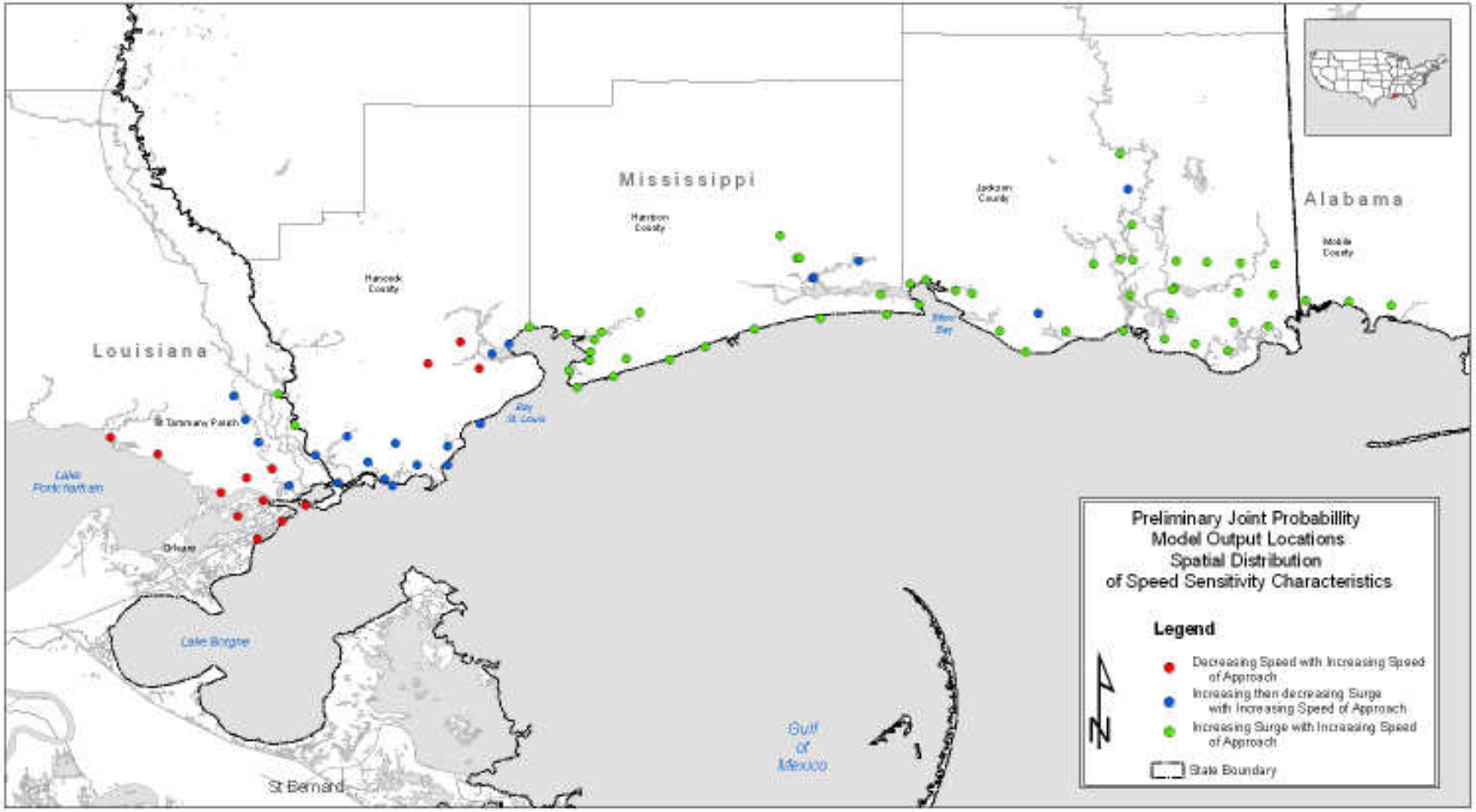

Figure 3-23. Preliminary JPM Output Locations Spatial Distribution of Speed Sensitivity Characteristics.

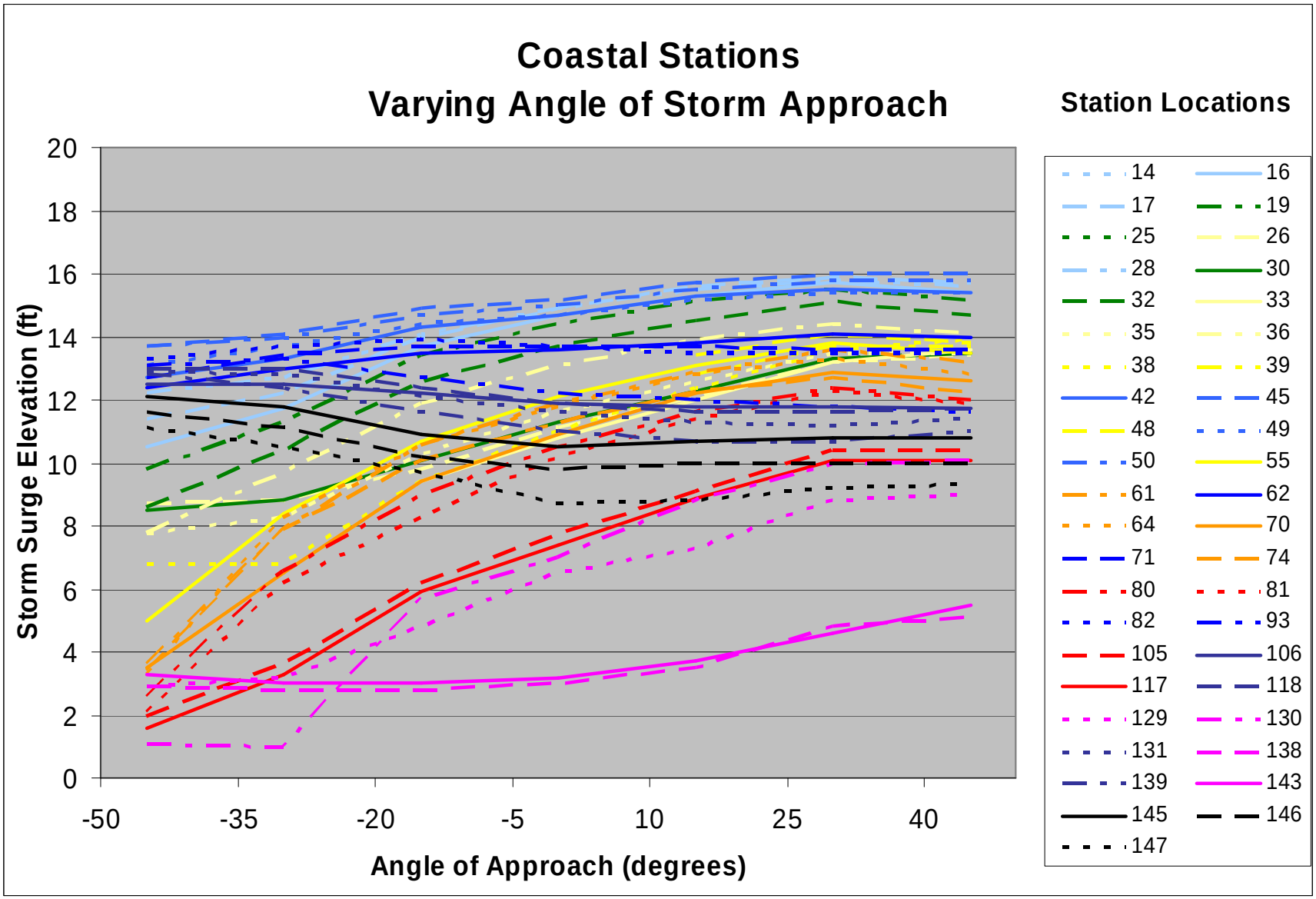

Figure 3-24. Coastal Stations Varying Angle of Storm Approach.

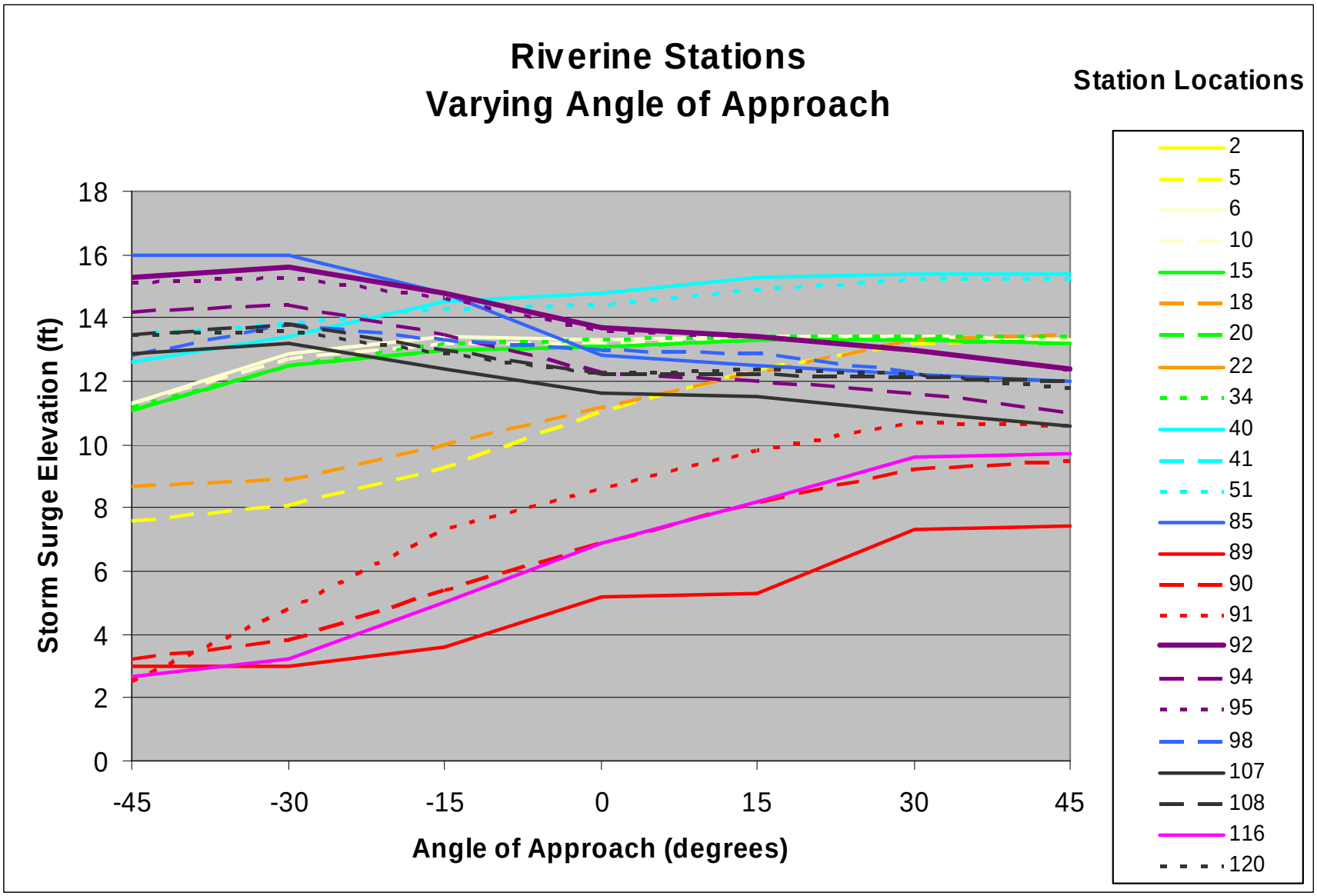

Figure 3-25. Riverine Stations Varying Angle of Storm Approach.

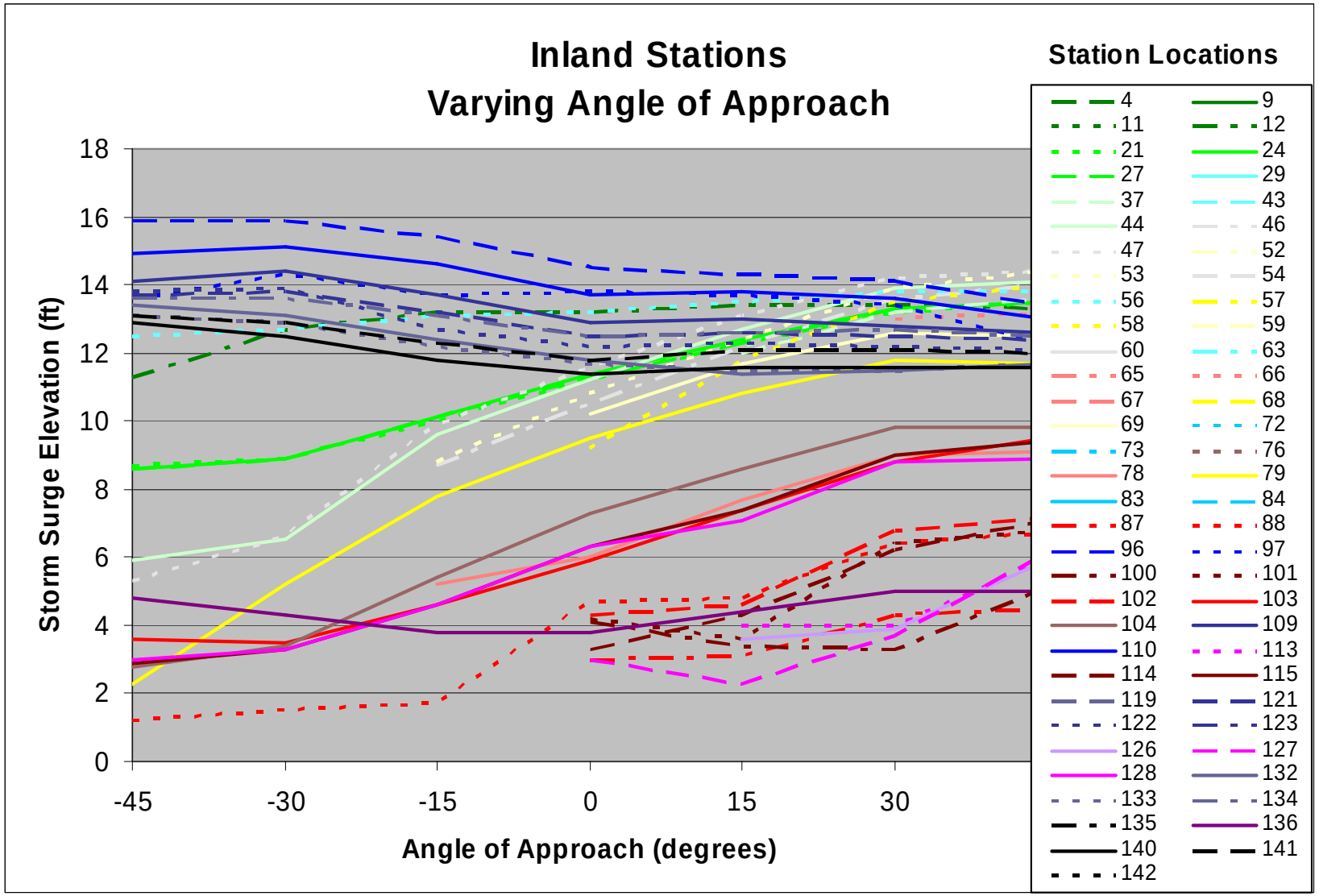

Figure 3-26. Inland Stations Varying Angle of Storm Approach.

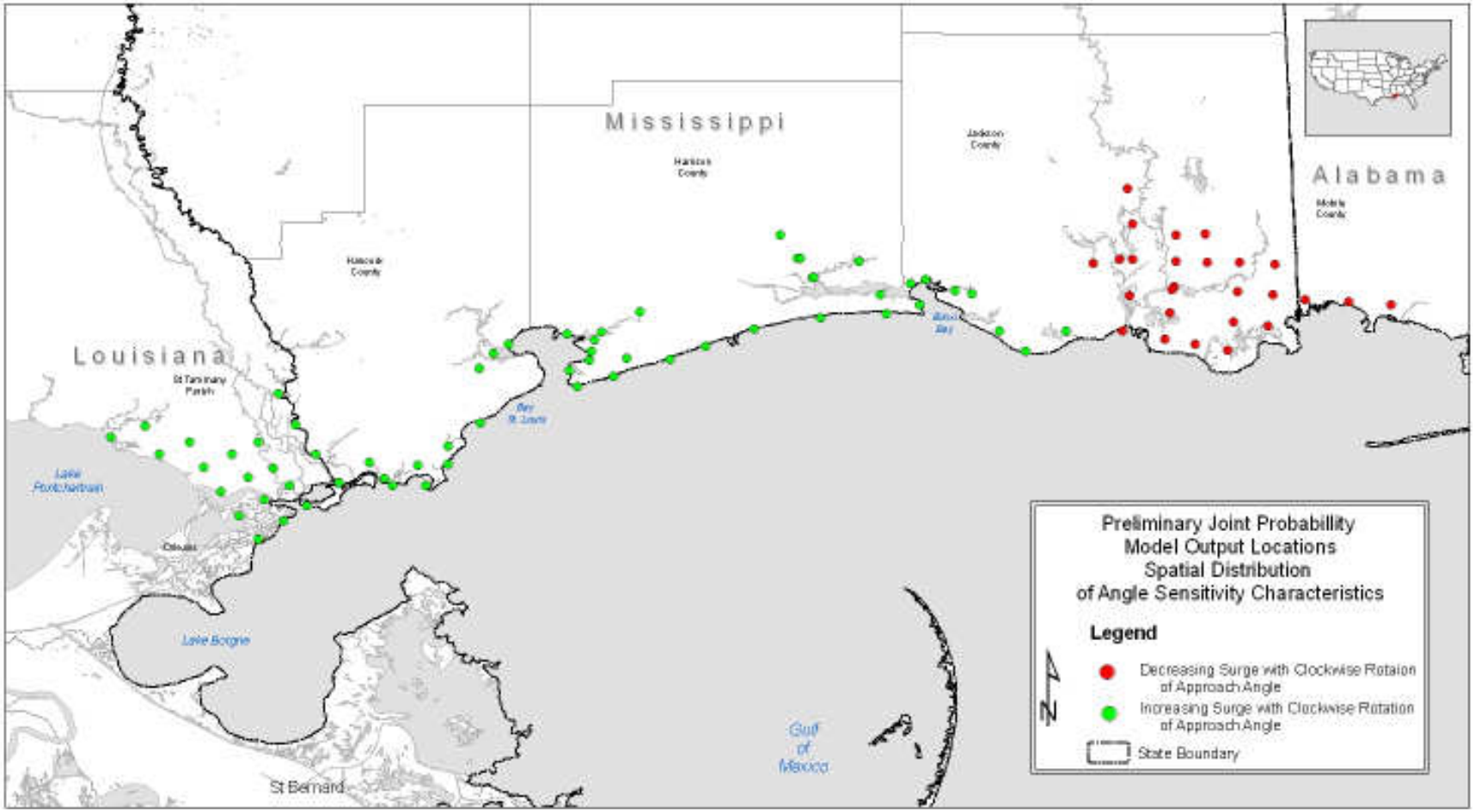

Figure 3-27. Preliminary JPM Output Locations Spatial Distribution of Angle Sensitivity Characteristics.

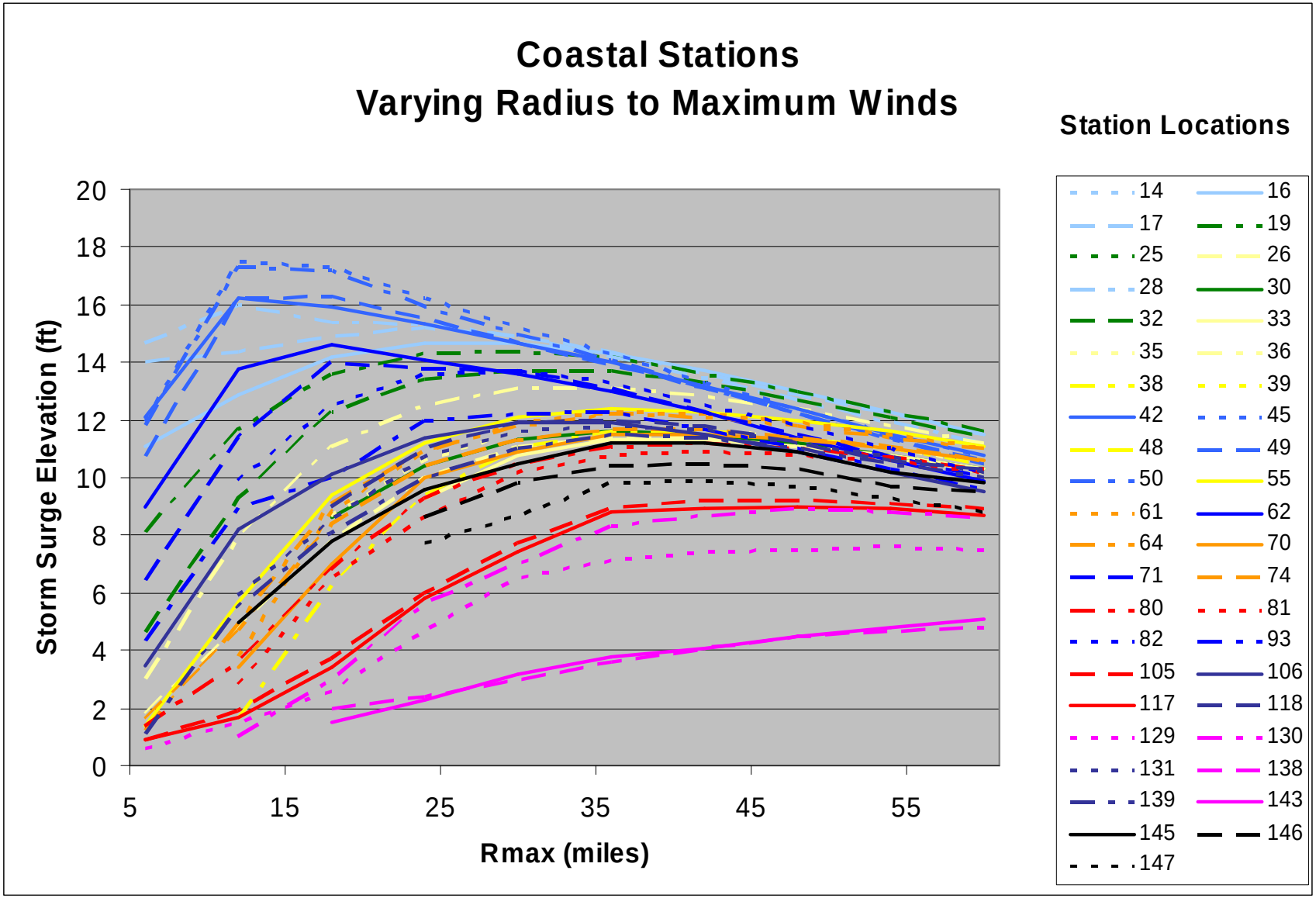

Figure 3-28. Coastal Stations Varying Radius to Maximum Winds.

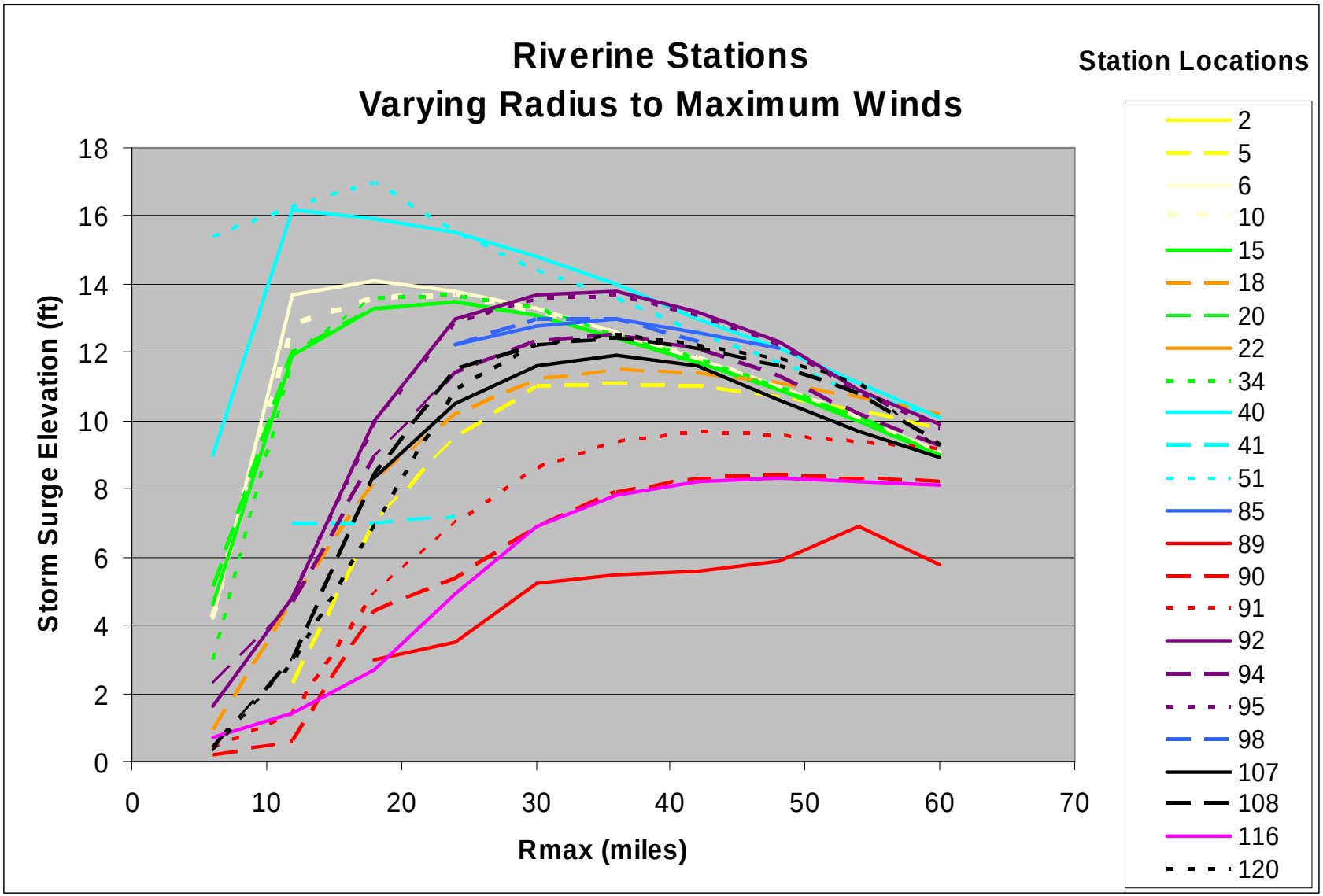

Figure 3-29. Riverine Stations Varying Radius to Maximum Winds.

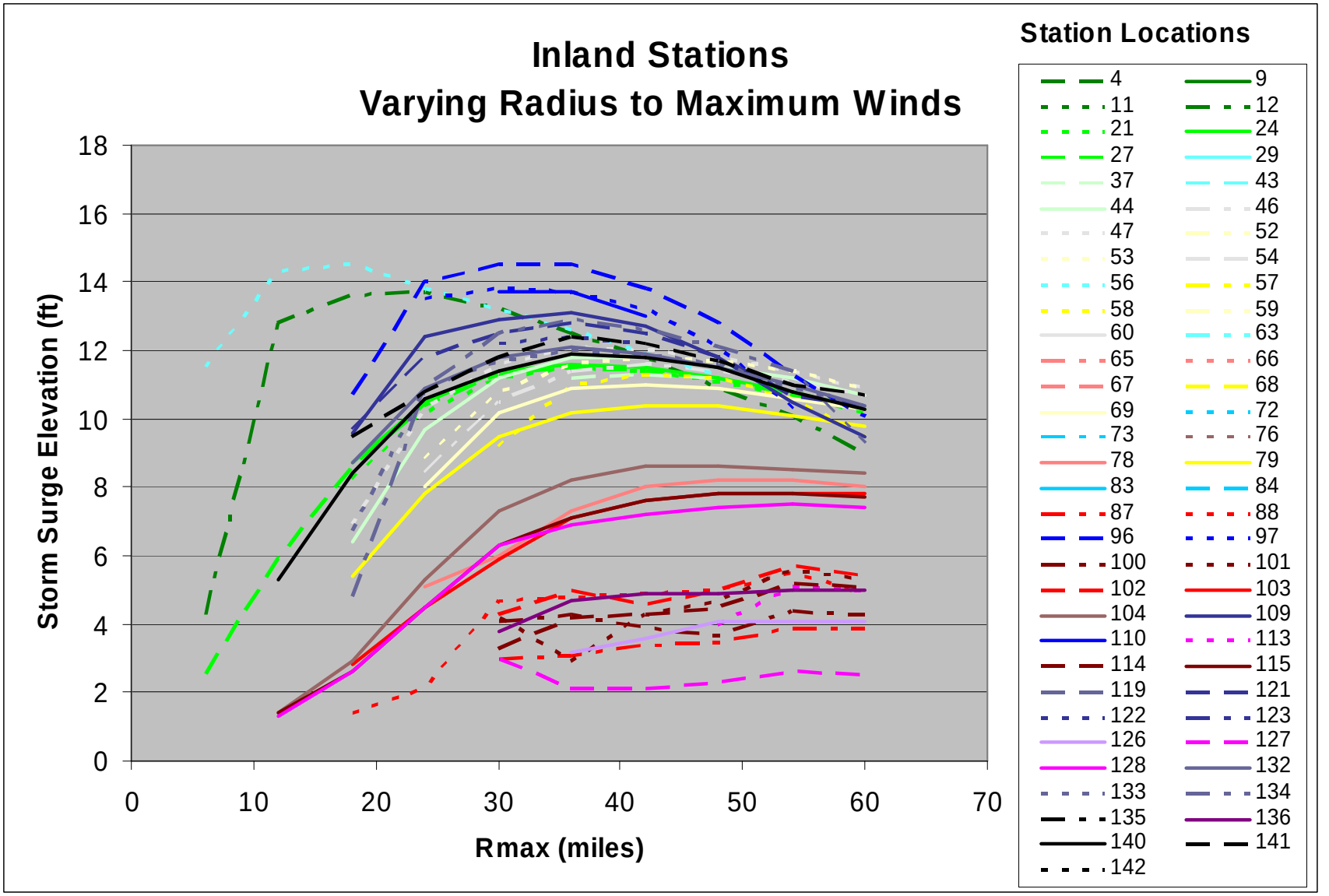

Figure 3-30. Inland Stations Varying Radius to Maximum Winds.

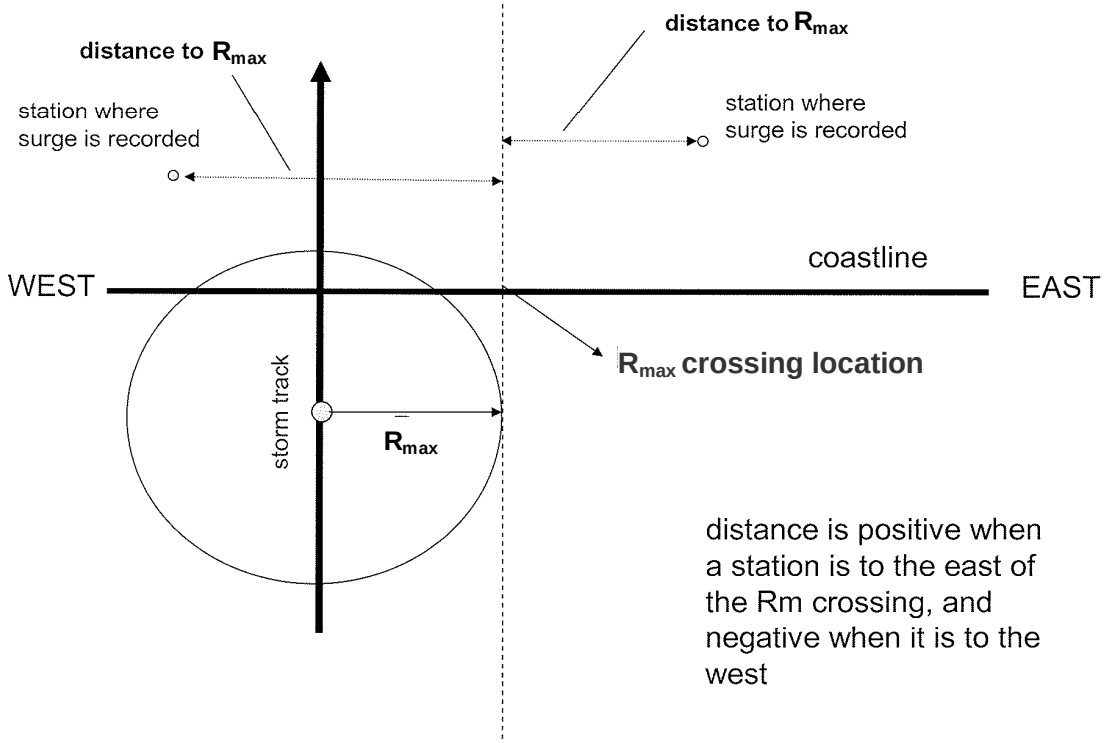

Figure 3-31. Distance Convention for Revised Analysis of Radius to Maximum Wind Sensitivity.

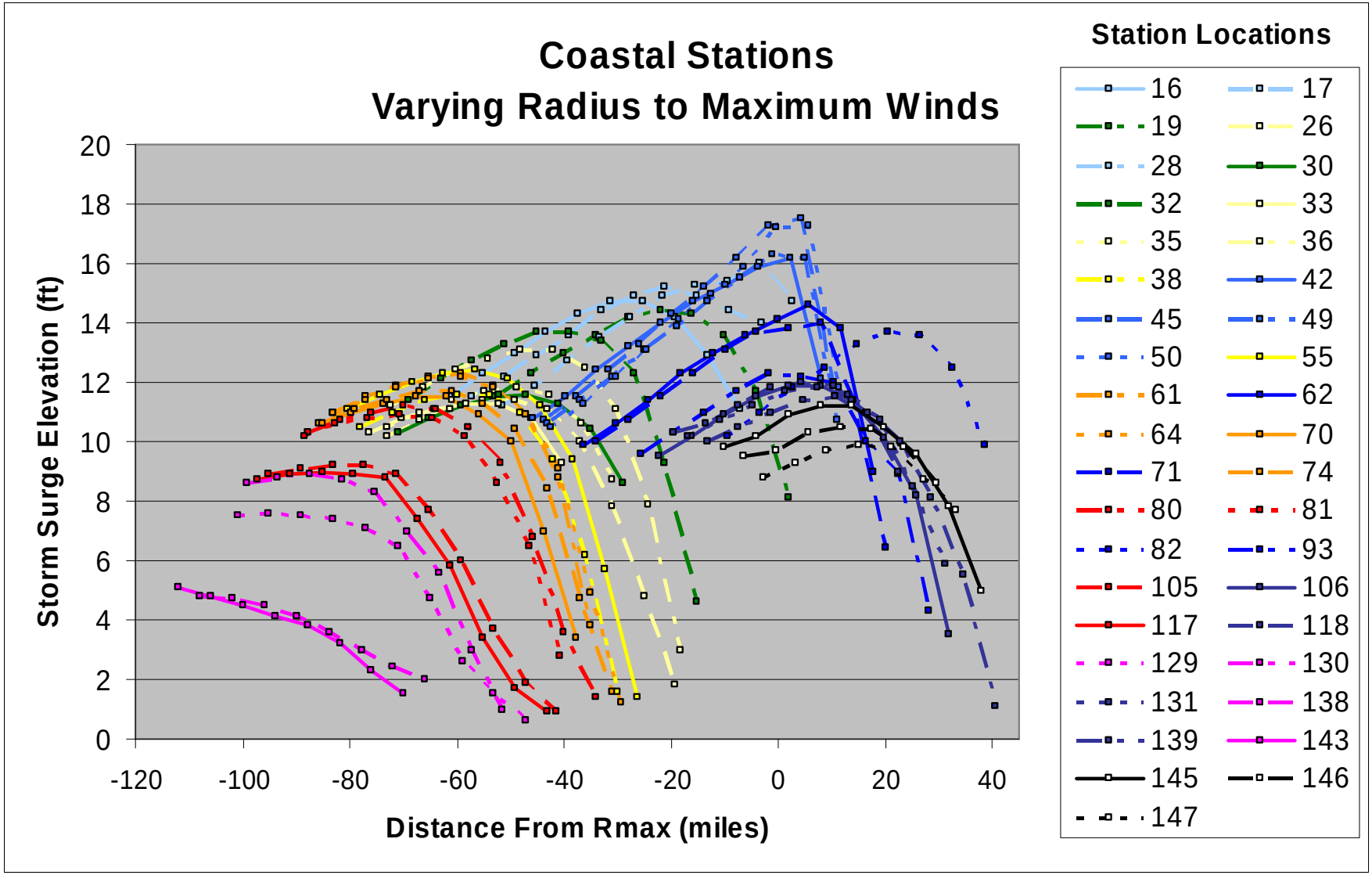

Figure 3-32. Coastal Stations Varying Radius to Maximum Winds.

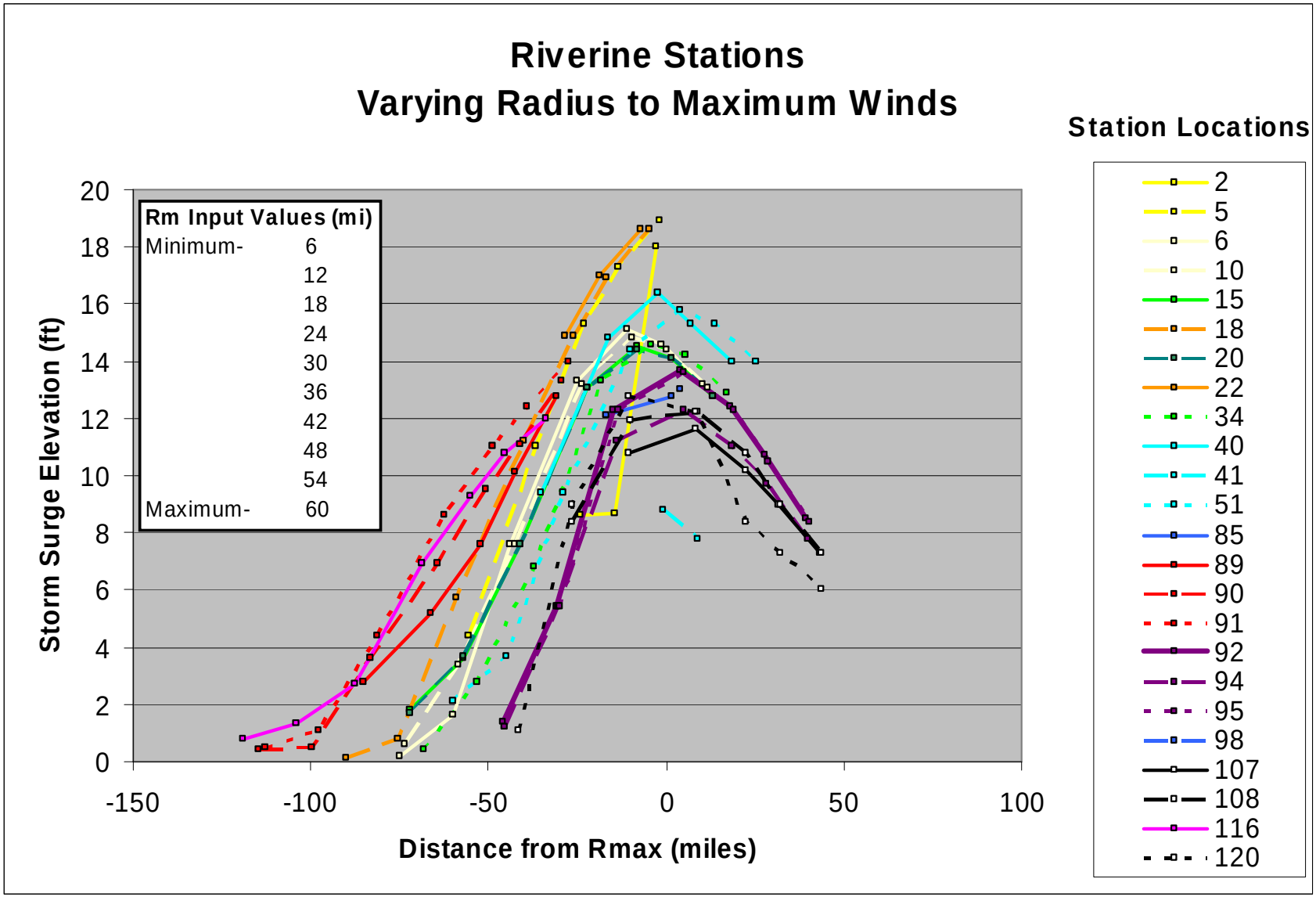

Figure 3-33. Riverine Stations Varying Radius to Maximum Winds.

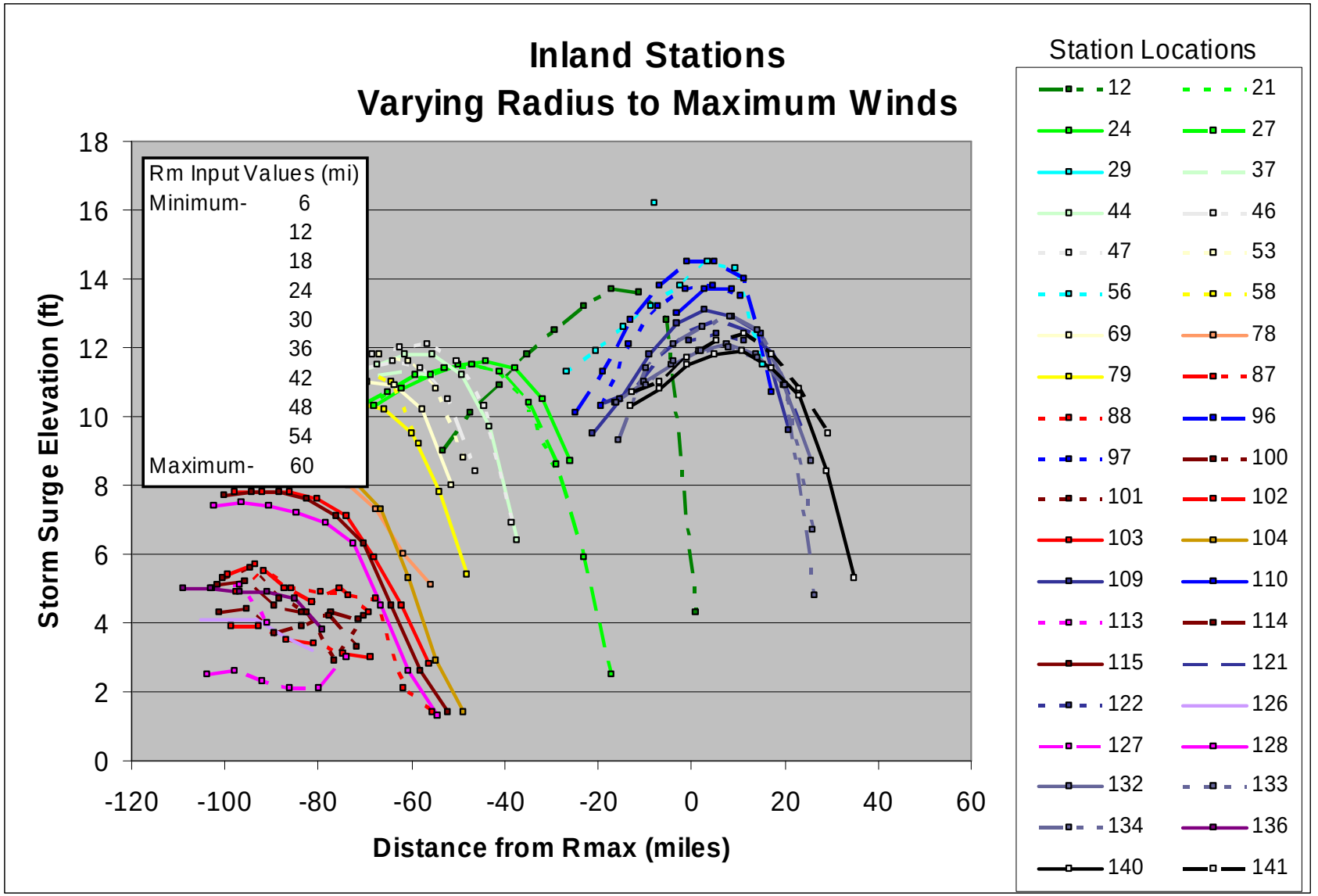

Figure 3-34. Inland Stations Varying Radius to Maximum Winds.

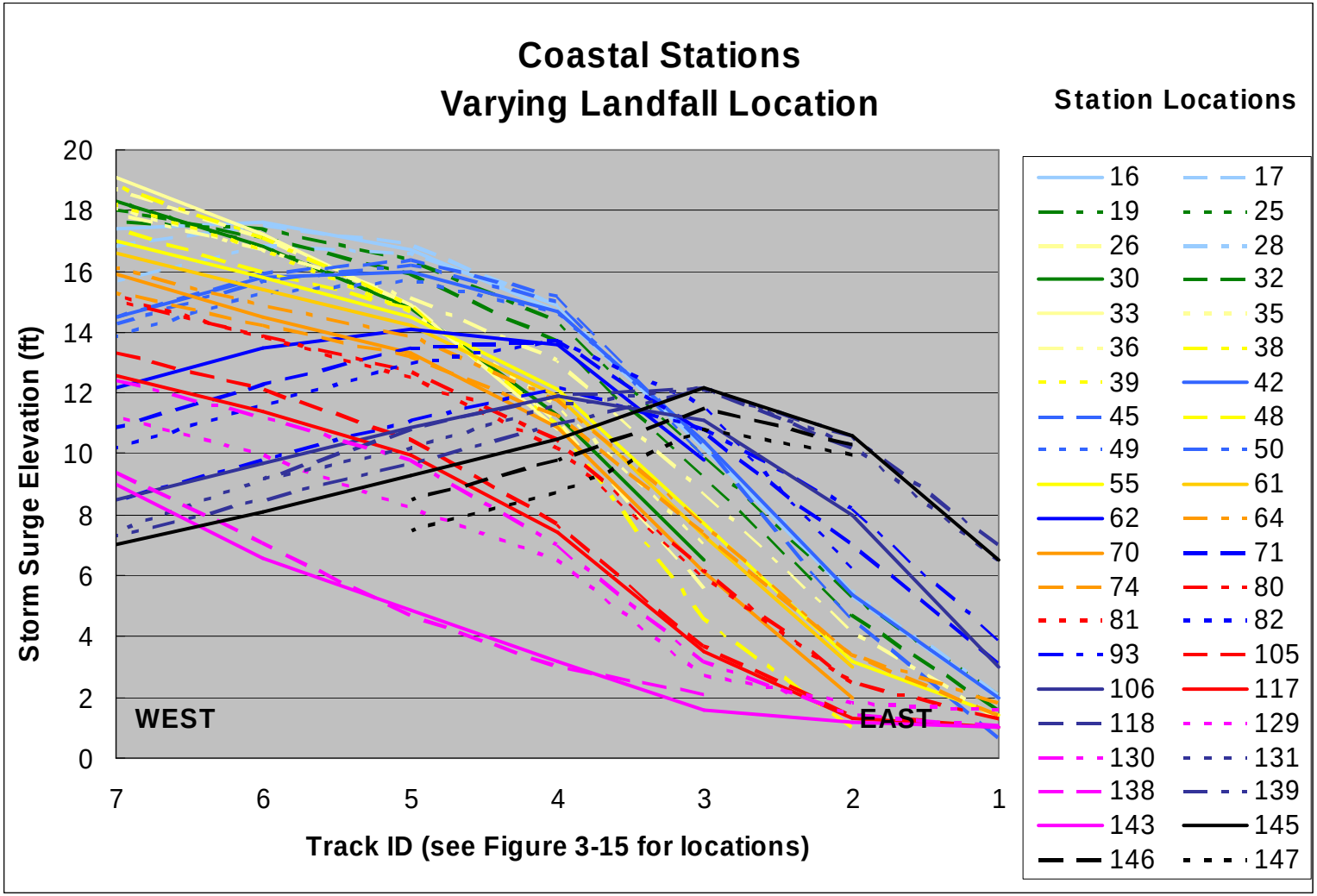

Figure 3-35. Coastal Stations Varying Landfall Location.

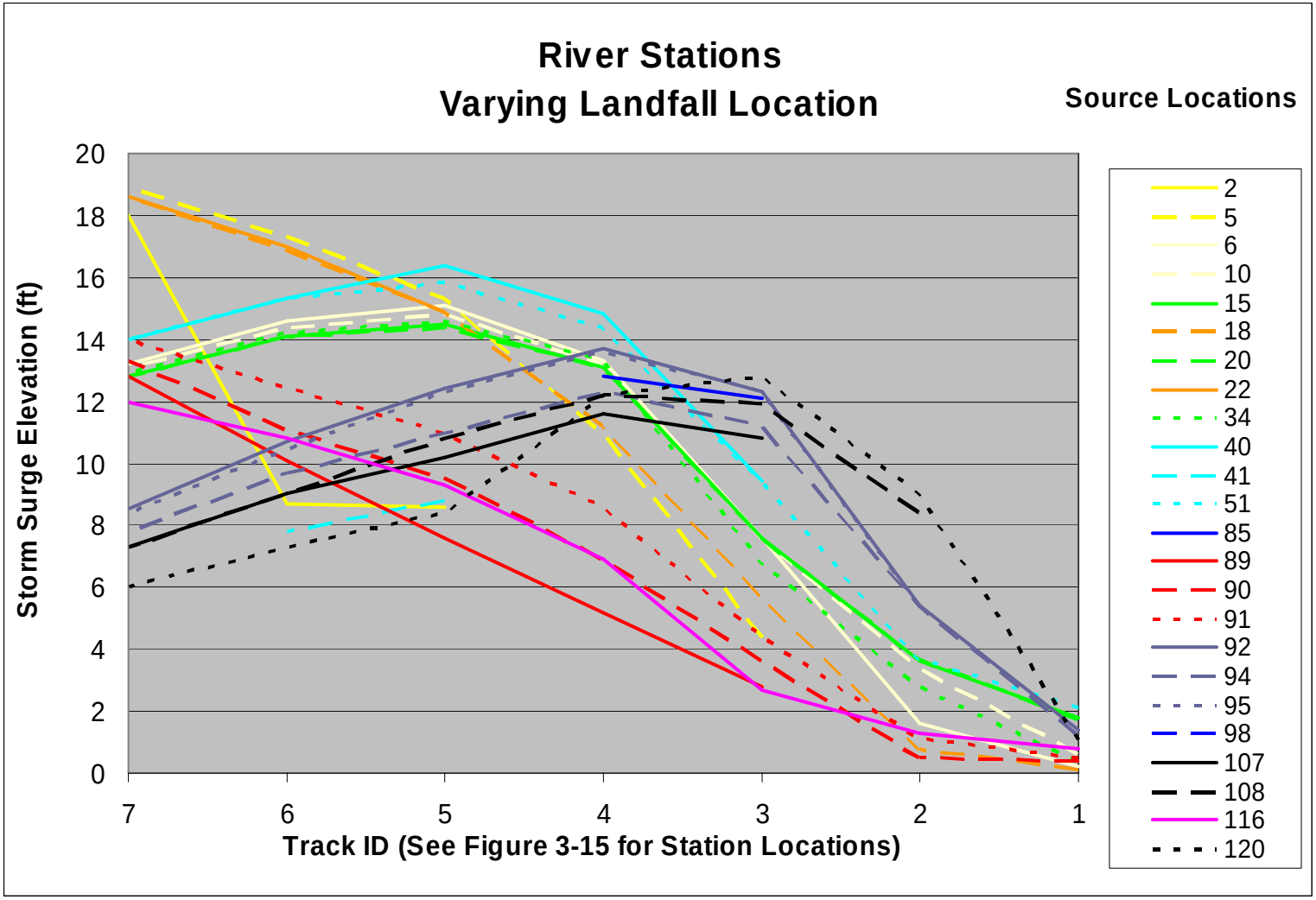

Figure 3-36. Riverine Stations Varying Landfall Location.

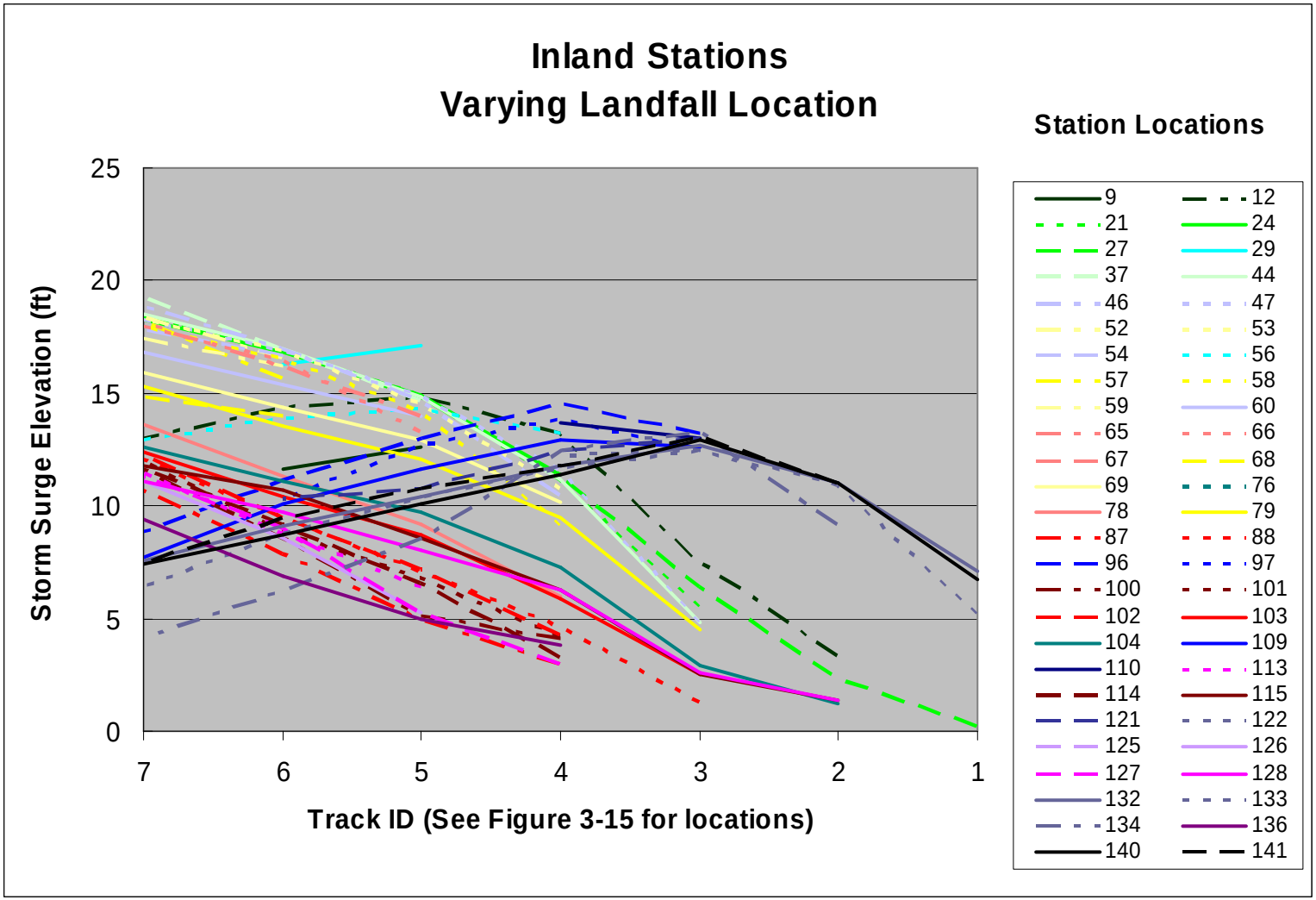

Figure 3-37. Inland Stations Varying Landfall Location.

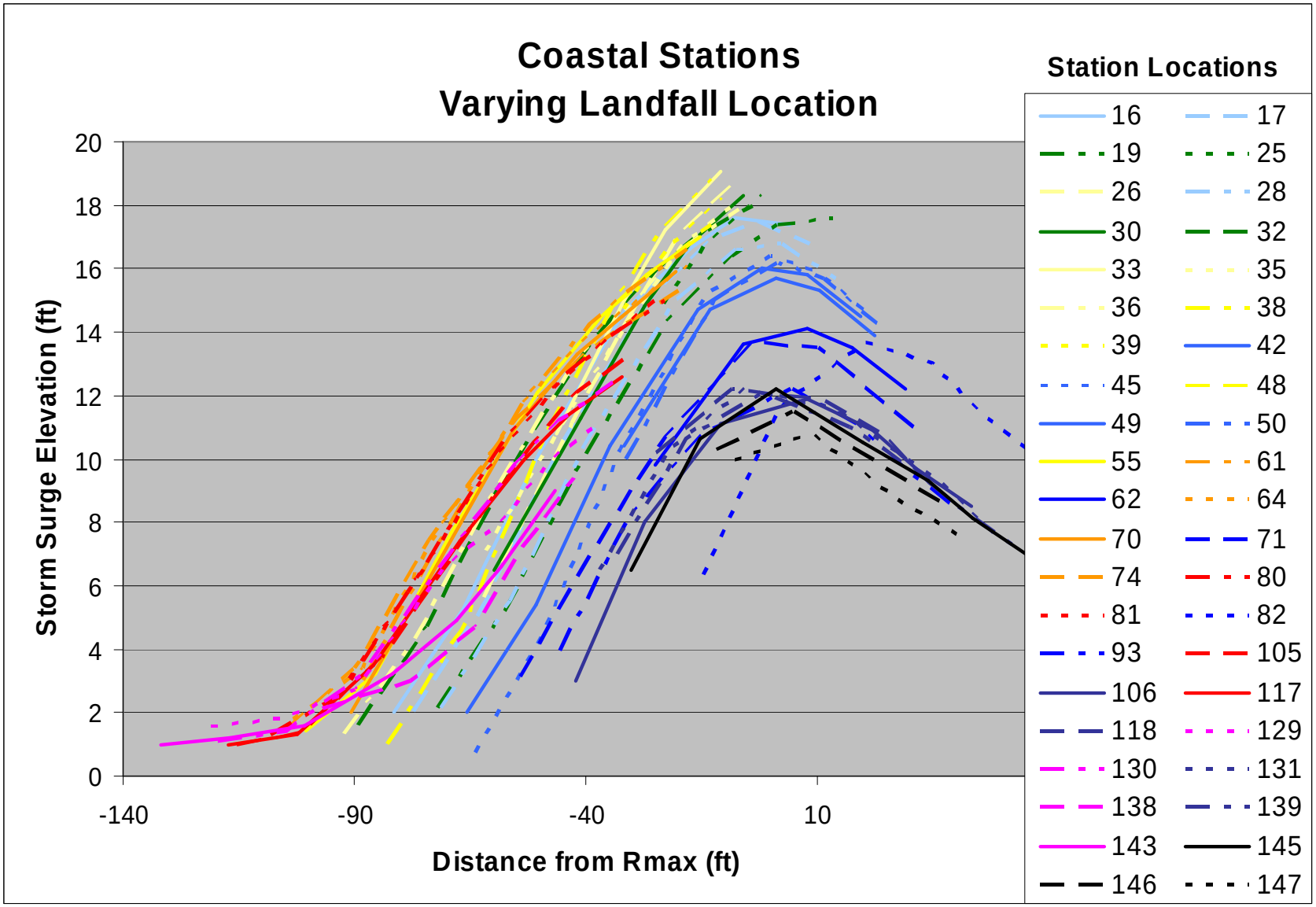

Figure 3-38. Coastal Stations Varying Landfall Location.

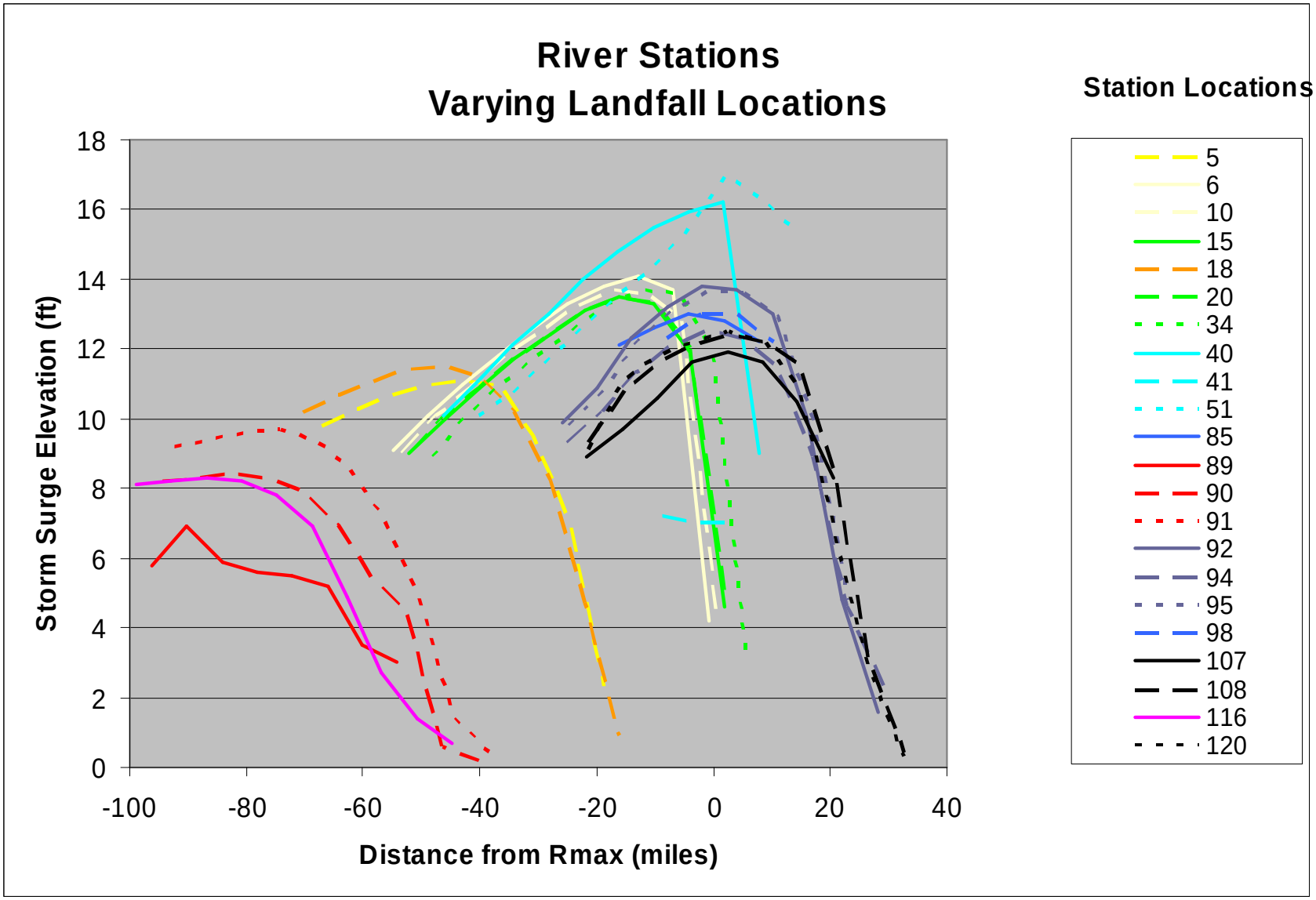

Figure 3-39. Riverine Stations Varying Landfall Location.

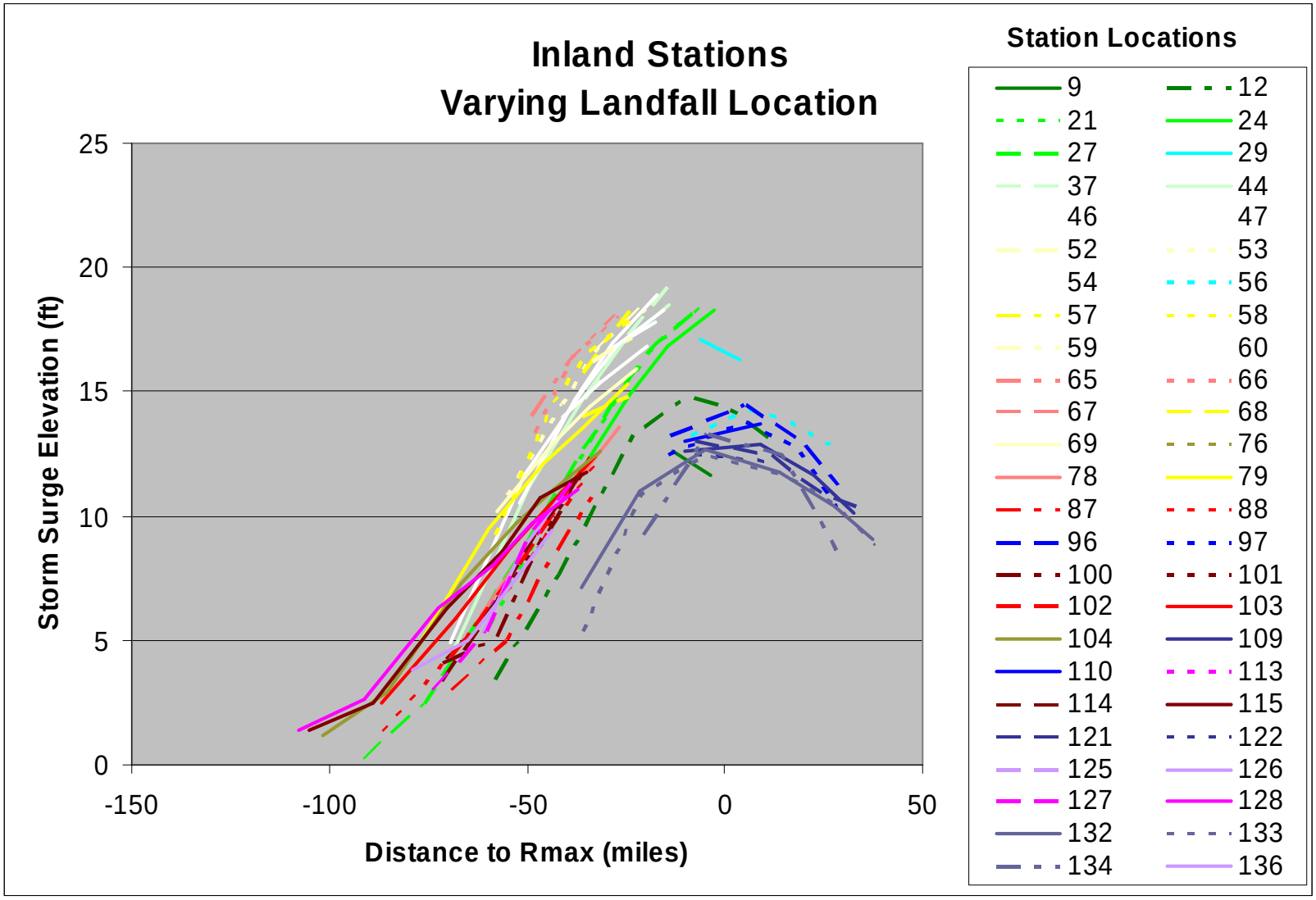

Figure 3-40. Inland Stations Varying Landfall Location.

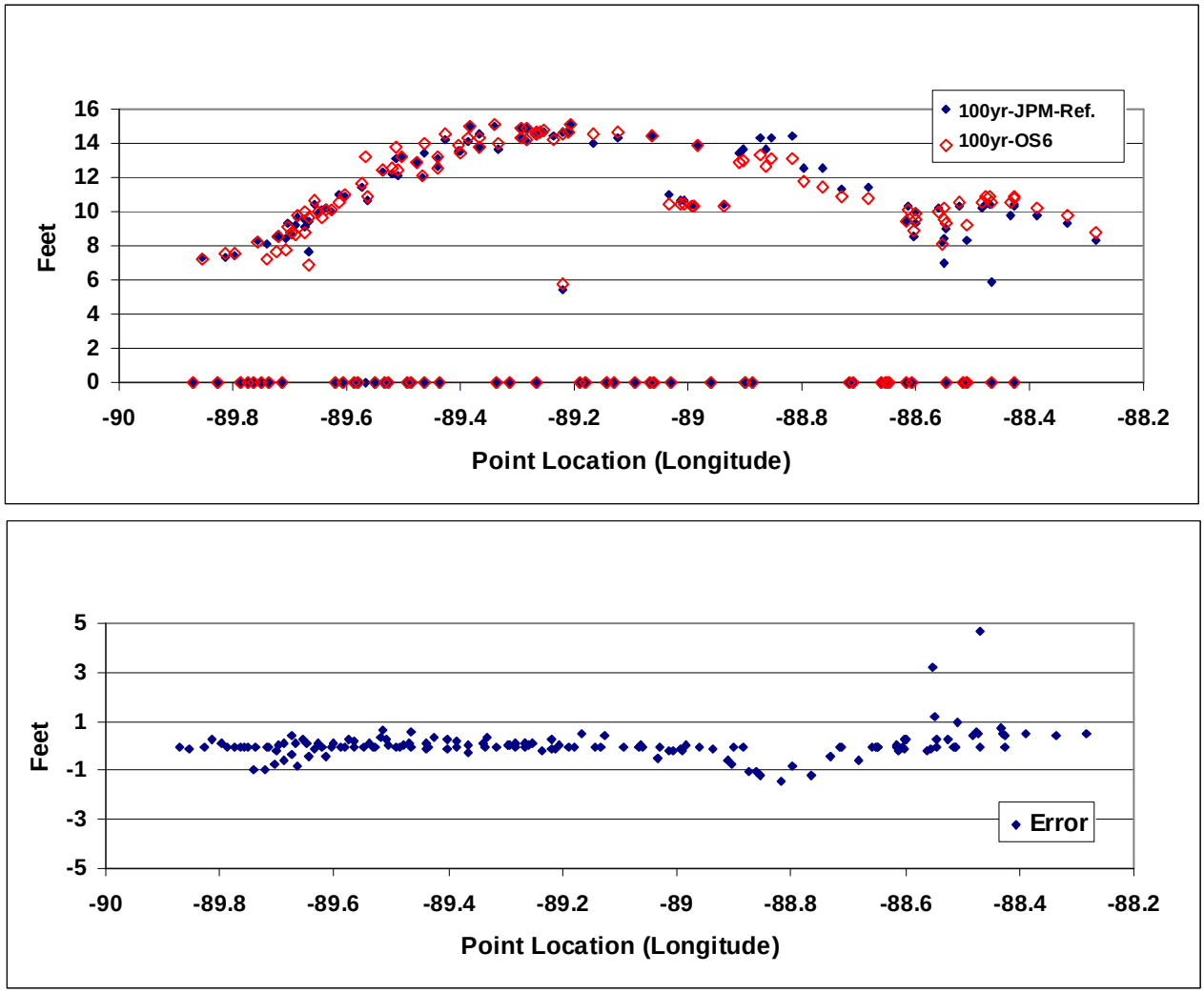

Figure 3-41. Comparison of Surge Elevation JPM-OS-6 with JPM-Reference (top) and Error Between Surge Elevations in JPM-OS-6 and JPM-Reference (bottom).

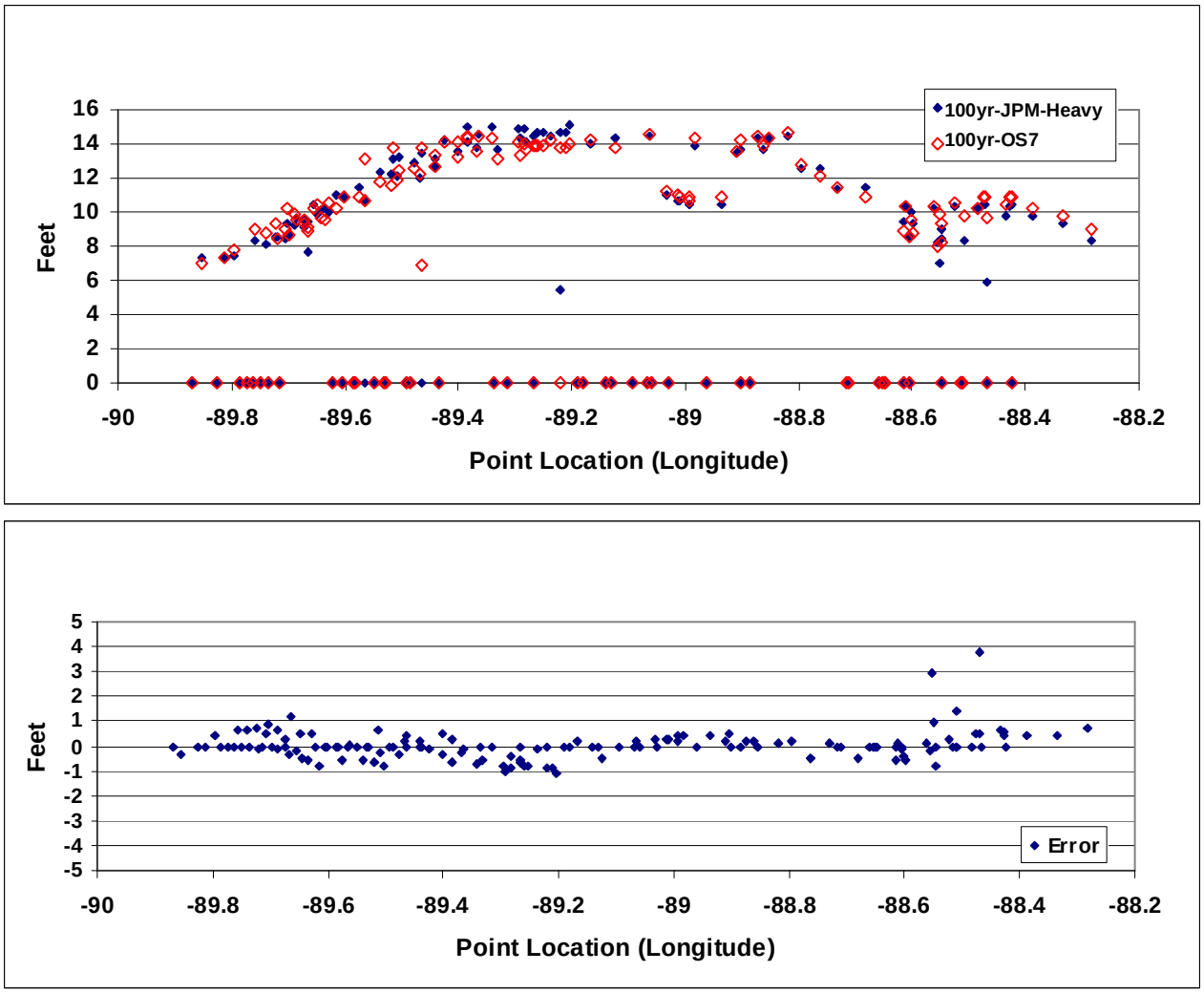

Figure 3-42. Comparison of Surge Elevation JPM-OS-7 with JPM-Reference (top) and Error Between Surge Elevations in JPM-OS-7 and JPM-Reference (bottom).

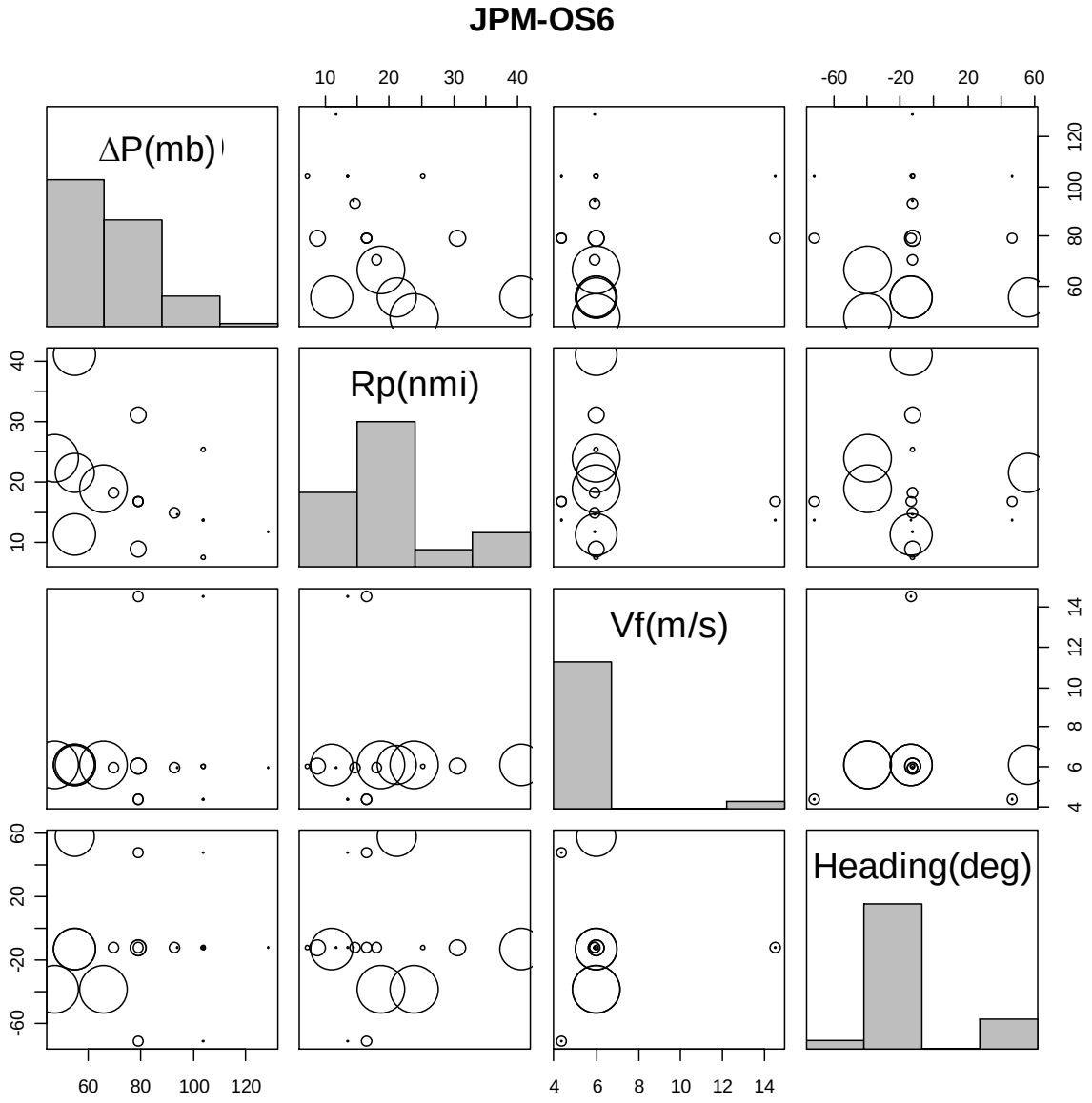

Figure 3-43. Graphical Representation of the JPM-OS-v6 Scheme for One Landfall Location.

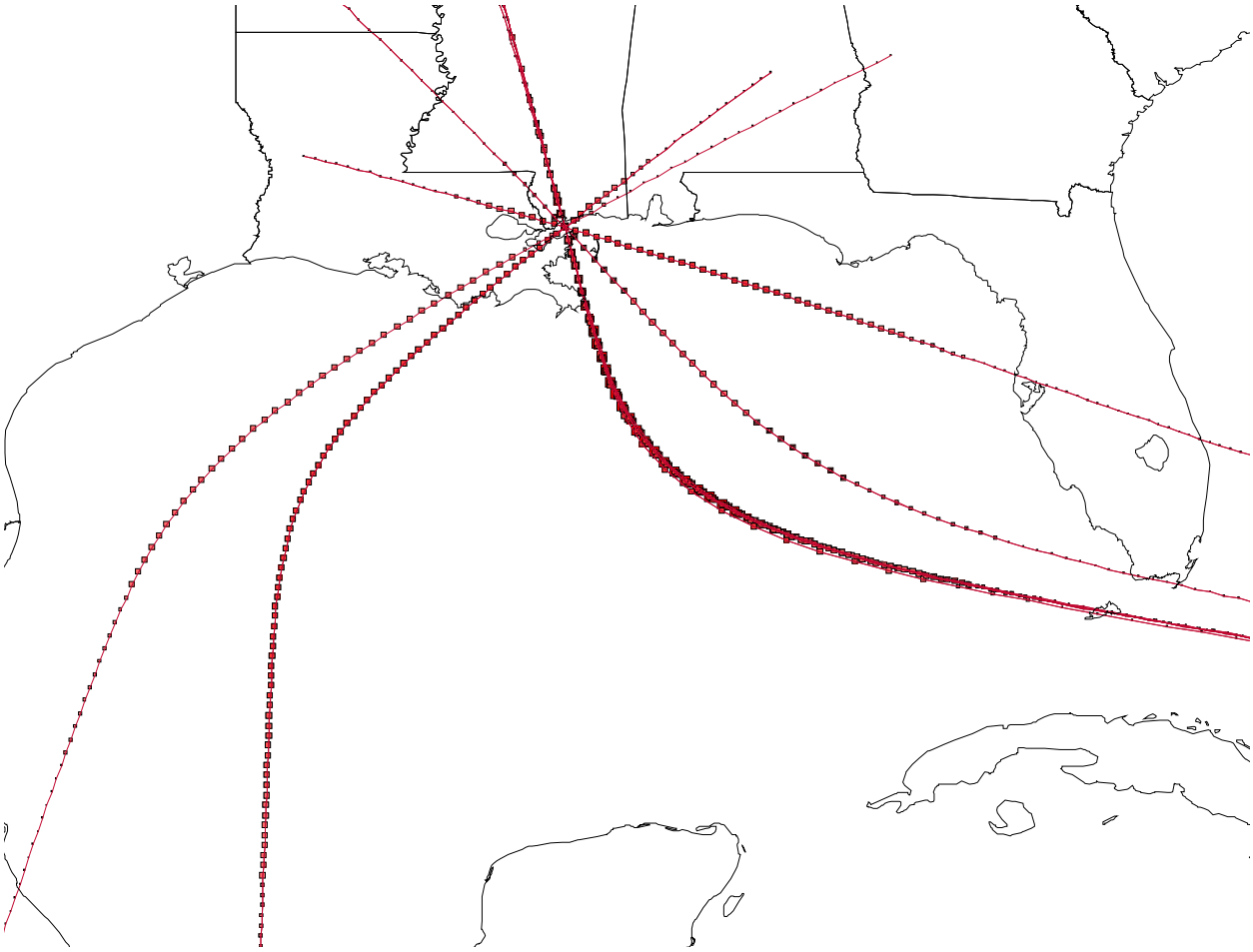

Figure 3-44. Sequential Positions (dots) Along the Master Tracks of the Synthetic Storms in the JPM-OS Representation of the Greater Storms.

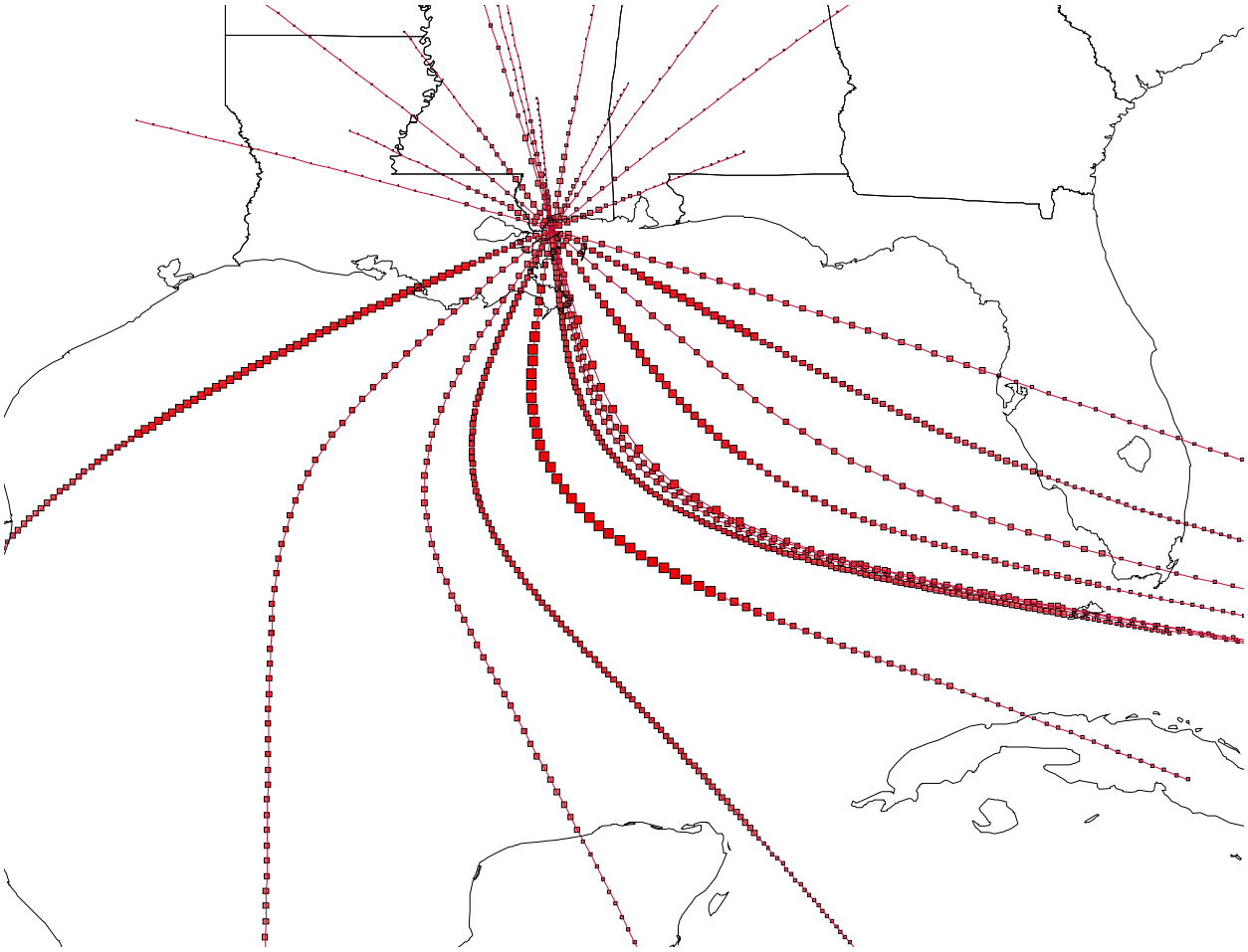

Figure 3-45. Sequential Positions (dots) Along the Master Tracks of the Synthetic Storms in the JPM-OS Representation of the Lesser Storms.

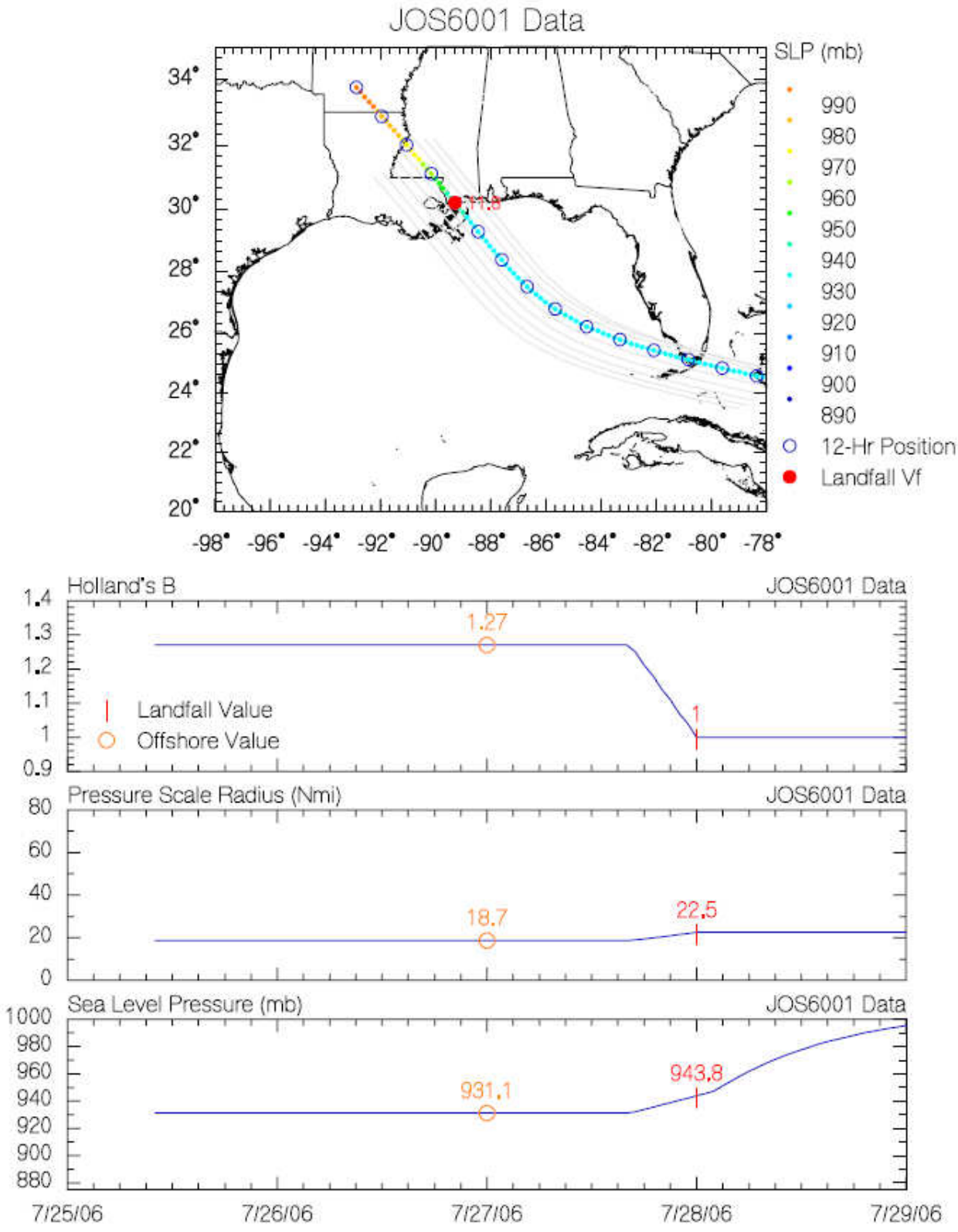

Figure 3-46. Track and Evolution of Storm Parameters for One Synthetic Storm.

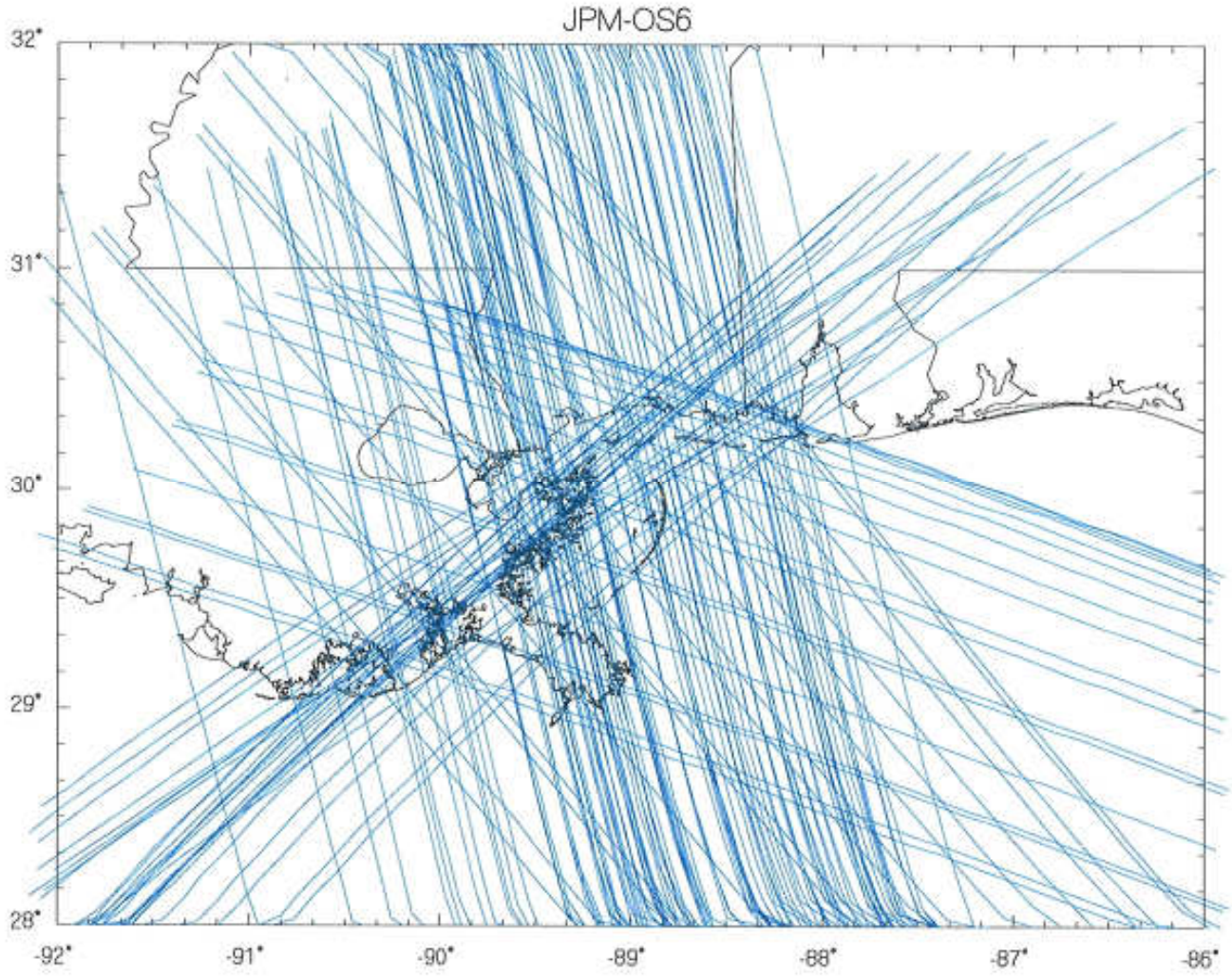

Figure 3-47. Track Paths for the 152 JPM-OS-6 Storm Set.

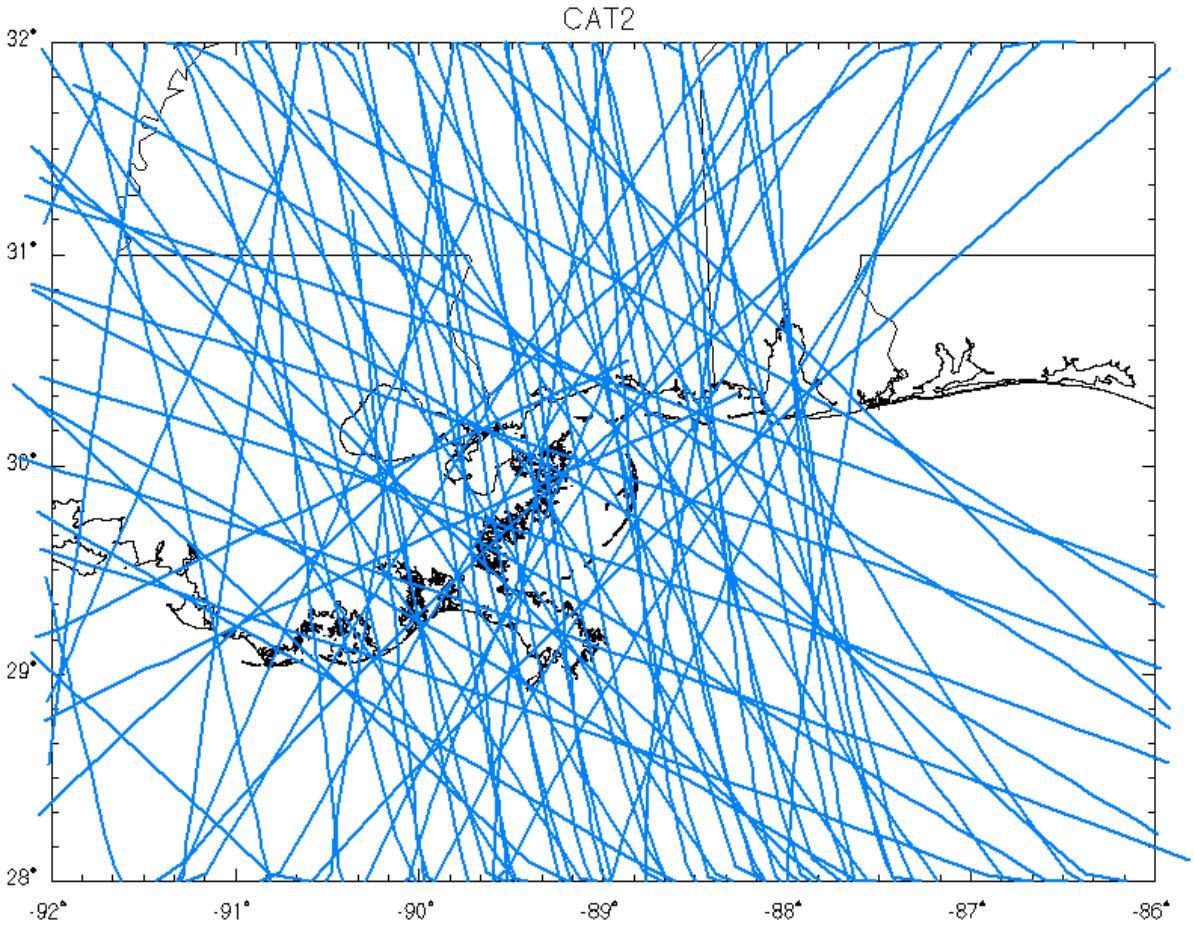

Figure 3-48. Track Paths for the 76 Category 2 Storm Set.

4.1 NUMERICAL MODELS

4.1.1 Introduction

As discussed in Section 3.4, numerical modeling was used to determine the maximum surge elevation caused by each synthetic storm at 7,898 points across the Mississippi coastal zone. This permitted evaluation of the function given by Equation 9. The series of 228 synthetic storms defined as JPM-OS-6 were simulated in the multi-component numerical model framework. For convenience, the term framework is used in referring to the whole sequence of numerical models that include the PBL (TC96), WAM (OWI-3 G), SWAN (ver. 40.51), and ADCIRC (ver. 46.52-03) models. The major numerical models used in this project are briefly described below without reference to their use. Sources of additional information on these models are also identified. These brief descriptions are followed by more detailed chapter sections covering the setup and operation of each model, how each was calibrated or verified (or both), and how the whole framework was used. The NOAA SLOSH model, which was used in some of the auxiliary simulations, was explained in Section 3.2.1.

4.1.2 Numerical Model Framework

The simulations of each of the synthetic storms involved developing time-varying representations of:

1) Hurricane wind and atmospheric pressure fields along pre-determined tracks
2) Wave conditions in the deep Gulf of Mexico
3) An initial estimate of the surge elevations to support nearshore wave modeling
4) Waves and surf zone conditions near and across the flooded mainland and barrier island zones
5) Wave setup
6) Overland flooding (surge plus wave setup)

This sequence is similar to the approach used by many past coastal flood hazard analyses. It differs from previous FEMA methods in that the wave setup is directly included in the representation of storm surge from each of the synthetic storms. This change permits the effect of the wave setup to be included directly into the statistical analysis of the stillwater elevations.

Figure 4-1 shows a flow chart of the model framework. Although this made for good compatibility between the project needs and capabilities, it also made it necessary to check the work at each stage. The specifications for each synthetic storm, defined by a unique set of the five basic storm parameters, and of the tracks for the model runs, were developed by Risk Engineering. These were transmitted to OWI. The OWI version of the PBL model was used to develop data files with time series of the moving wind and atmospheric pressure. OWI transmitted these output files to both D. Slinn and URS. OWI also used these files as inputs to their version of the WAM model (WAM –OWI13 G) to create files representing the deep Gulf wave conditions over the course of each storm. The outputs of the WAM modeling were transmitted to D. Slinn. The WAM results were input into the SWAN model to continue tracking the storm waves in nearshore and shallow water areas.

The model simulations of nearshore wave conditions required an estimate of the time history of surge levels over the duration of each synthetic storm. This estimate was made by applying the PBL storm meteorological outputs to a streamlined ADCIRC model and grid. This streamlined ADCIRC model had been reduced to a total of about 50,000 nodes so that it could run much faster than the full ADCIRC model. The streamlined ADCIRC model produced files with the time series of the surges for each synthetic storm, which were then passed to the SWAN models along with the PBL meteorological and deep Gulf wave inputs. The output of the SWAN modeling was a time series file of the radiation stress forcing needed as an input to the main ADCIRC model. Finally, the files from the PBL and SWAN models were input into the main ADCIRC model. This final ADCIRC modeling was carried out at the parallel cluster computing facilities.

The following subsections describe the elements of the model framework system used in this project. Detailed supporting project reports provide much more detail about each model and each step in the modeling process.

4.1.3 Planetary Boundary Layer (PBL) Model

The PBL model, also called the Tropical Boundary Layer model, is an application of a theoretical model of the horizontal airflow in the boundary layer of a moving vortex. This model can provide a description of the time-space evolution of the surface winds in the boundary layer of a tropical cyclone given the simple model parameters available in historical storms. This model solves, by numerical integration, the vertically averaged equations of motion that govern a boundary layer subject to horizontal and vertical shear stresses. The equations are resolved in a Cartesian coordinate system, whose origin translates at constant velocity, V_f, with the storm center of the pressure field associated with the hurricane. Variations in storm intensity and motion are represented by a series of quasi steady-state solutions.

The model used in this study included two major upgrades to the original model given by Chow (1971). The first upgrade (Cardone et al. 1992) mainly involved replacing the empirical scaling law with a similarity boundary layer formulation to link the surface drag, surface wind, and the model's vertically averaged velocity components. The second upgrade (Cardone et al. 1994) added spatial resolution and generalized the pressure field specification. A more complete description of the theoretical development of the model as upgraded is given by Thompson and Cardone (1996).

The model is driven by parameters derived from data in historical meteorological records. The outputs are time-histories of the wind and pressure fields. The evolving wind field is computed from pre-determined variations of the meteorological parameters along the storm track. These computations result in "snapshots," that are evaluated as often as is necessary to describe different stages of storm intensity, and then interpolated to form the entire time history of the hurricane.

The model pressure field is described as the sum of an axially symmetric component and a large-scale pressure field of constant gradient. This symmetric component is described in terms of an exponential pressure profile, which has the following parameters:

- P_o = minimum central pressure
- P_{far} = far-field pressure

- R_p = scale radius of exponential pressure profile
- Holland B = profile peakedness parameter

Holland B is an additional scaling parameter whose significance was discussed by Holland (1980). As noted in Section 3.2.4.6, this parameter was not included among the basic five parameters. However, as explained in the previous report sections it was accorded special treatment to account for spatial gradients in the shore-approach zone.

The model is maintained by OWI.

4.1.4 SWAN Model

The SWAN model is a non-stationary third-generation wave model (Holthuijsen et al. 1993; Ris 1997). The SWAN model is based on a numerical solution of the discrete spectral action balance equation and is fully spectral over the total range of wave frequencies and over the entire 360° range. The wave propagation is based on linear wave theory including the effect of currents. The processes of wind generation, dissipation, and nonlinear wave-wave interactions are represented explicitly with state-of-the-art, third-generation formulations. The fully spectral attribute provides for the simulation of short-crested, random wave fields propagating simultaneously from widely varying directions. SWAN simulates the following physical phenomena:

- Wave propagation in time and space
- Shoaling
- Refraction due to current and depth
- Frequency shifting due to currents and non-stationary depth
- Wave generation by wind
- Nonlinear wave-wave interactions (both quadruplets and triads)
- Whitecapping, bottom friction, and depth-induced breaking
- Blocking of waves by current

Note that neither reflection nor diffraction is explicitly modeled in SWAN, but diffraction effects can be simulated by applying directional spreading of the waves.

The SWAN computations can be made on both a Cartesian and a curvilinear grid in a Cartesian coordinate system. Nested runs can be made with the regular grid option. Efficient computing times are achieved in practical applications by using a fully implicit propagation scheme (in time and space). SWAN provides many output quantities including two-dimensional spectra, significant wave height and mean wave period, average wave direction and directional spreading, root-mean-square of the orbital near-bottom motion, and wave-induced force (based on the radiation-stress gradient).

4.1.5 ADCIRC Model

ADCIRC is a numerical model developed for simulating water level and circulation on continental shelves, at coastlines, and within estuaries (Westerink and Luettich 1991). The

model is based on a finite element in space and a finite difference solution in time to the Generalized Wave-Continuity Equation (GWCE) and the depth-integrated momentum equations. These equations have been formulated using the traditional hydrostatic pressure and Boussinesq approximations. They include the Coriolis and radiation stress gradient terms. The finite element method in space allows for the use of highly flexible, unstructured grids, providing for very high-resolution of bathymetry and topography along complex coastlines and inland bays and estuaries. ADCIRC can be run using either a Cartesian or a spherical coordinate system.

ADCIRC can be forced with elevation boundary conditions, normal flow boundary conditions (river inputs), surface stress boundary conditions (wind fields), and tidal potentials. Documentation for the model is available online at http://www.adcirc.org/index.htm.

Two varieties of the ADCIRC model were used. A serial version was used to support the nearshore wave analyses. A much more detailed set of hydrodynamic model runs were carried out on a version for use on a parallel-cluster computer platform. Unless otherwise noted, reference to the ADCIRC model means this parallel version.

These models are supported by USACE and their authors.

4.2 MODEL SETUPS

Each of the three main numerical models used in this study had its own model grid. These grids supported the cascade of modeling needed for the complete analysis. The PBL model output drove the ADCIRC models and the WAM wave model. The SWAN model was used in order to include depth-dependent wave transformations approaching the shore nested grid for the SWAN model where needed. These grids are described below.

4.2.1 The PBL Grid

For this study, OWI. developed wind velocity and barometric pressure fields 10 meters above the water surface using PBL, a tropical cyclone model (Thompson and Cardone 1996). PBL model uses two nested grids. The basin scale grid (18-30.8N 98-80W) has a resolution of 0.1 degree and the Regional scale grid (28.5-30.75N 91-88W) has a resolution of 0.025 degree.

4.2.2 The WAM Grid

In addition to providing the wind and pressure fields for hurricanes, OWI operated its third-generation wave model (OWI13 G). The OWI13 G model was set up on a 6 nmi grid covering the Gulf of Mexico. Wave model spectra were archived at 54 grid point locations along the agreed boundary of the SWAN modeling. The supporting project report titled *Hindcast Wind and Waves Forcing in Support of the URS FEMA Mississippi Coastal Flood Map Update* contains more detail about these grids and model setup.

4.2.3 The SWAN Grids

To develop the input files for the ADCIRC model, which represent the radiation stress gradients due to breaking waves, a series of nested grids for the SWAN model needed to be set up. This model was operated on grids of two scales. A regional grid extended from the shoreline to approximately 200 km offshore. This grid was about 300-km wide and centered on the

Mississippi coast. This regional grid had a resolution of 2.5 km and did not extend overland. The spectral ocean wave model was set up to interface with the regional grid of the SWAN model at 54 points along the mutual boundary.

To calculate the actual gradients of the wave radiation stresses at 15-minute time intervals, a series of nine detailed SWAN model grids were set up along the Mississippi shoreline. These detailed grids extended inland to the expected limit of surge inundation. Their resolutions were 180 m in the shore normal direction and 160 m in the longshore direction. They extended 54 km offshore and were 24 km across. Adjoining grids overlapped.

These grids and the model setup are described in more detail in the supporting project report titled *Wave Setup Methodology for the FEMA Mississippi Flood Study*.

4.2.4 The ADCIRC Grid

Unlike the other models, the ADCIRC grid has an open mesh triangular structure. Before the Mississippi Coastal Analysis Project started, an elaborate ADCIRC grid for the region had been developed in several stages by a group at Notre Dame University under the direction of Dr. Joannes Westerink. That effort was started in the early 1990s for the USACE studies of tides. Over a period of years, this grid development effort expanded to storm surge simulations in Louisiana resulting in an evolutionary growth of the grid for areas in the Gulf of Mexico. At the time that the Mississippi Coastal Analysis Project began, this grid had approximately 400,000 nodes. The open ocean boundary ran along a straight line between Nova Scotia and Venezuela so that the western North Atlantic, the Caribbean Sea, and all of the Gulf of Mexico were incorporated. This version of the ADCIRC grid covered some of the inland areas of Mississippi (Grid Versions TF01-v6), which was made available as a starting point for the Mississippi Coastal Analysis Project. However, the near-coastal and overland portions of this grid were not of adequate quality for this project.

The URS Team developed a detailed ADCIRC grid covering the area of the three coastal counties of Mississippi, Mississippi Sound, the barrier islands, and a portion of the Gulf of Mexico. The latitude of 30º13'N, located seaward of the barrier islands, marked the southern limit of this new grid. This new grid was married into the existing ADCIRC grid representing the western North Atlantic, Caribbean Sea, open Gulf of Mexico, and overland areas outside of the boundaries of Mississippi. This resulted in a project-specific ADCIRC grid designated as MS11-g.

The MS11-g grid has a nominal minimum spacing of 80 m. Because an automated gridding routine was used, some grid elements were slightly smaller. The overall grid spacing was variable from this lower limit, used to resolve detailed features, to an upper limit of 500 m in the nearshore coastal and overland areas (it is up to about 45 km in the open Atlantic). These large grid elements were only used where the relief of the seafloor or land was very small. The Surface Water Modeling System (SMS) was used in the grid development process.

The shape of the coastal lands and the sea floor are represented in the ADCIRC model with an unstructured triangular finite-element grid. The elevations of the land or sea bed are at the nodes, which are the vertices of the triangles.

The water depths were taken from the data set compiled by the Northern Gulf Littoral Initiative (Sawyer et al. 2001). Most of the data had been surveyed by the National Ocean Survey and

Naval Oceanographic Office. Available data were augmented with information from NOAA Navigation Charts.

Data for the shoreline position and the land elevations were taken from Light Detection and Ranging (lidar) surveys by EarthData International, Woolpert, and USACE. Elevation data for the coastal areas, including the barrier islands, were available for both before and after Hurricane Katrina, with the oldest taken in March 2003. Hydrologic features, such as rivers, streams, and tidal creeks, were delineated from the lidar data. Lidar data were combined with aerial photographs to distinguish embankments and roadways more than 1 ½ ft above the surrounding ground that would affect overland flooding. The depths of waterways and rivers were determined from navigation charts, previous surveys, or were approximated through a method that relied on morphological similarity. A number of river and stream cross-sections were available from earlier FEMA river flood studies. Where these data were missing, the stream depths were estimated by comparing measured depths for steams with the same stream order based on the Strahler stream ordering system (Chorley, 1972).

The types and dimensions of flow controlling structures, such as bridges, culverts, and similar structures, were either located in the archives of the Mississippi Department of Transportation or measured by field reconnaissance teams. A field reconnaissance was also carried out along the shoreline to map the seawall and similar features. The details of these data and their reduction are described in the supporting project report titled *HMTAP Task Order 18 Geospatial Technology Task Report*. The field reconnaissance is described in the supporting project report titled *HMTAP Task Order 18 Field Investigation of Continuous Seawall South Side of US Highway 90 in Mississippi and the ADCIRC Grid Development Report* (URS 2005). More detailed explanation of the field reconnaissance and the process of creating the ADCIRC grid are given in the supporting project report titled *Grid Generation Report*.

The ADCIRC unstructured triangular finite element grid required a variety of adjustments to overcome numerical instabilities that were experienced in some of the trial computer runs. It was discovered that it was necessary to distribute a minimum number of grid elements across narrow features, such as valleys, mounds, tidal creeks, and streams, for them to be properly recognized. Three grid elements were needed for streams and tidal water bodies, and five elements were needed for narrow relief features, such as stream valleys. As a consequence, minor topographic distortions were required. For example, rivers and creeks appear wider in the ADCIRC grid than on a map. The elevations of these grid nodes were adjusted to maintain approximately the same hydraulic radius. In some places, especially along the coast, these distortions were compounded by low relief and the required minimum spacing of grid nodes. When small low islands, low-lying coastal areas adjacent to waterways, and other features are spatially averaged the shape of the shoreline becomes generalized. Engineering judgment, based on experience with the minimal effect of these generalizations on the way the ADCIRC model computes the flows, was used to decide on the limits of topographic distortions in the grid.

The ADCIRC model has sub-grid element features to represent embankments and other linear narrow features. However, it does not have sub-grid element features to represent streams or ditches. Therefore, all streams that can be shown must be resolved by the grid elements. To accommodate this requirement, the details of the stream network were simplified to eliminate minor features. Positive relief features, such as embankments and roadways, were represented with weir sub-grid elements. Gaps were provided in the weirs for bridges and overpasses.

Some of the grid features were adjusted to accommodate wave setup in the hydrodynamic calculations. Wave setup is forced by breaking waves and must be represented on scales of 100 m or less. Therefore, where wave setup was expected to be significant, the ADCIRC grid was adjusted to have grid elements of corresponding size.

Auxiliary ADCIRC input files containing coefficients for surge flow drag (Manning's N), directional wind drag (boundary-layer roughness-lengths), and wind-blocking coefficients at each of the grid nodes in the MS11-g grid were developed (refer to the supporting project report titled *Summary of Work Performed by Ayres Associates in Support of URS Storm Surge Modeling for FEMA Region 4*). As explained in that report, special software was used to develop these coefficients from land use data based on the U.S. Geological Survey National Land Cover Dataset (USEPA, 2001, see http://edc.usgs.gov/products/landcover/nlcd.html) and the State-by-State Gap Analysis Study (see http://gapanalysis.nbii.gov). More details concerning these coefficients, their derivation, and applications can be found in the supporting project report titled *Grid Development Report*.

The final step in developing the MS11-g grid was performed by one of the ADCIRC model authors (Dr. Joannes Westerink of Notre Dame) who developed the detailed ADCIRC model grid for the USACE studies in Louisiana. To ensure that the Mississippi and Louisiana grids fit together into a seamless combination with similar properties, Dr. Westerink made final adjustments to some of the representations of detailed topography and flow-controlling structures. This resulted in a complete grid (SL-15) with good spatial resolution in coastal Mississippi and Louisiana that could be used for both USACE and FEMA projects.

The combined grid has a total of 2.13 million nodes. However, a great many of these nodes were located in overland portions of western and central Louisiana (because of the USACE needs) and these places, west of the Mississippi River, were of only limited interest to the Mississippi study. Therefore, the ADCIRC grid was de-refined for coastal and inland locations west of the Mississippi River for the final evolution of the MS11-g grid. The final grid was reduced to 900,450 nodes. The effect of this de-refining was to reduce the time required to perform a single storm simulation (wall clock run time of the parallel cluster) from 17 hours to 7 hours, which saved approximately 80 days in the project schedule. The de-refining process specifically avoided changing any of the ADCIRC grid nodes in the places east of the Mississippi River.

A more complete discussion of the MS11-g grid can be found in the supporting project report titled *ADCIRC Grid Generation Report*.

In addition to the MS-11g ADCIRC grid, a lower resolution grid was also developed and used for SWAN wave modeling. This ADCIRC grid had about 58,000 nodes and did not extend over land.

The model domain is the North West Atlantic Basin, including the Caribbean Sea and the Gulf of Mexico. Spatial resolution of the mesh ranges from a node spacing of approximately 160 km in the Atlantic Ocean to roughly 6 km element sizes along the northern Gulf Coastal boundaries. The use of this model grid is explained in Section 4.4.1.1 of this report and in the supporting project report titled *Wave Setup Methodology for the FEMA Mississippi Flood Study*.

4.3 CALIBRATION AND VERIFICATION OF MODELS

4.3.1 PBL Model Calibration and Validation

The PBL model was originally validated against winds measured in several storm studies by the offshore industry as part of the Ocean Data Gathering Joint Industry Project (ODGP). It has since been applied to nearly every recent hurricane affecting the U.S. offshore area, to all major storms affecting the South China Sea since 1945, and to storms affecting many other foreign basins including the Northwest Shelf of Australia, Tasman Sea of New Zealand, Bay of Bengal, Arabian Sea, and Caribbean Sea. Comparisons with over-water measurements from buoys and rigs support an accuracy specification of ± 20 degrees in direction and ± 2 meters/second in wind speed (1-hour average at 10-meter elevation). Many comparisons have been published (see e.g., Ross and Cardone 1978; Cardone and Ross 1979; Forristall et al. 1977; 1978; Forristall 1980; Cardone et al. 1992; and Cardone and Grant 1994).

4.3.2 ADCIRC Calibration and Validation

The model was calibrated for Hurricane Katrina (2005) and then validated for Hurricanes Betsy (1965) and Camille (1969). For each storm, measured high water marks (HWMs) were used as a basis for comparison with the ADCIRC simulation results. Wind and tide inputs taken from the historic data represented each storm. The measured and simulated peak surge values at each measurement point were compared to quantify the calibration and validation.

The wind field used to represent the Katrina storm was provided by OWI., and the details of that wind field can be found in the supporting project report titled *Hindcast Wind and Wave Forecasting in Support of URS FEMA Mississippi Coastal Flood Map (Update)*. Wind fields for both Camille and Betsy were also provided, but are of lesser quality due to the reduced availability of data for those wind fields.

Measured Data

Observed surge elevations for Hurricane Katrina were available from FEMA and the USGS. Shortly after landfall of Hurricane Katrina on August 29, 2005, URS team identified and surveyed 312 coastal high water marks (CHWMs) in the three coastal counties of Mississippi. The USGS identified an additional 90 CHWMs. These data were reviewed and used for Katrina calibration (FEMA 2006).

Storm surge elevation data for Hurricanes Betsy and Camille were collected from several sources (NOAA 1997, USACE 1965). Table 4-1 lists the various storm surge elevation data sources and their reported datum.

Table 4-1. Storm Surge Data Sets Used to Verify the ADCIRC Model for Hurricanes Betsy and Camille Simulations.

HWM Elevation Data Source	Reported Datum	Exact HWM Coordinates Given in Report	Hurricane
NOAA, 1992	National Geodetic Vertical Datum of 1929 (NGVD29), (ft)	Map	Betsy and Camille
USACE, 1965	Mean Sea Level (MSL) (ft)	Table of Coordinates	Betsy
URS, 2006	NAVD29 (ft)	Map and Table	Katrina

The project datum is North American Vertical Datum of 1988 (NAVD88) and all of the observed data not already referenced to this datum were converted using the NOAA Tides and Currents Web site (NOAA 2005), as well as National Geodetic Survey (NGS)-published benchmarks.[5] The differences between MSL, NGVD29, and NAVD88 were determined at 17 tidal stations along the Mississippi coast and used to convert the observed elevations to NAVD88.

The observed elevations were reviewed to determine if they were suitable for use in the ADCIRC model calibration. In some instances, one surge elevation within a small and uniform geographical area was significantly different than those in the surrounding area. If there was no obvious cause, these points were removed from the dataset. The effect of wind-generated waves on the surge values was also considered. The model calibrations represented the hurricane surge and the effects of wave-induced setup due to radiation stress forces, but not peak water elevations due to wave amplitudes. Therefore, each observation point was reviewed to determine if it was sufficiently sheltered from wind-generated waves such that the observed HWM represented the stillwater surge elevation. Any points that were likely affected by surface waves were removed from the data set. The locations of the observations and the final elevations referenced to NAVD88 used in the calibration and validation are shown in Figures 4-2 through 4-4 for each of the three calibration storms. Observation points for Hurricane Katrina are shown in Figures 4-2a, 4-2b, and 4-2c; observation points for Hurricane Camille are shown in Figures 4-3a, 4-3b, and 4-3c; and observation points for Hurricane Betsy are shown in Figures 4-4a, 4-4b, and 4-4c.

ADCIRC Calibration

The PBL model wind and pressure field time series files for Hurricane Katrina from OWI had been extensively hand-crafted to maximize agreement with a wide variety of measurements from satellites, Doppler radar, ocean data buoys, Hurricane Hunter aircraft surveys, and other sources. Their work was instructive with respect to the degree that modern "hand-crafting" methods can improve the representations of the time-varying wind and pressure fields compared with early representations, for which good measurements were sparse. This points out that the major cause of systematic differences between the modeled surge heights and the measured CHWMs is most likely found in the wind and pressure field representations, especially for older storms.

[5] (www.ngs.noaa.gov)

The calibration of the ADCIRC model consisted of adjusting the friction parameters in a series of model simulations. Both Manning's N and the wind-drag coefficient were varied until a reasonable fit to the data was obtained. The calibration criteria were set by reviewing the variability in the measured data. The difference between the simulation and measured data need not be more accurate than the variability within the measured data. The calibration criteria used required at least 70 percent of the comparisons with the measured data to be less than 1.5 ft. The results of the calibration are shown in Figures 4-5 and 4-6. Figures 4-5a, 4-5b, and 4-5c show comparison maps of the measured and simulated peak surges in Hancock, Harrison, and Jackson Counties. The same data are summarized in Table B-1 (see Appendix B). A frequency plot of the differences between the measured and simulated data is shown in Figure 4-6. The plot shows that 74 percent of the comparisons were within the 1.5-foot criterion.

ADCIRC Validation

The calibrated ADCIRC model was validated with simulations of Hurricanes Betsy and Camille. Initial simulations were made and reviewed for accuracy by comparing the simulated and measured peak surges. The evaluation revealed that the uncertainties in the Betsy and Camille wind fields and storm tracks were exacerbating the differences in the comparisons due to larger uncertainty in the parameters of R_p, Holland B, and track. Examination of the first simulations for both storms showed that differences between the modeled and measured HWMs were regional and systematic. That is, the sign of the difference was unchanged over large areas where the land use and vegetation changed. This indicated that imprecision related to the wind and atmospheric pressure fields most likely caused the differences. The PBL model and its inputs to the ADCIRC model were adjusted to improve the fit between the measured and modeled surge levels by modifying the details of the wind and pressure fields in the modeled storms. The modifications that were made had to be justified within the constraints of the measured meteorological data for the storms. This form of re-interpretation of the measured data is similar in concept to the present practices of the work the NHC now carries out after major hurricane landfalls where CHWMs and surge modeling help in the interpretation of the relatively sparse measured data.

For Hurricane Camille, the results of the initial simulations indicated that the surge was over-predicted and that the track was probably too far to the east. Therefore, the wind forcing was adjusted so that the central pressure was increased by 1 mb and the track was shifted westward by 0.03 degree. These small adjustments to the wind forcing greatly improved the comparisons.

The results for the validation using Hurricane Camille are shown in Figures 4-7 and 4-8. Figures 4-7a, 4-7b, and 4-7c show comparison maps of the measured and simulated peak surges in Hancock, Harrison, and Jackson Counties. The same data are summarized in Table B-2 (see Appendix B). A frequency plot of the differences between the measured and simulated data is shown in Figure 4-8. The plot shows that 75 percent of the comparisons were within the 1.5-ft criterion.

For Hurricane Betsy, several iterations were made before converging to an acceptable wind and pressure field. The final set resulted from changing the Holland B parameter by 0.05, increasing the storm radius by 2 nmi, and shifting the wind maxima angle by 20 degrees. All changes were well within the uncertainty range of the available meteorological data. These small adjustments to the wind forcing greatly improved the comparisons.

The results for the validation using Hurricane Betsy are shown in Figures 4-9 and 4-10. Figures 4-9a, 4-9b, and 4-9c show comparison maps of the measured and simulated peak surges in Hancock, Harrison, and Jackson Counties. The same data are summarized in Table B-3 (see Appendix B). A frequency plot of the differences between the measured and simulated data is shown in Figure 4-10. The plot shows that 95 percent of the comparisons were within the 1.5-ft criterion.

In both the Betsy and Camille cases, the wind- and water-drag coefficients that had been determined in the Katrina simulations were left unchanged. With the new interpretations of the storm meteorological data, the results of the validation runs were acceptable.

To gain a sense of what an acceptable level of agreement should be, the measured CHWM data from all three of the calibration/verification storms (Katrina, Camille, and Betsy) were analyzed.

The average measurement error (ε_{meas}) was obtained by forming groups of the individual CHWM measurement locations that *should* be similar due to their similar geographic location. These groups were determined by reviewing the local topography and the distances between points. The final selection of groupings was such that each point in the group could reasonably be expected to have nearly the same surge elevation. Where the measured points were not grouped or were widely scattered, they were not used. This process resulted in 19 data clusters from the three storms. The size of the data clusters varied from 4 to 24 points, with a median number of 9 points per cluster. The mean surge elevation for each group was calculated by averaging the surge elevations of all points in the group. At each point, the difference between the measured value and the group mean for the cluster containing the point was calculated (*See the project documents in the Technical and Sceintific Notebook*). All of these differences were pooled and treated as a single data set. The sample mean and variance of this data set were then determined. The standard deviation was 1.3 ft. Although there is no widely accepted measure for the "goodness of fit" between measured and modeled storm surge data, in this case the fit was adequate and no further effort was warranted.

4.3.3 SWAN Model Calibration and Validation

The SWAN model has been used extensively in the engineering community and has been calibrated to a wide range of conditions. There is an extensive body of literature indicating that both WAM and SWAN are state-of-the-art models for predicting waves accurately in coastal waters. The literature demonstrates the SWAN model capabilities and agreement with theory, laboratory measurements, and field data under a wide variety of circumstances. This literature is extensively referenced in the project report: *Wave Setup Methodology for the FEMA Mississippi Flood Study*.

A project-specific model validation was conducted. Two historical hurricanes that occurred in the area were simulated and a comparison made with wave height data that were available at various points. NOAA maintains a number of wave buoys in the Gulf of Mexico and the information is available online at the National Data Buoy Center (NDBC) Web site. The locations of several of these buoys are indicated in Figure 4-11.

Two of the buoys were located within the region of interest, and all of the buoys were used for comparisons with model predictions for Hurricanes Georges (1998) and Katrina (2005). Buoy 42007 is of primary interest because it is located in shallow water inside of the barrier islands. Buoy 42040 is located outside of the barrier island chain. Figures 4-12 and 4-13 show the

agreement between the model predictions and the NDBC buoys during Hurricane Katrina. Note that two of the Buoys, 42003 and 42007, broke during the peak of the storm, and so complete model validation could not be obtained. The agreement, however, was very good until the buoys failed. At Buoy 42040, the SWAN model under-predicts the peak wave height. The measured peak wave heights were approximately 17 m at this buoy, but both the WAM and SWAN models only predicted about 12 or 13 m. This difference is explained in the following paragraph.

Figures 4-14 and 4-15 show similar results for Hurricane Georges, the largest hurricane of 1998. For this hurricane, all four buoys survived the storm and the model predictions and the buoy data at all of the buoys, including Buoy 42040, show favorable agreement. The better agreement at Buoy 42040 for Hurricane Georges than for Hurricane Katrina can be explained in terms of the hurricane paths and model sensitivity. Hurricane Georges passed nearly directly over this buoy location, while this buoy was on the edge of Hurricane Katrina's strong winds. The swath of the observed peak significant wave heights for Hurricanes Georges and Katrina are shown in Figure 4-16. These data indicate that the eye of the storm passed directly over Buoy 42040 for Georges but passed to the west for Katrina. For the Katrina simulation, the buoy is located in a region where there was a large spatial gradient in the wave heights. Thus, small uncertainties in the wave field can explain the differences noted between the modeled and simulated wave heights at this location.

In addition to these validations, comparisons were made to the Steady-State Spectral Wave Model (STWAVE) (Smith et al. 1999) and other models. Also, grid resolution studies were conducted to ensure that the SWAN model grids were providing sufficient resolution for the computations. The details of these additional studies can be found in the supporting project report titled *Wave Setup Methodology for the FEMA Mississippi Flood Study.*

4.4 NUMERICAL MODELING OF THE STORMS IN THE JPM-OS ANALYSIS

The overall work flow of the numerical modeling has been explained and is diagrammed on Figure 4-1. The main ADCIRC grid with 900,450 nodes required special computer resources. To support this modeling, the main ADCIRC grid with 900,450 nodes required the use of two super-computers operating full-time for the duration of the run phase of the project. In addition, FEMA arranged access to a parallel cluster operated by the U.S. Department of Energy. The use of these fast computational resources significantly reduced the duration of the project.

4.4.1 Special Considerations

The Mississippi Coastal Analysis Project introduced many innovations to previous FEMA methods for coastal flood hazard analyses. Among them, the wave setup was included in the hydrodynamic simulations and the astronomical tides were excluded from these simulations. Controlling the maximum duration of the simulations was necessary to maintain the production schedule. These subjects are discussed below.

4.4.1.1 Wave Setup

The hurricane wind fields from the PBL model were input to ocean wave models. The WAM-3G model was used to convert the wind-time series of the wind field to corresponding time series of deep water wave conditions. The results for each synthetic storm were then input to a SWAN

wave model. The SWAN model (version 40.51) was implemented with 72 directional bins (i.e., with 5 degree directional wave spectral bins) and with 26 frequency bins (from 0.03138 to 0.4177428 Hz) covering wave periods from approximately 32 seconds (sec) down to 1 sec (the last frequency bin for the highest frequency waves is centered at 2.4 sec periods, but represents waves from 0.0 to 2.4 sec).

It was necessary to have an estimate of the water depths each 15 minutes throughout the simulations so that depth-limit wave breaking and the resulting radiation stress gradients could be evaluated. It was necessary to have an estimate of the water depths due to the surge in both the flooded overland and offshore areas. This was accomplished using the wind and atmospheric pressures from the PBL model with a streamlined ADCIRC model with only 50,000 nodes (ADCIRC 50K). The grid of this model did not extend overland. Because storm wave breaking is a coastal phenomenon, the surge levels from the ADCIRC 50K model were projected inland so that overland depths could be approximated. The resulting time series were used as input to the SWAN model domains. The output of the SWAN model was configured to be the radiation stress input to the main ADCIRC model.

One special feature of the analysis was consideration of the influence of vegetation on wave setup. Although there are anecdotal observations that coastal vegetation acts to reduce storm surge heights, there is little formally known about these effects. A recent paper by Dean and Bender (2006) examined the reduction in the rate of wave setup increase across vegetated zones by considering the underlying physics. They concluded that the rate of wave setup development is reduced by a factor provided the vegetation is not overtopped. The magnitude of this factor is not well known and the theoretical analysis by Dean and Bender indicate that the rate of wave setup development can be reduced by up to a factor of 0.667 provided the waves do not overtop the height of the vegetation. However, the factor is zero when the waves do overtop the vegetation. For vegetation of inconsistent heights or mixed vegetation, an intermediate value of this factor is appropriate.

A procedure was developed to implement this effect in the ADCIRC modeling. The procedure requires information about the vegetation across the coastal region of Mississippi. USGS land use data and vegetation data from the Gap Analysis Program (GAP) were compiled by Ayres and Associates and used to estimate vegetation heights at each of the ADCIRC mesh nodes. The details of this procedure can be found in the supporting project report titled *Summary of Work Performed by Ayres Associates in Support of URS Storm Surge Modeling For FEMA Region 4*. The method also requires the water surface elevation during the storm simulation. Since the surge elevation is calculated during the simulation, the elevations are not known a-priori. As an approximation, the surge elevations developed using the ADCIRC 50K simulations were used to make the wave force adjustments.

The wave forcing adjustment procedure was automated in a Fortran code which applied the adjustment to the input wave forcing files. The input files contained the wave force value for each ADCIRC node at 30-minute intervals. For each interval, the water elevation from the 50K simulation at the corresponding time was compared to the vegetation height at the node. If the vegetation was flooded, but not overtopped, a reduction factor of ⅓ was applied to the wave force. This value of the reduction factor was used to account for the variability in real wave heights and shapes along with local variability in the height of the vegetation. The original wave force input file was then replaced with one containing the adjustments.

The use of a sophisticated wave model, such as SWAN, brought much more detailed physics to bear on the wave setup calculations than was the practice in earlier FEMA coastal flood hazard projects. Additional information is given in the supporting project report titled *Wave Setup Methodology for the FEMA Mississippi Flood Study*.

Figure 4-1 shows a flow chart representing the calculation of the time-dependent wave setup in the final hydrodynamic storm simulations with the main ADCIRC model. At each step, the results were fully checked, first by the originating team, and then by the next team in the sequence. These quality assurance procedures are described in the supporting project report titled *Grid Development Report.*

4.4.1.2 Duration of the Modeled Storms

A series of trials were conducted with the ADCIRC model to determine the duration of simulation needed to represent the full range of hurricanes to be modeled. The aggressive project schedule required that this duration be minimized. The results of these trial runs showed that a duration of 5.5 days was needed. Of this, 3 days represented a model spinup (i.e., model run time that allows the hydrodynamic calculations to adjust to each other). This testing is more fully described in the supporting project report titled *Production Run Report.*

4.4.1.3 Astronomical Tide

A series of ADCIRC model trial runs were carried out to determine whether the astronomical tide needed to be incorporated into each storm simulation. These ADCIRC runs were made with and without the time-varying water level due to the tide. When the tide levels were added to the no-tide runs, the differences in the total water levels were minimal for a wide range of inland locations. Based on these tests, the number of production runs was reduced by representing only mid-tide conditions. The effects of the astronomical tides were then accounted for later in the overall analyses as part of the statistical analyses (see Sections 3.3 and 5.2). The trial runs are further described in the supporting project report titled *Production Run Report.*

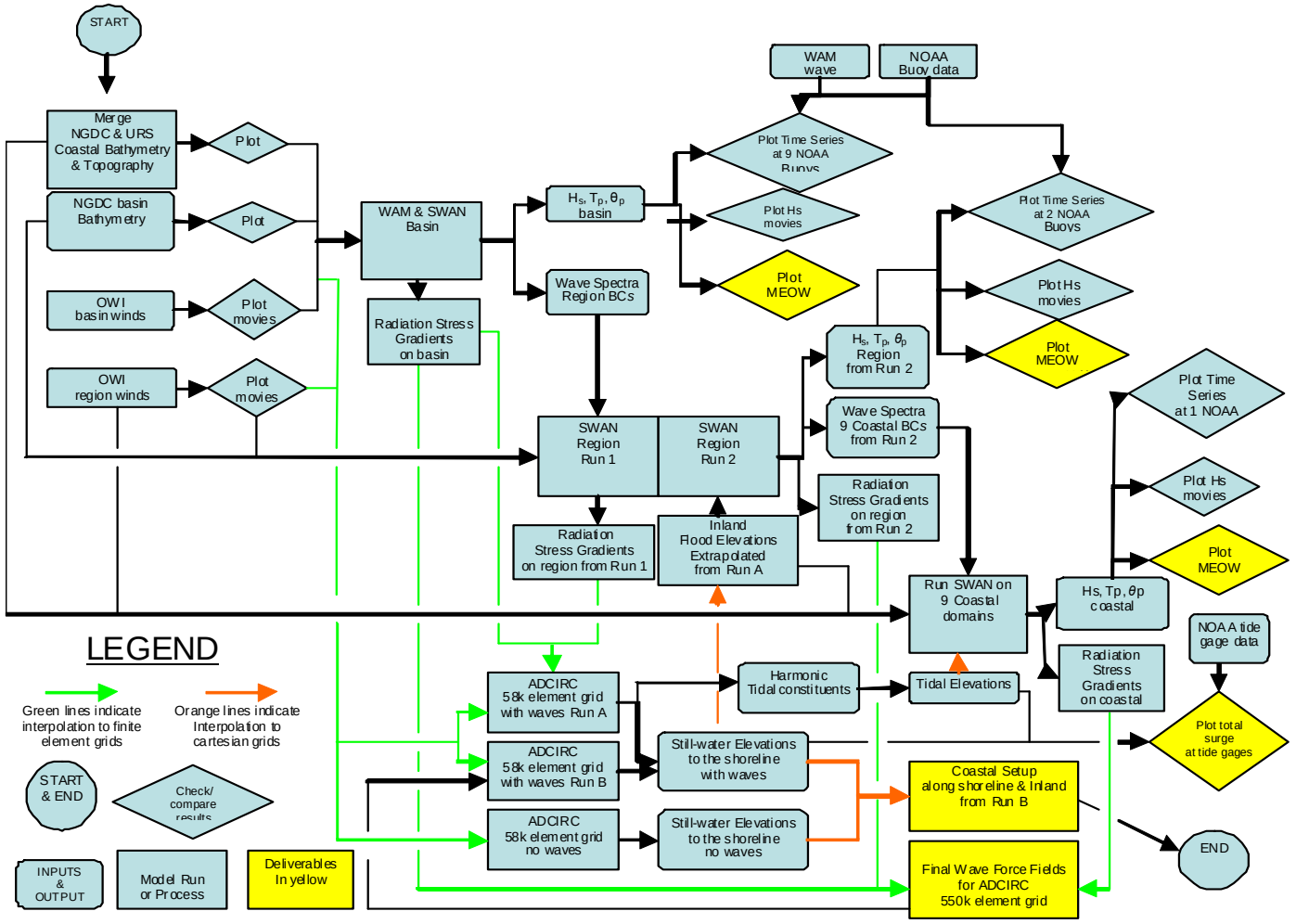

Figure 4-1. Flow Diagram Representing the Calculation Components of the Time-Dependent Wave Setup in the Final Hydrodynamic Storm Simulations with the Main ADCIRC Model.

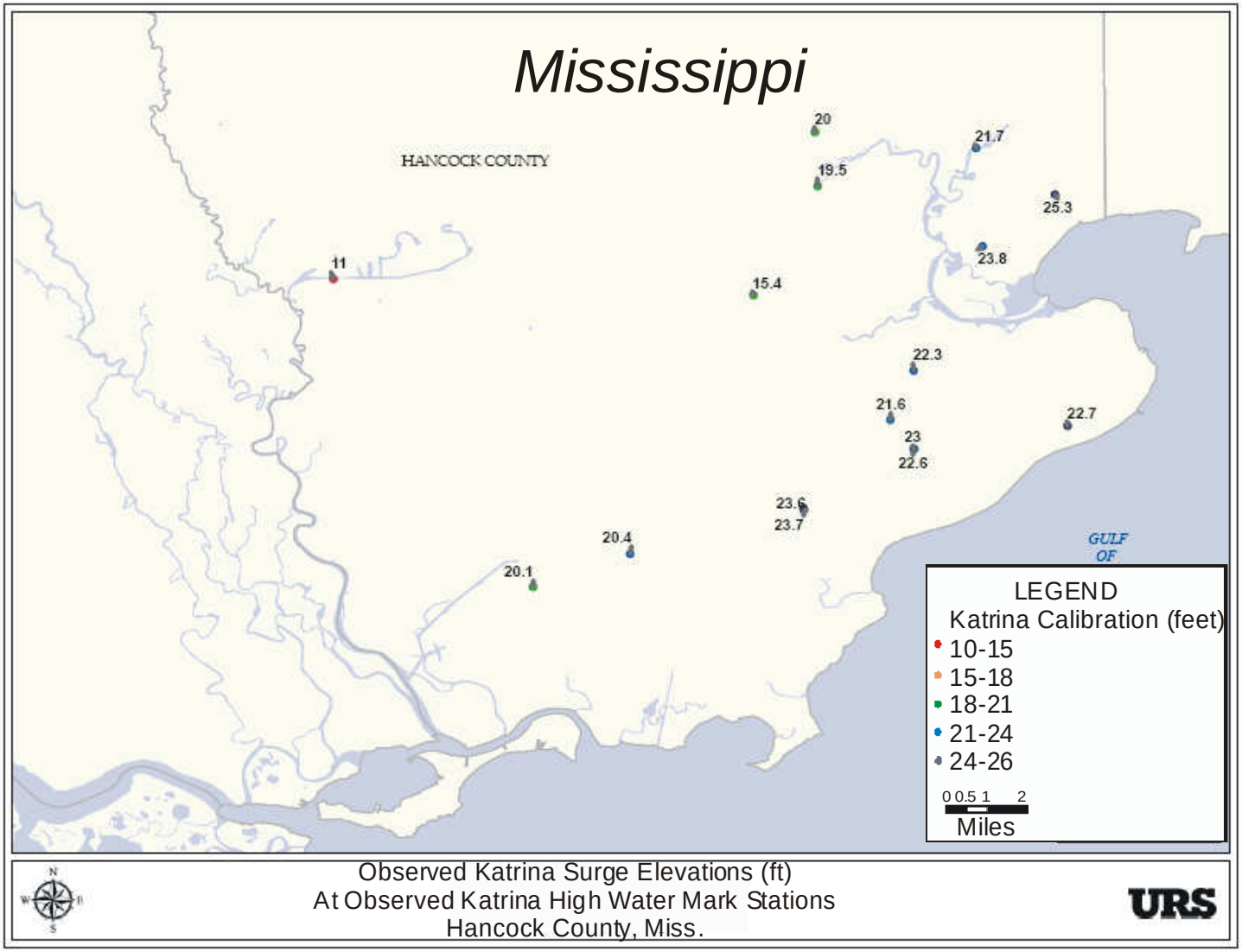

Figure 4-2a. Observation Points for Hurricane Katrina (Hancock County).

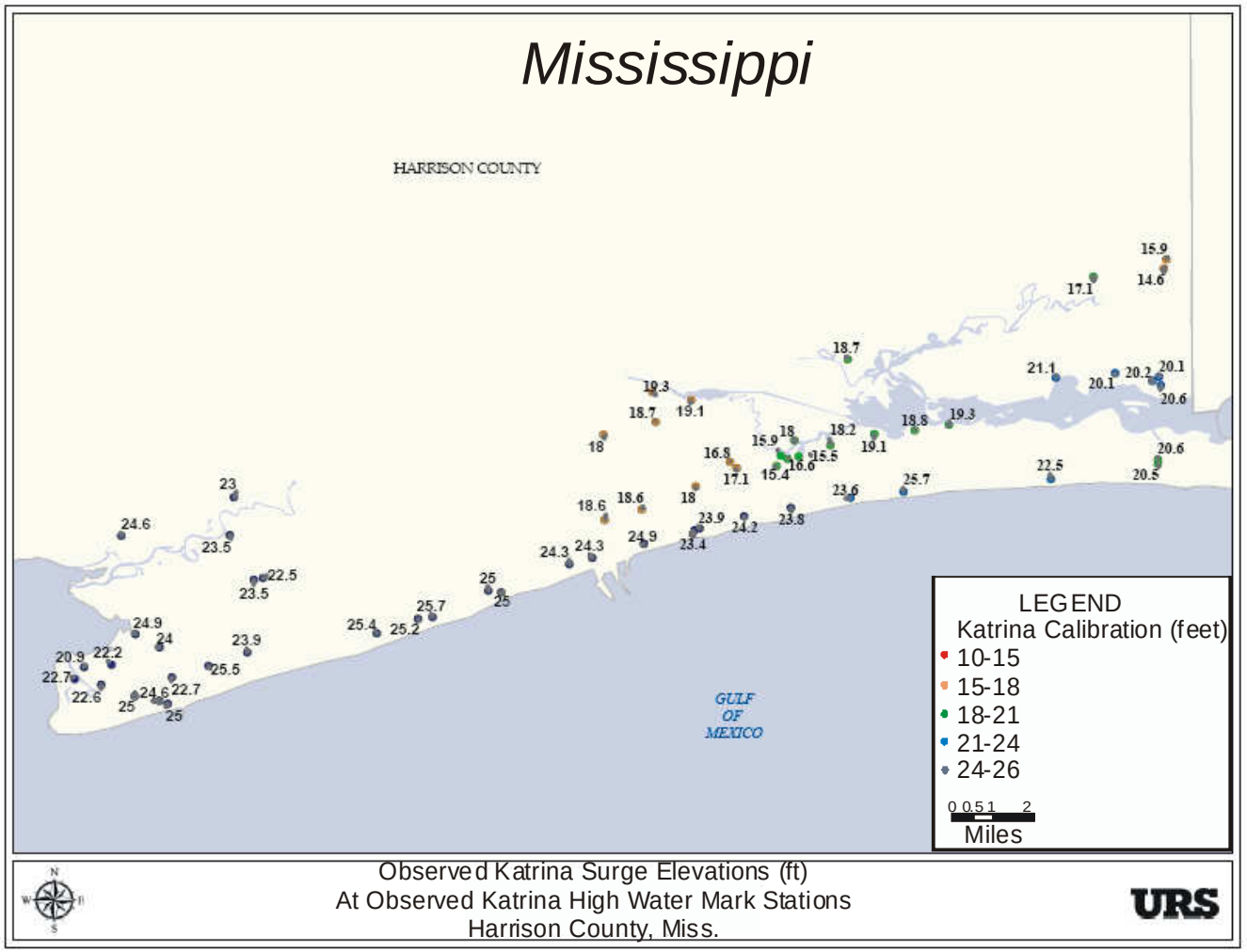

Figure 4-2b. Observation Points for Hurricane Katrina (Harrison County).

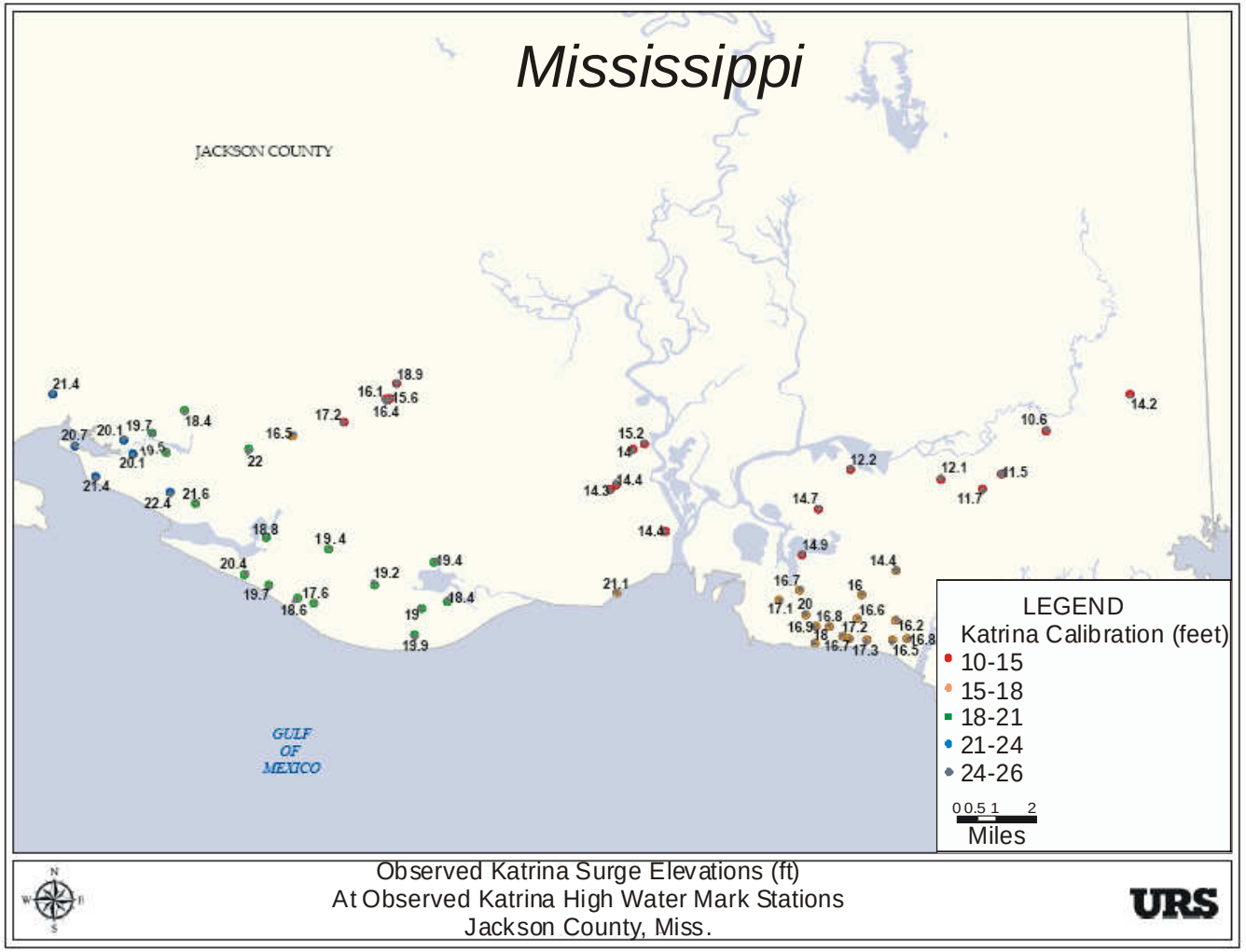

Figure 4-2c. Observation Points for Hurricane Katrina (Jackson County).

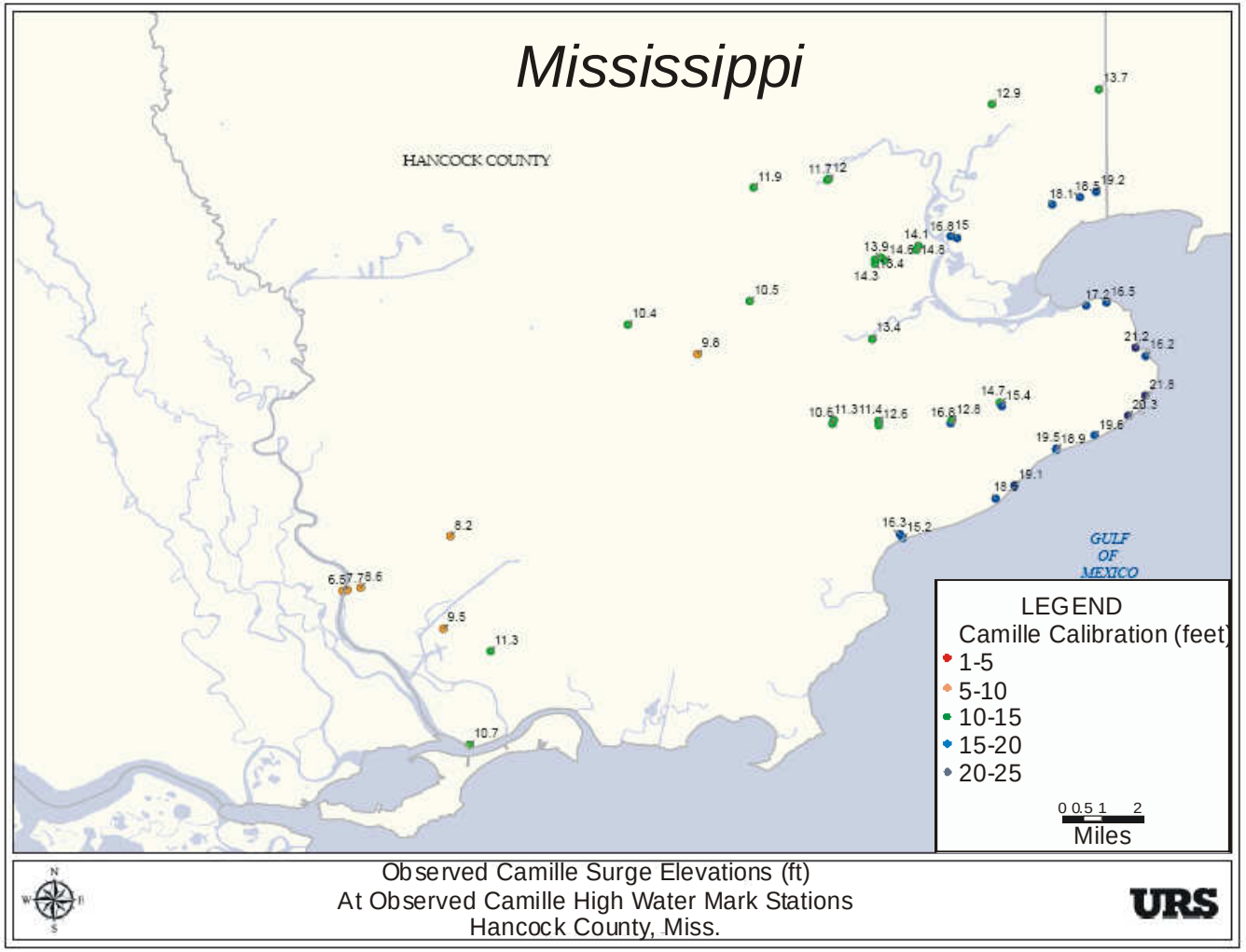

Figure 4-3a. Observation Points for Hurricane Camille (Hancock County).

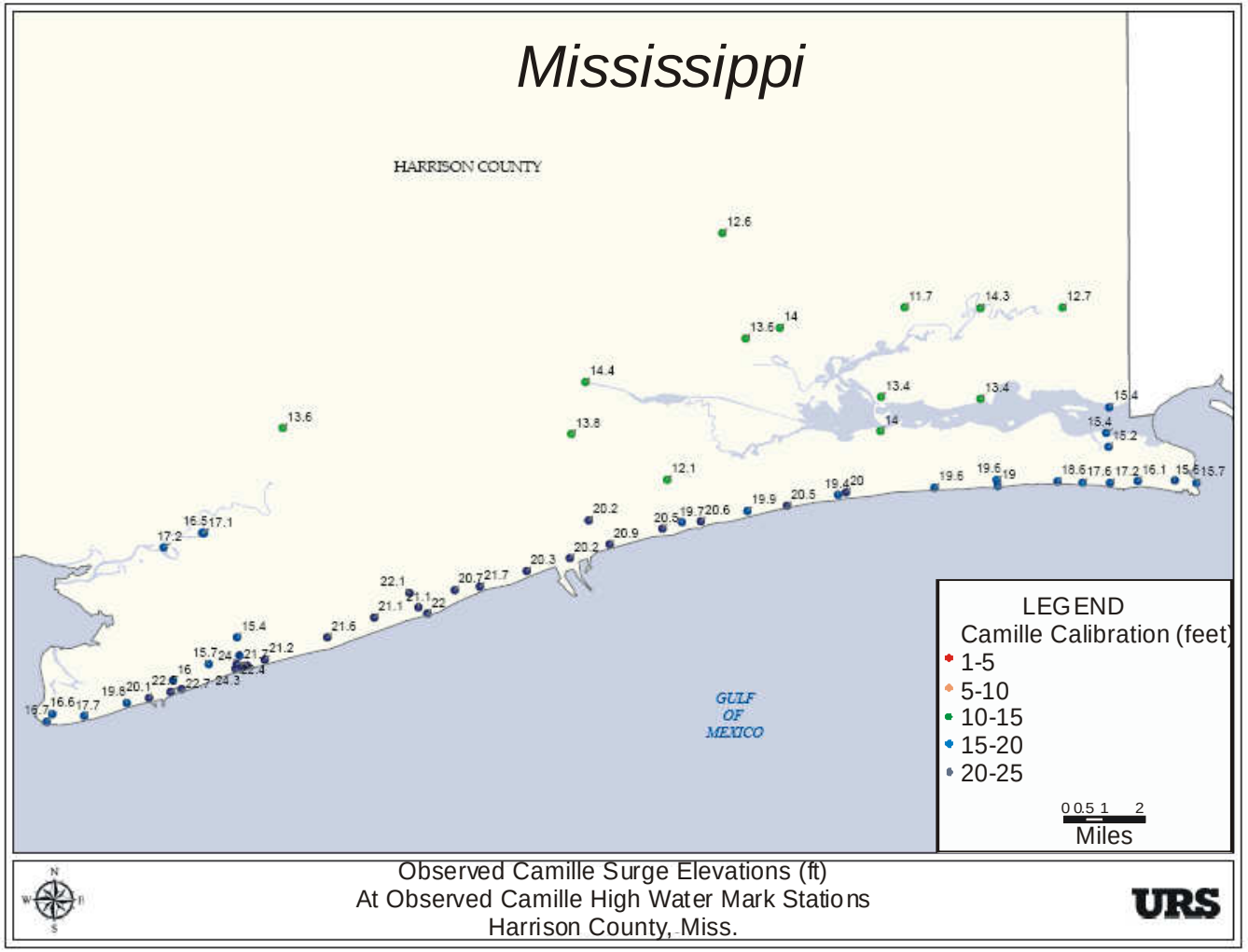

Figure 4-3b. Observation Points for Hurricane Camille (Harrison County).

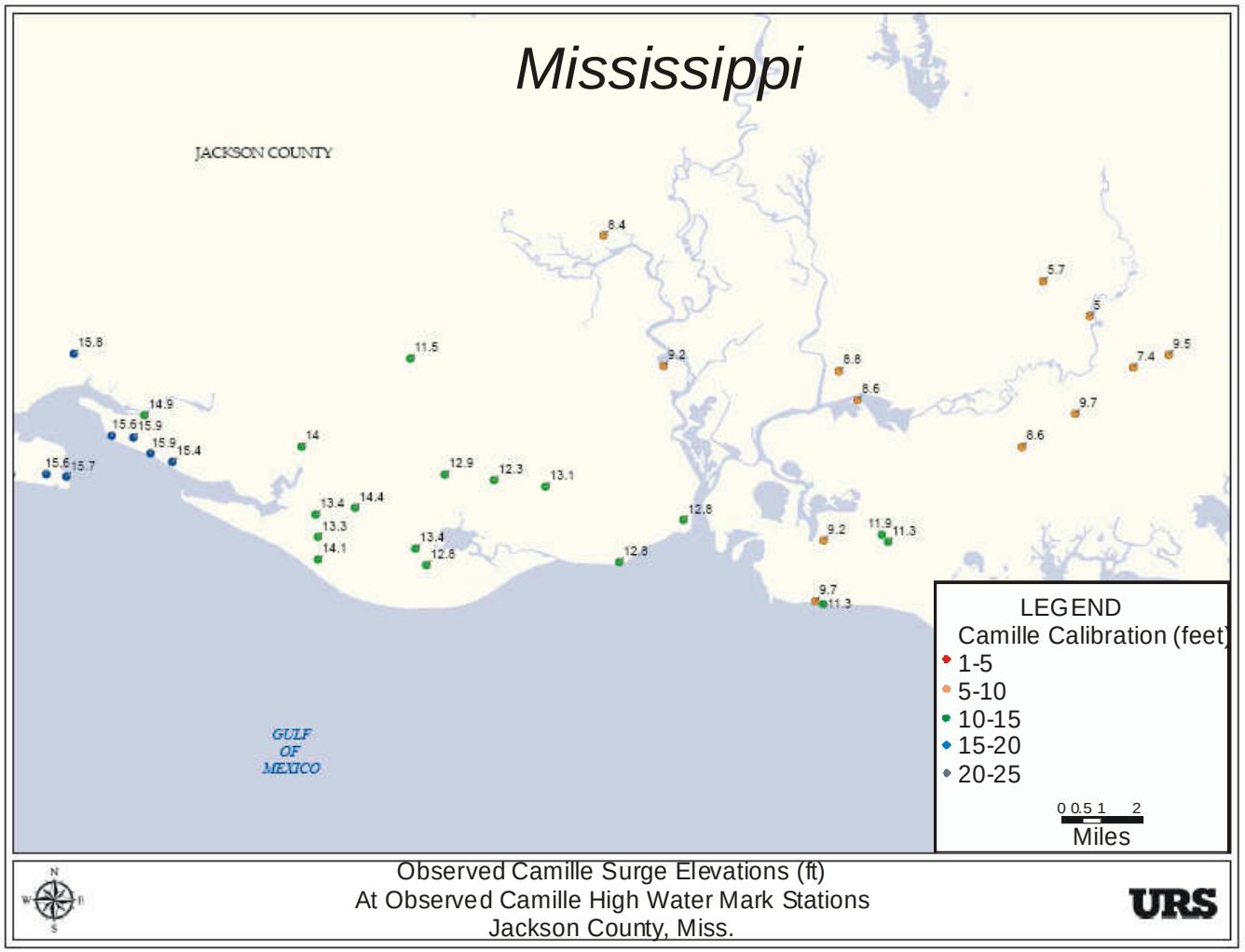

Figure 4-3c. Observation Points for Hurricane Camille (Jackson County).

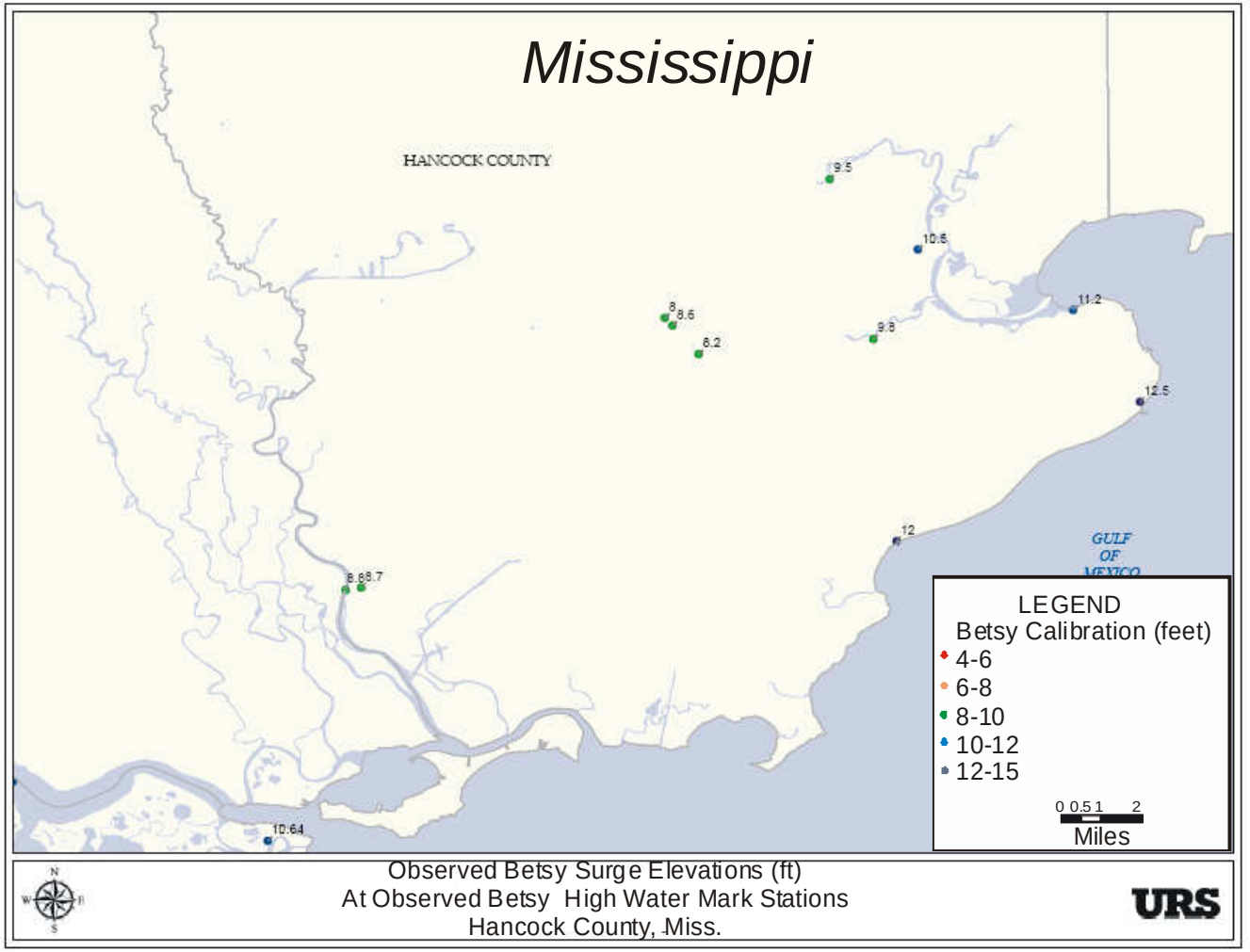

Figure 4-4a. Observation Points for Hurricane Betsy (Hancock County).

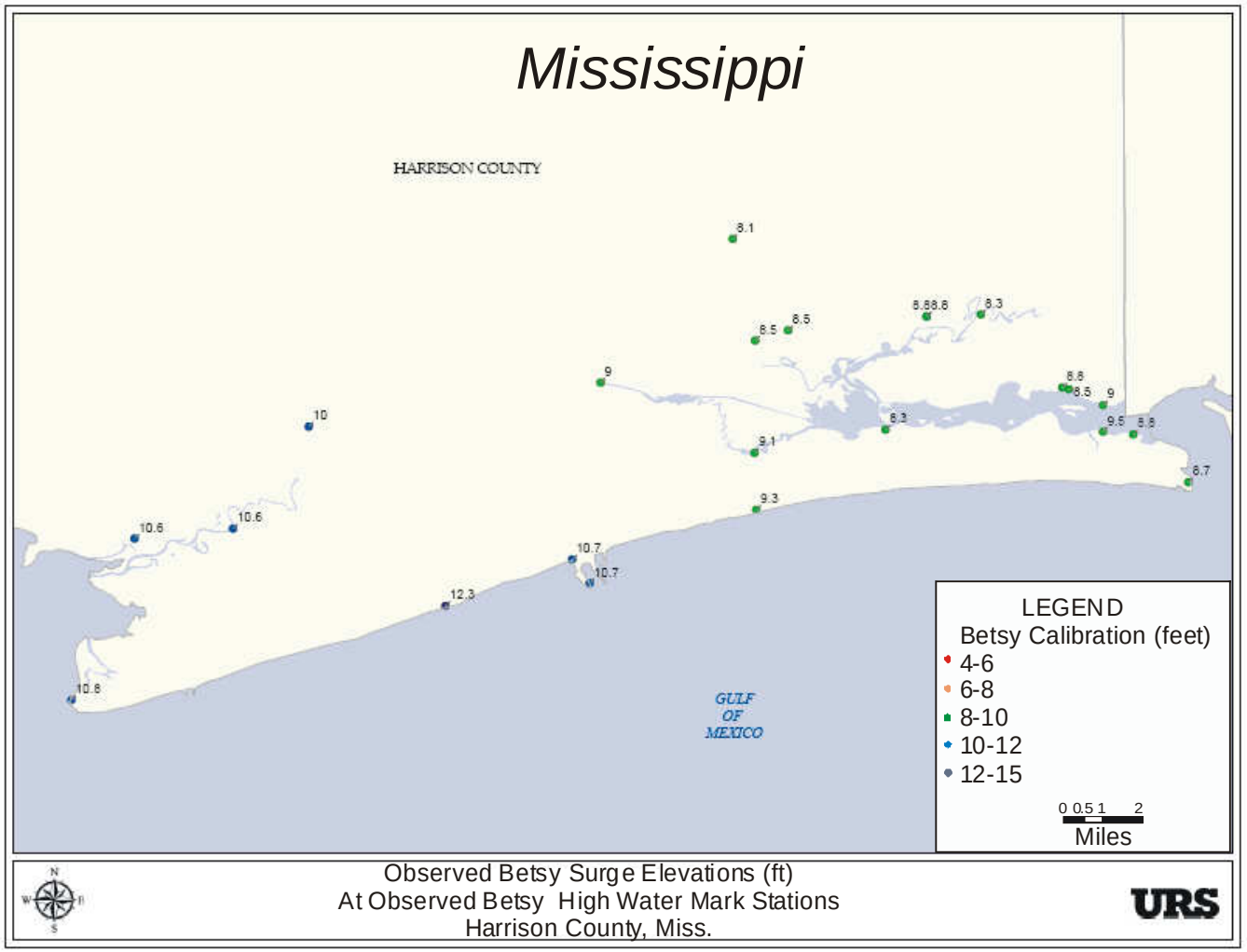

Figure 4-4b. Observation Points for Hurricane Betsy (Harrison County).

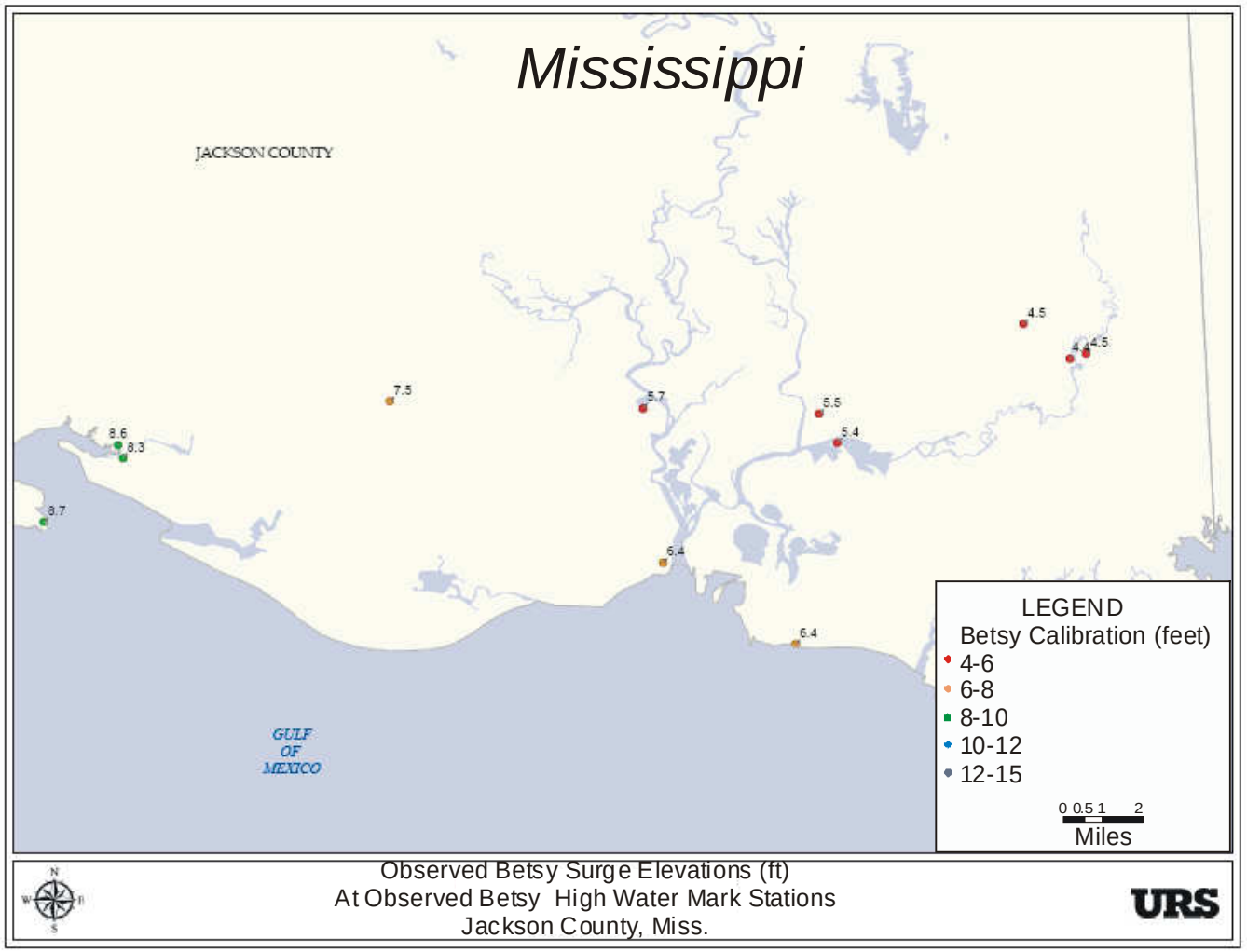

Figure 4-4c. Observation Points for Hurricane Betsy (Jackson County).

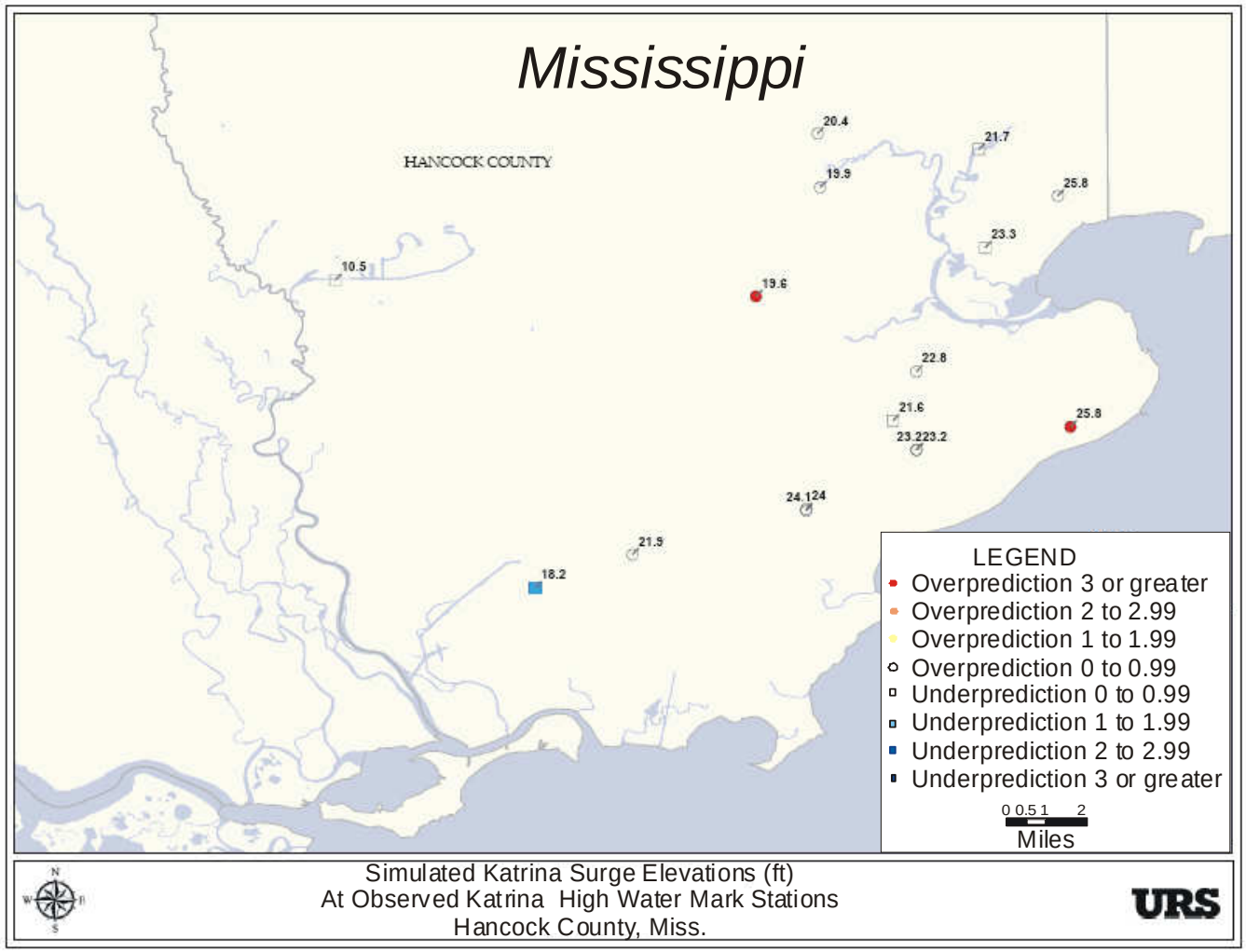

Figure 4-5a. Hurricane Katrina Comparison Maps for Hancock County (adjacent numbers indicate nearby co-located points).

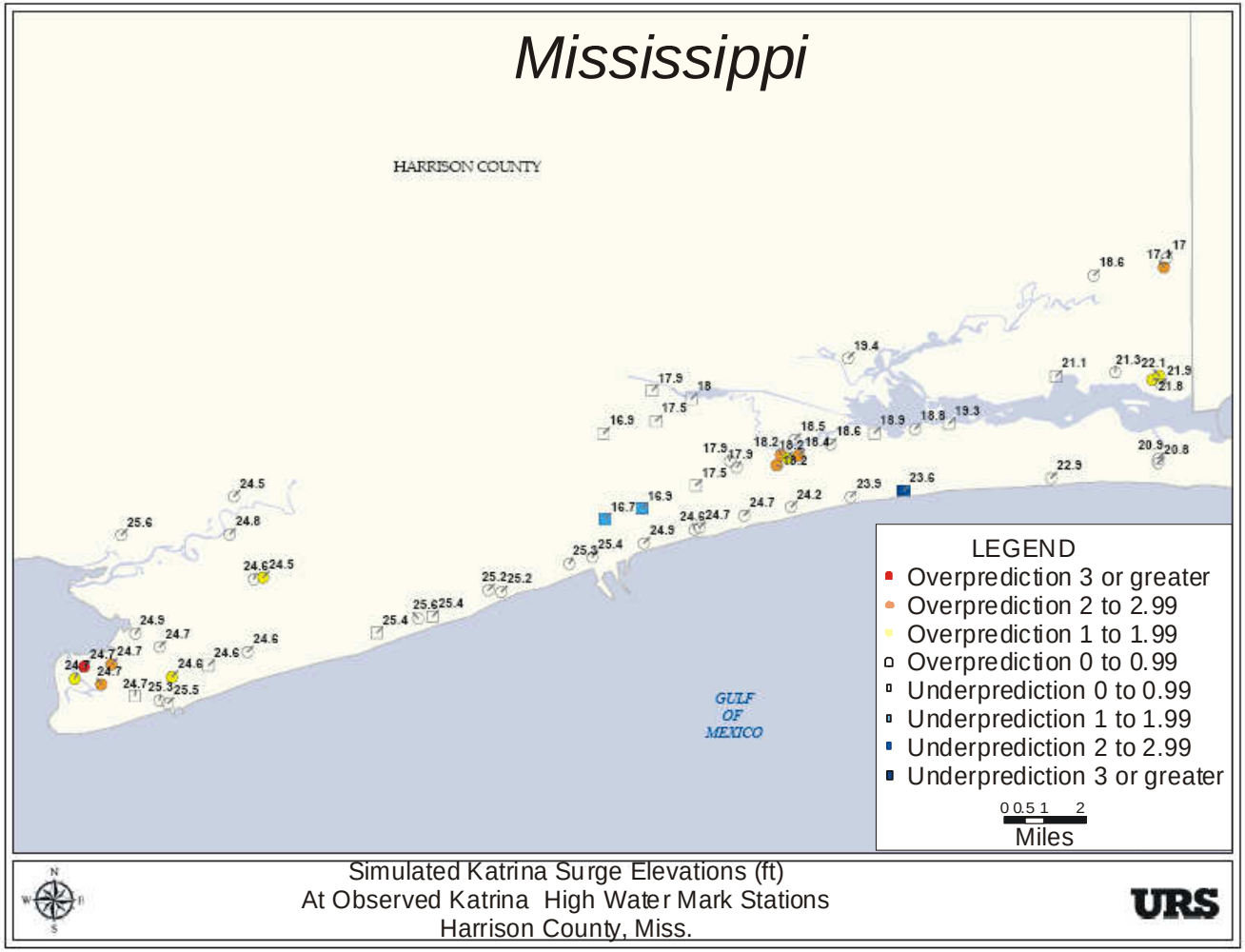

Figure 4-5b. Hurricane Katrina Comparison Maps for Harrison County (adjacent numbers indicate nearby co-located points).

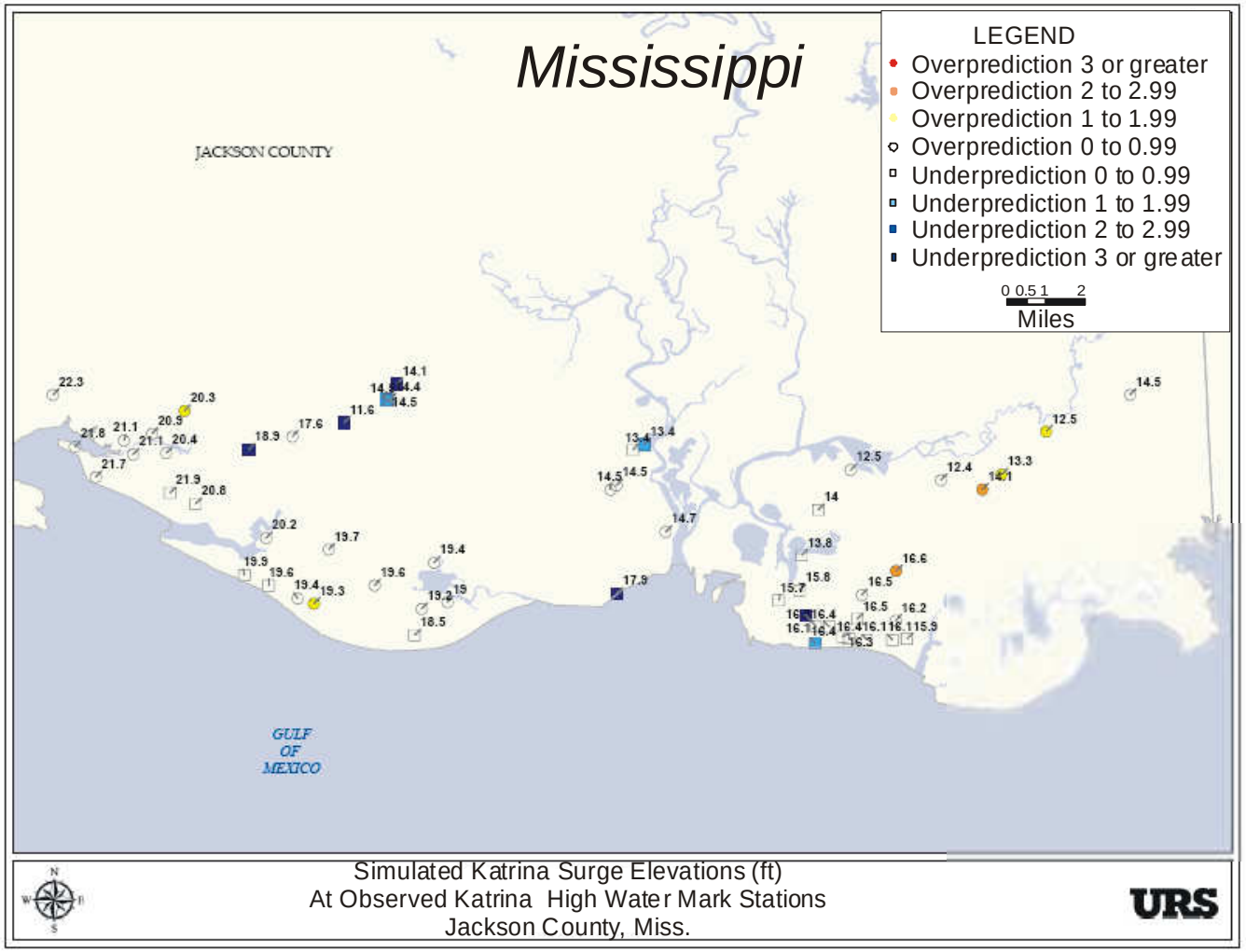

Figure 4-5c. Hurricane Katrina Comparison Maps for Jackson County (adjacent numbers indicate nearby co-located points).

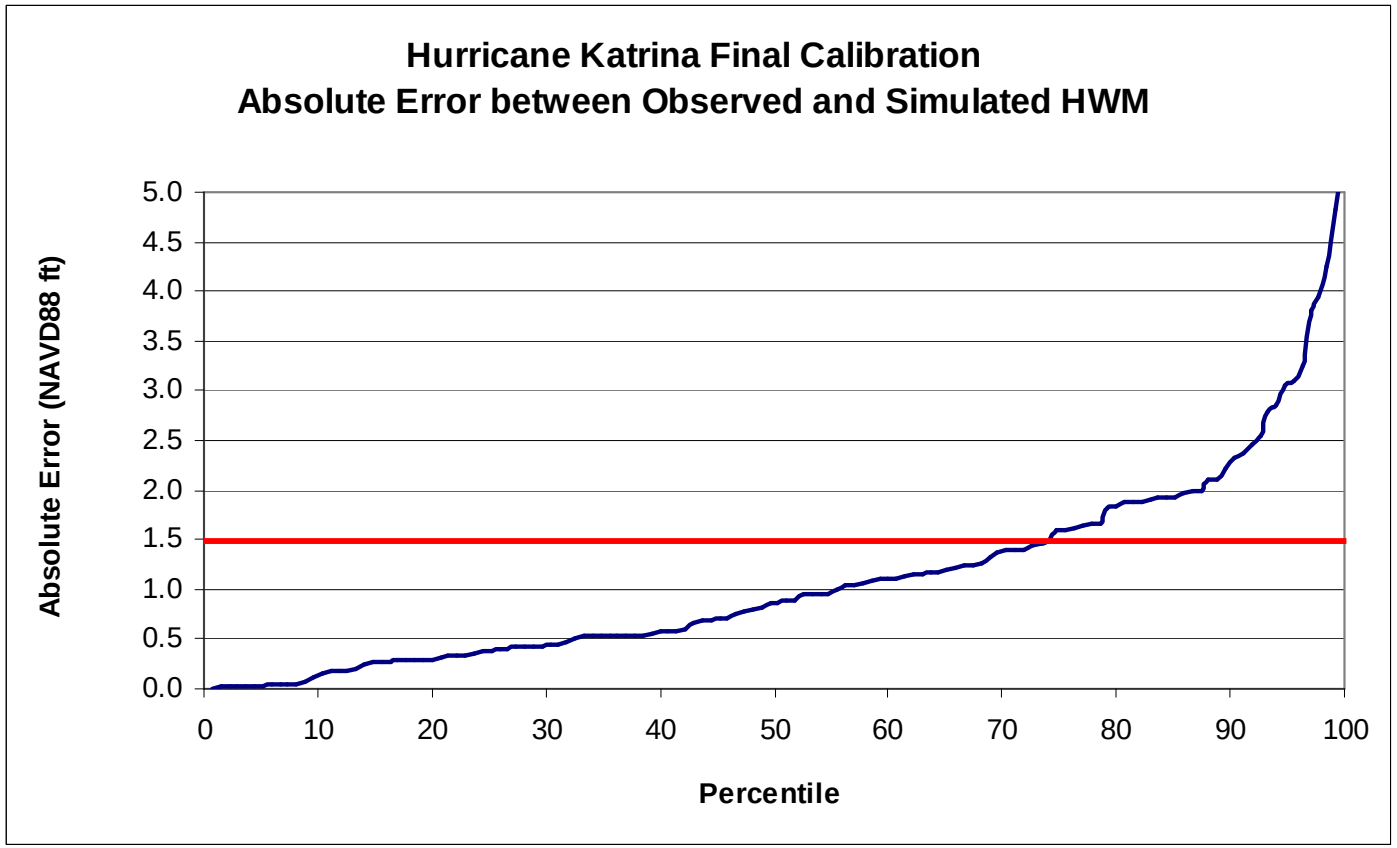

Figure 4-6. Frequency Distribution – Hurricane Katrina.

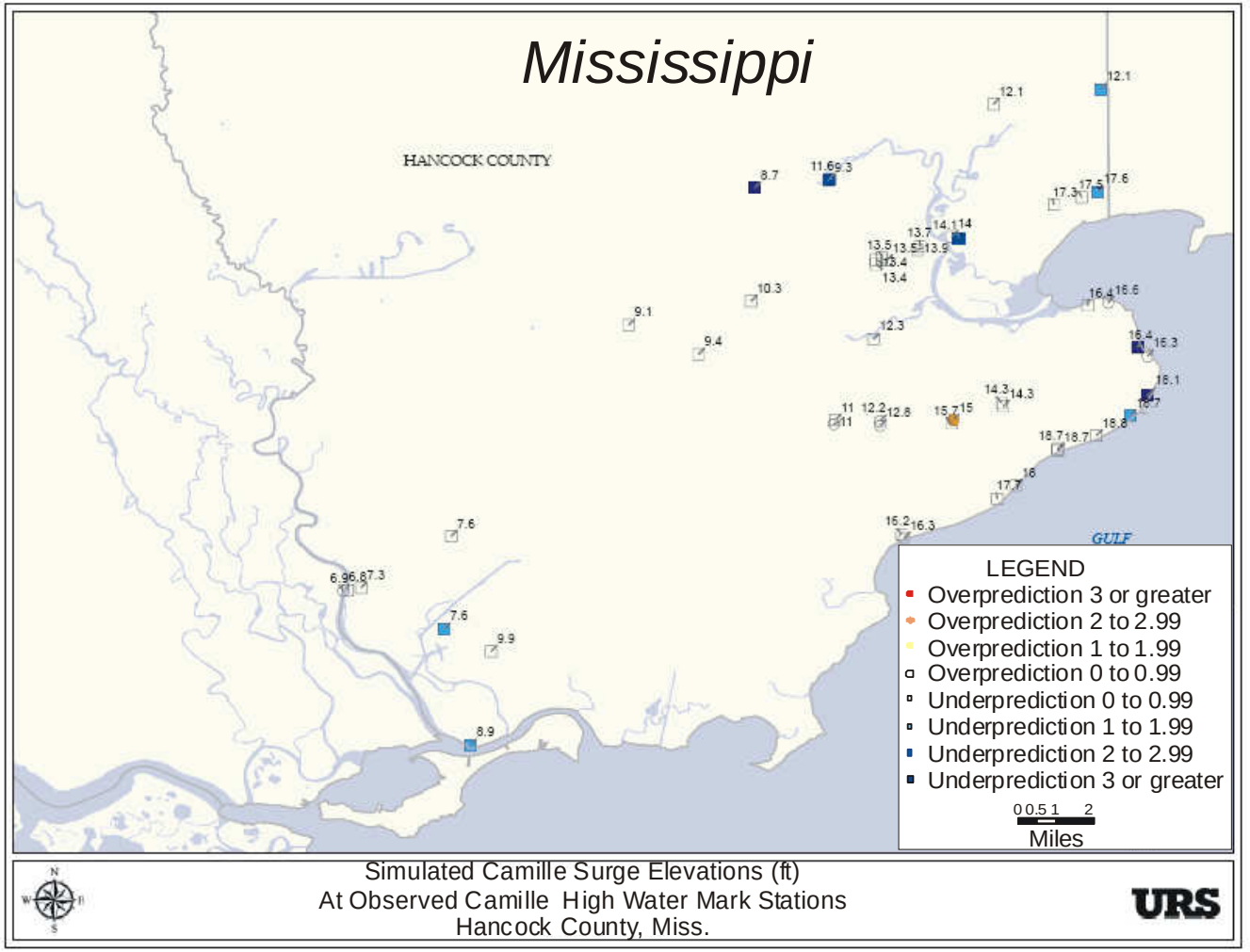

Figure 4-7a. ADCIRC Comparison Map for Hurricane Camille (Hancock County).

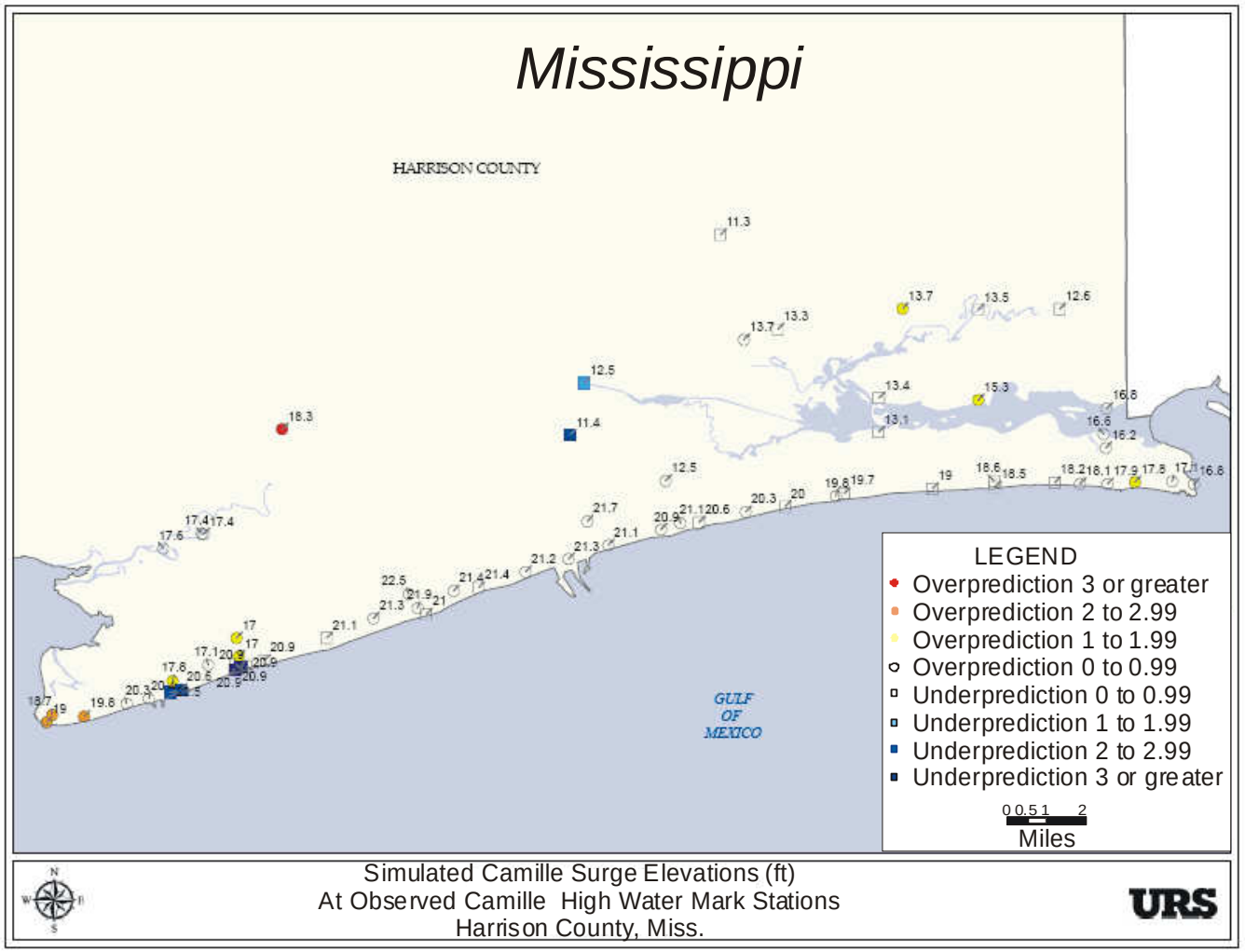

Figure 4-7b. ADCIRC Comparison Map for Hurricane Camille (Harrison County).

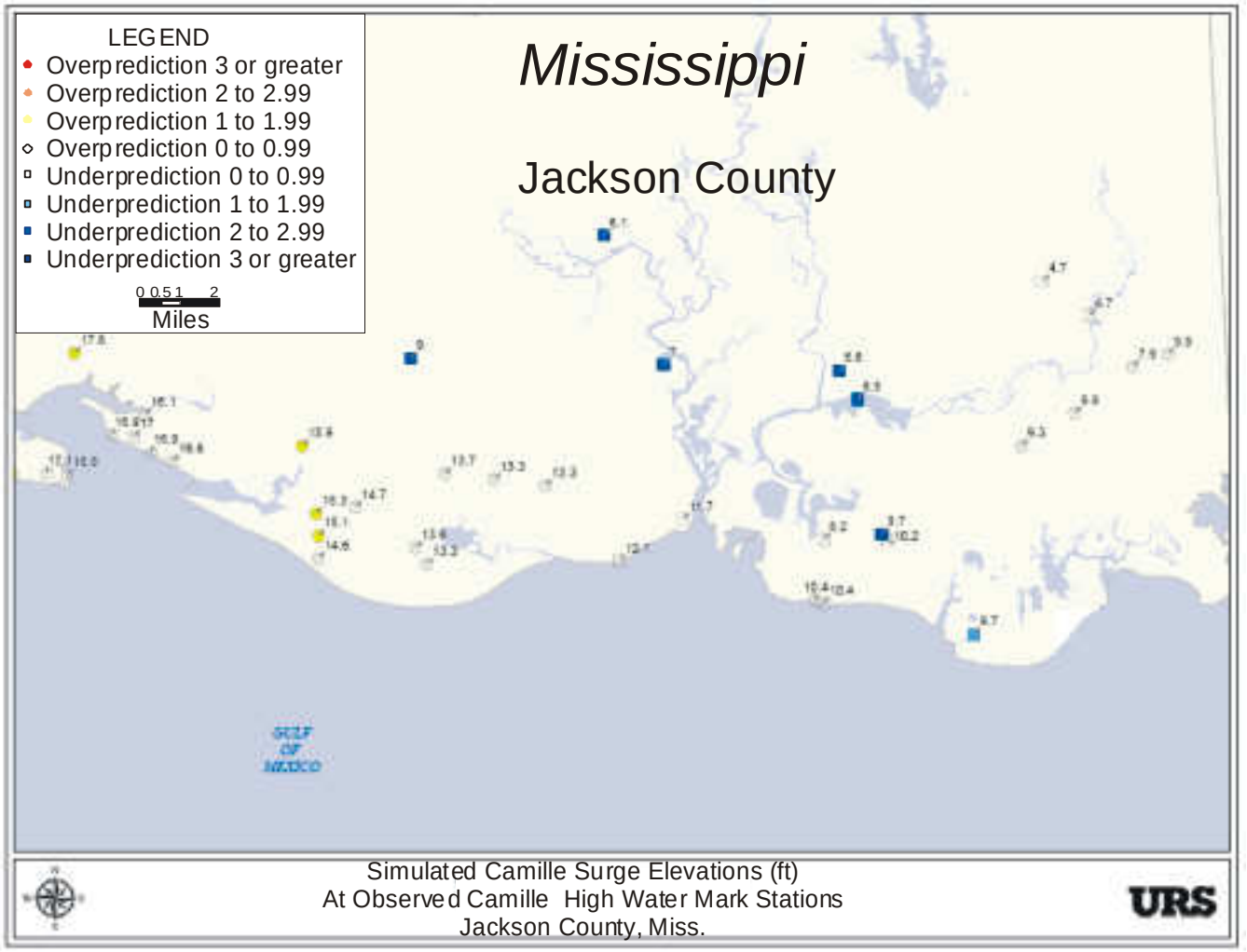

Figure 4-7c. ADCIRC Comparison Map for Hurricane Camille (Jackson County).

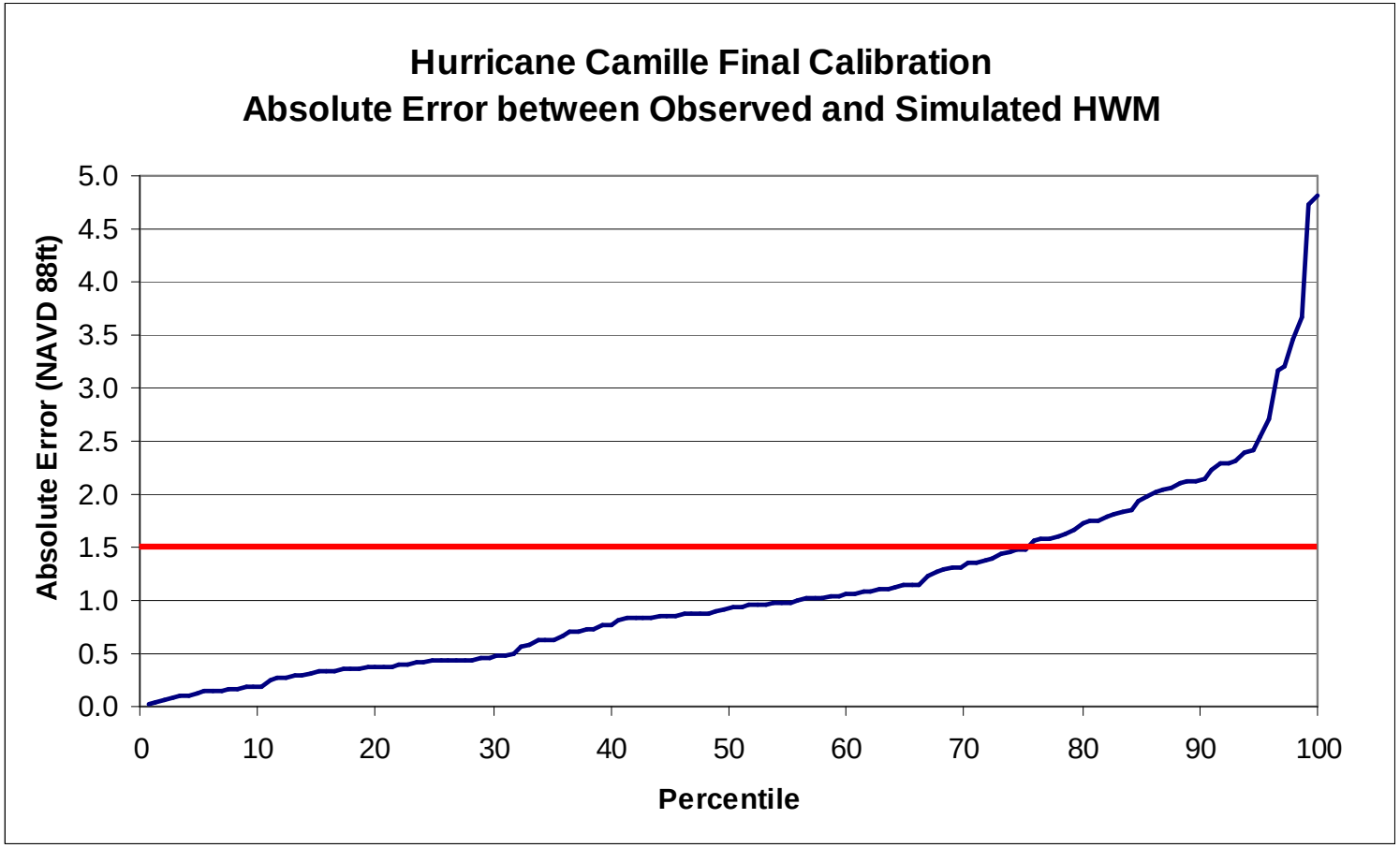

Figure 4-8. Frequency Distribution – Hurricane Camille.

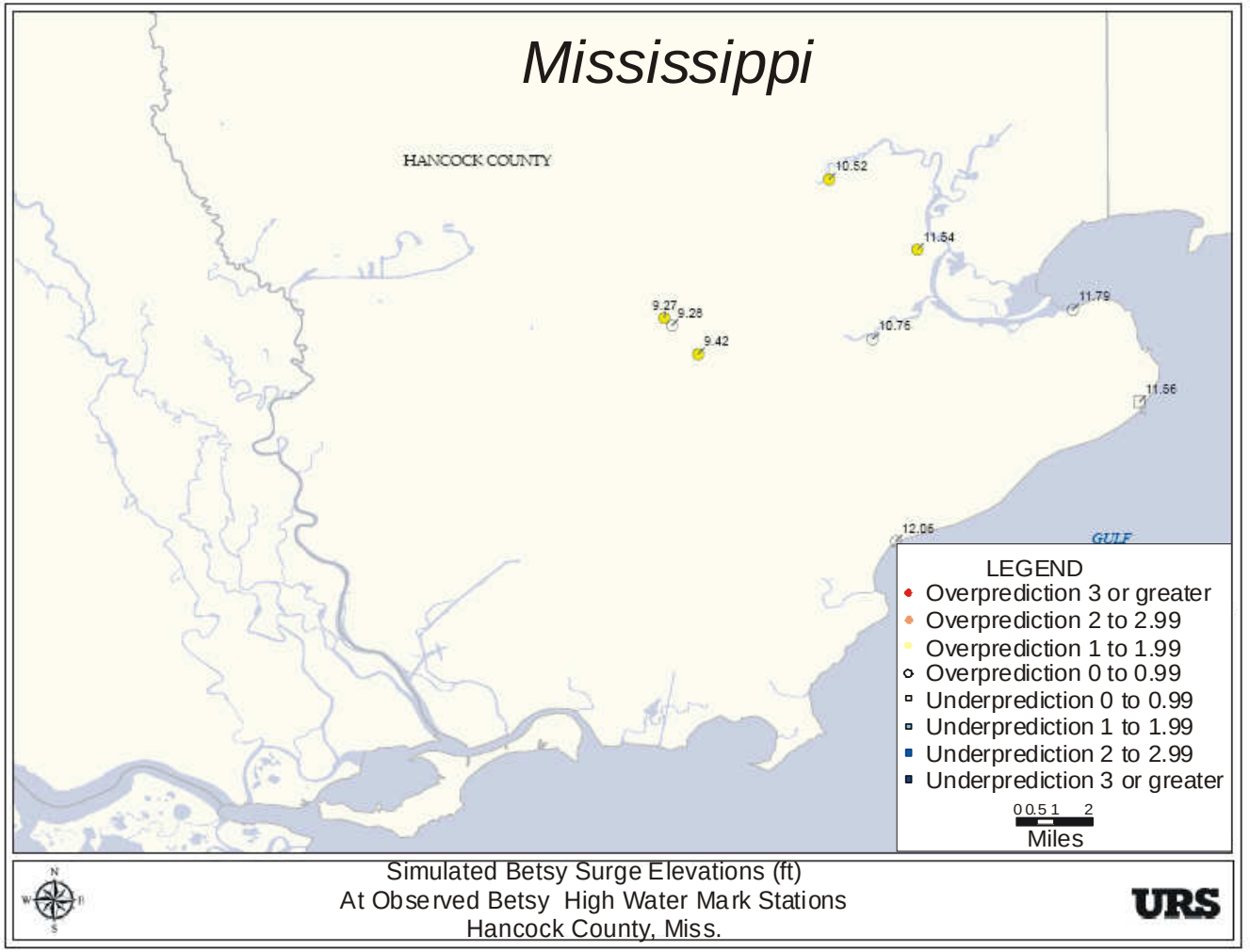

Figure 4-9a. ADCIRC Comparison Map for Hurricane Betsy (Hancock County).

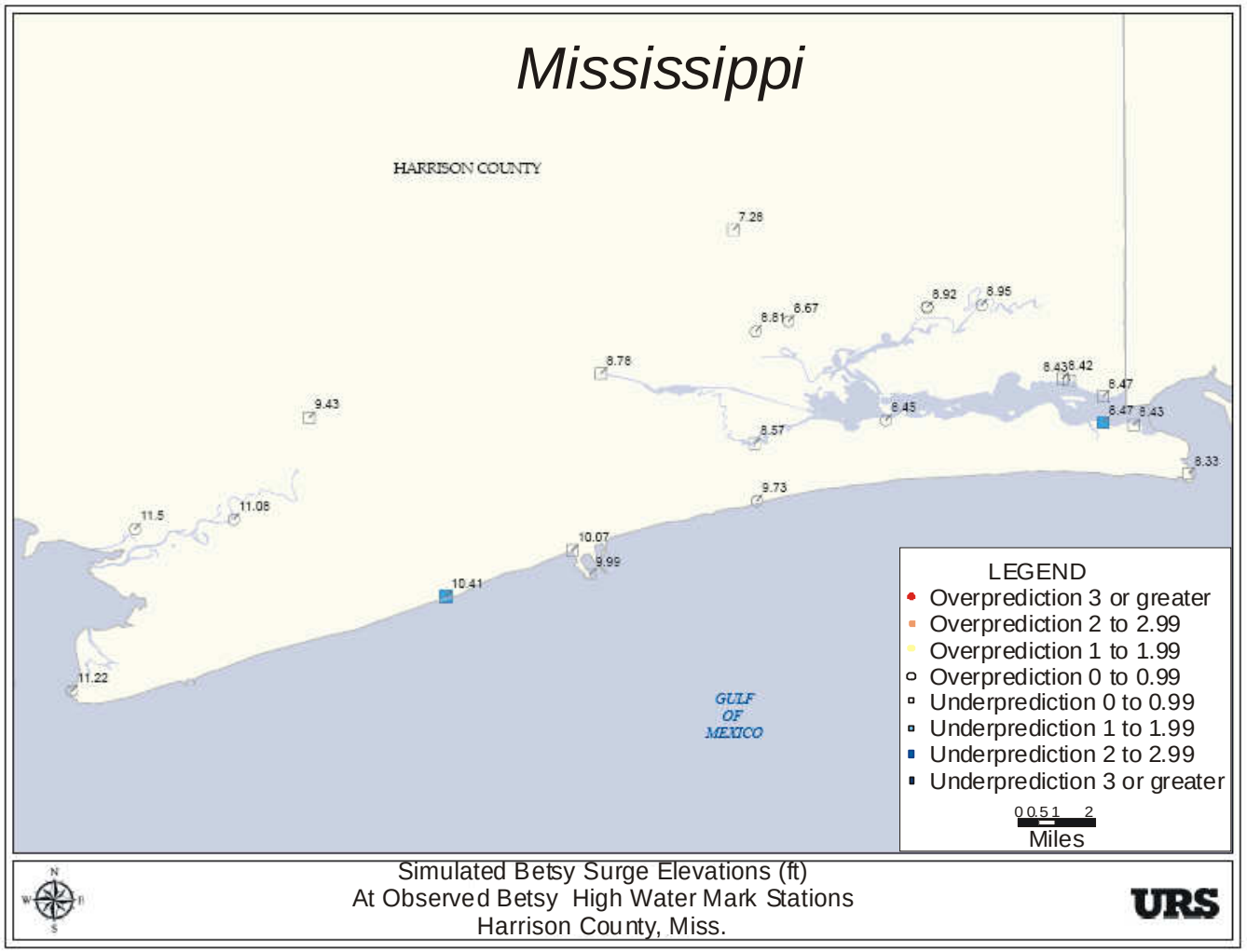

Figure 4-9b. ADCIRC Comparison Map for Hurricane Betsy (Harrison County).

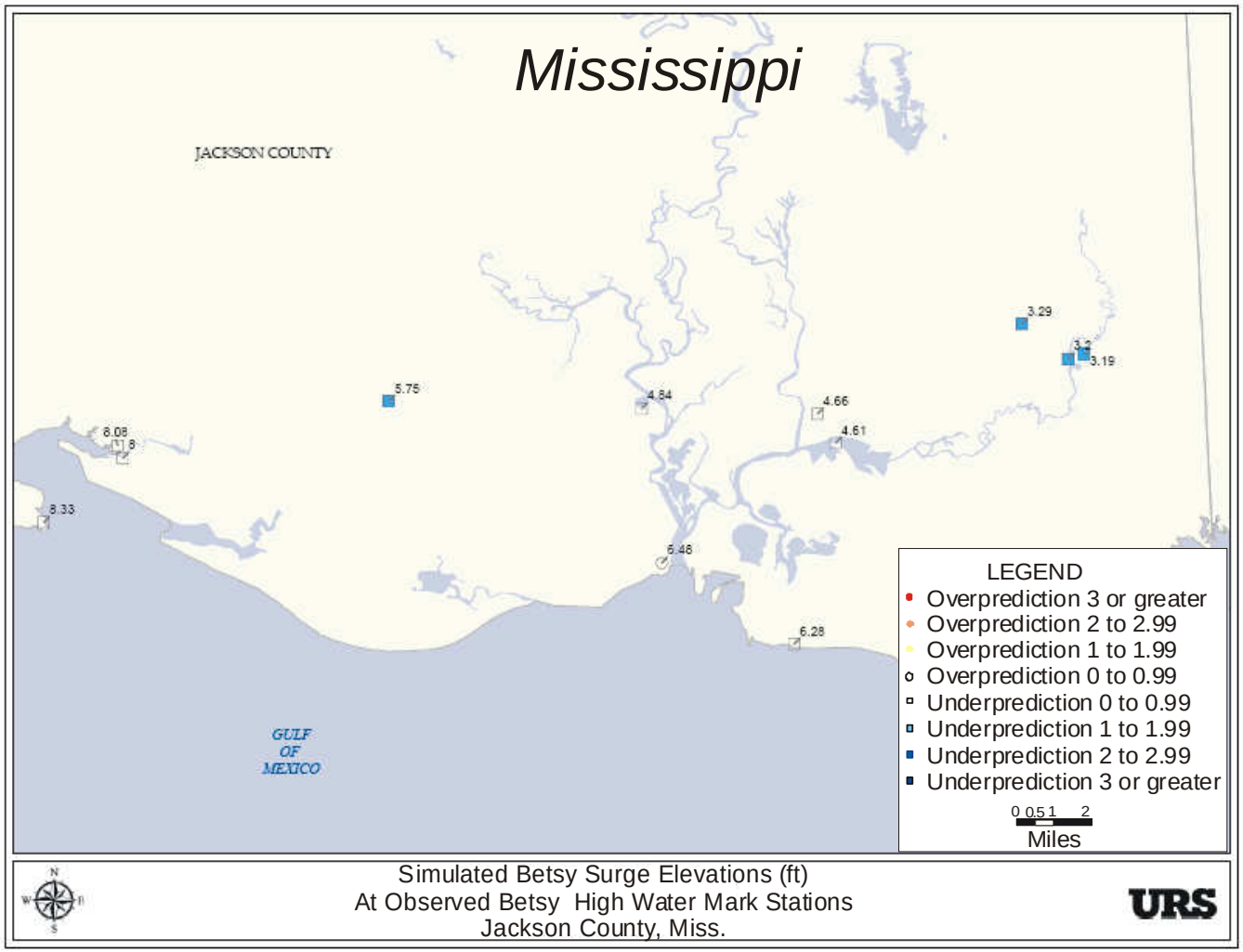

Figure 4-9c. ADCIRC Comparison Map for Hurricane Betsy (Jackson County).

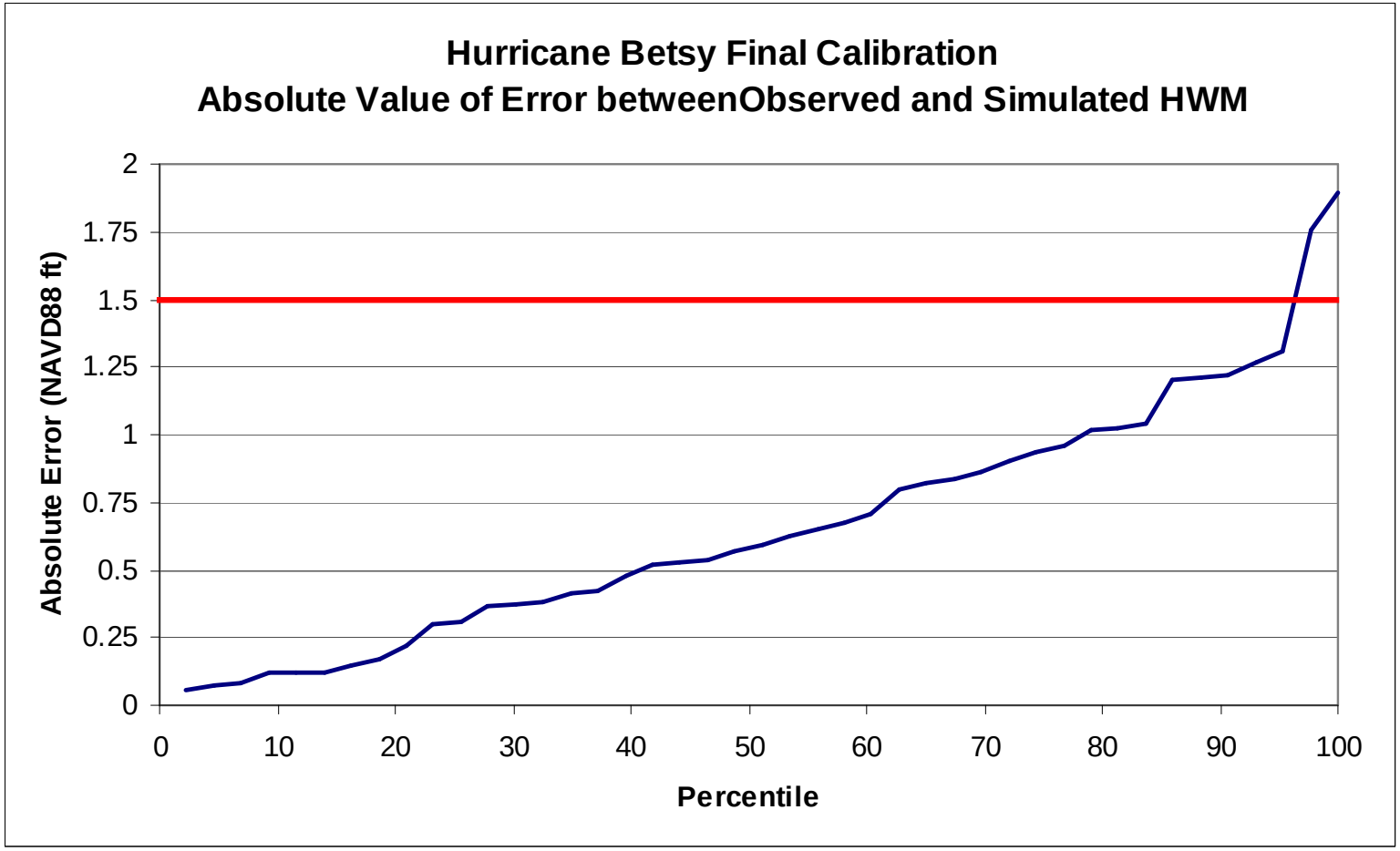

Figure 4-10. Frequency Distribution – Hurricane Betsy.

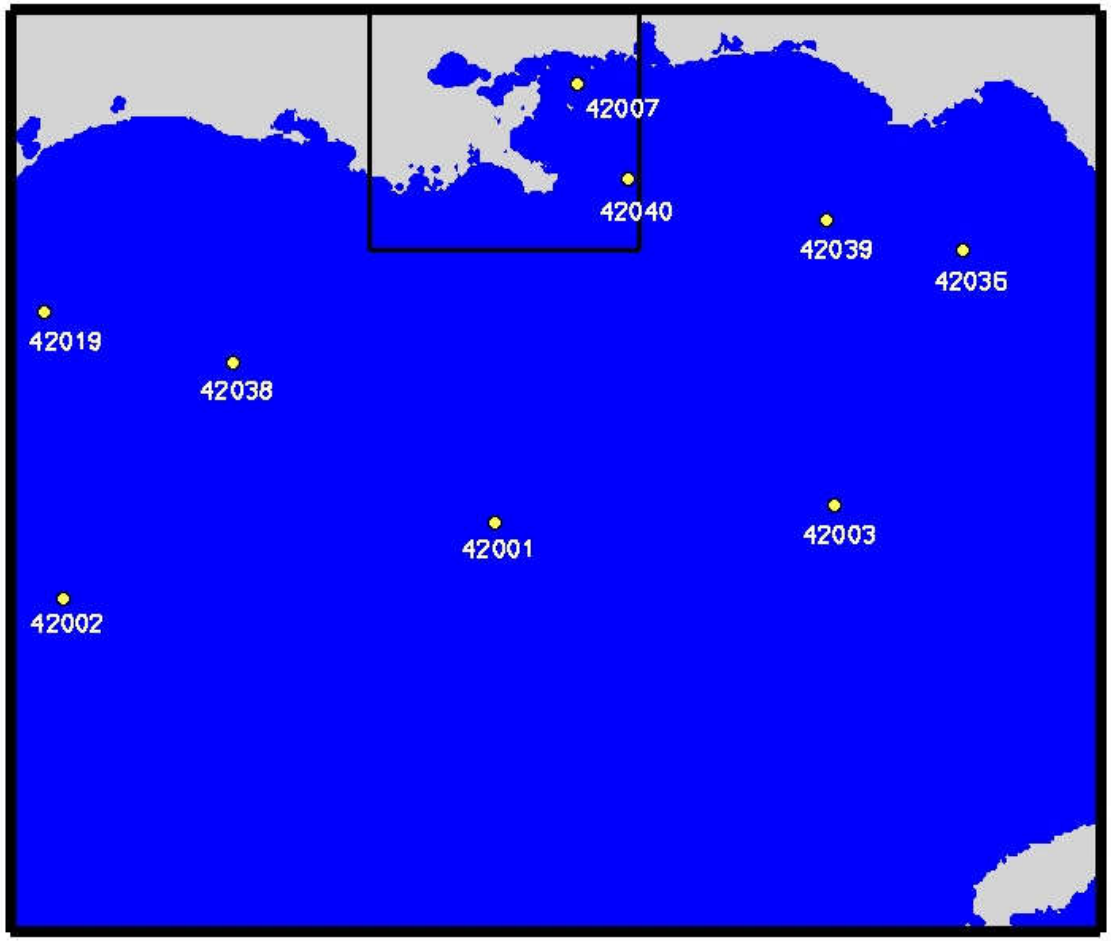

Figure 4-11. Location of NOAA Wave Buoys in the Gulf of Mexico.

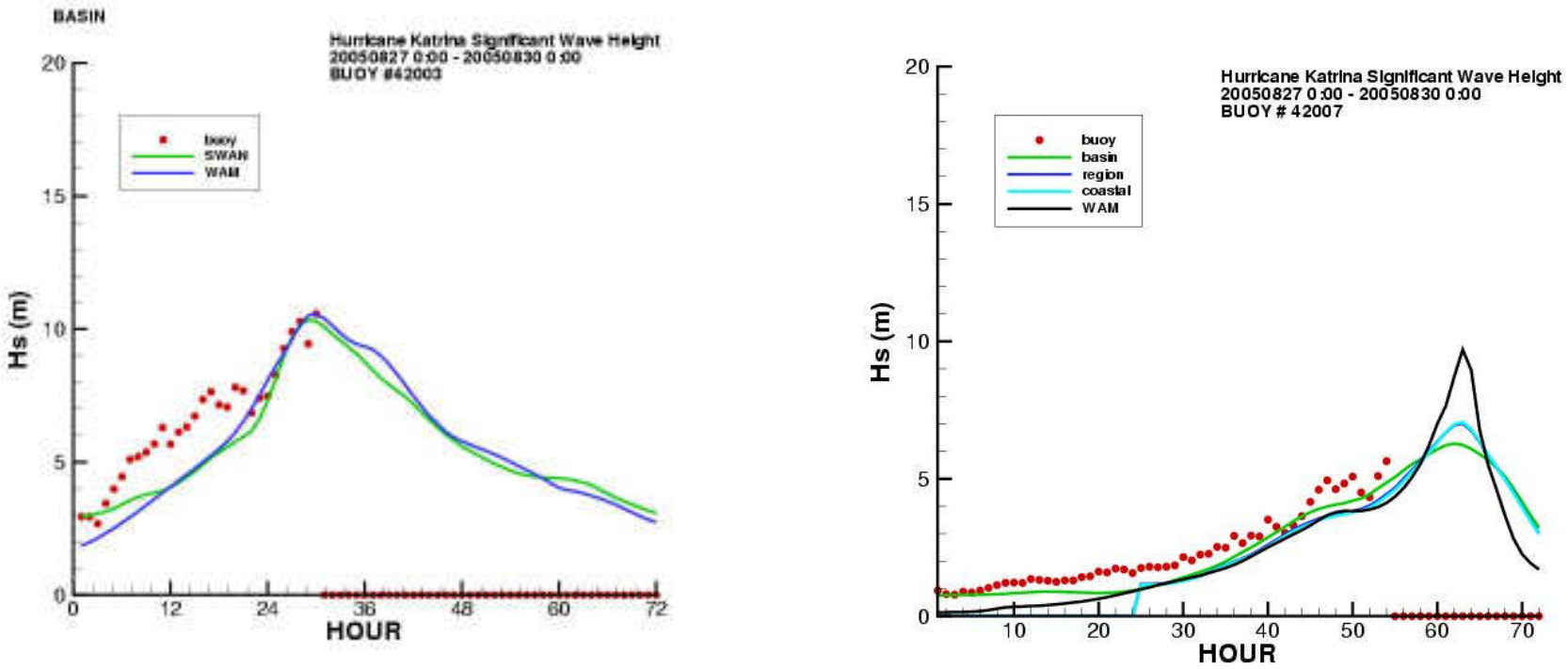

Figure 4-12. Comparison to Wave Buoy Results during Hurricane Katrina (2005) at Buoys 42003 and 42007.

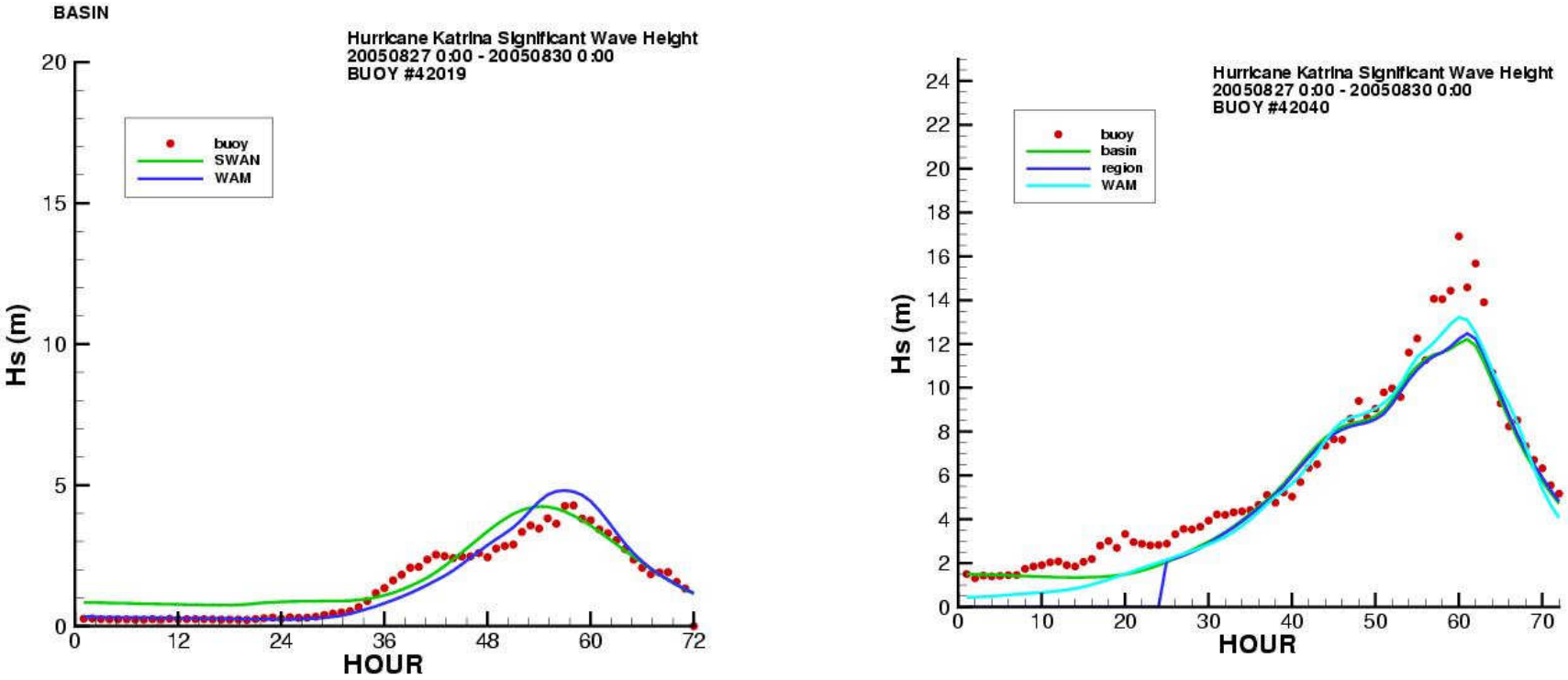

Figure 4-13. Comparison of Wave Model and Buoy Data during Hurricane Katrina (2005) at Buoys 42019 and 42040.

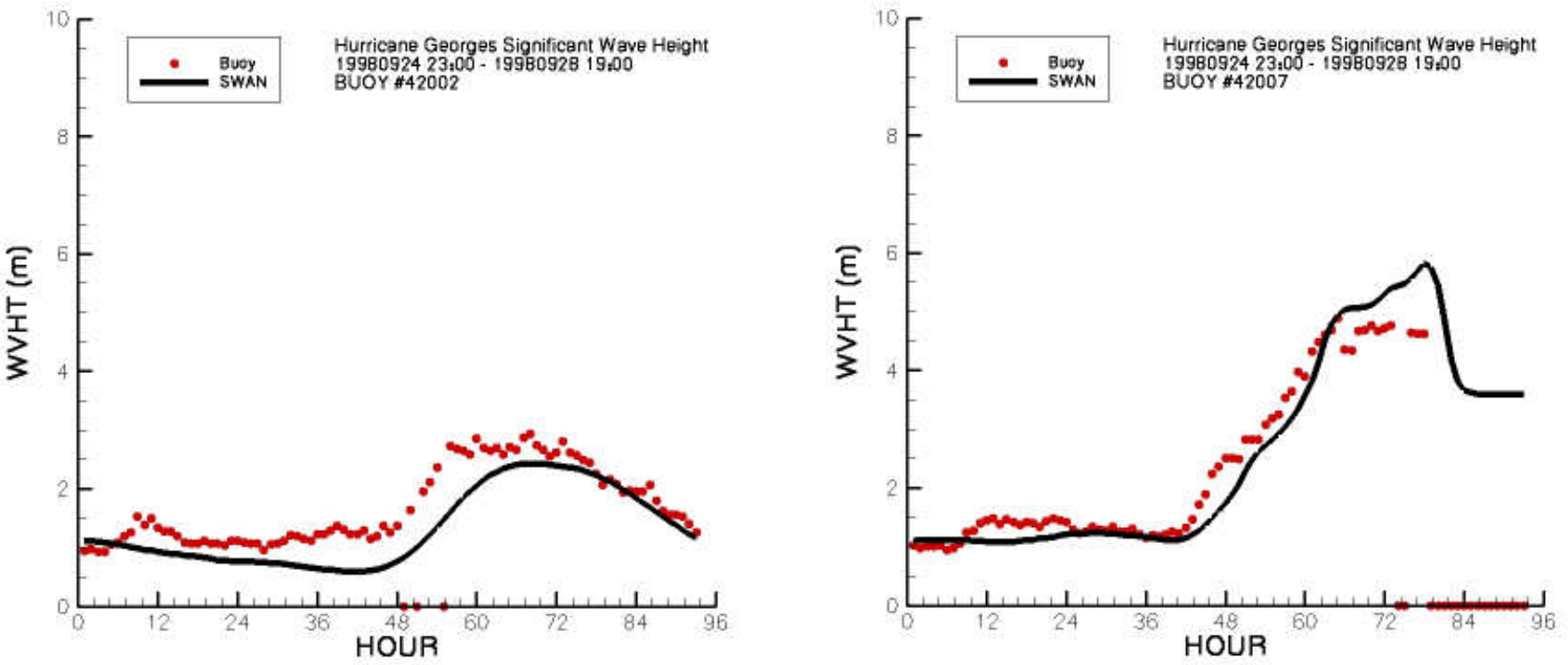

Figure 4-14. Comparison to Wave Buoy Results during Hurricane Georges (1998) at Buoys 42003 and 42007.

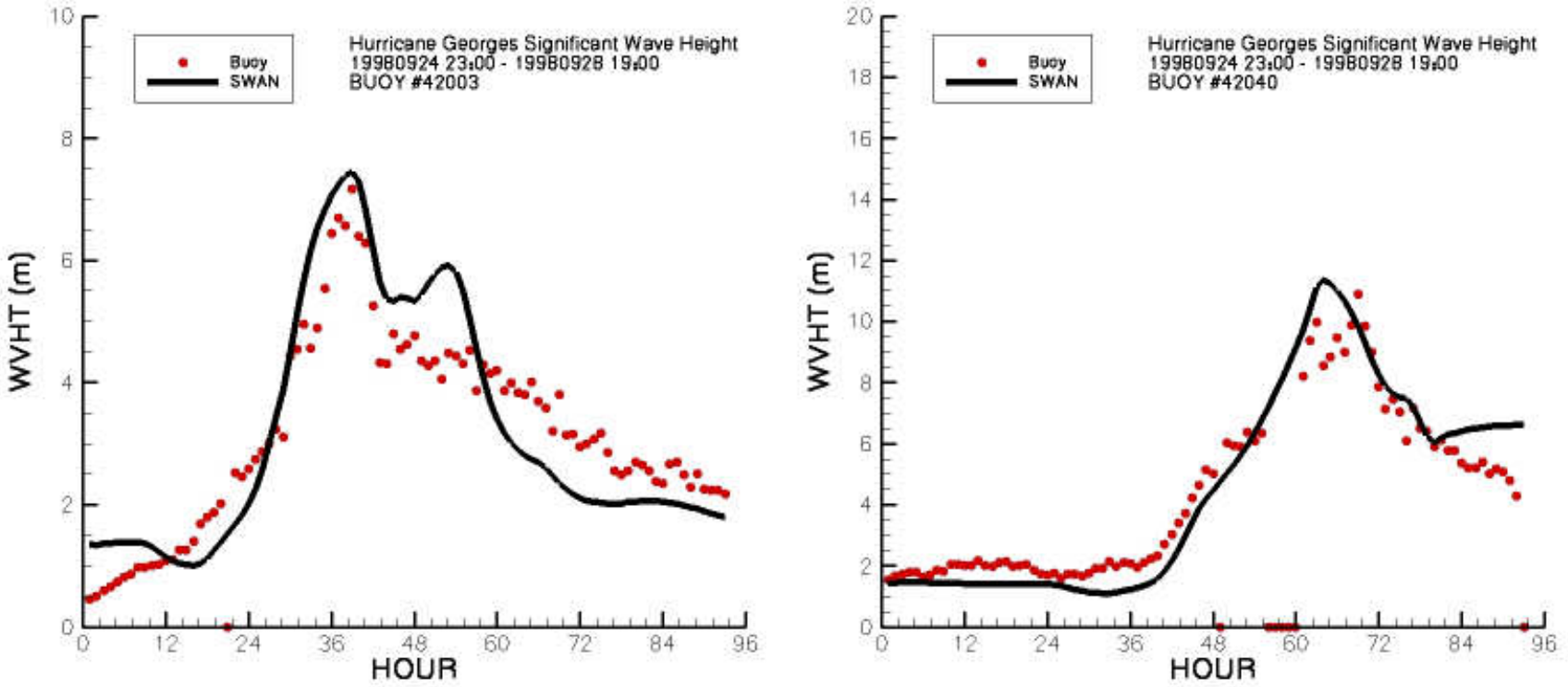

Figure 4-15. Comparison of Wave Model and Buoy Data during Hurricane Georges (1998) at Buoys 42019 and 42040.

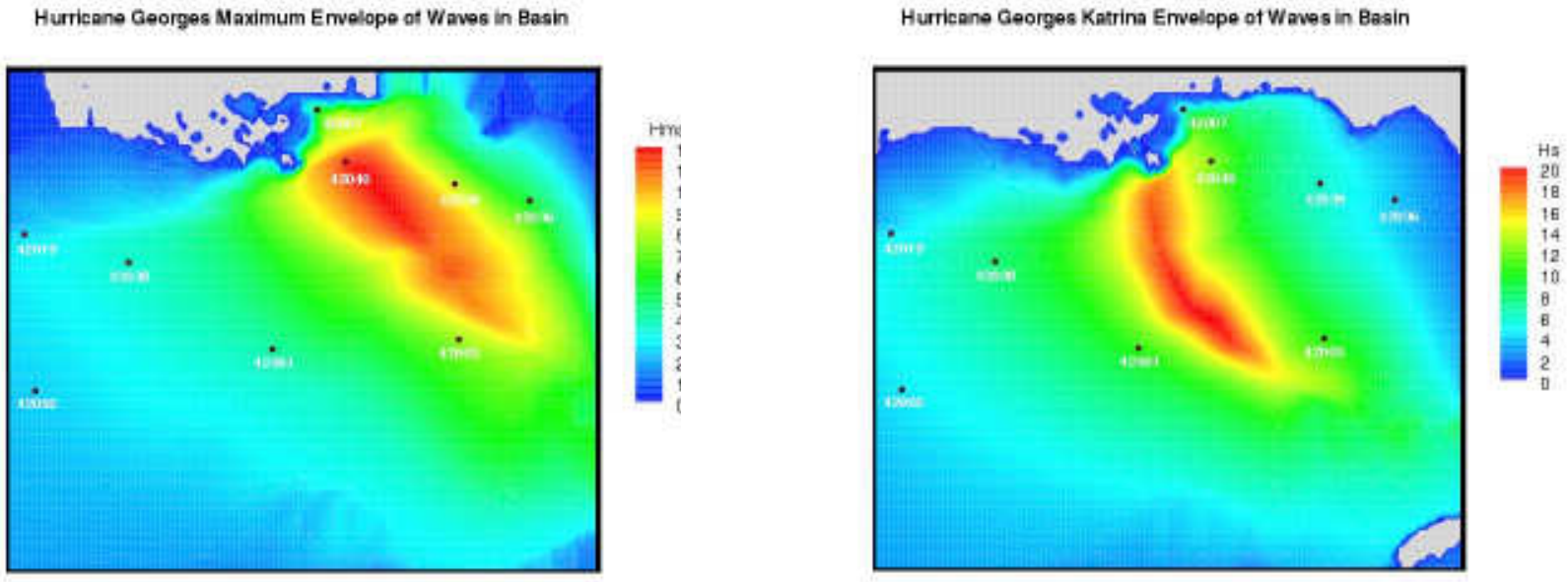

Figure 4-16. Maximum Significant Wave Heights during Hurricane Georges (right panel) and Hurricane Katrina (left panel) during the Simulations in the Basin Model Domains.

5.1 INTRODUCTION

Section 3 described the methods and procedures to characterize the historic hurricanes affecting the project area. It was pointed out that there are three classes of hurricane parameters in this analysis. One class is the five basic storm parameters (ΔP, R_{max}, V_f, θ, and S). The Holland B parameter (which is given special treatment) is the second class. A third class consists of the "epsilon" terms introduced in Section 3.3.1.1, which account for hurricane characteristics not included in the first two classes above, as well as for the limitations of the numerical hydrodynamic models, and for the effect of tide. The fundamental JPM analysis was carried out to the evaluation of surge heights with the numerical model framework for the family of synthetic storms defined by the JPM-OS-6 scheme. The results from these evaluations were then modified by the inclusion of the epsilon term (see Section 3.3 and Equation 6).

This report section describes how the size (more precisely, the standard deviation) of the epsilon term was determined and how the surge results were modified for the effect of epsilon. The methods used to complete the full JPM analysis and to provide the final definitions of the surge elevations for the 1-percent and 0.2-percent-annual-exceedance rate probabilities (note: these annual exceedance probability elevations are hereafter referred to as the Standard Annual Exceedance Levels or SAELs). Finally, the methods by which the results of these final analyses were combined with those of the USACE MsCIP project to obtain a unified set of SAELs are explained.

5.2 EVALUATION OF THE EPSILON COMPONENTS

The epsilon term related to the astronomical tide arises because a hurricane can make landfall at any phase of the tide. The value of this component was derived by taking the standard deviation of the tide based on predicted tides at NOAA Buoy: 8744117 for the 1-year period June 22, 2004 to June 21, 2005. The value of the standard deviation determined using this approach is:

$\sigma_1 = 0.65$ ft [6]

Section 3 notes that the Holland B parameter has both spatially systematic and temporally variable behaviors. The former are accounted for in the modeling by adjustments to the magnitude of the Holland B values as the storm comes within 90 nmi of the coast. It is also necessary to represent the effect of non-systematic variations of this parameter on surge levels.

The Holland B epsilon term was determined using the value given in Resio et al. (2007). This was based on modeled sensitivity tests carried out by USACE. It is defined in terms of the surge elevation:

$\sigma_2 = 0.15$ * surge elevation

and, therefore, it will be different for each synthetic storm and for each output point.

The modeling precision epsilon term was calculated as the standard deviation of the differences between simulations and measurements at common points:

[6] For the sake of simplicity, the standard deviation of ε_i will be denoted by σ_i and the standard deviation of the combined epsilon (i.e., $\varepsilon = \varepsilon_1 + \varepsilon_2 + \varepsilon_3 + \varepsilon_4$) will be denoted by σ_ε.

$$\sigma_3 = \sqrt{\sigma_{cal}^2 - \sigma_{meas}^2} \quad (10)$$

This term was calculated as the standard deviation of the difference between the simulated surge and measured surge at each observation point for all points used in the Katrina, Camille, and Betsy calibration and validation.

As described in Section 4.3.2, the σ_{meas} was obtained by forming groups of measurement from adjacent locations where it is reasonable to expect the same surge elevations due to their similar geographic location. The average elevation within each group was taken as a reasonable estimate of the true value. In each group, the average value was subtracted from the individual measurements. These differences from all groups were pooled and the overall standard deviation was determined as the measure of the characteristic measurement error. Using these methods, the simulation and measurement precision were:

σ_{cal} = 1.51 ft (estimate of calibration error)

σ_{meas} = 1.3 ft (estimate of measurement error),

yielding a value of

σ_3 = 0.77 ft

for the modeling errors.

In the hydrodynamic model calibration and validation process, the wind fields used to drive the hydrodynamic models are the so-called best winds, which are developed by combining inputs from a variety of data sources. In contrast, JPM synthetic storms use idealized wind and pressure fields.

Because the wind field represented in the JPM synthetic-storm modeling is not as good a representation of the wind field as that used to both validate the hydrodynamic models and to obtain estimates of the water elevation variability associated with the hydrodynamic-best wind modeling process, an additional variability term must be taken into account.

An estimate of the additional variability term associated with the use of PBL winds in the JPM process was obtained by re-modeling the calibration/validation storms using the PBL wind field algorithms alone to define the pressure field, and computing the water elevation variability either as a total variability (modeled minus observed) or an additional variability term (best wind model-Holland wind model). The variance associated with this additional model variability term must be added to the variances of any other variability terms used in the modeling process.

The variability associated with actual versus ideal winds was calculated as the standard deviation of the difference between the simulated surge for actual winds and ideal winds at the roughly 4,000 JPM points that had non-zero surge values. Prior to taking the standard deviation of the differences, the differences were shifted by a constant so that the average difference was zero. The final value of this term is:

σ_4 = 1.17 ft

The final value of the epsilon term was obtained by combining these components, under the assumption of independence, according to

$$\sigma_\varepsilon = \sqrt{\sigma_1^2 + \sigma_2^2 + \sigma_3^2 + \sigma_4^2} \tag{11}$$

Because the second term in the sum is a function of the surge height, this function was evaluated for each surge height value.

5.3 CALCULATION OF SURGE ELEVATIONS AND RECURRENCE INTERVALS, INCLUDING THE EFFECT OF EPSILON

During the model simulation of the synthetic storms, the maximum water level elevation in each event was determined and stored for each output point of interest. Over 9,000 model output points were distributed across the portion of the ADCIRC grid that could be inundated. The maximum spacing was 1 km. Closer spacing was used where warranted by local relief. For example, point spacing along stream channels was a maximum of 0.5 km. To avoid the possibility of under-coverage, the area covered by the output points was somewhat greater than would be inundated by even the greatest storms.

The calculation method for determining the stillwater elevations for given return intervals was made independently for each output point. For each of these points, the ADCIRC model simulations of each synthetic storm resulted in a maximum surge elevation, each with an associated rate.

The results of the 228 individual surges were processed at each point to estimate surge elevations associated with various return intervals. For each point, an initial histogram of the surge levels at a point was generated using 600 bins with an elevation width of 2 cm, spanning the range from 0 to 12 m (above the highest anticipated surge). The rate associated with each synthetic storm was accumulated into the appropriate bin. This process yielded the total rate Λ_j, where j is the bin index, which provides an approximation of the surge height annual-rate density function[7] at the point, similar to the example shown in Figure 5-1. Up to this point, the contribution of the epsilon terms described above is not considered. The procedure for the introduction of epsilon is described below.

Each bin's total rate Λ_j was modified according to the following equation:

$$\Lambda_j^{new} = \sum_{i=1}^{600} \Lambda_i \alpha_i \, e^{-\frac{1}{2}\left[\frac{(x_i - x_j)}{\sigma_{s_i}}\right]^2} \tag{12}$$

where *j* is the index of a specific bin, *i* is the general index for all bins, x is the bin's center value, and α_i is a normalizing constant defined below. The standard deviation σ_{s_i} is bin-dependent because σ_2 depends on the size of the calculated surge, as described earlier.

The normalizing constant α_i ensures that the total event probabilities are conserved. It is necessary due to the discrete implementation of the Gaussian function and because some of the

[7] This is not a probability density function because it does not integrate to unity. Instead, the rate Λ_j obtained for each bin is the annual rate of storms that cause the surge associated with that bin, at the grid point being considered.

normalizing constants in the Gaussian density function were omitted. The normalizing constant is calculated as:

$$\alpha_i = \frac{1}{\sum_{k=1}^{600} e^{-\frac{1}{2}\left[\frac{(x_i - x_k)}{\sigma_{\varepsilon_i}}\right]^2}} \quad (13)$$

An example of this redistribution is shown in Figure 5-2 for the contents of a single bin. The result after redistribution of all the bins is illustrated in Figure 5-3.

The modified histogram was then summed from the highest bin down to the lowest, resulting in an estimate of the cumulative surge distribution. This is illustrated in Figure 5-4, which shows the cumulative probability curve corresponding to the modified histogram in Figure 5-3. The surge height for any return period can then be interpolated from this curve. For example, the 100-year surge elevation corresponds to a cumulative rate of 1-percent-annual-exceedence rate, and is estimated to be about 4.5 m. The same procedure yields the 10-, 50-, and 500-year levels, corresponding to cumulative rates of 10-, 2-, and 0.2-percent-annual-exceedence rate.

5.4 COMBINING VALUES WITH JOINT FEDERAL COASTAL FLOOD ELEVATIONS

As a final step, the SAELs (i.e., the 2-percent, 1-percent and 0.2-percent-annual-exceedence rate surge levels) were compared to the corresponding results from the USACE MsCIP project. The median difference in the 1-percent-annual surge elevation was 0.07 ft between the results developed for this Mississippi Coastal Analysis Project Report and the corresponding USACE MsCIP results for more than 4,400 points scattered over the coastal counties. Over 90 percent of the values were within ± 1.0 ft of each other and none of the differences were more than 1.9 ft. Similar levels of agreement were found for the other statistical flood surfaces at the 10-percent and 2-percent annual exceedence rate levels.

Since the results compared acceptably well, they were combined to produce a single best estimate for the Mississippi coast. More details about the procedure that produced the combined results are available in the*Technical Support Data Notebook*. USACE has also been determining coastal flood levels for the adjacent areas of Louisiana, but because of schedule differences, those results were not available for final comparisons or for combination as were the MsCIP results.

5.5 THE 10-, 50- AND 500-YEAR SURFACES

The SAELs were determined for all of the ADCIRC output points. The number of these points varied because the lower frequency events flood further inland. These data formed the basis for the WHAFIS overland wave analysis and the preparation of the draft flood maps.

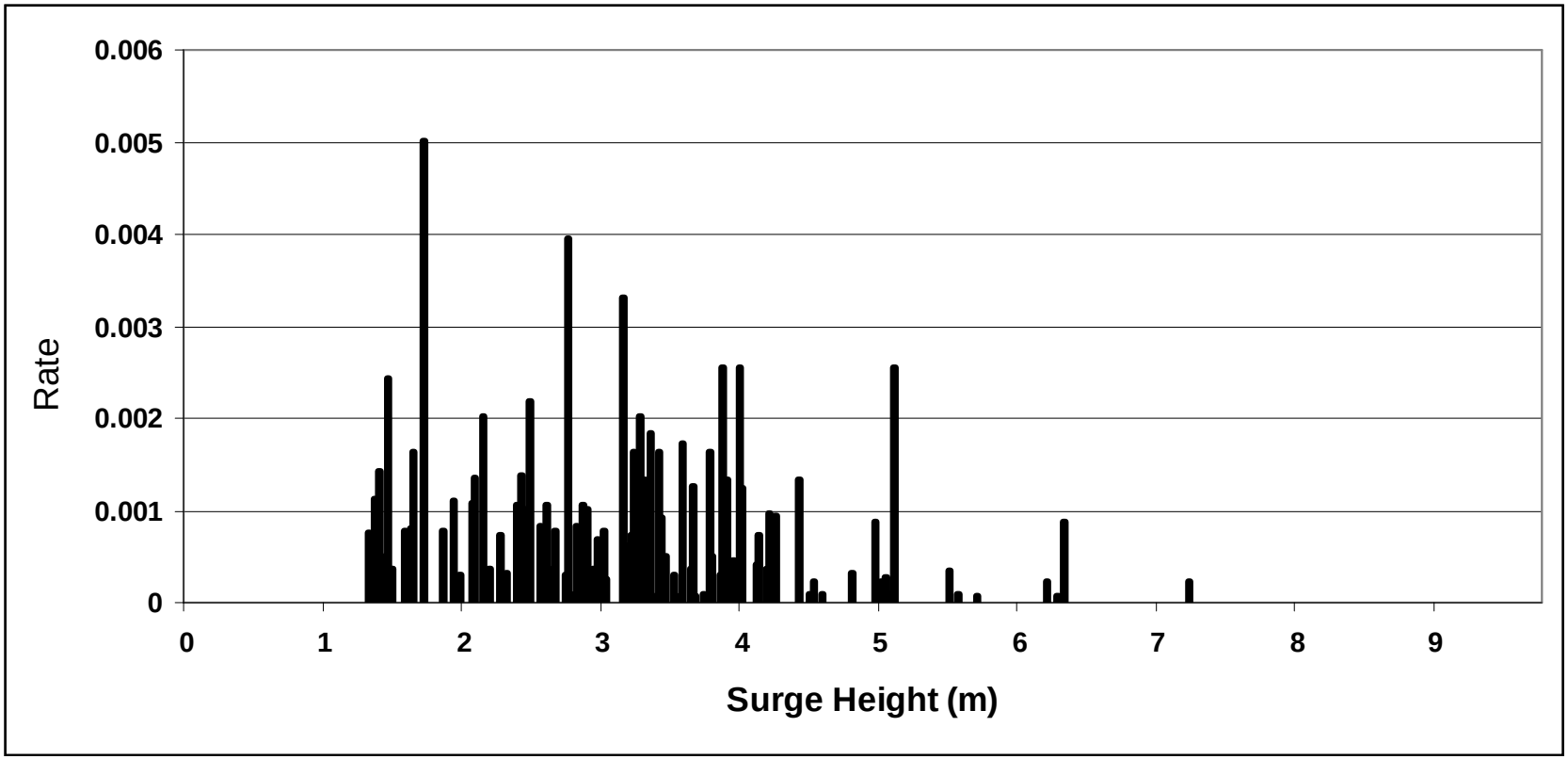

Figure 5-1. Histogram Generated for a Single JPM Point Based on Surges and Event Probabilities.

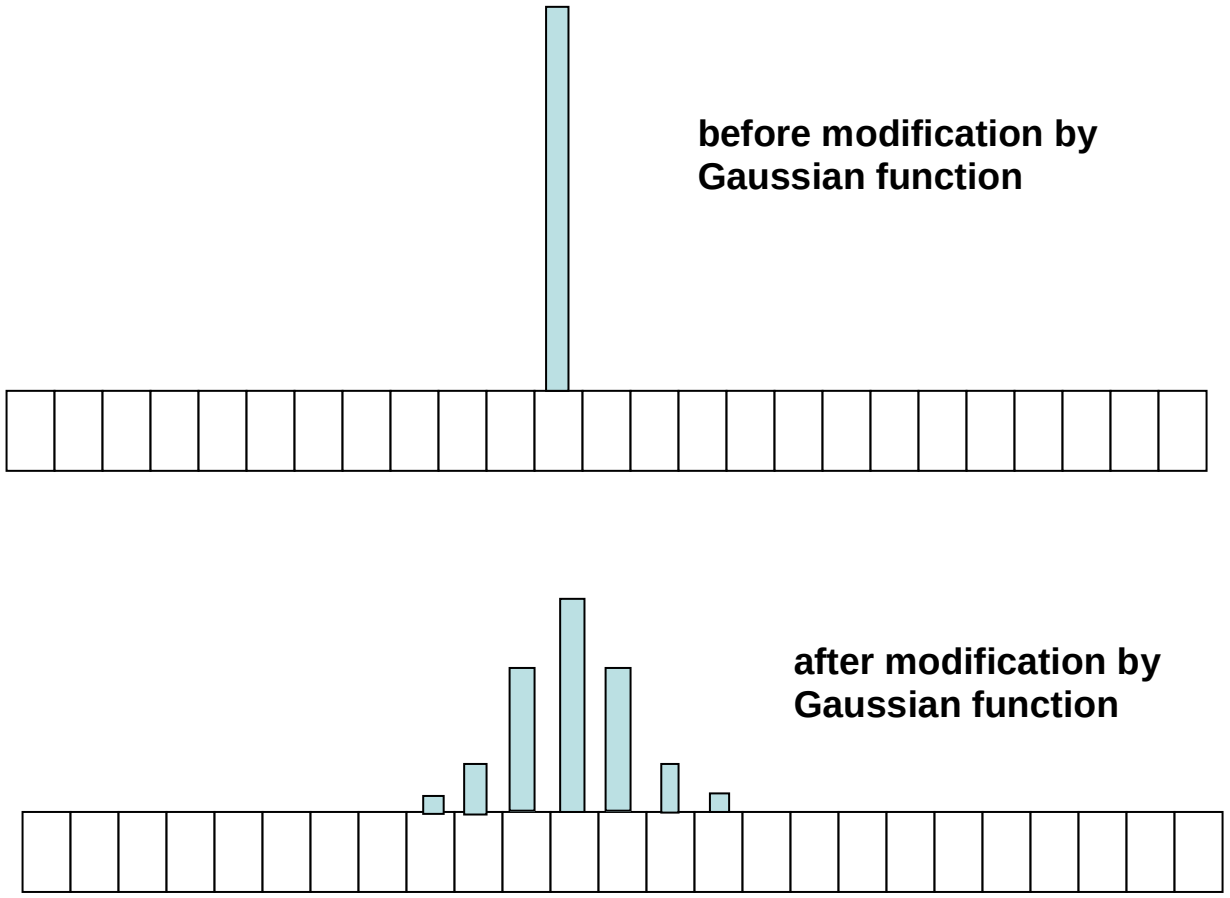

Figure 5-2. Example Application of the Epsilon Terms Using the Gaussian Function.

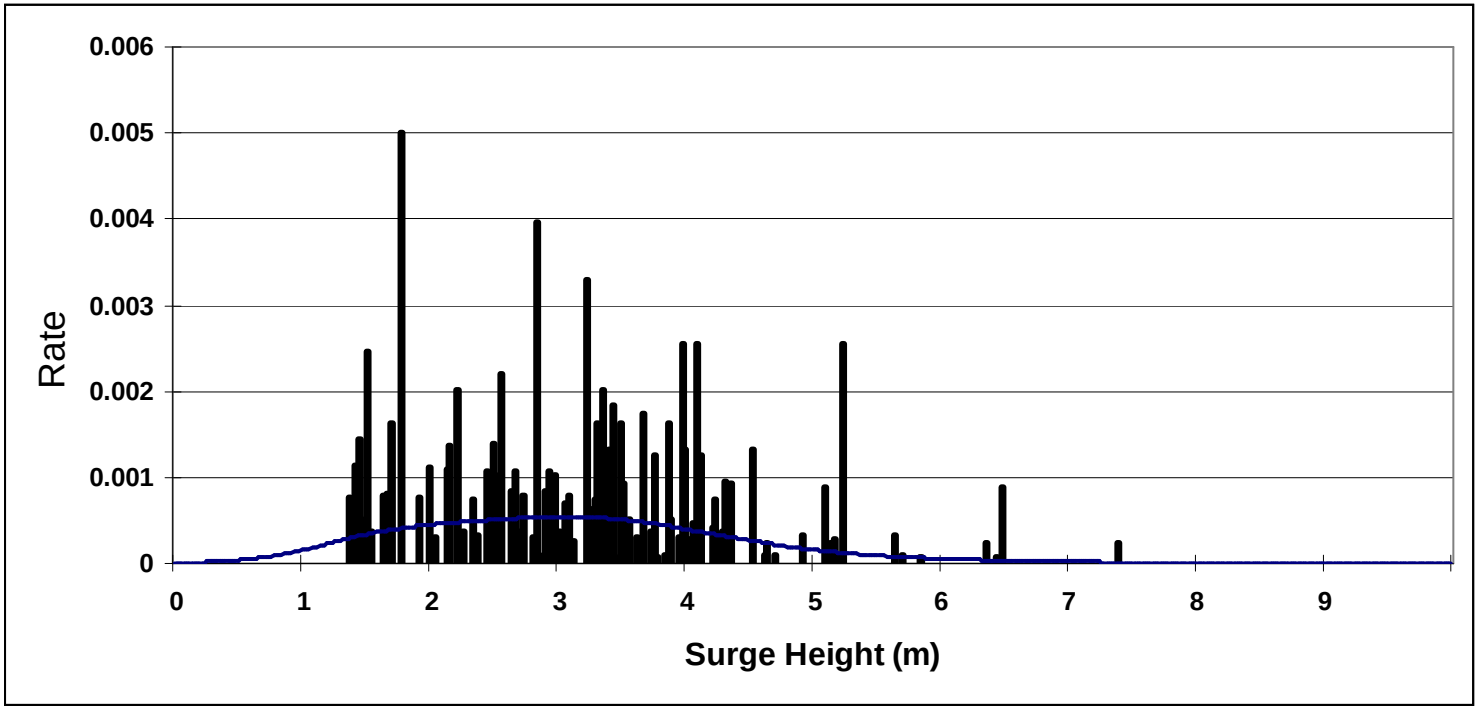

Figure 5-3. Histogram Following the Application of the Epsilon Term (blue line).

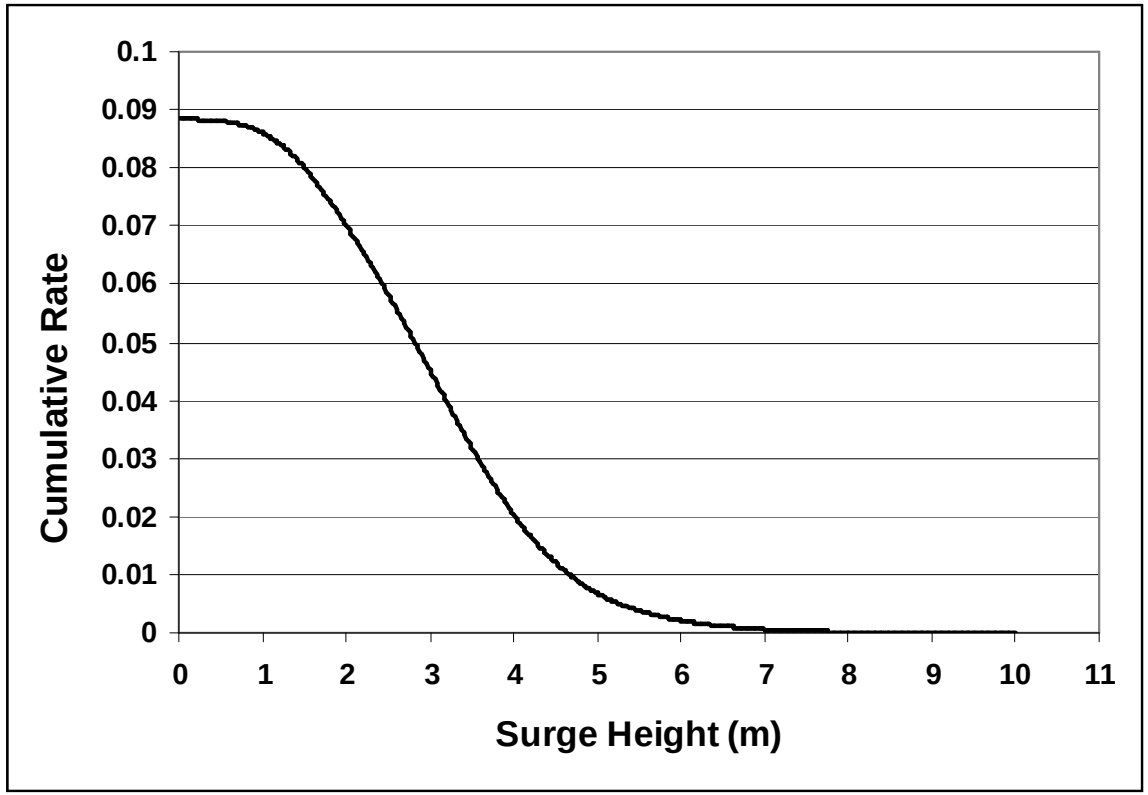

Figure 5-4. Cumulative Rate Plot and Determination of the 100-Year Surge.

6.1 WAVE HEIGHT ANALYSES FOR FLOOD INSURANCE STUDIES (WHAFIS)

The work described in the foregoing sections of this report resulted in determinations of the stillwater elevations (SWELs) and included the effects of wave setup. While these data can be used immediately to delineate 100- and 500-year floodplain boundaries, additional overland wave modeling using the 100-year SWELs is necessary to determine the BFEs and flood hazard zones (VE and AE) that are depicted on DFIRMs. This analysis is summarized in this report section. Much more detail about these methods and the quality assurance procedures are given in the supporting project report titled *Detailed Wave Analysis and Mapping Report.*

6.2 TRANSECT AND MODELING RESOURCES

The wave modeling and flood hazard mapping required multiple high-resolution geospatial datasets, including terrain (topography and bathymetry) and aerial imagery.

6.2.1 Terrain

For topography, pre-Hurricane Katrina lidar data for the three counties, which were collected between 2003 and 2005 by the State of Mississippi and NOAA, were merged with post-Katrina (September-October 2005) lidar data collected along the coast by USACE.

The bathymetric data obtained from the Northern Gulf Littoral Initiative (NGLI) reflect data gathered by multiple Federal and State agencies, universities, and private contractors. The NGLI data were augmented, where necessary, by NOAA navigation charts.

All terrain data were provided in the North American Vertical Datum of 1988 (NAVD88). The 1982-1983 composite NOAA shoreline (zero-ft contour) was used.

6.2.2 Aerial Imagery

Both pre-Katrina and post-Katrina high-resolution orthophotographs were available. Because the wave modeling and mapping were to be based on the vegetation and development patterns in existence at the time of the study (rather than some assumed future condition following recovery), the post-Katrina imagery was used. This imagery, dated September 15, 2005, originated from the U.S. Department of Agriculture.

6.3 WAVE TRANSECT SELECTION

For the Mississippi Coastal Analysis Project, the initial transect layout was developed following the procedures outlined in FEMA's *Guidelines and Specifications.* Each transect was intended to be representative of a particular reach along the coast with similar physical characteristics. After consulting available aerial imagery and effective Flood Insurance Studies, transect sites were chosen to capture the variability in coast orientation and coastal topography, large-scale vegetation distribution, and development patterns. Care was taken to ensure that transects crossed key secondary flooding sources in inland areas, such as bays and tidal rivers.

A few crossing transects were included in the initial layout to better resolve overland wave patterns over peninsulas. In East Biloxi (Harrison County) and Bay St. Louis (Hancock County),

flooding and wave effects from both easterly and southerly directions pose substantial hazards. As a result, crossing transects in these orientations were included.

The final layouts of the coastal transects for Jackson, Hancock, and Harrison Counties are shown in Figures 6-1 through 6-3. These 161 transects reflect an increase of 55 percent over the 104 transects modeled in the 1980s Effective Flood Insurance Studies for the Mississippi coast.

6.4 FIELD RECONNAISSANCE

Field reconnaissance along the Mississippi coast was carried out over a 2-week period in early June 2006 to document key features not visible on the imagery, such as building foundations (open versus enclosed) and vegetation types and characteristics (size, density, etc.).

6.5 STILLWATER ELEVATIONS

The 1-percent-annual-exceedence rate stillwater elevations were uploaded into the Geographic Information Systems (GIS)-based modeling tools, the WISE Coastal Module, and GeoFIRM coastal tools and interpolated to the nearest corresponding point (wave transect station) on the transects. Elevations were converted to feet rounded to the nearest tenth. The results were then examined to ensure there were no erroneous interpolations within the floodplain or extrapolations into above-surge areas at the floodplain boundary.

6.6 STORM-INDUCED EROSION

The ground elevations near the shoreline recorded in the post-Katrina LiDAR data were assumed to reflect eroded conditions. Thus, no storm-induced erosion assessment was applied to any transect in the Mississippi Coastal Analysis Project.

6.7 WAVE HEIGHT MODELING

The hydrodynamic forces associated with waves pose a substantial additional hazard to buildings beyond simple inundation. The 2-D wave modeling that resulted in including the contribution of wave setup to the SWELs was described in Section 4.4.1.1. A different suite of models was applied to map the spatial distribution wave heights that are associated with the base flood. The latest version of the program Wave Height Analyses for Flood Insurance Studies (WHAFIS), version 4.0, is capable of calculating the effects of open fetches and obstructions on the growth and attenuation, respectively, of wave heights on a detailed scale (i.e., large property or lot scale) for both the 100- and 500-year flood levels.

6.7.1 Input Preparation

For each of the 161 coastal transects, detailed ground profiles were extracted from the high-resolution digital terrain surface (i.e., the Triangulate Irregular Network (TIN) in the WISE Coastal Module and the Digital Elevation Model [DEM] in the GeoFIRM Coastal Tools). These were then edited to WHAFIS profiles, with appropriate resolution, eliminating redundancy and negligible variations. To enforce consistency, an initial station of zero and elevation of 0 ft were adopted throughout this study.

The procedure for determining the Initial Elevation (IE) station location in WHAFIS varied slightly depending on which GIS-based modeling toolset was used for transect modeling. For transects modeled in the WISE Coastal Module, the TIN interpolated a 0-ft elevation from the lidar topographic data and bathymetric grid. WHAFIS profile IE stations were then placed where the ground data showed the elevation to be 0 ft (NAVD88). This elevation contour was found to deviate significantly (e.g., 10s to 100-200 ft or more) from the NOAA composite shoreline in some locations (see Figure 6-4). This lack of spatial coincidence is not unreasonable given the age of the NOAA dataset, which is 22-23 years older than the 2005 lidar data. Spot checks of the terrain data showed that most of the problem areas were located in Hancock County. The NOAA shoreline appeared consistent enough with current (2005) conditions in Jackson County to be burned into the GeoFIRM DEM as a 0-ft contour. As a result, the IE stations for all transects in this reach (Jackson County transects 24 to 55) were aligned with the NOAA shoreline.

The remaining stations in the WHAFIS profile were generated in a straightforward manner.

6.7.2 Incident Wave Conditions

The extensive 2-D wave modeling, described in Section 4.4.1.1, was primarily directed towards incorporating wave setup in the ADCIRC hydrodynamic model simulations of the synthetic storms. However, this work also provided the basis to develop 100-year and 500-year significant wave heights and wave periods at the approximate location of the IE station for each of the 161 wave transects. The procedures used to identify the wave conditions that corresponded to the time of the maximum surge elevations used in the recurrence interval analysis are described in detail in the supporting project report titled *Wave Setup Methodology for the FEMA Mississippi Flood Study.*

6.7.3 WHAFIS Modeling

WHAFIS 4.0 runs were executed for all 161 wave transects. The resulting 100-year wave height profiles were automatically subdivided by WHAFIS 4.0 into flood hazard zones (VE and AE) and whole-foot BFEs to the limit of the 100-year floodplain. Application of these results for floodplain mapping is discussed in Section 7.

6.7.4 500-Year Wave Modeling

WHAFIS profiles were extended where necessary to encompass the entire 500-year floodplain, and station-elevation pairs were also populated with 500-year SWELs derived from a surface generated from the corresponding JPM point data. The same field reconnaissance data and aerial imagery were used to model the new segments of the WHAFIS profiles falling below the 500-year SWEL. Input wave heights and periods were provided for 500-year wave analyses. The source of these inputs is described in the supporting project report titled *Wave Setup Methodology for the FEMA Mississippi Flood Study*.

6.8 WAVE RUNUP MODELING

Slopes steeper than 1-on-10 on the transects were designated for calculation of wave runup. This involved 14 transects, or less than 10 percent of the total. The Technical Advisory Committee for

Water Retaining Structures (TAW) runup model was adapted for use as explained in the supporting project report titled *Detailed Wave Analysis and Mapping Report*.

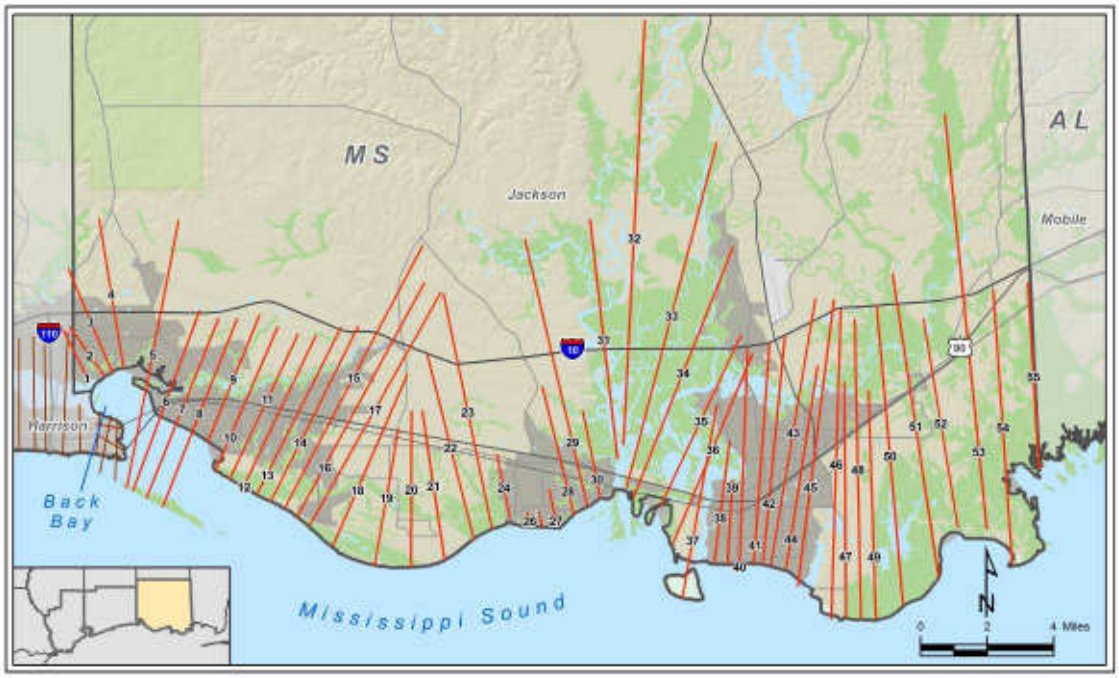

Figure 6-1. Transect Location Map for Jackson County.

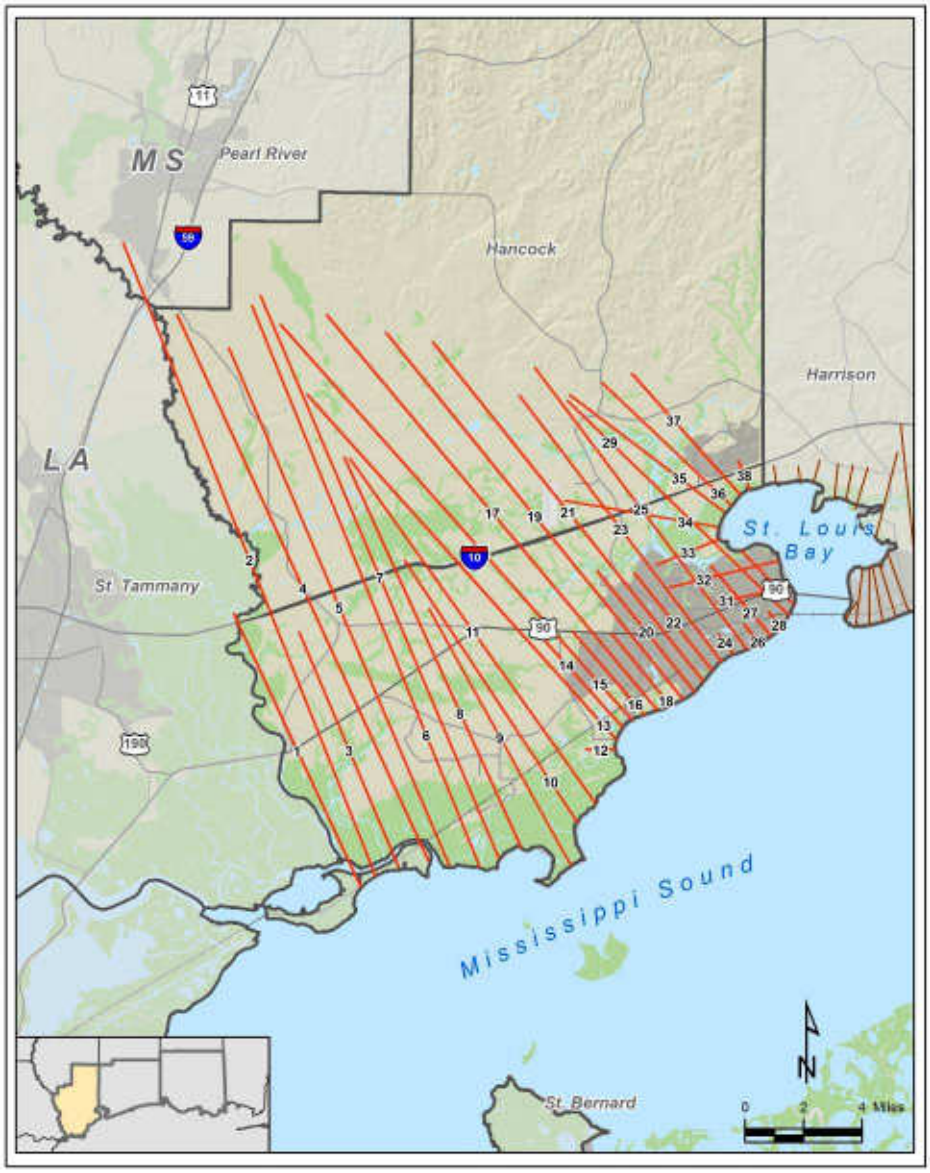

Figure 6-2. Transect Location Map for Hancock County.

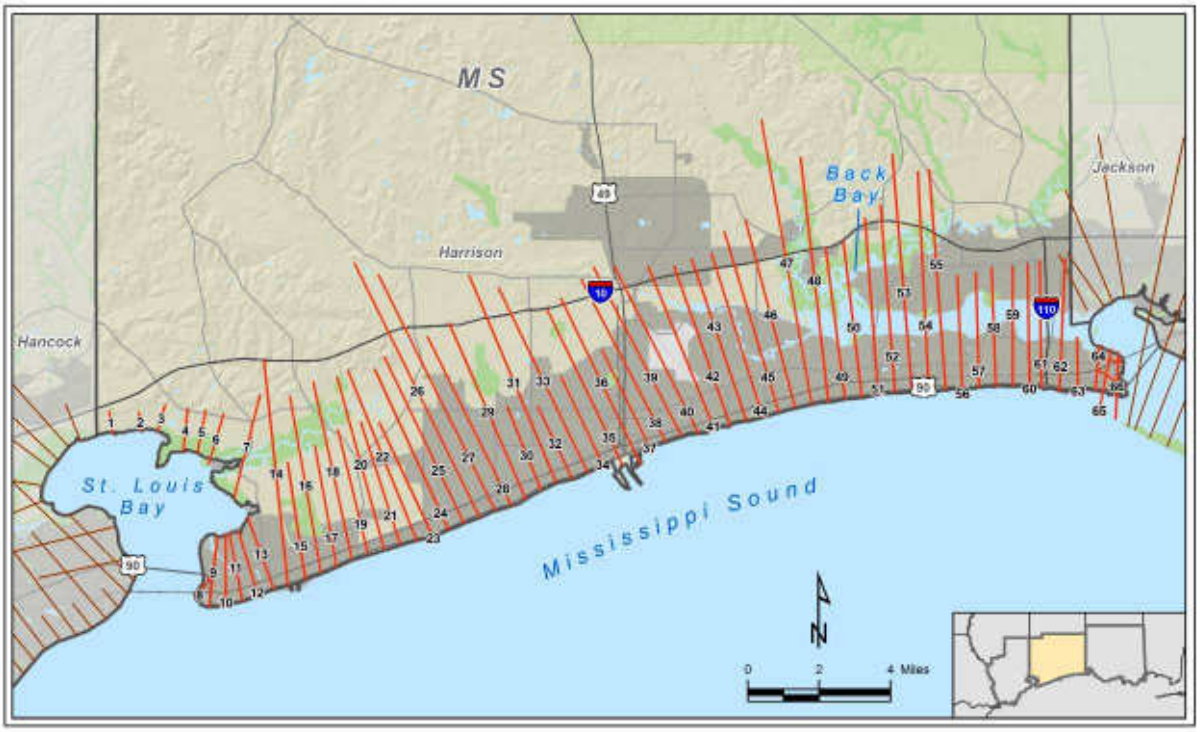

Figure 6-3. Transcect Location Map for Harrison County.

Figure 6-4. NOAA Composite Shoreline (in red) Compared to 2005 Orthoimagery from Bay St. Louis (Hancock County).

7.1 INTRODUCTION

The BFE Work Maps were one of the major project deliverables. These were delivered to State contractors who prepared the final maps. This section describes the procedures for creating the Work Maps. More detail on these subjects and a description of the related quality assurance procedures is given in the supporting project report titled *Detailed Wave Analysis and Mapping Report.*

7.2 100-YEAR AND 500-YEAR FLOODPLAIN BOUNDARIES

Both the WISE Coastal Module and GeoFIRM Coastal Tools use standard GIS utilities to spatially analyze the available terrain and SWEL data and to generate initial 1-percent- and 0.2-percent-annual-chance (100- and 500-year) floodplain boundaries. This produced a very irregular initial boundary, as well as many small, isolated areas that were inconsistent with the prevailing conditions in the area (e.g., dry islands within flooded areas, small ponds with no direct hydraulic connection to a coastal flooding source). With the initial mapping as a guide, the final boundaries were manually drawn.

7.3 WAVE ANALYSIS RESULTS

The BFEs for the Zone VE and Zone AE special flood hazard areas were determined using the WHAFIS results. After examining the results to determine what features were controlling (elevation, land-use, etc.), the zones were averaged to make sure all reaches had appropriate minimum dimensions that were within at least 0.2 tenths of the map scale or 100 ft in width (any reaches <100 ft were generally not included due to map scale limitations, but sometimes 40 to 50 ft widths were accommodated). All of the results were hand-checked and corrected based on engineering judgment.

7.4 HAZARD ZONE AND BFE MAPPING

All hazard zone and BFE mapping followed the FEMA February 2007 *Atlantic Ocean and Gulf of Mexico Guidelines Update.* There was only one case, along the coast of Jackson County, in which the primary frontal dune criteria were applied to the Zone VE mapping.

7.5 MAPPING OF THE INLAND LIMIT OF MODERATE WAVE ACTION

Flood Insurance Rate Maps currently depict Zone VE areas, or the Coastal High Hazard Area, where high velocity flow due to wave action can cause structural damage to building foundations and other critical elements. Damage observed following numerous coastal storms over the last 15 years has shown a need to either lower the threshold for defining the Zone VE (wave height of 3 ft or greater) or to subdivide the Zone AE in such a way to show which areas have sufficient wave hazards to recommend more restrictive building practices.

FEMA has recently elected to map an advisory line at the limit of the 1.5-ft wave height that subdivides the Zone AE. In March 2007, FEMA issued a procedures memorandum that provided guidance on the identification and mapping of the 1.5-ft wave height line, also known as the Limit of Moderate Wave Action (LiMWA).

To map the LiMWA, the full WHAFIS 4.0 wave profile was analyzed, and points were plotted along each transect where the wave height crossed 1.5 ft.

Then, like a flood zone gutter, the LiMWA was plotted via interpolation between transects. In runup-dominated areas, the LiMWA was placed immediately landward of the Zone VE to Zone AE gutter, per the current FEMA guidance, and was tied in with adjacent wave height-dominated zone mapping. To aid in the utility of this new flood map data layer, every effort was made to keep the line as a continuous feature throughout the study area, even when flood zones were at minimum widths. The LiMWA was discontinued in instances when there were no Zone AE areas (i.e., zones went directly from VE to X500). The LiMWA was truncated at the point where the last Zone AE pinched out at the 100-year boundary.

Andorka Gal, J.H., L.H. Holthuijsen, J.C.M. de Jong, and A.T.M.M. Kieftenburg. 1998. "Wave transformation near a quasi-1D coast," 26th International Conference on Coastal Engineering, Copenhagen, 150-160.

Bea, R.G., N.W. Lai, A.W. Niedoroda, and G.H. Moore. 1983. "Gulf of Mexico Shallow-Water Wave Heights and Forces," Offshore Technology Conference; Vol/Issue: 3; May 2,1983; Houston, TX.

Benjamin, J.R., and C.A. Cornell. 1970. *Probability, Statistics, and Decisions for Civil Engineers*, New York: McGraw Hill.

Blake, E.S., J.D. Jarrell, E.N. Rappaport, and C.W. Landsea. 2005. *The Deadliest, Costliest, and Most Intense United States Tropical Cyclones From 1851 to 2004 (And Other Frequently Requested Hurricane Facts)*, NOAA Technical Memorandum NWS TPC-4.

Booij, N., R.C. Ris, and L.H. Holthuijsen. 1999. "A third-generation wave model for coastal regions, Part I, Model description and validation," *Journal Geophysical Research* C4, 104, 7649-7666.

Booij, N., L.H. Holthuijsen, and IJ.G. Haagsma. 1998a. "Comparing the second-generation HISWA wave model with the third-generation SWAN wave model," 5th International Workshop on Wave Hindcasting and Forecasting, Jan. 27-30, 1998, Melbourne, FL, 215-222.

Booij, N., L.H. Holthuijsen, and R.C. Ris. 1998b. "Shallow water wave modeling," Oceanology International 98, The Global Ocean, Brighton, Conference Proceedings, 3, 483-491.

Booij, N., L.H. Holthuijsen, N. Doorn, and A.T.M.M. Kieftenburg. 1997a. "Diffraction in a spectral wave model," Proceedings 3rd International Symposium on Ocean Wave Measurement and Analysis, WAVES'97, ASCE, 243-255.

Booij, N., L.H. Holthuijsen, and R. Padilla-Hernandez. 1997b. "Numerical wave propagation on a curcilinear grid," Proceedings 3rd International Symposium on Ocean Wave Measurement and Analysis, WAVES'97, ASCE, 286-294.

Booij, N., L.H. Holthuijsen, and R.C. Ris. 1996. "The SWAN wave model for shallow water," Proceedings of the 25th International Conference on Coastal Engineering, Orlando, FL, Vol. 1, pp. 668-676.

Borgman, L.E., M.C. Miller, H.L.Butler, and R.D. Reinhard. 1992. "Empirical simulation of future hurricane storm histories as a tool in engineering and Economic Analysis," ASCE Proceedings for Civil Engineering in the Oceans V. College Station, TX. 2-5 November 1992.

Cardone, V. J. and C. K. Grant. 1994. "Southeast Asia meteorological and oceanographic hindcast study (SEAMOS)," OSEA 94132. 10th Offshore Southeast Asia Conference, 6-9 December. 1994.

Cardone, V. J., A. T. Cox, J. A. Greenwood, and E. F. Thompson. 1994. *Upgrade of tropical cyclone surface wind field model*, Miscellaneous Paper CERC-94-14, U.S. Army Corps of Engineers.

Cardone, V. J., C.V. Greenwood, and J. A. Greenwood. 1992. *Unified program for the specification of tropical cyclone boundary layer winds over surfaces of specified*

roughness, Contract Rep. CERC 92-1, U.S. Army Corps of Engineers Waterway Experiment Station, Vicksburg, MI.

Cardone, V. J. and D. B. Ross. 1979. *State-of-the-art wave prediction methods and data requirements*, Ocean Wave Climate ed. M. D. Earle and A. Malahoff. Plenum Publishing Corp., 1979, 61-91.

Cavaleri, L. and L.H. Holthuijsen. 1998. "Wave modeling in the WISE group," Proceedings of the 26th International Conference on Coastal Engineering, Copenhagen, 498-508.

Chorley, R.J. [ed.], 1972, Spatial Analysis in Geomorphology, Harper & Row, N.Y., 393 pps.

Chouinard, L.M. and C. Liu. 1997a. "Model for Recurrence Rate of Hurricanes in Gulf of Mexico," *Journal of Waterway, Port, Coastal and Ocean Engineering*, Vol. 123, No. 3, pp. 113-119.

Chouinard, L.M., C. Liu, and C.K. Cooper. 1997b. "Model for Severity Rate of Hurricanes in Gulf of Mexico," *Journal of Waterway, Port, Coastal and Ocean Engineering*. Vol. 123, No. 3, pp. 120-129.

Chow, S. H. 1971. *A study of the wind field in the planetary boundary layer of a moving tropical cyclone*, Master of Science Thesis in Meteorology, School of Engineering and Science, New York University, New York, NY.

Cooper, C.K. 1992. "A Preliminary Case for the Existence of Hurricane Alleys in the Gulf of Mexico," Offshore Technology Conference 6831. May 4-7, 1992, Houston, TX, USA.

Dean, R. and C.J. Bender. 2006. "Static Wave Set-Up with Emphasis on Damping Effects by Vegetation and Bottom Friction," *Journal of Coastal Engineering*, Vol. 53, pp 149-156.

Diaconis, P. (1988). Bayesian numerical analysis. Statistical Decision Theory and Related Topics IV (pp. 163--175).

Efron, B. 1982. *The Jacknife, the Bootstrap, and Other Resampling Plans*, Society for Industrial and Applied Mathematics, Philadelphia, PA.

Federal Emergency Management Agency. 2006. *Final Coastal and Riverine High Water Mark Collection for Hurricane Katrina in Mississippi*, FEMA-1604-DR-MS.

Federal Emergency Management Agency. 2003. *Guidelines and Specifications for Flood Hazard Mapping Partners*, Appendix D.

Federal Emergency Management Agency. February 2007. *Atlantic Ocean and Gulf of Mexico Guidelines Update.*

Forristall, G. Z. 1980. "A two-layer model for hurricane driven currents on an irregular grid," *Journal of Physical Oceanography*, 10, 9, 1417-1438.

Forristall, G. Z., E. G. Ward, V. J. Cardone, and L. E. Borgman. 1978. "The directional spectra and kinematics of surface waves in Tropical Storm Delia," *Journal of Physical Oceanography*, 8, 888-909.

Forristall, G.Z., R. C. Hamilton and V. J. Cardone. 1977. "Continental shelf currents in tropical storm Delia: observations and theory," *Journal of Physical Oceanography*. 7, 532-546.

Frank, N. 1970. "Atlantic Tropical Systems of 1969," *Monthly Weather Review*, p.307-314.

Gorman, R.M. and C.G. Neilson. 1999. "Modelling shallow water wave generation and transformation in an intertidal estuary," *Coastal Engineering*, 36, 197-217.

Goudeau, D.A. and W.C. Conner.1968. *Storm Surge over the Mississippi River Delta Accompanying Hurricane Bettsy, 1965,* American Meteorological Society, 96:2.

Hamilton, R.C. and Steere, D.B. 1969. *Ocean Gathering Program Report No. 2 Covering Hurricane Camille (17 August 1969),* Baylor, CO. Consulting Report, Oct. 8, 1969, 27 pps.

Hebert, Paul J., J.D. Jarrell and M. Mayfield. 1996. The Deadliest, Costliest, and Most Intense United States Hurricanes of this Century (And Other Frequently Requested Hurricane Facts), NOAA Technical Memorandum NWS TPC-1.

Ho, F.P. and V.A. Myers. 1975. *Joint Probability Method of Tide Frequency Analysis applied to Appalachicola Bay and St. George Sound, Florida*, NOAA Tech Rep. WS 18, 43p.

Ho, F. P., J.C. Su, K. Hanevich, R.J. Smith, and F.P. Richards. 1987. *Hurricane Climatology for the Atlantic and Gulf Coasts of the United States,* NOAA Technical Report NWS 38.

Holland, G. J. 1980. "An analytical model of the wind and pressure profiles in hurricanes," *Monthly Weather Review*, 1980, 108, 1212-1218.

Holthuijsen, L.H. 1998. "The concept and features of the ocean wave spectrum, Provision and engineering/operational application of ocean wave spectra," COST Conference, UNESCO, 21-25 Sept., 1998, Paris, keynote address, in press.

Holthuijsen, L.H., A. Herman, and N. Booij. 2003. "Phase-decoupled refraction-diffraction for spectral wave models," *Coastal Engineering*, 49, 291-305.

Holthuijsen, L.H. and L. Cavaleri. 1998. "Activities of the WISE group," 5th International Workshop on Wave Hindcasting and Forecasting, Jan. 27-30, 1998, Melbourne, FL, 433-437.

Holthuijsen, L.H., R.C. Ris, and N. Booij. 1998a. "A verification of the third-generation wave model SWAN," 5th International Workshop on Wave Hindcasting and Forecasting, Jan. 27-30, 1998, Melbourne, FL, 223-230.

Holthuijsen, L.H., N. Booij, and J.G. Haagsma. 1998b. "Comparing 1st-, 2nd- and 3rd-generation coastal wave modeling," 26th International Conference on Coastal Engineering, Copenhagen, 140-149.

Holthuijsen, L.H., N. Booij and R. Padilla-Hernandez. 1997a. "A curvilinear, third-generation coastal wave model," Conference on Coastal Dynamics '97, Plymouth, England, 128-136.

Holthuijsen, L.H., N. Booij, R.C. Ris, J.H. Andorka Gal, and J.C.M. de Jong. 1997b. "A verification of the third-generation wave model 'SWAN'along the southern North Sea coast," Proceedings of the 3rd International Symposium on Ocean Wave Measurement and Analysis, WAVES'97, ASCE, 49-63.

Holthuijsen, L.H., N. Booij, and R.C. Ris. 1993. "A spectral wave model for the coastal zone," Proceedings of the 2nd International Symposium on Ocean Wave Measurement and Analysis, New Orleans, LA, July 25-28, 1993, New York, pp. 630-641.

Hong, X., S. W. Chang, S. Raman, L. K. Shay, And R. Hodur (2000). The Interaction between Hurricane Opal (1995) and a Warm Core Ring in the Gulf of Mexico. Monthly Weather Review, v. 28, p.1347.

Hsu, T. W., S. H. Ou, and J. M. Liau. 2005. "Hindcasting nearshore wind waves using a FEM code for SWAN," *Coastal Engineering*, 52, 177-195.

Irish, J., D. Resio, and J. Ratcliff (2008). The influence of storm size on hurricane surge. Journal of Physical Oceanography, in press.

Jelesnianski, C.P., J. Chen, and W.A. Shaffer. 1992. *SLOSH: Sea, lake, and overland surges from hurricanes*. NOAA Technical Report NWS 48, NOAA, Washington, DC.

Levinson, David . 2007. NOAA National Climate Data Center, pers. comm.

McGuire, R.K., C.A. Cornell, and G.R. Toro. 2005. "The Case for Using Mean Seismic Hazard," *Earthquake Spectra*, v. 21, no. 2, p. 879-886.

Miller, A.C., and T.R. Rice (1983). "Discrete approximations of probability distributions," Management Science, 29, 3, 352-361.

Minka, T. P. (2000) Deriving quadrature rules from Gaussian processes, Technical Report, Statistics Department, Carnegie Mellon University. Available on-line at http://research.microsoft.com/~minka/papers/minka-quadrature.ps.gz.

Myers, V.A. 1975. *Storm Tide Frequencies on the South Carolina Coast*, NOAA Tech Rep. NWS-16, 79p.

National Oceanic and Atmospheric Administration. 2005. Tides and Currents, http://tidesandcurrents.noaa.gov. Nov. 2005.

NOAA, 1997. Hydrographic Survey Digital Database. Vol. 1, 3rd. ed., National Oceanic and Atmospheric Administration.

O'Hagan, A. (1991). Bayes-Hermite quadrature. J Statistical Planning and Inference, 29, 245--260.

Padilla-Hernandez, R. and J. Monbaliu. 2001. "Energy balance of wind waves as a function of the bottom friction formulation," *Coastal Engineering*, 43, 131-148.

Padilla-Hernandez, R., J. Monbaliu, and L.H. Holthuijsen. 1998. "Intercomparing third-generation wave model nesting," 5th International Workshop on Wave Hindcasting and Forecasting, Jan. 27-30, 1998, Melbourne, FL, 102-112.

Resio, D.T., S.J. Boc, L. Borgman, V. Cardone, A. Cox, W.R. Dally, R.G. Dean, D. Divoky, E. Hirsh, J.L. Irish, D. Levinson, A. Niedoroda, M.D. Powell, J.J. Ratcliff, V. Stutts, J. Suhada, G.R. Toro, and P.J. Vickery. 2007. *White Paper on Estimating Hurricane Inundation Probabilities*. Consulting Report prepared by USACE for FEMA.

Ris, R.C. 1997. *Spectral modeling of wind waves in coastal areas*, (Ph.D. Dissertation Delft University of Technology, Department of Civil Engineering), Communications on Hydraulic and Geotechnical Engineering, Report No. 97-4, Delft, The Netherlands.

Ris, R.C. and L.H. Holthuijsen. 1997. "Modelling of current induced wave-blocking in a spectral wave model," 8th International Biennial Conference on Physics of Estuaries and Coastal Seas, J. Dronkers and M.B.A.M. Scheffers (eds.), The Hague, 139-144.

Ris, R.C. and L.H. Holthuijsen. 1996. "Spectral Modeling of current induced wave-blocking," Proceedings of the 25th International Conference on Coastal Engineering, Orlando, FL, Vol. 1, pp. 1247-1254.

Ris, R.C., L.H. Holthuijsen, and N. Booij. 1994. "A spectral model for waves in the near shore zone," Proceedings of the 24th International Conference on Coastal Engineering, October 1994, Kobe, Japan, pp. 68-78.

Rogers, W.E., P.A. Hwang, and D.W. Wang. 2003. "Investigation of wave growth and decay in the SWAN model: three regional-scale applications," *Journal of Phys. Oceanography*, 33, 366-389.

Ross, D. B. and V. J. Cardone. 1978. *A comparison of parametric and spectral hurricane wave prediction products. Turbulent Fluxes through the Sea Surface, Wave Dynamics, and Prediction,* A. Favre and K. Hasselmann, editors, 647-665.

Scheffner, Norman W. 2006. "Summary of EST Sensitivity Simulations Using the SLOSH model and a Single Hypothetical Storm with Multiple Landfall Points," Unpublished Data Report for URS (8/2/2006).

Scheffner, Norman W. and Leon E. Borgman. 1996. "The Empirical Simulation Technique, a Bootstrap-Based Life Cycle Approach to Frequency Analysis," 7th International Symposium on Stochastic Hydraulics, MacKay, Queensland, Australia, July 29-31, 1996.

Scheffner, N.W., L.E. Borgman, and D.J. Mark.1996."Empirical Simulation Technique Based Storm Surge Frequency Analysis," *ASCE Journal of Waterways, Ports, Coastal and Ocean Engineering*, Vol. 122, No.2 March/April1996.

Simpson, R.H., A. L. Sugg, G.B. Clark, N.L. Frank, J.R. Hope, P.J Hebert, R.L. Kraft, and J.M. Pelissier. 1979. "The Atlantic Hurricane Season of 1969," *Monthly Weather Review*, p. 293–306.

Shen, W. 2006. "Does the size of hurricane Eye Matter With its Intensity?", Geophysical Research Letters 33, L18813.

Smith, J. M., D. T. Resio, and A. K. Zundel.1999. *STWAVE: Steady-State Spectral Wave Model. Report 1: User's Manual for STWAVE Version 2.0*, Instructional Report CHL-99-1, U.S. Army Engineer Waterways Experiment Station, Vicksburg, MS.

Thompson, E. F. and V. J. Cardone. 1996. "Practical modeling of hurricane surface wind fields," *ASCE Journal of Waterway, Port, Coastal and Ocean Engineering*. 122, 4, 195-205.

Toro, G.R., C.A. Cornell, V.J. Cardone, and D.B. Driver. 2004. "Comparison of historical and deductive methods for the calculation of low-probability seastates in the Gulf of Mexico" Proceedings of the OMAE-04 Conference, ASME.

U.S. Army Corps of Engineers. 1965. *Hurricane Betsy*, Serial No. 1621, New Orleans, LA.

U.S. Army Corps of Engineers (Mobile District). 1970. *Report on Hurricane Camille (14-22 August 1969)*, USACE Mobile District Report. 80 pps.

U.S. Environmental Protection Agency. 2001. National Landcover Data (NCLD 2001). http://www.epa.gov/mrlc/nlcd-2001.html

Van der Westhuysen, A.J., M. Zijlema and J.A. Battjes. 2007. "Nonlinear saturation-based whitecapping dissipation in SWAN for deep and shallow water," *Coastal Engineering*, 54, 151-170.

Vickery, P. 2007. Hurricane Landfall Pressures. Unpublished Data Report for URS (11/06/ 2007).

Vickery, P.J., and L.A. Twisdale. 1995. "Wind-field and Filling Models for Hurricane Wind-Speed Predictions," *Journal of Structural Engineering*, ASCE, 121(11), 1700-1709.

Wamsley, T. 2007. *Mississippi Coastal Improvement Project Final Report*. Engineering Appendix.

Wen, Y.K. and H. Banon. 1991. "Development of Environmental Combination Design Criteria for Fixed Platforms in the Gulf of Mexico," OTC 6540, Offshore Technology Conference, Houston, TX, May 1991.

Westerink, J.J. and R.A. Luettich. 1991. *Tide and storm surge predictions in the Gulf of Mexico using model ADCIRC-2D,* Report to the U.S. Army Engineer Waterways Experiment Station, July, 1991.

Zijlema, M. and A.J. van der Westhuysen. 2005. "On convergence behaviour and numerical accuracy in stationary SWAN simulations of nearshore wind wave spectra," *Coastal Engineering*, 52, 237-256.

Appendix A
Acronyms

ADCIRC	ADvanced CIRCulation
BFE	Base Flood Elevation
BRICKA	Betsy, Rita, Ivan, Camille, Katrina, Andrew hurricane tracks
CAT2	Category 2
CHL	Coastal Hydraulics Laboratory
CHWM	Coastal High Water Mark
C-MAN	Coastal Marine Automated Network
CP	Central Pressure of the Storm
CRP	Coastal Reference Point
CVSE	Cross validation square error
DEM	Digital Elevation Model
DFIRM	Digital Flood Insurance Rate Map
ERDC	Environmental Research and Development Center
ERS-2	European Remote Sensing Satellite
EST	Empirical Statistical Technique
FEMA	Federal Emergency Management Agency
GAP	Gap Analysis Program
GIS	Geographic Information System
GOES	Geostationary Operational Environmental Satellite
GWCE	Generalized Wave-Continuity Equation
HMTAP	Hazard Mitigation Technical Assistance Program
HWM	High Water Mark
HPO	Hurricane Protection Office
HURDAT	HURricane DATabase
IDIQ	Indefinite Delivery/Indefinite Quantity
IE	Initial Elevation card in WHAFIS
ICZ	Initial Capture Zone
IPET	Interagency Performance Evaluation Taskforce
JPM	Joint Probability Method
JPM-OS	Joint Probability Method-Optimum Sampling
LaCPR	Louisiana Coastal Protection and Restoration Project
lidar	Light Detection and Ranging
LiMWA	Limit of Moderate Wave Action

MsCIP	Mississippi Coastal Improvement Project
MSL	Mean Sea Level
MWL	Maximum Winds making Landfall
NAVD	North American Vertical Datum
NBDC	National Buoy Data Center
NCEP	National Centers for Environmental Prediction
NFIP	National Flood Insurance Program
NGLI	Northern Gulf Littoral Initiative
NGS	National Geodetic Survey
NGVD	National Geodetic Vertical Datum
NHC	National Hurricane Center
NHRD	National Hurricane Research Division
NLCD	National Land Cover Dataset
NOAA	National Oceanic and Atmospheric Administration
NWS	National Weather Service
ODGP	Ocean Data Gathering Joint Industry Project
OWI	Oceanweather, Inc.
PBL	Planetary Boundary Layer
QUIKSCAT	Quick Scatterometer
R_{max}	Radius to Maximum Winds
RMS	Root Mean Square
R_p	Pressure Scale Radius
$R_{p(o)}$	R_p offshore
S_i	Point of Landfall
SAEL	Standard Annual Exceedence Level
SLOSH	Sea, Lake, and Overland Surges for Hurricanes model
SMS	Surface Modeling System
STWAVE	Steady-State Spectral Wave Model
SWAN	Simulating Waves Nearshore
SWEL	Stillwater Elevation
TAW	Technical Advisory Committee for Water Retaining Structures
TIN	Triangulate Irregular Network
TOPEX	TOPography EXperiment

TROP	TROPical file
TSDN	Technical Support Data Notebook
URS	URS Group, Inc.
USACE	U.S. Army Corps of Engineers
USGS	U.S. Geological Survey
V_f	Forward speed of the storm center
WAM	Wave Application Model
WHAFIS	Wave Height Analyses for Flood Insurance Studies
WISE	Watershed Information System
ΔP	Central atmospheric pressure deviation
θ	Storm track azimuth
λ	Storm rate

Appendix B
Comparison of Simulated and Measured Surge Elevations

Table B-1. Comparison of Simulated and Measured Surge Elevations for Hurricane Katrina.

Longitude	Latitude	Measured (ft)	Simulation (ft)	Comparison(ft)
-89.61847	30.35083	11.00	10.48	-0.52
-89.54668	30.24011	20.10	18.18	-1.92
-89.51177	30.25189	20.40	21.86	1.46
-89.46735	30.34494	15.40	19.65	4.25
-89.44942	30.26839	23.60	24.02	0.42
-89.44931	30.26771	23.70	24.13	0.43
-89.44528	30.40367	20.00	20.39	0.39
-89.44432	30.38425	19.50	19.86	0.36
-89.41819	30.30018	21.60	21.58	-0.02
-89.40986	30.28970	22.60	23.17	0.57
-89.40985	30.31793	22.30	22.84	0.54
-89.40975	30.28971	23.00	23.17	0.17
-89.38736	30.39787	21.70	21.68	-0.02
-89.38503	30.36259	23.80	23.28	-0.52
-89.35903	30.38123	25.30	25.83	0.53
-89.35445	30.29803	22.70	25.76	3.06
-89.28464	30.32322	22.70	24.69	1.99
-89.28118	30.32760	20.90	24.71	3.81
-89.27509	30.32118	22.60	24.71	2.11
-89.27141	30.32836	22.20	24.74	2.54
-89.26786	30.37490	24.60	25.59	0.99
-89.26300	30.31707	25.00	24.73	-0.27
-89.26280	30.33945	24.90	24.91	0.01
-89.25426	30.31538	24.60	25.28	0.68
-89.25411	30.33465	24.00	24.70	0.70
-89.25115	30.31434	25.00	25.53	0.53
-89.24968	30.32381	22.70	24.59	1.89
-89.23659	30.32795	25.50	24.55	-0.95
-89.22894	30.37507	23.50	24.83	1.33
-89.22745	30.38870	23.00	24.49	1.49
-89.22254	30.33289	23.90	24.56	0.66
-89.22022	30.35902	23.50	24.55	1.05
-89.21695	30.35964	22.50	24.46	1.96
-89.17612	30.33969	25.40	25.39	-0.01
-89.16127	30.34489	25.20	25.63	0.43
-89.15612	30.34560	25.70	25.37	-0.33
-89.13613	30.35511	25.00	25.16	0.16
-89.13138	30.35449	25.00	25.20	0.20
-89.10695	30.36459	24.30	25.26	0.96
-89.09876	30.36690	24.30	25.40	1.10
-89.09467	30.41131	18.00	16.89	-1.11
-89.09424	30.38058	18.60	16.67	-1.93
-89.08097	30.38436	18.60	16.93	-1.67
-89.08016	30.37187	24.90	24.94	0.04

Longitude	Latitude	Measured (ft)	Simulation (ft)	Comparison(ft)
-89.07725	30.42677	19.30	17.91	-1.39
-89.07594	30.41580	18.70	17.46	-1.24
-89.06319	30.42382	19.10	17.98	-1.12
-89.06202	30.37693	23.40	24.59	1.19
-89.06156	30.39267	18.00	17.47	-0.53
-89.06024	30.37756	23.90	24.68	0.78
-89.04928	30.40147	16.80	17.91	1.11
-89.04690	30.39926	17.10	17.92	0.82
-89.04425	30.38181	24.20	24.73	0.53
-89.03255	30.40000	15.40	18.20	2.80
-89.03096	30.40371	15.90	18.22	2.32
-89.02859	30.40245	16.60	18.23	1.63
-89.02734	30.38491	23.80	24.19	0.39
-89.02607	30.40919	18.00	18.47	0.47
-89.02461	30.40344	15.50	18.35	2.85
-89.01324	30.40745	18.20	18.63	0.43
-89.00694	30.43836	18.70	19.40	0.70
-89.00598	30.38851	23.60	23.88	0.28
-88.99747	30.41147	19.10	18.85	-0.25
-88.98695	30.39073	25.70	23.60	-2.10
-88.98297	30.41284	18.80	18.83	0.03
-88.97063	30.41490	19.30	19.26	-0.04
-88.93399	30.39528	22.50	22.88	0.38
-88.93223	30.43185	21.10	21.07	-0.03
-88.91872	30.46811	17.10	18.55	1.45
-88.91097	30.43344	20.10	21.32	1.22
-88.89759	30.43061	20.20	21.80	1.60
-88.89560	30.40229	20.60	20.90	0.30
-88.89559	30.40077	20.50	20.77	0.27
-88.89518	30.43213	20.10	22.09	1.99
-88.89454	30.42906	20.60	21.86	1.26
-88.89349	30.47108	14.60	17.05	2.45
-88.89258	30.47438	15.90	16.96	1.06
-88.85492	30.44341	21.40	22.28	0.88
-88.84625	30.42288	20.70	21.77	1.07
-88.83805	30.41086	21.40	21.68	0.28
-88.82693	30.42525	20.10	21.13	1.03
-88.82327	30.41988	20.10	21.06	0.96
-88.81571	30.42814	19.70	20.93	1.23
-88.81010	30.42037	19.50	20.37	0.87
-88.80866	30.40467	22.40	21.86	-0.54
-88.80293	30.43701	18.40	20.33	1.93
-88.79857	30.40025	21.60	20.81	-0.79
-88.77929	30.37213	20.40	19.86	-0.54
-88.77750	30.42183	22.00	18.91	-3.09
-88.77064	30.38672	18.80	20.17	1.37

Longitude	Latitude	Measured (ft)	Simulation (ft)	Comparison(ft)
-88.76966	30.36800	19.70	19.65	-0.05
-88.76033	30.42692	16.50	17.65	1.15
-88.75815	30.36278	18.60	19.36	0.76
-88.75180	30.36080	17.60	19.25	1.65
-88.74598	30.38222	19.40	19.71	0.31
-88.73990	30.43236	17.20	11.63	-5.57
-88.72784	30.36806	19.20	19.58	0.38
-88.72324	30.44160	16.10	14.50	-1.60
-88.72278	30.44107	16.40	14.51	-1.89
-88.72278	30.44107	16.40	14.51	-1.89
-88.72179	30.44168	15.60	14.43	-1.17
-88.71905	30.44763	18.90	14.08	-4.82
-88.71194	30.34832	19.90	18.51	-1.39
-88.70924	30.35873	19.00	19.18	0.18
-88.70432	30.37692	19.40	19.45	0.05
-88.69907	30.36135	18.40	18.99	0.59
-88.63450	30.40590	14.30	14.47	0.17
-88.63219	30.40764	14.40	14.47	0.07
-88.63200	30.36482	21.10	17.85	-3.25
-88.62554	30.42165	14.00	13.43	-0.57
-88.62112	30.42380	15.20	13.40	-1.80
-88.61277	30.38915	14.40	14.68	0.28
-88.56798	30.36208	17.10	15.70	-1.40
-88.55977	30.36605	16.70	15.76	-0.94
-88.55891	30.37984	14.90	13.75	-1.15
-88.55739	30.35623	20.00	16.07	-3.93
-88.55378	30.34499	18.00	16.39	-1.61
-88.55332	30.35175	16.90	16.33	-0.57
-88.55240	30.39791	14.70	14.02	-0.68
-88.54808	30.35159	16.80	16.36	-0.44
-88.54287	30.34772	17.20	16.32	-0.88
-88.54024	30.34688	16.70	16.37	-0.33
-88.53962	30.41361	12.20	12.54	0.34
-88.53709	30.35470	16.60	16.50	-0.10
-88.53526	30.36414	16.00	16.53	0.53
-88.53315	30.34635	17.30	16.12	-1.18
-88.52309	30.34633	16.50	16.08	-0.42
-88.52187	30.35400	16.20	16.21	0.01
-88.52161	30.37373	14.40	16.60	2.20
-88.51726	30.34685	16.80	15.93	-0.87
-88.50395	30.40968	12.10	12.39	0.29
-88.48757	30.40595	11.70	14.07	2.37
-88.47990	30.41195	11.50	13.34	1.84
-88.46235	30.42889	10.60	12.48	1.88
-88.42915	30.44342	14.20	14.48	0.28

Table B-2. Comparison of Simulated and Measured Surge Elevations for Hurricane Camille.

Longitude	Latitude	Measured (ft)	Simulation (ft)	Comparison(ft)
-89.615567	30.238617	6.47	6.94	0.47
-89.613900	30.238917	7.67	6.85	-0.82
-89.611528	29.412755	1.84	2.71	0.87
-89.609177	30.239764	8.55	7.25	-1.30
-89.576868	30.258284	8.16	7.58	-0.58
-89.562488	30.216879	11.34	9.86	-1.48
-89.513122	30.334269	10.42	9.06	-1.36
-89.488051	30.323697	9.83	9.41	-0.42
-89.469285	30.342788	10.50	10.32	-0.18
-89.467901	30.383611	11.89	8.73	-3.16
-89.441467	30.386283	11.67	9.27	-2.40
-89.440979	30.386637	11.97	11.63	-0.34
-89.439570	30.298591	10.64	11.03	0.39
-89.439077	30.300042	11.34	11.04	-0.30
-89.425305	30.329087	13.37	12.25	-1.12
-89.424359	30.356083	14.25	13.38	-0.87
-89.424299	30.357629	13.45	13.44	-0.01
-89.423011	30.299631	11.43	12.24	0.81
-89.422902	30.298044	12.63	12.82	0.19
-89.422147	30.358417	13.85	13.50	-0.35
-89.420693	30.357326	14.55	13.54	-1.01
-89.415267	30.258922	16.34	16.24	-0.10
-89.414317	30.257500	15.17	16.32	1.15
-89.409450	30.361144	14.77	13.89	-0.88
-89.408663	30.362598	14.06	13.69	-0.37
-89.397147	30.298837	16.81	15.71	-1.10
-89.397117	30.366053	14.98	13.96	-1.02
-89.396655	30.300014	12.81	15.03	2.22
-89.394814	30.365416	16.79	14.09	-2.70
-89.382326	30.413589	12.94	12.11	-0.83
-89.380940	30.271756	18.64	17.69	-0.95
-89.379412	30.306282	14.70	14.34	-0.36
-89.378728	30.305023	15.41	14.34	-1.07
-89.374183	30.276500	19.07	18.03	-1.04
-89.360632	30.377440	18.13	17.29	-0.84
-89.359144	30.289739	19.54	18.68	-0.86
-89.359083	30.289200	18.87	18.68	-0.19
-89.350650	30.380150	18.47	17.52	-0.95
-89.348441	30.341171	17.23	16.35	-0.88
-89.345326	30.294453	19.55	18.81	-0.74
-89.344847	30.382069	19.16	17.57	-1.59
-89.343879	30.418899	13.72	12.14	-1.58

Longitude	Latitude	Measured (ft)	Simulation (ft)	Comparison(ft)
-89.341133	30.342283	16.47	16.65	0.18
-89.333259	30.301570	20.34	18.74	-1.60
-89.330667	30.326067	21.17	16.36	-4.81
-89.327159	30.308774	21.83	18.15	-3.68
-89.327071	30.322918	16.20	16.30	0.10
-89.289650	30.304417	16.67	18.97	2.30
-89.287515	30.307308	16.64	18.71	2.07
-89.275554	30.306673	17.74	19.79	2.05
-89.259576	30.311506	19.83	20.28	0.45
-89.251179	30.313409	20.13	20.40	0.27
-89.245761	30.370008	17.20	17.61	0.41
-89.243042	30.315699	22.63	20.50	-2.13
-89.242166	30.320076	16.03	17.83	1.80
-89.239034	30.316736	22.73	20.63	-2.10
-89.231200	30.375467	16.47	17.40	0.93
-89.230531	30.375250	17.10	17.38	0.28
-89.228825	30.326181	15.73	17.11	1.38
-89.218740	30.324391	24.33	20.87	-3.46
-89.218333	30.326100	22.37	20.94	-1.43
-89.218192	30.336156	15.43	16.98	1.55
-89.217752	30.230250	15.87	16.85	0.98
-89.217279	30.329360	15.33	16.99	1.66
-89.216517	30.325150	24.07	20.87	-3.20
-89.214367	30.325617	21.67	20.89	-0.78
-89.207713	30.327741	21.23	20.91	-0.32
-89.200987	30.414969	13.60	18.33	4.73
-89.184249	30.336191	21.63	21.15	-0.48
-89.166643	30.343665	21.13	21.30	0.17
-89.153433	30.352842	22.07	22.50	0.43
-89.150013	30.347536	21.13	21.89	0.76
-89.146700	30.345197	21.97	21.01	-0.96
-89.136452	30.353914	20.73	21.39	0.66
-89.127045	30.355208	21.73	21.37	-0.36
-89.109446	30.361078	20.33	21.19	0.86
-89.093209	30.365981	20.23	21.27	1.04
-89.092642	30.412691	13.82	11.40	-2.42
-89.087397	30.432188	14.41	12.48	-1.93
-89.086183	30.380117	20.17	21.66	1.49
-89.078339	30.371206	20.93	21.06	0.13
-89.058427	30.377020	20.47	20.90	0.43
-89.056697	30.395401	12.13	12.53	0.40
-89.051131	30.379563	19.73	21.13	1.40
-89.044071	30.379845	20.63	20.55	-0.08
-89.035952	30.488298	12.59	11.28	-1.31
-89.027267	30.448635	13.61	13.68	0.07
-89.026634	30.383728	19.93	20.31	0.38

Longitude	Latitude	Measured (ft)	Simulation (ft)	Comparison(ft)
-89.014433	30.452618	14.01	13.29	-0.72
-89.011773	30.385705	20.53	19.96	-0.57
-88.992617	30.389808	19.37	19.76	0.39
-88.989589	30.390666	20.03	19.70	-0.33
-88.976600	30.413807	14.03	13.09	-0.94
-88.976382	30.426625	13.42	13.37	-0.05
-88.967590	30.460335	11.71	13.69	1.98
-88.956307	30.392483	19.63	19.01	-0.62
-88.939103	30.459981	14.32	13.48	-0.84
-88.939102	30.425919	13.41	15.25	1.84
-88.933018	30.395373	19.63	18.65	-0.98
-88.932683	30.393150	18.97	18.53	-0.44
-88.910183	30.394795	18.63	18.18	-0.45
-88.908326	30.460237	12.71	12.57	-0.14
-88.900768	30.394382	17.63	18.06	0.43
-88.891869	30.413079	15.43	16.65	1.22
-88.891067	30.407850	15.17	16.18	1.01
-88.890746	30.422743	15.42	16.77	1.35
-88.890445	30.394217	17.23	17.86	0.63
-88.880069	30.395029	16.13	17.75	1.62
-88.866061	30.395241	15.63	17.09	1.46
-88.858065	30.394217	15.73	16.82	1.09
-88.855154	30.442950	15.82	17.56	1.74
-88.840175	30.410451	15.63	16.95	1.32
-88.831592	30.409731	15.93	17.04	1.11
-88.827221	30.418581	14.93	16.07	1.14
-88.824822	30.403440	15.93	16.88	0.95
-88.816133	30.400017	15.37	16.65	1.28
-88.765025	30.406170	14.03	15.85	1.82
-88.759456	30.379275	13.42	15.27	1.85
-88.758571	30.370390	13.31	15.06	1.75
-88.758488	30.361422	14.11	14.55	0.44
-88.743894	30.381912	14.42	14.70	0.28
-88.722015	30.441124	11.51	8.97	-2.54
-88.719973	30.365742	13.40	13.64	0.24
-88.715667	30.359235	12.79	13.30	0.51
-88.708395	30.395117	12.89	13.72	0.83
-88.688875	30.392820	12.30	13.27	0.97
-88.668494	30.390237	13.11	13.26	0.15
-88.645550	30.489825	8.42	6.11	-2.31
-88.639345	30.360366	12.80	12.09	-0.71
-88.621793	30.438119	9.24	6.95	-2.29
-88.613933	30.377089	12.82	11.68	-1.14
-88.561753	30.344925	9.65	10.36	0.71
-88.558592	30.343675	11.25	10.35	-0.90
-88.558518	30.369042	9.19	8.17	-1.02

Longitude	Latitude	Measured (ft)	Simulation (ft)	Comparison(ft)
-88.552390	30.436072	8.75	6.63	-2.12
-88.545072	30.424612	8.55	6.54	-2.01
-88.535431	30.371175	11.89	9.74	-2.15
-88.533000	30.368383	11.27	10.21	-1.06
-88.498855	30.331305	11.45	9.70	-1.75
-88.479988	30.406000	8.64	9.27	0.63
-88.471583	30.471660	5.74	4.66	-1.08
-88.458916	30.419174	9.74	9.88	0.14
-88.453291	30.457941	5.04	4.70	-0.34
-88.436007	30.437633	7.43	7.88	0.45
-88.421937	30.442616	9.53	9.91	0.38
-88.558592	30.343675	11.25	10.35	-0.90
-88.558518	30.369042	9.19	8.17	-1.02
-88.552390	30.436072	8.75	6.63	-2.12
-88.545072	30.424612	8.55	6.54	-2.01
-88.535431	30.371175	11.89	9.74	-2.15
-88.533000	30.368383	11.27	10.21	-1.06
-88.498855	30.331305	11.45	9.70	-1.75
-88.479988	30.406000	8.64	9.27	0.63
-88.471583	30.471660	5.74	4.66	-1.08
-88.458916	30.419174	9.74	9.88	0.14
-88.453291	30.457941	5.04	4.70	-0.34
-88.436007	30.437633	7.43	7.88	0.45
-88.421937	30.442616	9.53	9.91	0.38

Table B-3. Comparison of Simulated and Measured Surge Elevations for Hurricane Betsy.

Longitude	Latitude	Measured (ft)	Simulation (ft)	Comparison(ft)
-89.50018	30.33675	8.00	9.27	1.27
-89.44100	30.38663	9.50	10.52	1.02
-89.49741	30.33395	8.60	9.28	0.68
-89.48803	30.32369	8.20	9.42	1.22
-89.42537	30.32909	9.80	10.76	0.96
-89.40938	30.36123	10.50	11.54	1.04
-89.41702	30.25645	12.00	12.06	0.06
-89.35366	30.33961	11.20	11.79	0.59
-89.32965	30.30653	12.50	11.56	-0.94
-89.26892	30.37129	10.60	11.50	0.90
-89.29344	30.30822	10.80	11.22	0.42
-89.23052	30.37521	10.60	11.08	0.48
-89.20102	30.41494	10.00	9.43	-0.57
-89.14784	30.34502	12.30	10.41	-1.89
-89.09862	30.36314	10.70	10.07	-0.63
-89.09164	30.35385	10.70	9.99	-0.71
-89.02754	30.40479	9.10	8.57	-0.53
-89.02681	30.38245	9.30	9.73	0.43
-89.08744	30.43216	9.00	8.78	-0.22
-89.02726	30.44861	8.50	8.81	0.31
-89.01444	30.45262	8.50	8.67	0.17
-89.03598	30.48831	8.10	7.28	-0.82
-88.96055	30.45804	8.80	8.92	0.12
-88.90503	30.42954	8.50	8.43	-0.07
-88.89193	30.42331	9.00	8.47	-0.53
-88.89189	30.41307	9.50	8.47	-1.03
-88.90770	30.43023	8.80	8.42	-0.38
-88.88006	30.41203	8.80	8.43	-0.37
-88.96055	30.45804	8.80	8.92	0.12
-88.97660	30.41387	8.30	8.45	0.15
-88.93934	30.45880	8.30	8.95	0.65
-88.85856	30.39324	8.70	8.33	-0.37
-88.82922	30.42364	8.60	8.08	-0.52
-88.82726	30.41857	8.30	8.00	-0.30
-88.72194	30.44108	7.50	5.75	-1.75
-88.62189	30.43822	5.70	4.84	-0.86
-88.61396	30.37714	6.40	6.48	0.08
-88.56165	30.34486	6.40	6.28	-0.12
-88.54513	30.42462	5.40	4.61	-0.79
-88.55234	30.43611	5.50	4.66	-0.84
-88.47161	30.47173	4.50	3.29	-1.21
-88.45326	30.45793	4.40	3.20	-1.20
-88.44680	30.46001	4.50	3.19	-1.31

Appendix C

Summary of the Hurricane Major Characteristics

a. Rate (ΔP>48 mb)=2.88E-4E-4 storms/km/yr
   Rate (ΔP 31-48 mb) =2.57E-4 storms/km/yr
b. Can treat landfall location as uniformly distributed
c. Azimuth:
   i. ΔP >48 mb, Beta ($r = 10.229$, and $t = 11.747$)
   ii. ΔP 31-48 mb, normal (mean=-9.9 deg, σ =58.7 deg; truncate at ± 90 deg)
d. ΔP: three-parameter Weibull (see Eqs. 3 and 4)
   i. ΔP>48mb, ΔP_0=48mb, U=48.6 mb, k=1.8
   ii. ΔP 31-48 mb, U=46.6 mb, k=1.95
e. R_p (offshore) given ΔP: lognormal
   i. ΔP>48mb
      1. mean (nmi): $406.2\Delta P^{-0.711}$
      2. sigma (nmi): $187.7\Delta P^{-0.711}$
   ii. ΔP 31-48 mb
      1. mean (nmi): $79.58\Delta P^{-0.33}$
      2. sigma (nmi): $36.78\Delta P^{-0.33}$
f. V_f: lognormal
   i. ΔP>48mb
      1. mean (meters/second [m/s]); 6.6
      2. sigma (m/s): 2.8
   ii. ΔP 31-48 mb
      1. mean (m/s); 5.5
      2. sigma (m/s): 2.5